Non-photochemical quenching mechanisms in plants - light induced reorganization of the thylakoid membrane

Inaugural dissertation

for the attainment of the title of doctor
in the Faculty of Mathematics and Natural Sciences
at the Heinrich Heine University Düsseldorf

presented by

Suman Paul
from India

Mülheim an der Ruhr, May 2014

from the institute for Max-Planck-Institut für Chemische Energiekonversion
at the Heinrich Heine University Düsseldorf

Published by permission of the
Faculty of Mathematics and Natural Sciences at
Heinrich Heine University Düsseldorf

Supervisor: Prof. Dr. Alfred R. Holzwarth
Co-supervisor: Prof. Dr. Claus A. M. Seidel

Date of the oral examination: 25/06/2014

Dedicated to Sir Jagadish Chandra Bose

A physicist, botanist and fine man

Believe you can and you're halfway there.

TABLE OF CONTENTS

Summary

The safe harnessing of natural sunlight is intimately related with the dissipation of excess energy accumulated on the photosystem II (PSII) antenna, in order to protect the reaction centers (RC) and other parts of the photosynthetic apparatus from oxidative damage. Non-photochemical quenching (NPQ) is one of the main mechanisms to achieve that goal. It is generally considered as a fully reversible mechanism, which starts within seconds of light fluctuations and capable of photoprotection to a large extent. The rapid part of NPQ, termed as qE, is initiated by the pH gradient across the thylakoid membrane and dependent on the presence of 22 kDa PsbS protein. At low pH, light associated xanthophyll cycle conversion, i.e. de-epoxidation of violaxanthin (V) into zeaxanthin (Z), switches on a second mechanism, qZ, where the excited chlorophylls, most likely located on the peripheral photosystem II (PSII) antenna are quenched. In the literature, the functional models were developed based on the static picture of thylakoid membrane, where, PSII and PSI are confined to grana stacks and stroma lamella. This information is by far, not sufficient to understand the real NPQ state, where fluctuating sunlight, as experienced in natural habitat is known to trigger architectural switches inside the photosynthetic machinery. In addition, vascular plants, when grown under higher light intensity demonstrated a significantly higher photoprotection capacity compared to the typical controlled light grown plants cited in the literature. A two-site (qE and qZ) NPQ model was unsuitable to explain the three-four-fold increases in their NPQ values.

The thesis addressed these questions principally by time-resolved fluorescence spectroscopy performed on intact leaves under various physiological dark and/or light adapted states. The high signal-to-noise signals were registered at exceptionally high dynamic range with picosecond resolution. This allowed the extremely complex fluorescence kinetics to be successfully interpreted on the basis of multicomponent analysis and target models. Detailed energy and/or electron transfer pathways and quenching kinetic schemes were also investigated. The results were used to build structural models to understand the light induced dynamicity inside the thylakoid membrane. In some cases, further clues were collected using electron microscopy (EM) and pigment analysis, done in collaboration. Subsequently, all these information are compiled to understand: a) the complete behavior of thylakoid membrane, b) how extra photons are dissipated as heat and c) the site(s) and mechanism(s) involved.

Studies were performed on intact leaves of *Arabidopsis thaliana*, *Monstera deliciosa*, *Prunus laurocerasus* and *Hedera helix*, where the latter 3 species are evergreens and were known to dissipate more than 90% of incident sunlight. *Arabidopsis* remained the most preferred choice because of the availability of a large number of mutants, where desired chlorophyll pigment(s) was eliminated. Plants grown under various light conditions are elected, such as, low-light (60-70 μmol photons m^{-2} s^{-1}), high-light (600-700 μmol photons m^{-2} s^{-1}), natural fluctuating sunlight (1400-1600 μmol photons m^{-2} s^{-1}) and also artificial sun-flecks caused by short light pulses (1000 μmol photons m^{-2} s^{-1}) staying for 20-s on every 5 min interval. In addition, acclimatization of low-light grown *Monstera* plants to high irradiation was also studied. Measurements were performed on dark-adapted (unquenched) and high light-adapted (quenched) leaf-disks. In a response towards light-induced stress, the kinetic modelling revealed three principle changes in the energy transfer dynamics of PSII, while the PSI kinetics generally remained unaltered. It is concluded that NPQ in these plants is associated with: 1) zeaxanthin-dependent increase in the deactivation of PSII-attached antenna (k_D); 2) PsbS-dependent formation of a novel far-red fluorescence compartment, functionally detached from photosystem II or photosystem I; 3) A direct energy-transfer between the PSII and PSI compartments was established for high light and natural fluctuating sunlight grown plants. The kinetic data provided support for the presence of two-independent quenching sites, reminiscent of qE and qZ mechanisms proposed earlier, where qE was associated with the pH-induced detachment of the light-harvesting antenna (LHCII) and subsequent quenching by PsbS protein and qZ mechanism was the Z dependent quenching of remaining PSII complex. The direct energy-transfer from PSII to oxidized P700 reaction center unveiled a novel quenching mechanism, termed as energy-spillover or (Q_{so}). This mechanism is recognized as the most efficient way of photoprotection of PSII.

The extensive research carried in this thesis acknowledges that thylakoid membrane is extremely responsive towards light, contrary to the classical static model. The folding of grana stacks and also the membrane architecture are found to adjust with surrounding light to achieve highest photosynthesis turnover and lowest oxidative damage. Plants grown at high light or natural sunlight possesses exceptionally higher photoprotection or NPQ capacity, mainly due to the spillover of extra energy to photosystem I. This mechanism also visualized in electron microscopy as dissolution of the appressed region. For normal light (such as SF) or low-light grown plants, qE and qZ remains as the dominating form of quenching carried by the photosystem II antenna proteins.

Zusammenfassung

Die sichere Nutzung von natürlichem Sonnenlicht ist eng verbunden mit der Ableitung der am Photosystem II (PSII)-Antenne angesammelten überschüssigen Energie, um die Reaktionszentren (RC) und anderen Teile des Photosyntheseapparates vor oxidativen Schäden zu schützen. Nicht-photochemische Löschung (nonphotochemical quenching, NPQ) ist einer der wichtigsten Mechanismen, um dieses Ziel zu erreichen. Es wird im Allgemeinen als vollständig reversibler Mechanismus betrachtet, der in der Lage ist innerhalb von Sekunden Lichtschwankungen auszugleichen und somit die Photoprotektion enorm auszuweiten. Der schnelle Teil des NPQ, bezeichnet als qE, wird durch den pH-Gradienten an der Thylakoidmembran initiiert und ist abhängig vom Vorhandensein des 22 kDa PsbS Proteins. Bei einem niedrigen pH-Wert schaltet eine durch Licht ausgelöste Konversion des Xanthopylls, d.h. die Deepoxidierung von Violaxanthin (V) zu Zeaxanthin (Z) einen zweiten Mechanismus qZ, bei dem die angeregten Chlorophylle, die sich üblicherweise an den äußeren Antennen des PSII befinden, „gelöscht“ werden. In der Literatur wurden die Funktionsmodelle üblicherweise auf der Grundlage des statischen Bildes von Thylakoidmembranen , bei dem PSII und PSI durch Granastapel und Stromalamellen begrenzt sein sollen, entwickelt. Diese Information reicht bei weitem nicht aus, um die tatsächlichen NPQ-Zustände zu verstehen, bei dem ständig wechselnde Sonneneinstrahlung, wie im natürlichen Lebensraum üblich, dazu dient, architektonische Schalter innerhalb der photosynthetischen Maschinerie auszulösen. Außerdem zeigten Topfpflanzen, wenn sie unter höheren Lichtintensitäten gewachsen sind, auch eine deutlich höhere Lichtschutzkapazität im Vergleich zu den typischerweise in der Literatur beschriebenen Lichtbedingungen angebauten Pflanzen. Ein zweistufiges NPQ-Modell (qE und qZ) war ungeeignet die drei- bis vierfache Erhöhung der NPQ-Werte zu erklären.

Die vorliegende Arbeit behandelt diese offenen Fragen vornehmlich durch zeitaufgelöste Fluoreszenzspektroskopie an intakten Blättern unter Zuhilfenahme verschiedener physiologischer Zustände (dunkel und / oder Licht angepasst). Das hohe Signal-zu-Rausch-Verhältnis wurde in einer außergewöhnlich hohen Dynamik im Pikosekunden-Zeitbereich aufgezeichnet. Dies ermöglicht es die äußerst komplexen Fluoreszenzkinetiken auf der Basis von Mehrkomponentenanalysen und Kinetik-Modellierungsansätzen („Target Analysis“) erfolgreich zu interpretieren. Detaillierte Energie-und/oder Elektronentransferwege und kinetischen Möglichkeiten zur Löschung

Zusammenfassung

wurden ebenfalls untersucht. Die Ergebnisse wurden verwendet, um strukturelle Modelle zu bauen, die die lichtinduzierte Dynamik in der Thylakoidmembran besser verstehen lassen. In einigen Fällen wurden auch weitere Anhaltspunkte zum Verständnis der zugrundeliegenden Mechanismen mittels Elektronenmikroskopie (EM) und Pigmentanalyse in Zusammenarbeit mit anderen Forschungseinrichtungen gesammelt. Anschließend werden alle diese Informationen zusammengetragen, um: a) das vollständige Verhalten der Thylakoidmembran zu verstehen, b) zu erfahren wie zusätzliche Photonen als Wärme abgeführt werden und c) welche Komponenten und Mechanismen beteiligt sind.

Die Untersuchungen wurden an intakten Blättern von Arabidopsis thaliana , Monstera deliciosa , Prunus laurocerasus und Hedera helix durchgeführt, wobei die letzteren 3 Spezies zu den immergrünen Pflanzen gehören und bei denen bekannt ist, dass sie mehr als 90% der einfallenden Sonnenlichts umwandeln. Arabidopsis wurde bevorzugt verwendet aufgrund der großen Anzahl von verfügbaren Mutanten, bei denen ausgesuchte Chlorophyllpigmente einfach eliminiert werden konnten.

Wir haben uns für Pflanzen entschieden, die unter verschiedenen Lichtbedingungen angezogen wurden. Die Bedingungen wie folgt: wenig Licht (60-70 µmol Photonen m^{-2} s^{-1}), Starklicht (600 bis 700 µmol Photonen m^{-2} s^{-1}), natürlich schwankendes Sonnenlicht (1400-1600 µmol Photonen m^{-2} s^{-1}) und künstliche Lichtflecken, die durch kurze Lichtpulse (1000 µmol Photonen m^{-2} s^{-1}) alle 5min für 20 s. erzeugt werden. Darüber hinaus untersuchten wir auch die Adaption von unter low-light Bedingungen gewachsenen Monstera Pflanzen an eine höhere Lichteinstrahlung. Die Messungen wurden an dunkeladaptierten (ungelöschten) und an hohe Lichtmengen angepasste (gelöschte) Blattschnipsel durchgeführt. Als Antwort auf lichtinduzierten Stress zeigen sich beim kinetischen Modellieren drei grundsätzlichen Änderungen in der Energietransferdynamik des PSII , während die PSI- Kinetik grundsätzlich unverändert blieb. Daraus wird geschlossen, dass in diesen Pflanzen NPQ im Zusammenhang steht mit: 1) Zeaxanthin abhängigen Anstieg der Deaktivierung des PSII, bei dem die Antenne angelagert ist (k_D); 2) PsbS abhängige Bildung einer neuen, funktionell von Photosystem II oder Photosystem I abgelösten Struktur mit einer neuen im fernroten Bereich liegenden Fluoreszenz; 3) Einer direkten Energieübertragung zwischen den PSII und PSI Systemen bei unter Starklicht und natürlich schwankendem Sonnenlicht gewachsenen Pflanzen etabliert. Die kinetischen Daten unterstützen die Möglichkeit zur Anwesenheit von zwei unabhängigen Löschorten und erinnern an früher vorgeschlagene

Mechanismen qE und qZ, bei denen qE wurde mit der pH -induzierten Ablösung der Lichtsammelantennen (LHCII) und anschließendem Löschen durch das PsbS Protein verknüpft war und der qZ Mechanismus war die von Z abhängige Löschung des restlichen PSII -Komplexes. Die direkte Energieübertragung vom PSII zum oxidierten P700 Reaktionszentrum offenbart einen neuen Löschmechanismus, der als Energieüberlauf (Q_{SO}) bezeichnet wird. Dieser Mechanismus wird als die effizienteste Möglichkeit der Photoprotektion des PSII anerkannt.

Bei der Ausführlichkeit dieser Arbeit zeigt sich deutlich, dass das hier vorgestellte Thylakoidmembransystem im Gegensatz zum klassischen statischen Modell sehr empfindlich auf Licht reagiert. Es wurde erkannt, dass die Faltung der Granastapel und auch die Struktur der Membran zu einer Anpassung an das Umgebungslicht führt, um höchste Umsätze und geringste oxidative Schäden bei der Photosynthese zu erreichen. Pflanzen, die bei künstlichem Starklicht oder natürlichem Sonnenlicht gewachsen sind besitzen einen deutlich höheren Lichtschutz oder eine verstärkte NPQ Kapazität, aufgrund des Überleitens der überschüssigen Energie hin zum Photosystem I. Dieser Mechanismus zeigt sich ebenfalls auch in der Elektronenmikroskopie als Auflösung der zusammengepressten Bereiche der Thylakoidmembran. Bei unter normalen Lichtbedingungen (z.B. SF) oder Low-Light angezogenen Pflanzen bleiben qE und qZ als hauptsächliche Möglichkeit zur Löschung, welche durch Photosystem II Antennenproteine realisiert werden.

Abbreviations and symbols

Car	carotenoid
Chl	chlorophyll
CS	charge separation
DAS	decay-associated (emission) spectrum
DCMU	3-(3′,4′-dichlorphenyl)-1,1-dimethylurea
DES	deepoxidation state
ΔpH	transthylakoid proton gradient
EET	excitation energy transfer
F_0	fluorescence from open PS II reaction centre particles in dark-adapted state
F_{max}	fluorescence from closed PS II reaction centre particles in dark-adapted state
F_{npq}	fluorescence from closed PS II reaction centre particles in light-adapted state
HL	high light
kDa	kilodalton
LHC	light-harvesting complex
LHC I	light-harvesting complex I of PS II
LHC II	light-harvesting complex II of PS II
LL	low light
Lut	lutein
MGDG	monogalactosyldiacylglycerol
NL	natural sunlight
NPQ	non-photochemical quenching
Nx	neoxanthin
OEC	oxygen-evolving-complex
Pheo	pheophytin
PQ	plastoquinone
PS	photosystem
PS I	photosystem I
PS II	photosystem II
qE	fast reversible component of non-photochemical quenching
RC	reaction centre
RP	radical pair
r.t.	Room tempearture
SA(E)S	species-associated (emission) spectrum
SF	sun-flecks, caused by short high light pulses (20 s) on every 5 min
SPT	single-photon timing
V	violaxanthin
VAZ	violaxanthin/antheraxanthin/zeaxanthin
VDE	violaxanthin-de-epoxidase
w.t.	wild type
XC	xanthophyll cycle
Z	zeaxanthin
ZEP	zeaxanthin epoxidase

Chapter 1 : Introduction

1.1. Thylakoid membrane - structure and function

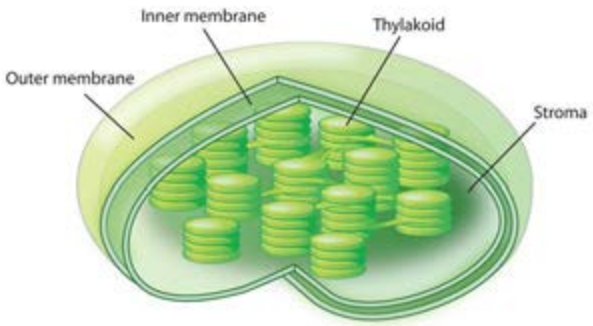

Figure 1.1: Structure of a chloroplast. Reproduced from Nature Education 2010.

Thylakoids are highly structured flat compressed membrane-bound vesicles, embedded into the chloroplasts (Figure 1.1), where light dependent reactions of photosynthesis take place. The outer chloroplast envelope consists of two membranes, with slightly differing lipid composition, spaced 2-10 nm apart. The chloroplast membrane is permeable for small molecules and certain metabolites, mediated by special transporter proteins. Thylakoids have 'sac-like' (Menke 1962) structures (appressed region) known as **grana**, which are stacked discs of membrane approximately 300-600 nm in diameter while the non-stacked (non-appressed) regions are called **stroma lamellae**. A chloroplast can have 10-20 grana, which are connected by lamellae (Mustárdy, Buttle et al. 2008). Grana and lamella differ in their protein composition. Thylakoids are surrounded by an amorphous aqueous space rich in soluble protein and ribosomes, called stroma, where CO_2-fixation takes place. The space enclosed by thylakoids is called lumen.

1.1.1. Lateral segregation in thylakoid membrane

The protein complexes are distributed unevenly in the thylakoids (Andersson and Anderson 1980). Photosystem I (PSI) and ATP synthase are primarily located in the stroma lamellae and grana margins, while Photosystem II (PSII) is found almost exclusively in the grana; Cytochrome b_6f complex (Cyt b_6f) is distributed equally in both. At the interface between PSII-rich grana and PSI-rich stroma, there are the so-called 'fret' domain (also called Margin, as in Figure 1.2), where the density of both RCs are high (Kaftan, Brumfeld et al. 2002). Such domains in the grana margins are extremely important during the dynamic organization of thylakoid membranes, due to the interactions between both RCs. This lateral heterogeneity of protein complexes and the thylakoid stacking itself are maintained by attractive forces between the light harvesting antenna protein complexes (LHCII) surrounding PSII (Ryrie, Anderson et al. 1980). The structure is thought to serve at least two primary objectives in photosynthesis, the maximization of PSII yield (Barber, Chow et al. 1980) and photoprotection (Horton and Black 1981, Chow, Kim et al. 2005).

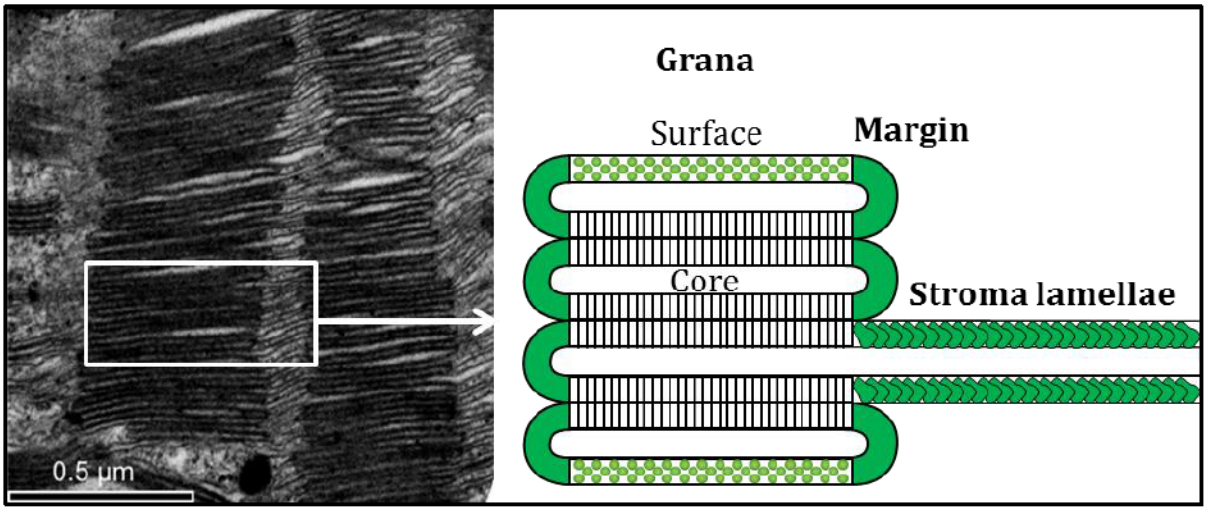

Figure 1.2: Organization of grana and stroma lamellae in thylakoid membrane. Electron micrograph (left) was acquired by Onno Muller at the University of Colorado, USA.

Recent proteomic results of thylakoid fractions have identified at least 335 different proteins, 89 in the lumen, 116 are integral membrane proteins, 62 are peripheral proteins on the stroma side and 68 are peripheral proteins on the lumen-side (van Wijk 2004). Integral membrane proteins play key roles in light-harvesting and light-dependent reactions of photosynthesis. There are four major protein complexes in the thylakoid membrane that run photosynthetic light reactions.

1.1.1.1. Photosystem I (PSI)

PSI has a reaction centre (RC; chlorophyll dimer), called P700; electron acceptors, such as A_0 (chlorophyll), A_1 (a phylloquinone), three 4Fe-4S iron-sulphur centers, including F_X, F_A, and F_B and over 20 carotenoids (Figure 1.3A). The RC and the four chlorophyll (Chl) a/b binding peripheral antenna proteins (LHCI; Lhca1-4) are distributed into two distinct loosely associated moieties, called PsaA and PsaB (Amunts, Drory et al. 2007). In each case, the polypeptide chains are folded into five transmembrane α-helices. In addition to peripheral antenna, PSI also contains a small amount of 'red' chlorophylls with shifted absorption bands (Croce, Chojnicka et al. 2007). PSI is extremely efficient, almost every photon that is absorbed is used for driving electron transport with quantum yield near to unity (Boichenko, Hou et al. 2001). PSI is responsible for $NADP^+$-reduction.

1.1.1.2. Photosystem II (PSII)

In the native state, PSII has a dimeric RC, P680, where each monomer is made of at least 20 protein subunits (Kamiya and Shen 2003, Barber, Ferreira et al. 2004, Umena, Kawakami et al. 2011). The largest subunits carrying chlorophyll pigments are the

centrally located D1 (PsbA) and D2 (PsbD) proteins carrying the two special pairs Chls (P_{D1} and P_{D2}), two accessory Chls (Chl_{accD1} and Chl_{accD2}), two pheophytins (Pheo) and two quinones (Q_A and Q_B) (Loll, Kern et al. 2005), as illustrated in Figure 1.3B. This complex further contains two large chlorophyll-pigment proteins, CP43 (PsbC) and CP47 (PsbD) (Kern, Biesiadka et al. 2007). In higher plants, the PSII core is surrounded by the peripheral membrane proteins; like the minor complexes CP24, CP26, CP29 and major light-harvesting complex II (LHCII). Additional redox cofactors are also present, such as a tyrosine (Tyr_Z), manganese-Ca complex, iron, cytochrome b_{559} and carotenoids. Like PSI, in PSII also, the homologous proteins D1 and D2 are interlocked to create a pseudo-symmetrical C2 handshake motif (Broser, Gabdulkhakov et al. 2010), where each of the polypeptide chains is folded into five transmembrane α-helices. The cofactors P_{D1}, Chl_{accD1} and $Pheo_{D1}$ constitute the active pathway (D1 branch) for electron transfer (Holzwarth, Müller et al. 2006). The second D2 branch contains symmetrically related cofactors, such as, P_{D2}, Chl_{accD2} and $Pheo_{D2}$ but inactive in primary electron transport. Rather, it hosts a β-carotene, which is able to quench the triplet chlorophyll (^3Chl) produced at closed PSII-RCs under strong light (Martinez-Junza, Szczepaniak et al. 2008). The nonheme iron (Fe^{2+}) and bicarbonate ions (HCO_3^-/CO_3^{2-}) are located between the two quinones.

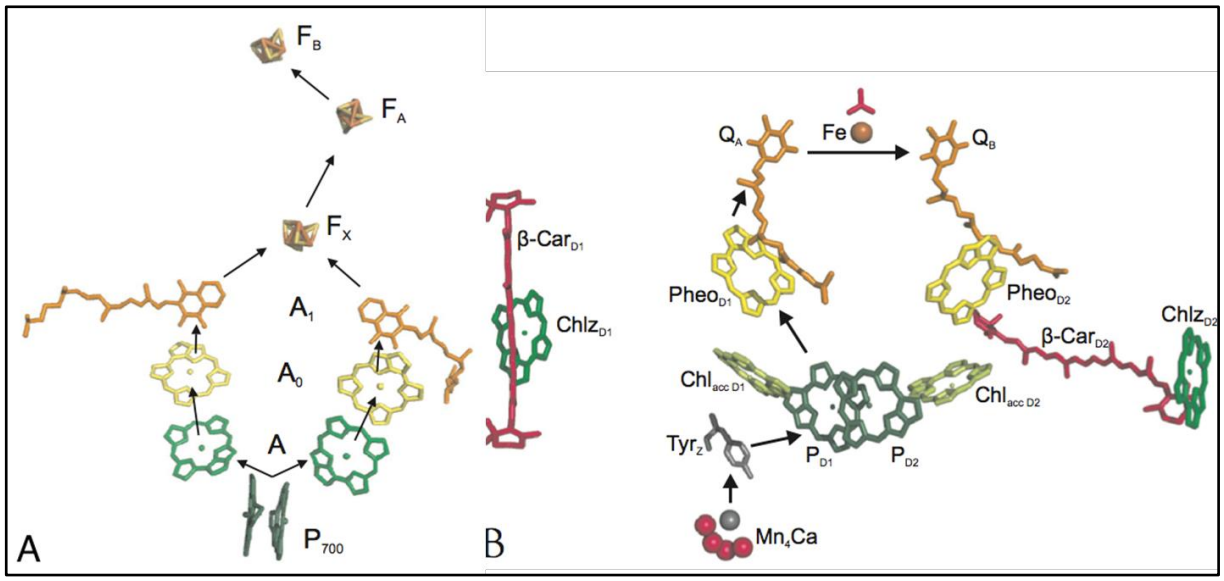

Figure 1.3: Structural arrangement of the cofactors involved in the primary reactions of Photosystem I (PSI, left-A) and Photosystem II (PSII, right-B). The pathways of electron transfers are indicated by arrows.

In green plants, PSII structure deserves a special attention. The core structure is surrounded by an antenna complex that accounts for nearly 70% of the total protein in plant chloroplast membrane (Remelli, Varotto et al. 1999). The LHCII antenna exists as a trimer and consists of multiple Lhc units of at least four types (LHCIIa-d) made by the

combination of six different chlorophyll a/b-binding proteins (Lhcb1-6). Each monomeric LHCII contains a single polypeptide of 230-250 amino acid residues (24-29 kDa), 8 Chl a, 6 Chl b and two luteins (Minagawa and Takahashi 2004, Standfuss, Terwisscha van Scheltinga et al. 2005). A very small amount of other xanthophyll molecules, such as, violaxanthin (0.2-0.4 mol) and neoxanthin (1.0 mol) are also present (Connelly, Müller et al. 1997). In addition, it contains one tightly bound native phospholipid (phosphatidylglycerol, PG). The secondary structure of LHCII contains three transmembrane α-helices H1, H3 and H4, which span the thylakoid membrane. The detailed investigation into the structure of complete PSII-LHCII has revealed the presence of a supercomplex consisting of a dimeric PSII core, designated as C2, and LHCII trimers at different binding positions, designated as 'S', 'M' and 'L', in which they refer to 'strongly', 'moderately' and 'loosely' bound LHCII complexes, respectively (Boekema, van Roon et al. 1999). Several combinations of these attached LHCII have been isolated, such as, C_2S_2M, $C_2S_2M_2$ and $C_2S_2M_2L$. A recent report, however, has indicated that the association of 'L' trimer occurs very rarely (Yakushevska, Keegstra et al. 2003), whereas $C_2S_2M_2$ and C_2S_2 are the most abundant (Barera, Pagliano et al. 2012). Figure 1.4 is a schematic illustration of the commonly available $C_2S_2M_2$ supercomplex. The PSII-LHCII macrostructure is dependent upon the presence of Mg^{2+}-ions, which screen the negatively charged residues on the stromal and luminal sides of the LHCII proteins and allow a tight association both within and between the membranes (Barber 1982, Daum, Nicastro et al. 2010).

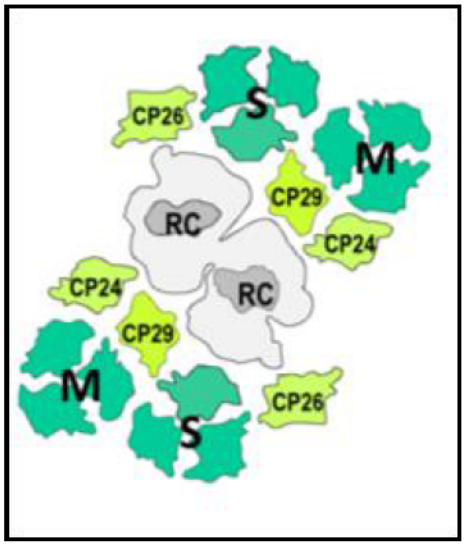

Figure 1.4: Schematic illustration of PSII-LHCII supercomplex, including various minor Lhcb proteins.

1.1.1.3. ATP synthase (ATP-ase)

ATP-ase is an enzyme, which produces ATP at the expense of the proton motive force (pmf) formed by the light-driven electron-transfer reactions (Engelbrecht and Junge 1997). It consists of two regions. The F_0-portion is located within the membrane, while the F_1-portion above the membrane (McCarty 1992). The proton intake and mechanism of ATP production is shown in Figure 1.5.

1.1.1.4. Cytochrome b_6f complex (Cyt b_6f)

Cyt b_6f mediates the electron transport between PSII and PSI (plastoquinol to plastocyanin, Figure 1.5) and converts the redox energy into part of the proton gradient used for ATP formation. Cyt b_6f exists as a dimer, where each monomer consists of c-type cytochrome f (Cyt f), the Rieske iron-sulfur protein (FeS), cytochrome b_6 (Cyt b_6) and a subunit IV (suIV) (Cramer, Martinez et al. 1994, Kurisu, Zhang et al. 2003).

Cyt b_6f complex is responsible for linear and cyclic electron transfers (Joliot and Johnson 2011). PSII and PSI along with Cyt b_6f drive the electron transfer from water to $NADP^+$, in the so-called linear electron transfer mechanism (LET, discussed below). However, under certain conditions, electrons from the reducing side of PSI may return towards the Cyt b_6f complex and/or plastoquinol pools (PQ) rather than to $NADP^+$. This mechanism is called cyclic electron transfer (CET), where ATP is synthesized without any NADPH (Foyer, Neukermans et al. 2012). This 'extra' ATP is used later in carbon-fixation and other processes, such as starch synthesis.

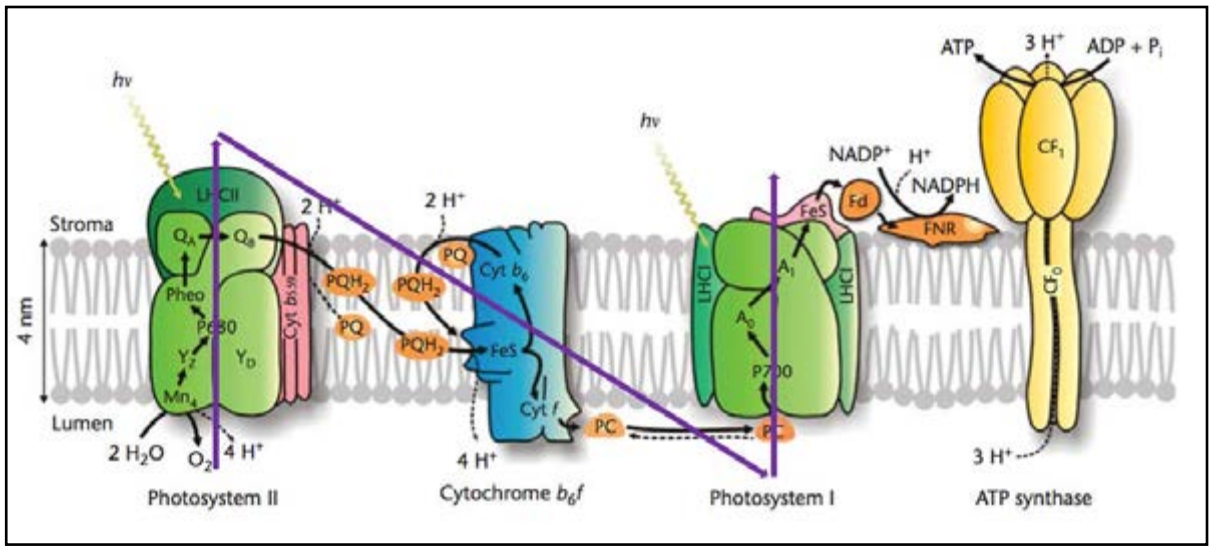

Figure 1.5: Schematic presentation of the protein complexes and cofactors involved in the primary photochemical reactions and the proton transport inside thylakoid membrane of oxygenic photosynthetic organisms. The Z-scheme is shown in magenta-color. The image is modified from "Photosystem II (2010); Encyclopedia of Life Sciences (ELS)"; with permission from John Wiley & Sons.

The functions of these individual protein complexes are concerted to perform primary photochemical reactions: light energy is absorbed by the light-harvesting antenna systems that excites PSII RC, P680; electrons are extracted by the water-oxidizing manganese–oxygen–calcium cluster (Mn_4O_xCa, where $x \geq 4$ is the number of bridging oxygens) and then travel through the tyrosine (Tyr_Z), P680, Chl_{accD1}, $Pheo_{D1}$ into the plastoquinone (PQ) pool. After receiving two electrons, doubly reduced PQ (Q_B^{2-}) is released from the PSII complex, which is then oxidized by the Cyt b_6f complex. This

complex donates electrons to PSI RC, P700 via the soluble plastocyanin (PC) in the thylakoid lumen. Electrons released from P700 are transferred to ferredoxin (Fd), then to the ferredoxin-$NADP^+$ oxidoreductase (FNR), which finally reduces $NADP^+$ to NADPH. The direction of electron flow from oxygen-evolving-Mn-cluster (OEC) to NADPH production is shown in Figure 1.5 and is known as 'Z-scheme'.

1.2. Dynamic regulation of thylakoid membrane

The static picture of the thylakoid membrane concerning its folding, heterogeneous distribution of proteins and kinetics of excitation energy between PSII and PSI has been obtained based on *in vitro* experiments on isolated thylakoid membranes, often treated with cationic salts (Papageorgiou and Govindjee 2011). The structural views on appression of thylakoid membrane and distribution of excitation and interaction between different pigment-protein complexes cannot be static, however, because the cation salts can dynamically modulate or mask the electric charge of the lipids and proteins, leading to altered membrane folding. During past decades, there were very limited evidences gathered, finding insights into the *in vivo* three-dimensional structure of thylakoid membrane. Improved topological and functional model would be useful to answer many open questions about whole chain and/or intersystem electron transport.

Apart from such static models, the behaviour of thylakoid membrane has been studied widely towards various long-term adaptations and environmental factors, including light intensity and colour (Anderson, Horton et al. 2012). There are long-term (acclimation) and short term (adaptation) changes (Heldmaier and Werner 2003) affecting the distribution of PSII and PSI, and the degree of thylakoid appression do occur abundantly in nature. Many of these processes are reversible, while some causes permanent changes.

1.3. Light adaptation and acclimatization strategies in plants

The intensity and colour of natural sunlight has a wide temporal and spatial variation. This is an important ecological factor for the natural habitation in tropical forests where the photon flux that reaches the deep shade is about 3-10% compared to the actual direct sunlight over the canopy. This light is also enriched in far-red wavelengths (FR) (Ballaré, Scopel et al. 1995), due to the selective absorption of photosynthetically active radiation (PAR; 400-700 nm) by surrounding taller trees. In addition, rapid and irregular changes in light intensity also occur. These changes can be caused by clouds (sunflecks) or shading by neighbouring vegetation in natural environments. Diurnal and

seasonal changes in light quality and quantity regularly modulate the light input into the photosynthetic membrane (Pearcy 1990).

Light signals are perceived over a wide range of wavelength by distinct photoreceptors (Briggs and Olney 2001) including POR (Armstrong, Runge et al. 1995), phytochromes (at least five-types) (Smith 2000, Sharrock 2008), cryptochromes or blue-light photosynthetic receptors (Ahmad and Cashmore 1996) and UV-B receptors (Heijde and Ulm 2012) that may affect photo-adaptation and photo-acclimatization of organisms; and efficiently used by the light harvesting antenna that funnels the light energy into the PSII reaction centers, where actual photochemistry takes place. The regular and/or drastic fluctuations that occur in natural climate make it necessary to develop acclimatization strategies to ensure the safe harnessing of sunlight. At low light intensities the photochemical yield requires the maximum light capture by the antenna proteins and its optimal distribution between PSII and I. This low-light condition has been termed as light-starvation. Under strong light the rates of energy absorption by the PSII antenna, transfer to reaction centers and subsequent linear electron transport rates are not matched (Holzwarth 2008) and regulating processes are required to protect the photosystems against over-excitation. A fundamental thermodynamic limitation arises as the linear electron transport rates are much slower than the energy transfer (Holzwarth, Müller et al. 2006), which leads to saturation and subsequent closures of reaction centers. As a result, the fraction of light energy that is actually used to drive the photochemistry is reduced and potentially harmful excited products start to accumulate. This kind of light-saturation eventually affects almost every event that occurs inside the photosynthetic membrane. Therefore, light adaptations in plants are vital and inevitable for a sustained photosynthetic efficiency and also to reduce the long-term light induced damage to a minimum (Adams III, Muller et al. 2013).

Higher plants have evolved a multilevel network of adaptation/acclimatization mechanism that can be divided into four major groups:

1.3.1. Type-A, long-term acclimatization: The responses may begin within hours and may take days or weeks. Changes can be morphological that are usually visible. It can also involve reallocation of resources between the component processes of photosynthesis.

Certain long-term acclimatization involves changes in the whole organism. The classic example is the light-regulated gene expression during biogenesis of chloroplasts from its

progenitor proplastids and etioplasts (Pogson and Albrecht 2011). In higher plants and algae, this depends on the concerted action of two genetic systems located in the nucleus and in the plastid. Current evidences support a complex mechanism involving many proteins at transcriptional level (Schrubar, Wanner et al. 1991); posttranscriptional (Rochaix 2001), translational or protein modification (Gruissem and Tonkyn 1993), and posttranslational (Lisitsky, Liveanu et al. 1995) regulatory processes have also been detected. Normally photomorphogenetic events are initiated by two principle pathways, photointerconversion of phytochrome or by cryptochrome triggered by blue light.

The action of light can be inductive. The responses can be fast and reversible, such as the orientation of leaf to track the sun. The perpendicular orientation will ensure the maximum exposure, while; a parallel leaf position will greatly minimize it. However, this is not an absolute in natural habitation, due to a huge amount of scattered light available from all directions. These light-guided leaf movements are carried out by the pulvinar motor tissue (Koller, Björkman et al. 1995). Specific light signals also control the movements of shoot organs.

A similar light-driven reversible adaptation mechanism is the chloroplast movement that occurs on the cellular level. The chloroplasts either move away from the direction of the strong light (avoidance response) or accumulate in an area irradiated with weak light (accumulation response). The movements are essentially complete within minutes and can control the light absorption into photosystem up to 20% (Brugnoli and Björkman 1992). Chloroplast avoidance movement is not only limited to plants, but can be seen in algae, mosses and ferns too. The underlying mechanisms from light perception to actin-based movements have been identified through molecular genetic approach (Kong and Wada 2014). A blue-light photoreceptor, phototropin have been identified recently in *Arabidopsis thaliana*, the fern *Adiantum capillus-veneris* and in the moss *Physcomitrella* (Suetsugu and Wada 2007). There are obstacles such as large vacuoles and other cellular organelles, which can limit the chloroplast movement.

In other long-term changes, plants avoid shade by decreasing leaf blade and elongating petiole and internodes. In absence of light, in dicots, a subapical part of the stem is curved backward like a hook, due to differential elongations in the concave and convex sectors. In light, however, this is reversed and the hook progressively disappears towards maturity. Some plants deposit inorganic salt crystals on leaf surface and/or develop air-filled hairs. Some desert plants have developed a number of adaptations to

increase leaf reflectance and that way they reduce the amount of absorbed light (Brown and Mies 2012).

1.3.2. Type-B, short-term adaptations: They are primary responses under fluctuating light. The changes are generally reversible and occur within minutes of environmental change. The mostly cited short-term adaptation mechanism is known as non-photochemical quenching (NPQ), where the excess excitation that is already absorbed by the light-harvesting antenna gets dissipated harmlessly as heat (Johnson, Young et al. 1994).

In plants, the photosynthetic organisms dissipate the excess energy by at least four different quenching processes, such as, the energy-dependent quenching, qE (Krause, Vernotte et al. 1982), zeaxanthin (Z)-dependent quenching, qZ (Nilkens, Kress et al. 2010), photoinhibitory quenching, qI (Krause 1988) and state-transition, qT (Allen, Bennett et al. 1981). The first three of these mechanisms qE, qZ and qI together are classified as NPQ, whereas qT is rather a regulatory mechanism that balances the excitation between PSII and PSI.

1.3.2.1. Energy-dependent, qE, mechanism is derived from its relation with the energization of the thylakoid membrane (Horton, Ruban et al. 1996). The molecular basis for this mechanism is under debate, however, today it is generally accepted that as soon as the excitation energy exceeds the capacity of the electron transport processes in the reaction centre, the PSII antenna switches to a photoprotective light energy dissipation state and the absorbed energy is safely dissipated as heat (Ruban, Johnson et al. 2012). This type of quenching state can be formed and relaxed on a seconds to minutes timescale and associated with acidification of chloroplast lumen and protonation of PsbS protein (Li, Gilmore et al. 2004).

1.3.2.2. Zeaxanthin-dependent, qZ, quenching mechanism is the reversible light-dependent synthesis of the carotenoid zeaxanthin (Z) from its epoxide homologue violaxanthin (V) (Nilkens, Kress et al. 2010). Since its successful isolation in 1964 (Krinsky 1964) on plants, numerous studies have been performed on the relationship between zeaxanthin and NPQ (Demmig-Adams and Adams 1990, Jahns and Holzwarth 2012) suggesting zeaxanthin as the pigment responsible for quenching. In the so called "gear-shift" model (Frank, Cua et al. 1994), Z was proposed as a direct quencher with an electronic state (S1) lower than the lowest excited Chl-(Qy)-state. V cannot quench because its S1 state is higher in energy than the Qy of Chl a. However, this model of

direct quenching has recently been disproved. Femtosecond transient absorption studies on zeaxanthin-deficient (*npq1*) and zeaxanthin-enriched (*npq2*) *Arabidopsis thaliana* mutants revealed that quenching of Chl singlet is not dependent on energy transfer to any Car (Müller, Lambrev et al. 2010). The other possible mode of quenching by zeaxanthin is as indirect quencher. Mechanisms, suggest that the presence of zeaxanthin affects the conformation and/or organization of Chl binding proteins in a way that increase in Chl fluorescence occurs. The indirect quenching role for zeaxanthin also suggest that protonation of lumen exposed acidic residues in chlorophyll binding proteins are a prerequisite. The location and mechanism of the proposed conformational changes are controversial.

1.3.2.3. Photoinhibition of PSII, qI, quenching type is a consequence of prolonged or pronounced excess light absorption; either exposure of low-light grown plants or leaves to high light, or exposure to moderate light in presence of one or more additional stresses, such as chilling. The molecular mechanism(s) of photoinhibition remains to be elucidated since its first introduction in 1956 (Kok 1956). It is generally agreed that PSII is more susceptible to photoinhibition and the damaged component is mainly the D1 protein (Mellis 1999), although there are also damages to other PSII proteins, such as the D2 protein, cytochrome b_{559}, CP43 and CP47, but at a much slower rate (Schuster, Timberg et al. 1988, Yamamoto and Akasaka 1995, Zer and Ohad 1995, Jansen, Mattoo et al. 1999). PSI is less prone to photoinhibition with the exception of some chilling sensitive species (Kudoh and Sonoike 2002) and is not studied in much detailed because of several reasons: limited combinations of plant species and environmental conditions, the non-regulatory aspect of PSI photoinhibition and methodological inefficiency to accurately determine the stress level in PSI .

PSII photoinhibition occurs in all organisms capable of oxygenic photosynthesis, from vascular plants to single cell cyanobacteria. Several mechanisms have been proposed based on their origin and function: (a) mechanisms, where the donor side is partially or completely inactive (donor side photoinhibition). In such circumstances, the electron donation from Tyr_Z to $P680^+$ is inhibited and/or slowed down leading to the production of long-lived highly oxidizing radicals $P680^+$ and Tyr_Z at the donor side. As a result PSII electron transport activity is drastically reduced and oxidation of nearby amino acids, pigments and other redox components occur (Jegerschöld, Virgin et al. 1990, Barbato, Friso et al. 1992, Aro, Virgin et al. 1993); (b) mechanisms, in which the activity of the acceptor side is limiting while the donor side is active (acceptor side photoinhibition). In this mechanism, the primary quinone electron acceptor Q_A is either doubly reduced and

leaves its site in D2 protein under strong illumination (Styring, Virgin et al. 1990, Vass, Styring et al. 1992) or it becomes non-functional due to binding with chemical substrate. Such condition lead to the recombination of primary radical pair ($P680^{+}Pheo^{-}$) and generation of triplet Chl. Triplet Chl then reacts with molecular oxygen and produces singlet oxygen, which damages PSII (Vass, Styring et al. 1992); (c) accumulation of PSII centers with impaired electron donation from the Mn-cluster has been demonstrated under UV-A and UV-B illumination (Sarvikas, Hakala et al. 2006), recently also extended to blue and green light in the visible spectrum (Ohnishi, Allakhverdiev et al. 2005, Hakala-Yatkin, Mantysaari et al. 2010). In this mechanism a photoinhibition of PSII donor side (inactivation of OEC) is followed by the destruction of PSII reaction centre (two-step donor side mechanism of photoinhibition) (Ohnishi, Allakhverdiev et al. 2005). The another less popular mechanism occurs in low-light (Keren, Berg et al. 1997) when the chances of charge recombination reactions in PSII and subsequent production singlet oxygen are higher. PSII can also be inhibited by weakly coupled chlorophyll (free chlorophyll mechanism) or by cytochromes or iron-sulphur centers (Jung and Kim 1990).

1.3.2.4. State transition, qT, is a regulatory mechanism responsive towards the colour/wavelength of the irradiating light, was first reported in the plant photosynthetic membrane isolated from *Pea* leaves in 1981 (Allen, Bennett et al. 1981). It was originally proposed as qT component of NPQ during the 'dark' relaxation kinetic of preilluminated barley leaves at saturating light intensities (Quick and Stitt 1989).

It is a reversible phosphorylation of the light harvesting complex in PSII (LHCII) and typically occurs under dim-light (Mullineaux and Emlyn-Jones 2005). According to the classical model, 'State 1' prevails when plants are exposed to far-red light (PSI excitation), which dephosphorylate LHCII. Conversely 'State 2' is the reverse mechanism, when the plants are exposed to blue or red light (PSII excitation), favouring the LHCII phosphorylation (Allen and Forsberg 2001). The phosphorylation of LHCII proteins is regulated in chloroplast stroma (Aro and Ohad 2003) by the redox state of the electron transfer chain (ETC) (Zito, Finazzi et al. 1999, Finazzi, Zito et al. 2001) through a mechanism dependent on the *Stt7*/*STN7* kinase (Depège, Bellafiore et al. 2003, Bellafiore, Barneche et al. 2005, Bonardi, Pesaresi et al. 2005) and a protein phosphatase called thylakoid-associated phosphatase (TAP38) (Pribil, Pesaresi et al. 2010) or PPH1 (Shapiguzov, Ingelsson et al. 2010). However, a recent report has questioned the role of cyclic electron transport in state transition (Takahashi, Clowez et al. 2013).

1.3.3. Type-C, changes in PSII/PSI stoichiometry with light

Within each chloroplast, in higher plant thylakoid membrane the changes in PSII/PSI stoichiometry occur due to the redox signals generated, when there is an excitation imbalance between PSII and PSI (Kim, Glick et al. 1993). PSII/PSI stoichiometry is also affected by light quality (Pfannschmidt, Nilsson et al. 1999). In nature, shady environments are enriched in far-red light creating an excitation imbalance favouring the PSI (Fujita, Ohki et al. 1987).

It is a responsive mechanism towards the acclimatory changes in the surroundings affecting the structure of photosynthetic apparatus to maintain optimal electron transport and minimizing photodamage (Chow, Melis et al. 1990). The PSII/PSI ratio has been reported to vary from 1.1-1.9 in thylakoids isolated from *Pea* plants grown under PSII-light (550-660 nm), to 2.2-4.0 in the corresponding thylakoids from plants grown in PSI-light (>660 nm) (Melis 1984, Chow, Goodchild et al. 1990). Similar values are reported for wild-type barley (Kim, Glick et al. 1993) and mustard seedlings (Pfannschmidt, Nilsson et al. 1999). A recent study has also confirmed these numbers (Fan, Hope et al. 2007).

Several mechanisms have been proposed: an increase in the number of PSI reaction centers in relation to PSIIs, may suggest an enhanced cyclic electron flow around PSI, increasing ATP/NADPH ratio and providing extra ATP to compensate for the decline in light intensity (Bailey, Walters et al. 2001). In high light, the number of PSII reaction centers increases, associated with other regulatory mechanisms to protect the cell against photodamage (Sonoike, Hihara et al. 2001).

1.3.4. Organizational structure of the Sun and Shade leaves

The photosynthetic apparatus inside a leaf is responsive and flexible towards the changes in the environment. Certain genotypes have characteristics to express different phenotypes in different environment (phenotypic plasticity) (Bradshaw 1965), including adaptation to a shady environment (shade-adapted plants). Additionally, genotypes can acclimate to shade and change their biochemical, physiological and morphological characteristics. The term shade plant, therefore, refers to an 'adapted' phenotype or an 'acclimated' genotype. Similarly, the term sun plant refers to a plant grown in high-light conditions, but it is also used to indicate a shade-avoiding species or ecotype. The terms sun leaf and shade leaf refer to leaves that have developed at high and low irradiance, respectively (Boardman 1977).

There are differences in chloroplast structure between shade and sun leaves. Shade chloroplasts tend to be larger, contain more thylakoid membranes and show higher levels of stacking into appressed region than those found in sun plants (Maxwell, Marrison et al. 1999). The higher proportion of appressed to non-appressed membranes found in shade chloroplast is largely the result of increased LHCII content (Walters 2005), which is also reflected by their lower Chl a/b ratios (Biswal, Pattanayak et al. 2012). Chlorophyll a and b, both are associated with light harvesting antenna, while only Chl a is found in cores and reaction centers. Shade plants have high chlorophyll/Rubisco ratio, due to smaller number of cell layers and a smaller volume of stroma, where Calvin-cycle enzymes are located, per chloroplast. Sun leaves have more stroma-exposed thylakoid membranes, which contain the larger amount of Rubisco, b_6f cytochromes and ATPase. Therefore, sun chloroplasts are adapted to light-sufficient CO_2-deficient conditions, while shade chloroplasts are adapted to perform optimally under light deficient CO_2-sufficient condition.

Sun/shade leaves can occur together in a same plant, providing their chloroplasts are exposed to different light conditions. The classic example is the differences seen in chloroplasts found at the periphery (high light) or interior (shade) of a single tree crown. Recently, it is realized that a season-long developmental time scale is not required for sun/shade chloroplasts to develop; the granal numbers and granal areas increases after only a 10 min shade treatment, this effect is, however, fully reversible with 10 min of high light (Rozak, Seiser et al. 2002).

1.4. Importance of NPQ - roles of qE and qZ

The seasonal, diurnal and other natural reasons for the fluctuation in sunlight intensities put excess excitations into photosynthetic antenna that cannot be carried further by linear electron transport as the latter being much slower than the former. This imbalance is the primary source for the formation of reactive oxygen species (ROS), which are harmful and can destruct nearby amino acids, photosynthetic proteins, oxidize lipids and lead eventually to cell death (Van Breusegem and Dat 2006).

The higher plants, therefore, evolved mechanisms to convert this excess oxidative stress into heat and dissipate harmlessly. Based on the relaxation kinetics of excited Chl, earlier studies have proposed four different quenching processes, qE, qZ, qI and qT, as we described above (Krause and Weis 1991). Recent studies on the state transition deficient *Arabidopsis* mutant *STN7* have disproved the role of qT as a component in NPQ (Bellafiore, Barneche et al. 2005, Nilkens, Kress et al. 2010).

Under most natural conditions, regular to moderate light stresses, qE and qZ represent the dominating form of energy dissipation and are easily reversible (Niyogi and Truong 2013). The physical process that gives rise to quenching remains elusive; however, according to the present understanding, certain changes in the thylakoid membrane are correlated:

• a significant decrease in LHCII fluorescence when all PSII reaction centers are open (Johnson and Ruban 2010)
• acidification of the thylakoid is crucial (Müller, Li et al. 2001)
• conversion of violaxanthin (V) to zeaxanthin (Z) via the xanthophyll cycle (Jahns and Holzwarth 2012)
• the kinetics is greatly dependent upon the protonation of PsbS protein (Li, Gilmore et al. 2004), which is not a part of PSII-core complex, but, rather randomly distributed in the membrane
• conformational changes in the antenna of PSII (Johnson, Pérez-Bueno et al. 2009)
• detachment and subsequent oligomerization of LHCII from PSII-supercomplex (Holzwarth, Miloslavina et al. 2009)

These facts summarize the existing hypothesis for both the location and mechanism. The availability of specific mutants made it possible to investigate the role of different components and their interdependence (Müller, Li et al. 2001, Jahns and Holzwarth 2012, Ruban, Johnson et al. 2012). Reports suggest that qE occurs in the PSII reaction centre (Finazzi, Johnson et al. 2004, Ivanov, Hurry et al. 2008, Krupnik, Kotabov et al. 2013). The direct measurement of heat emission in the qE state confirmed this hypothesis (Ruban, Johnson et al. 2012), while the majority agrees that it occurs in LHCII (Horton, Wentworth et al. 2005, Johnson, Pérez-Bueno et al. 2009, Ruban, Johnson et al. 2012). The three PSII minor antennae CP29 (Lhcb4), CP26 (Lhcb5) and CP24 (Lhcb6) found to host majority of xanthophyll pigments and have pronation sites, and thus, can also act as potential sites of thermal dissipation (Andersson, Walters et al. 2001, de Bianchi, Dall'Osto et al. 2008). The relation and mutual dependence between qE and qZ had been a subject of intense debate (Johnson, Pérez-Bueno et al. 2009, Horton 2012). A recent study has proposed that these two quenching processes are independent from each other and are located on different sites (Holzwarth, Miloslavina et al. 2009). On a broad perspective, these proposals endorse a general conscience, where specific components of PSII-supercomplex are involved, including the three minor LHCs, the major LHCII and the PSII core based on their interactions with PsbS and/or xanthophyll cycle.

1.4.1. The xanthophyll cycle - the role of zeaxanthin

Demmig-Adams et al. first revealed a connection between the xanthophyll cycle and NPQ in 1990 before the details of PSII antenna structure was known (Demmig-Adams and Adams 1990). The cycle was discovered by Sapozhnikov in 1957 (Sapozhnikov, Krasovskaya et al. 1957) and later characterized by Yamamoto and Hager (Yamamoto, Nakayama et al. 1962, Hager 1966). It requires two enzymes, the de-epoxidase (VDE) and the epoxidase, which reversibly interconvert the carotenoids violaxanthin and zeaxanthin (Stransky and Hager 1970). Antheraxanthin is an intermediate product formed in both reactions (Yamamoto, Nakayama et al. 1962). In mature leaves it takes minutes to induce the synthesis of zeaxanthin from violaxanthin but hours for the back reaction. Therefore, zeaxanthin accumulated in light remains present in the dark for some time.

There are evidences that LHCII binds carotenoids of the xanthophyll cycle (Bonente, Ballottari et al. 2011). Solubilisations of LHCII-enriched membranes have localized violaxanthin at the monomer–monomer interface (Liu, Yan et al. 2004), a peripheral location ideal for a faster conversion by the de-epoxidase enzyme. The enzyme is activated (Fufezan, Simionato et al. 2012) under saturating light when the lumen pH reaches below 5.0 and a suitable reducing agent (such as ascorbate) is present (Hager 1969). The accumulation of zeaxanthin during NPQ was initially proposed as a direct quencher of chlorophyll-excited states (Demmig-Adams and Adams 1990). This model was later modified based on energy transfer from Chl to Z (Frank, Cua et al. 1994) or due to the formation of carotenoid cation in $Chl^{-}Z^{+}$ charge transfer (CT) state (Holt, Zigmantas et al. 2005, Ahn, Avenson et al. 2008, Avenson, Ahn et al. 2008). Such direct quenching mechanisms are assumed to be located in minor LHCs (CP24, CP26 and CP29) (Gilmore, Shinkarev et al. 1998, Holzwarth, Miloslavina et al. 2009, Miloslavina, de Bianchi et al. 2011) in PSII-antenna complex, since no such quenching of Z was detected *in vitro* studies of LHCII (Miloslavina, Wehner et al. 2008, Müller, Lambrev et al. 2010). Recent findings suggest that zeaxanthin can only have an indirect effect, activating a quenching process triggered by ΔpH and intrinsic to LHCII (Johnson, Havaux et al. 2007). This result is further supported by the fact that ΔpH dependency of qE is controlled by the de-epoxidation state (DES) (Rees, Young et al. 1989). In the absence of zeaxanthin, the violaxanthin pK for protonation is around 4.5 and it shifts to 5.5 after light-induced de-epoxidation. In violaxanthin deficient *Arabidopsis npq2* mutant, the pK was over 6 (Horton, Ruban et al. 1991). More evidences for an indirect effect of the xanthophyll cycle on qE come from the fact that violaxanthin slows down, while zeaxanthin exhibits

strong quenching in LHCII complexes, in presence of low detergent concentration and low pH (Horton, Ruban et al. 1996, Petrou, Belgio et al. 2013). Orientation of the xanthophyll head group to form J-type or head-to-tail aggregates was proposed as the determining feature (Horton, Ruban et al. 1999). Horton and Ruban has proposed the 'LHCII aggregation model' (Horton, Ruban et al. 1991) in this context. In this model, there are four different but interconnected states of LHCII antenna with different degrees of heat dissipation, roughly proportional to the degree of aggregation. Low pH and Z are two key parameters for achieving a deeply quenched state; quenching is only partial if any of them is mutually absent (Horton, Wentworth et al. 2005). The molecular basis of this model assumes conformational as well as structural reorganization in the major LHCII antenna. Binding of Z acts as allosteric regulator that switches the LHCII proteins from efficient light harvesting to a dissipative state (Gruszecki, Grudzinski et al. 2006). Recent studies have reported a substitution of violaxanthin bound to the L2 site in CP26 or CP29 with zeaxanthin increases the quenching in aggregated state (Morosinotto, Baronio et al. 2002, Ballottari, Girardon et al. 2010).

1.4.2. The role of PsbS protein

The protonation of a 22 kD protein (Ljungberg, Akerlund et al. 1986, Mishra and Ghanotakis 1993), called PsbS, was discovered to have strong effects on NPQ (Müller, Li et al. 2001). PsbS has two lumen-exposed glutamate residues, E122 and E226 (Bonente, Howes et al. 2008), as a sensor for luminal pH (Niyogi, Li et al. 2005). This protein is a member of Lhc superfamily, have four very hydrophobic transmembrane helixes (Kim, Sandusky et al. 1992), but does not contain the conserved histidine residues like other Lhc members (Bergantino, Segalla et al. 2003). *Arabidopsis npq4-1* mutant that is deficient of PsbS does not have any qE, although its light harvesting and photosynthetic efficiencies remains unchanged (Li, Björkman et al. 2000, Peterson and Havir 2000).

The exact role of PsbS in NPQ is controversial (Niyogi, Li et al. 2005). The protein does not bind pigments (Dominici, Caffarri et al. 2002) and therefore, does not likely to have any direct quenching effect (Crouchman, Ruban et al. 2006). However, *in vitro* reconstitution studies have found that zeaxanthin can bind to PsbS (Aspinall-O'Dea, Wentworth et al. 2002) and this binding can be the origin for an absorption change in the so-called 535 nm, associated with the formation of qE (Bergantino, Segalla et al. 2003). Wilk et al. have proposed a similar quenching mechanism, where a significant quenching in LHCII fluorescence is reported when both Z and PsbS are present (Wilk, Grunwald et al. 2013). However, this proposition is not supported by Bonete et al., where it was concluded that such binding between zeaxanthin and PsbS cannot be

responsible for qE (Bonente, Howes et al. 2008); although roles of other Lhcb type pigment-binding proteins were not excluded. Recent investigation of the structure of the PSII membranes by freeze-fracture microscopy, FRAP microscopy and detergent solubilization techniques revealed new information. PsbS decreased protein mobility in grana membrane (Goral, Johnson et al. 2012). The amount of membrane in crystalline domains increases in the absence of PsbS and decreases when PsbS is elevated (Kereïche, Kiss et al. 2010). PsbS enhances the Mg^{2+}-dependent grana stacking and association of PSII with LHCII (Kiss, Ruban et al. 2008). These observations support the view that PsbS, despite of directly participating in quenching, controls the association and interaction among various membrane protein complexes (Horton, Johnson et al. 2008, Kereïche, Kiss et al. 2010). This goes with the fact that PsbS is freely distributed in photosynthetic membrane (Dominici, Caffarri et al. 2002). Such regulatory behaviour of PsbS protein is further determined by studies showing that PsbS controls the dissociation of the B4C subcomplex consisting of LHCII M-trimer, CP24 and CP29, under light stress. Mutant plants lacking B4C subcomplex have strongly reduced heat dissipation capabilities (Betterle, Ballottari et al. 2009). The protonation of PsbS seems to promote such kind of dissociation (Betterle, Ballottari et al. 2009), most likely by a rearrangement of the PSII macro-organization (Horton, Johnson et al. 2008, Kiss, Ruban et al. 2008, Goral, Johnson et al. 2012), however, the biochemical mechanism is not understood yet. Although, PsbS is necessary *in vivo*, isolated thylakoids lacking PsbS does exhibit flexible NPQ in presence of enhanced ΔpH (Johnson and Ruban 2011), suggesting the hypothesis that direct protonation of LHCII antenna protein can bypass the need for PsbS.

1.4.3. Is it qE or qZ - identification of two-independent quenching sites

The introduction of qZ, as a component of NPQ only appeared recently (Nilkens, Kress et al. 2010). The analysis of NPQ dynamics for *Arabidopsis* under saturating light treatment for a prolonged period of time had three components: the well-characterized fast qE, reversible and dependent on the formation of ΔpH; the slow qI, quenching due to photoinhibition and the third, as an intermediate, qZ, a zeaxanthin dependent component, reversible but at a much reduced rate (10-15 min). The function of qZ does not directly depend on the acidification of lumen (Brooks, Sylak-Glassman et al. 2013).

The distinction between qE and qZ are not clearly defined in literature, primarily due to the fact that exact functions of the carotenoid-Z and PsbS protein in the NPQ mechanism are not known. In past years, many hypothesis were made, where it was generally

assumed that qE and qZ share a common conformational change within the PSII antenna induced by light and ΔpH (Johnson, Pérez-Bueno et al. 2009).

The recent progresses in non-invasive ultrafast Chl fluorescence technique and availability of specific NPQ-affecting mutants have added invaluable information. The possible existence of one or multiple quenching sites/mechanisms is under debate for a long time and the choice between qE and qZ remains to be investigated further. However, a recent finding has identified two independent sites (Figure 1.6), proposed to be located (1) on the major LHCII antenna (Q1-site) and (2) the monomeric PSII antenna proteins (Q2-site), based on their quenching dependencies on PsbS and Z, respectively (Holzwarth, Miloslavina et al. 2009). Below are some aspects of it:

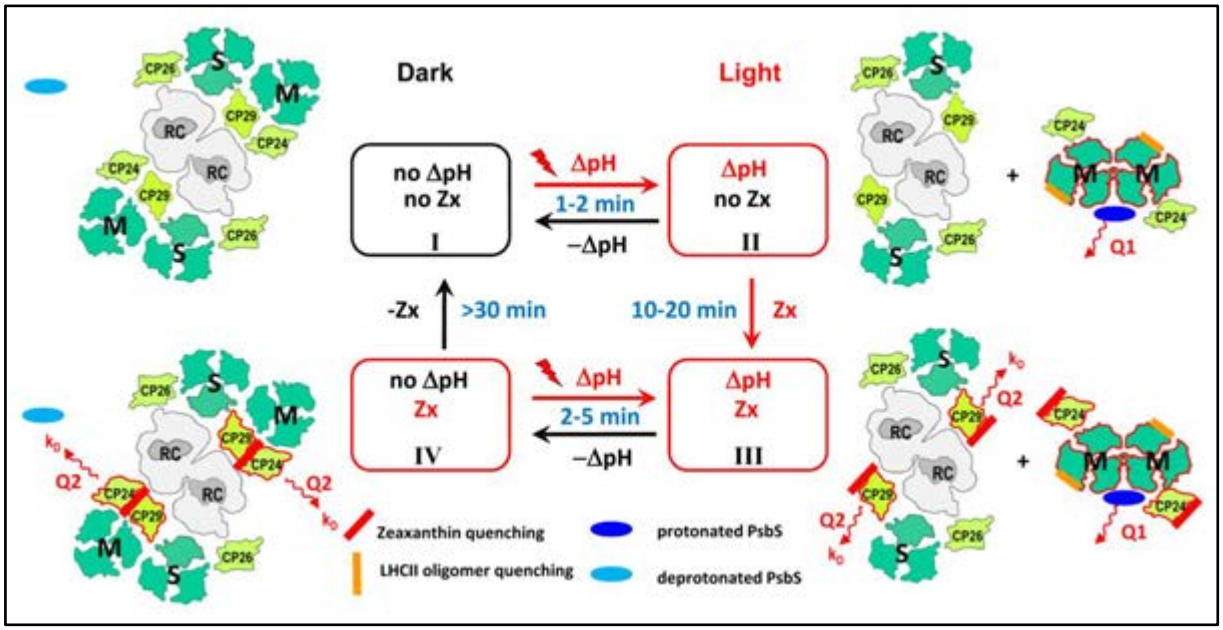

Figure 1.6: Schematic illustration of the 4-State-2-Site quenching model of the PSII supercomplex under high light adaptations. 'S' and 'M' denote strongly and moderately bound LHCII respectively. The dark-adapted states are on the left and light-adapted states are on the right. Q1 and Q2, the two quenching sites are labelled as wavy arrows. The red bars indicate the Z induced quenching of various antenna parts and the orange bars represent the quenching locations in detached LHCII oligomers. It is hypothesized that protonated PsbS protein (labelled as blue-ovals) might be attached to the LHCII oligomers. The minor antenna protein CP24 was also found to modulate the quenching in the detached LHCII in presence of Z (Miloslavina, de Bianchi et al. 2011). Adapted with permission from (Holzwarth and Jahns 2014).

1.4.3.1. The Q1-site (qE)

The quenching site Q1 is created in presence of PsbS, as in the PsbS-deficient *Arabidopsis npq4* mutant, it was absent (Holzwarth, Miloslavina et al. 2009). V to Z conversion is not mandatory for its function. The identification is based on the target analysis of spectrally resolved ultrafast fluorescence kinetics covering the entire PSII and PSI fluorescence region. Q1-site has distinct spectral characteristic, a strongly enhanced far-red (FR)

fluorescence, most likely due to the formation of Chl-Chl charge transfer (CT) state (Miloslavina, Wehner et al. 2008). The site is kinetically independent of either PSII or PSI (Holzwarth, Miloslavina et al. 2009), exclusively occurs at the expense of PSII antenna cross-section under quenching condition (Holzwarth, Miloslavina et al. 2009) and bears similarity with the *in vitro* aggregation studies on LHCII trimers (Mullineaux, Pascal et al. 1993, Miloslavina, Wehner et al. 2008). These findings suggest that Q1 mechanism is a PsbS-dependent quenching process, where a majorities of LHCII are detached from the PSII-supercomplex (Holzwarth, Miloslavina et al. 2009). Currently, it is unclear whether or not minor Lhcb proteins are also associated with this detached LHCII. A study on CP24 deficient *Arabidopsis* mutant has observed a strong reduction in the fast phase of its NPQ, among all other antenna deficient mutants (Kovács, Damkjær et al. 2006). Recently CP24 protein has also been detected as a component of free LHCII assemblies (Ferroni, Angeleri et al. 2014). This is in agreement with the existing hypothesis that minor antenna protein CP24 of PSII is extremely essential for light harvesting (de Bianchi, Dall'Osto et al. 2008) as well as for the function of Q1-site (Miloslavina, de Bianchi et al. 2011). Such PsbS-dependent quenching mechanism is most likely controlled by lumen pH (Müller, Li et al. 2001, Bergantino, Segalla et al. 2003) and reported to have a very fast activation and relaxation kinetics (1-2 min). Using a multi-wavelength spectrometer allowing slow, with a time-resolution in the ms range, time-dependent measurements of fluorescence spectra on intact leaves, it was confirmed that the FR-fluorescing component possesses the same spectral and PsbS-dependent characteristics as qE (Lambrev, Nilkens et al. 2010).

1.4.3.2. The Q2-site (qZ)

This site is not associated with the detachment of PSII antenna protein, rather it is a direct non-photochemical deactivation of PSII reaction centers, functionally coupled with strongly bound LHCII trimers and some minor Lhcb proteins (Holzwarth, Miloslavina et al. 2009, Miloslavina, de Bianchi et al. 2011). Q2-site is induced by high light, characterized as pronounced increase in the rate constant k_D, during the target analysis of time-resolved fluorescence kinetic data (Lambrev, Miloslavina et al. 2012). Studies on *Arabidopsis npq4* and *L17* mutants have revealed that this site remains functional, despite of any changes in the PsbS level (Holzwarth, Miloslavina et al. 2009); conversely, it is strongly modulated with the presence of Z and abolished totally in *npq1*-plants, which cannot accumulate zeaxanthin under strong (Holzwarth, Miloslavina et al. 2009). These findings suggest that Q2 site is an independent centre for PSII quenching and its firm Z-dependence is reminiscent of qZ mechanism. The induction of Q2 site is

expected to be in the range of 10-20 min, typical with the conversion of violaxanthin to zeaxanthin, followed by a slower relaxation phase (30-60 min) accompanied by Z epoxidation (Nilkens, Kress et al. 2010, Jahns and Holzwarth 2012).

1.5. More advanced models for NPQ

The fundamental limitation in the present models of NPQ is that these models were developed on the basis of the static picture of thylakoid membrane derived from plant tissues grown under constant lights, which is in a sense contrary to the actual fluctuating natural sunlight in real habitation. Recently efforts were made to study chloroplasts isolated from plants, where growing conditions are more similar to higher intensity natural fluctuating sunlight. In such situations, it is more likely that photosynthetic apparatus will respond differently to the external stimuli. An up-regulation in NPQ capacities has been noticed in *Arabidopsis thaliana*, when short artificial sunflecks were applied in regular intervals in addition to a constant growth light (Alter, Dreissen et al. 2012). The isolation of chlorophyll pigments has revealed higher levels in xanthophyll cycle pigments and the PsbS protein in these plants (Alter, Dreissen et al. 2012). Strong effects of such fluctuations in growing lights have been reported in other studies also (Tikkanen, Grieco et al. 2010, Hubbart, Ajigboye et al. 2012). It is believed that fluctuating light signals induce only marginal effect on PSII, whereas it can damage PSI (Suorsa, Järvi et al. 2012). Recently a protein, the so-called PROTON GRADIENT REGULATION5 (PGR5) has been identified in *Arabidopsis* that is believed to protect PSI by regulating linear electron transfer (Suorsa, Grieco et al. 2013). A recent note by Slavov et al. has indicated a mixing between PSII and PSI in chlorolichen *Parmelia*, induced by a major thylakoid reorganization, as an extremely efficient acclimation process (Slavov, Reus et al. 2013).

Chapter 2 : Aims of the thesis

From the hypothesis and models of photoprotection mechanisms, as presented in Chapter 1, it is evident that optimization of photosynthesis is largely dependent on the optimal control of photo-oxidative damage, particularly under fluctuating natural sunlight, when the chances of sudden over-exposure to much higher light intensity cannot be avoided (Müller, Li et al. 2001). Chloroplasts, particularly photosystem II (PSII) must adapt rapidly to the varying light levels. Non-photochemical quenching (NPQ) has been widely accepted as the fastest response. So far, NPQ mechanisms have been assessed in three categories, like, qT, qE and qI, depending on their mode of operation and relaxation kinetics (Krause and Weis 1991). In addition, recently, a zeaxanthin dependent quenching of PSII antenna, the so-called qZ mechanism, has gained importance (Nilkens, Kress et al. 2010, Jahns and Holzwarth 2012). According to current understanding, NPQ mechanisms are triggered by the acidification of luminal space when the rate of linear electron transport falls short under excessive irradiation (Holzwarth, Müller et al. 2006). Recent reports suggest that two quenching sites (Q1 and Q2) (Holzwarth, Miloslavina et al. 2009) get operational when the pH drops below 6 (cf. Figure 1.6) (Niyogi, Li et al. 2005). However, such functional NPQ models were developed based on the static structure of the dark-adapted thylakoid membranes, where the PSII in the grana are laterally separated from PSI in the stroma exposed regions (Papageorgiou and Govindjee 2011). This limits the existing NPQ models to a static thylakoid structure. However, the actual fluctuation in natural sunlight and short-term adaptation, as well as long-term acclimation were found to effect substantial reorganization of the thylakoid architecture (Anderson, Horton et al. 2012, Herbstová, Tietz et al. 2012). Therefore, it is imperative to gain insights into a more realistic photosynthetically active state under varying lights, incorporating the dynamics of the thylakoid. The most important aim of this thesis is to uncover the development and role of NPQ sites and processes on the basis of information obtained on plants grown under natural, highly variable light conditions.

We have chosen three evergreen plants, viz., *Monstera deliciosa*, *Prunus laurocerasus* and *Hedera helix* as model plants for our study. The principal reason for such selection is because these slow-growing species often dissipate over 90% of the sunlight they absorb and were found to exhibit up to three to four times higher maximal NPQ capacity as compared to the usually studied constant light grown plants (Demmig-Adams, Cohu

et al. 2012). Very likely also the extremely high NPQ values reached by sun-plants would not be achievable by the mechanisms known so far in literature. They also serve as an excellent model of plant acclimation to contrasting light environments – as these plants thrive equally in the extremely low-light-environment and in full sunlight (Demmig-Adams, Ebbert et al. 2006). One of the further aims is to characterize the molecular and structural basis of the higher NPQ capacities by comparing them with the NPQ characteristics of identical plants grown under low-light conditions. Another model organism for our study was *Arabidopsis thaliana*, because of the availability of a great number of mutants and its widespread use in molecular plant science and physiological studies.

In the present work, the fact also becomes apparent that NPQ regulation is a property of the intact plant leaf or the intact organism. Therefore, we applied non-invasive Chl fluorescence technique on intact leaves under conditions close to the physiological ones. The conventional steady state methods cannot distinguish the fluorescence signals deriving from various Chl and antenna components of the photosynthetic membrane. Such methods are also unsuitable to determine the exact contributions of photochemical and non-photochemical quenching (Holzwarth 1988, Holzwarth 1991, Holzwarth 2004). Time-resolved Chl fluorescence kinetics with picosecond resolution is, however, ideally suited as a non-invasive and direct method to probe the photochemical and non-photochemical energy-dissipating mechanisms in photosynthetic tissue. The regulation of NPQ will thus be addressed by applying picoseconds fluorescence measurements on intact plant leaves in this thesis. Furthermore, other techniques, such as, extraction of various chlorophyll pigments, electron microscopy were used in some cases.

We analysed and interpreted the data based on our previous knowledge acquired during *in-vitro* experiments on isolated parts of thylakoids, e.g., open and closed PSII particles, LHCII and PSI (Holzwarth, Müller et al. 2005, Ihalainen, Croce et al. 2005, Holzwarth, Müller et al. 2006, Miloslavina, Szczepaniak et al. 2006, Slavov, Ballottari et al. 2008, Lambrev, Miloslavina et al. 2012). The complete intact thylakoid membrane contains various fluorescing pigments; many of them have overlapping wavelengths. However, the important separation of the fluorescence components deriving from PSI and PSII, and the determination of the quenching parameters in the various states is made possible by global target analysis of the fluorescence kinetics, as the PSII and PSI components differ in their spectral shapes and lifetimes (Holzwarth 1996) depending on the origin of the fluorescence and state of the PSII RC (open vs. closed RCs) (Holzwarth 1988).

In the following the specific aims of each chapter are summarized.

- The long debated reason for 3-4 times higher NPQ capacities that were found in natural sunlight grown evergreen plants are investigated (Chapters 4 and 6).
- The molecular mechanisms for high light acclimatization in higher plants are studied, particularly when a typical low-light plant was irradiated to nearly 10 times higher light intensity for a prolonged period (Chapter 5).
- A more realistic functional/structural model of the photo-regulation in thylakoid membrane is developed, where the key issues like light induced reorganization is addressed (Chapter 7), a phenomenon that is missing so far in the literature. Roles of the carotenoid pigment zeaxanthin and PsbS protein in the quenching mechanism and/or light induced dynamic changes in thylakoids were also enquired by selecting suitable knockout *Arabidopsis* mutants.
- A real photoprotection scenario has been replicated on *Arabidopsis* genotypes, which were grown under artificially produced sun-flecks (Chapter 8), which is more close to natural conditions than constant growth light, against a controlled low-light condition.
- The specific roles of carotenoid zeaxanthin and PsbS in the NPQ mechanism, particularly during the quenching of LHCII antennas are investigated (Chapter 9). In this work, both LHCII and PsbS were inserted into reconstituted membrane in different proportions and quenching was studied by time-resolved fluorescence spectroscopy in presence and/or absence of zeaxanthin and also ΔpH.

Chapter 3 : Materials and methods

3.1. Fluorescence spectroscopy and time-correlated single photon counting

Fluorescence is a key experimental technique for studying photosynthesis because it can be measured in real time. It is highly sensitive, highly selective, non-destructive, and can also be applied easily to strongly scattering materials. Fluorescence itself does not play any role in the mechanism of photosynthesis; however, it is not surprising that light emission from plants has always played a central role in photosynthesis studies (Baker 2008, Stirbet and Govindjee 2011). The reason is that chlorophyll is an efficient fluorophore and its molecular environment, which is composed of large, complex, multi-functional, multi-component, compartmentalized, dynamic and highly organized supra-molecular units that determines the probability to emit fluorescence (Shiau and Franck 1947). The rapid development of time-resolved fluorescence methods starting from the 1960s (Murty and Rabinowitch 1965) provided more detailed information, adding a time dimension on the scale comparable to the rate of primary processes of photosynthesis (Holzwarth 1988, Holzwarth 1996). Time-correlated single photon counting (TCSPC) is one of the most sensitive techniques for recording low-level light signals with picosecond resolution and extremely high precision (O'Connor and Phillips 1984, Becker 2005). It is indispensable for the kinetic study of photosynthetic light reactions in pigment-protein complexes, cyanobacteria, diatoms and intact leaves.

3.1.1. The principle of time-correlated single photon counting

The principle of single photon timing stems from the concept of delayed coincidence measurements of radioactive decay originating from nuclear physics. In the TCSPC experiment the delayed coincidence between an exciting light pulse and the occurrence of the first fluorescence photon is being measured. According to the Ergodic theorem the time distribution of the photon emission from one excited molecule and of the fluorescence from an ensemble of these molecules have the same distribution probability. To measure it as a function of photon time delay the following procedure is used, as illustrated in Figure 3.1.

A pulsed excitation laser beam is split into two parts (Point-F). One of them excites a photodiode (PD), thereby; its electronic pulse determines a reference point. The other part of the beam excites the sample (Rotation cuvette, R). The emitted photon is

detected by a micro-channel-plate-photomultiplier (MCP). It is located after monochromator (MR) in order to be protected from scattered excitation light and to multiply the selected wavelength. PD and MCP forward their electronic pulses to the electronic clock, or time-to-amplitude converter (TAC). It creates a pulse of voltage, the amplitude of which is proportional to the difference between the arrival times of the PD and MCP pulses. With the help of an analog-to-digital converter (ADC) and a multichannel analyser (MCA) the voltage amplitudes produced by the TAC are converted and stored into channel numbers, where each channel counts the number of emission occurrences within a certain delay time interval. When many (typically millions) detected photons are counted, the computer will contain a histogram of the probability distribution of emitted fluorescence photons across delay times after excitation. The shape of the histogram matches exactly the time course of the fluorescing sample.

3.1.2. Laser system

The scheme of the laser system and optical setup used for the measurements is shown in Figure 3.1. A few details are described elsewhere (Müller 1992). The core of the TCSPC-apparatus is a dye laser system providing pulses of picoseconds duration. It consists of the mode-locked argon-ion laser (model 2030 with mode-locker 342A and mode-locker-driver 452, Spectra Physics) and a synchronously pumped dye laser (model 375 B, Spectra Physics) that is equipped with a cavity-dumper (model 344S with cavity-dump-driver 454, Spectra Physics). As a dye in this work DCM (4-dicyanomethylene-2-methyl-6-p-dimethylaminostyryl-4H-pyran, $C_{19}H_{17}N_3O$) was used, the emission interval of which is 610-710 nm. This laser system allows reaching 1-2 picosecond time resolution after the deconvolution of signals recorded with a high signal-to-noise ratio. The laser power was 10-15 mW for the cavity dumper repetition rate of 4 MHz. The stability of pulses during the measurements was controlled by an oscilloscope (Tektronix, model 485).

The intensity of the laser pulses was reduced to the required values by two neutral-density filters before entering the light-protected sample box. The geometry of optics in the sample box was set according to the type of measurement. A Glan-Thompson prism situated before the sample improved the vertical polarization purity of the laser beam. The fluorescence photons were detected perpendicular to the excitation direction by a micro-channel-plate photomultiplier with multi-alkali photocathode (R1564U-01, Hamamatsu).

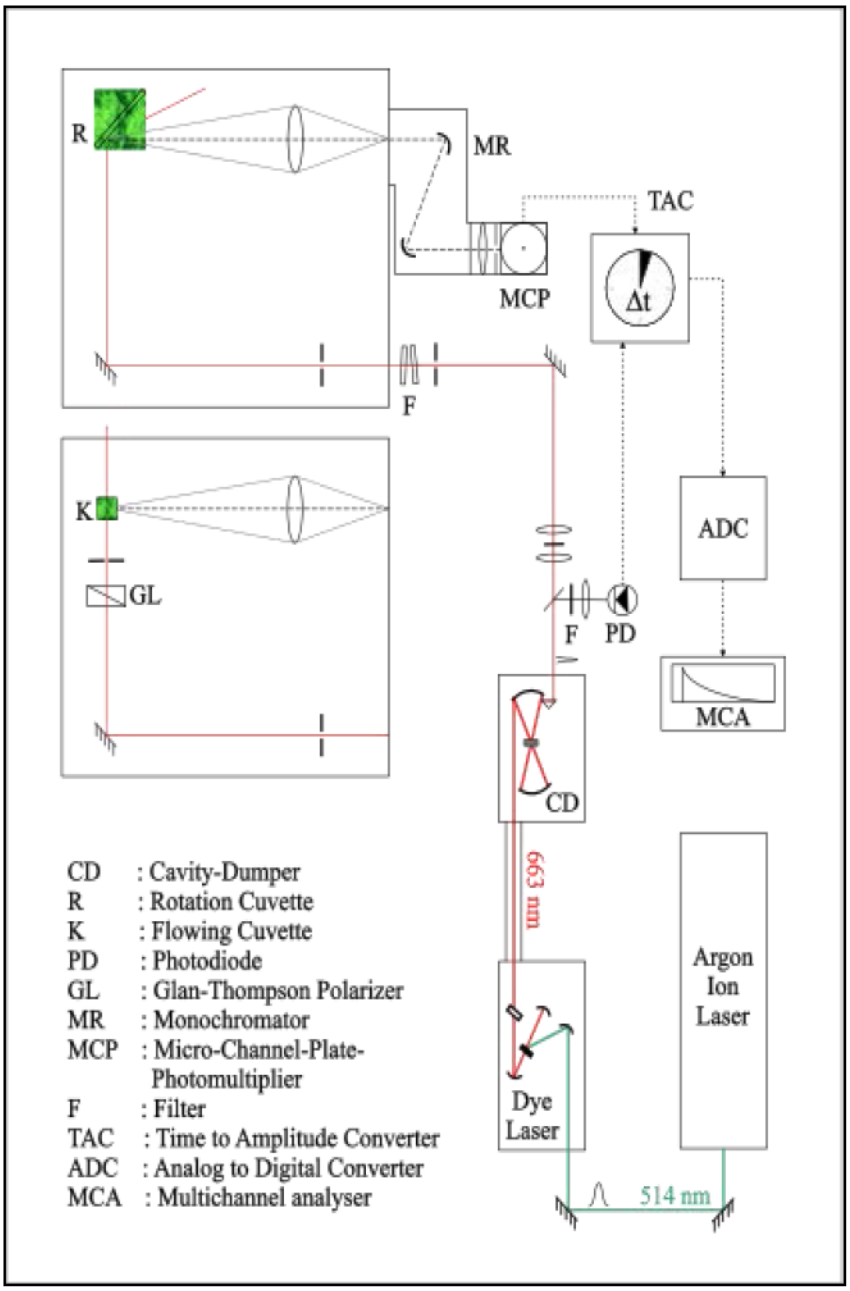

Figure 3.1: Schematic assembly of the TCSPC equipment used in this work. Excitation pulses are provided by the dye laser coupled to the cavity dumper. The dye laser is pumped by the argon-ion laser. The optical path of the excitation beam is depicted with a red line. The main part of the beam is collimated with lenses and a pinhole and, after passing a set of neutral-density filters to adjust for the desired pulse energy, is directed to the sample compartment and reflected away. Two possible arrangements depending on the type of cuvette, flowing (K) or rotation (R), are shown. The emitted fluorescence is focused onto the enter slit of a computer-controlled monochromator and the selected wavelength is detected by a MCP photomultiplier. The photomultiplier signal starts the TAC clock. The amplitude generated by the TAC (proportional to the time between excitation and detection) is digitized by the ADC and stored into a corresponding time channel by the multichannel analyzer

3.1.3. Detection electronics

The power supply (Oltronix A 3.4 k-40R) provides a highly stable voltage for the photomultiplier. The output signal of the photomultiplier is amplified from millivolt– into the volt-range (HP8447 F, Hewlett Packard amplifier) and split into two parts with a Star-splitter. One part of the pulse is transformed into a fast rectangular signal by a constant-fraction-discriminator (CFD Model 455 Quad, Tennelec,) in such a way that the triggering time becomes independent of the signal amplitude. The rectangular signals start the time-to-amplitude converter (TAC 862, Tennelec). The second part of the signal is again amplified (EG&G timing-amplifier, model 574) and analysed in an energy-discriminator (EG&G TD101/N). Through the pulse transformer it delivers information to the gate-entrance of the TAC whether the pulse amplitude lies within predetermined limits. Only a relatively small number of photomultiplier pulses will not fulfil this discrimination condition. To minimize the dead time of the system, the TAC works in the "inverse" principle. It means that the laser pulses do not start the TAC, but rather stops it (Müller 1992, Becker 2005).

3.1.4. Data analysis

The measured decay curve $I(t)$ represents a convolution, of the real fluorescence decay of the sample $F(t)$ and the instrument response function $P(t')$:

$$I(t) = \int_0^t P(t') \cdot F(t - t') dt' \qquad (1)$$

The instrument response function depends basically on the finite duration of the excitation pulse (it is not a δ-shaped excitation) and the final response time of the detection system employed. To overcome this problem the signal of a highly scattering sample (nonfluorescent), the important feature of which is that it responds to the exciting light without delay, was measured under exactly the same optical conditions as the investigated fluorescent sample. As scatterer, a dilute milk suspension in water was used. The signal measured from such a scatterer is usually the direct instrument response (Grinvald and Steinberg 1974, Holzwarth 1995).

The decay kinetics of photosynthetic complexes has in most cases a multiexponential form. In these cases the decay function $F(t)$ is determined as:

$$F(t, \lambda_{em}) = \sum_{i=1}^{n} A_i(\lambda_{em}) \cdot \exp(-t / \tau_i) \qquad (2)$$

The fluorescence decay function and amplitudes A_i here are not only time-dependent, but also dependent on the emission wavelength (λ_{em}); τ_i presents lifetimes. The analysis of measured fluorescence decay $I(t)$ is concentrated mostly on the identification of lifetimes and amplitudes by an iterative least-squares fit deconvolution (O'Connor and Phillips 1984). In essence, the procedure consists of calculating a theoretical decay function, $F(t, \lambda_{em})$, according to Eq. 2 and convoluting it with the measured instrument response function $P(t)$ to obtain a theoretical signal $G(t)$. The fitting parameters (amplitudes and lifetimes of the theoretical decay function) are varied to minimize the quadratic deviation χ^2, which is the criterion for best fit:

$$\chi^2 = \frac{1}{n-p-1}\sum_{i=1}^{n}\frac{(I_i - G_i)^2}{I_i}, \tag{3}$$

where n is here the total number of data points in the fit, p is the total number of independent fit parameters. The least-square fit procedure is done by the Levenberg-Marquardt algorithm (Marquardt 1963).

The goodness of fit can be evaluated by examining the plot of weighted residuals (r_i). The weighted residual in channel i is calculated from the equation:

$$r_i = \frac{I_i - G_i}{\sqrt{I_i}}. \tag{4}$$

When plotted against channel number, residuals from successful fits should be randomly distributed around zero.

3.1.4.1. Global analysis

In the global, or "simultaneous" analysis method fluorescence decay data taken at various conditions of emission wavelength, excitation wavelength, temperature, concentration, etc., are analysed in a combined procedure. The main idea is that certain parameters in fluorescence decay remain constant or change in a defined manner with other independent parameters. Then a combined analysis where several fluorescence decays are linked together becomes possible. It leads to a better accuracy in the values of the extracted parameters and allows the analysis of more complex systems and more closely spaced lifetime components.

The global analysis is focused mostly on the identification of lifetimes and amplitudes (see eq. 2). The obtained amplitudes of the decay lifetime components plotted against

emission wavelength after correction for stationary spectra (Holzwarth, Wendler et al. 1985) or detection time produce so called *decay-associated spectra* (DAS) (Holzwarth 1996). In the case when only one emitting species contributes to a given fluorescence lifetime, the corresponding DAS would represent the fluorescence emission spectrum of this species if it were isolated and then measured individually spectra (Holzwarth, Wendler et al. 1985). The DAS is then identical to the species-associated emission spectrum (SAES), which provides valuable information on the absorption cross-section and hence the antenna sizes of the decay components:

$$A(\lambda_{em}) = k_{rad} \cdot \sigma(\lambda_{exc}) \cdot N \cdot F(\lambda_{em}) \tag{5}$$

where k_{rad} is the radiative rate constant, $\sigma(\lambda_{exc})$ is the extinction or absorption cross-section at the excitation wavelength, $F(\lambda_{em})$ is the shape of the (normalized) fluorescence spectrum, and N is the number of chromophores contributing to the lifetime component. In practice several species having different emission spectra can take part in the observed fluorescence lifetime. In this case the DAS is a linear combination of their SAES. An illustration of that is the energy transfer occurring between two chromophores. This would produce a lifetime component with DAS having a positive maximum at the emission maximum of the donor and a negative maximum corresponding to the acceptor's fluorescence emission maximum.

Important values that one can also get from global analysis are the average lifetime τ_{av} and the relative fluorescence yield φ_i:

$$\tau_{av} = \frac{\sum_i A_i \tau_i}{\sum_i A_i} \tag{6}$$

$$\varphi_i = \frac{A_i \tau_i}{\sum_i A_i \tau_i} \tag{7}$$

Global analysis provides a mathematical description of the measured data, which is not, however, direct information in terms of a physical/chemical model. Rather these fitting parameters have to be used to derive the physical parameters of real interest to the understanding of the standard systems.

3.1.4.2. Target analysis

The goal of target analysis is to get physically relevant parameters directly, such as species-associated emission and absorption spectra (SAES and SAAS), rate constants (k_i) and concentrations or populations of components (x_i).

It allows to test different kinetic models on raw data and to describe energy transfer and/or electron transfer processes between chromophores or chromophore groups. The detailed procedures used in this work can be found in (Beauregard, Martin et al. 1991, Holzwarth 1996).

The time dependence of concentrations of excited species is found by solving the first order differential equation:

$$\frac{d\vec{X}(t)}{dt} = K \cdot \vec{X}(t) + \vec{B} \cdot l(t) \qquad (8)$$

where $\vec{X}(t)$– (n x 1) vector of concentrations of excited state species,

$\vec{B}$ is a vector of time zero absorbances of species,

$l(t)$ – excitation function,

K is the (n x n) kinetic transfer matrix describing the connectivity of the matrix,

K_{ij} – time constants k_{ij}.

$$K_{ii} = K_{0i} + \sum_{j=1,\, j\neq i}^{n} K_{ji}$$

The equation of the time dependence of fluorescence spectra $F(t, \lambda_i)$ is:

$$F(t,\lambda_i) = \sum_{j=1}^{n} e^{\gamma_j t} \cdot \sum_{m=1}^{n} S_m(\lambda_i) \cdot \left(U^{-1} \cdot \vec{B}\,(\lambda_{exc})\right)_j \cdot U_{jm} \qquad (9)$$

where γ_j – j^{th} eigenvalue of matrix K, $\gamma_j = -1/\tau_j$,

U – matrix of eigenvectors of K,

n – number of excited species m,

$S_m(\lambda_i)$ – SAES for m^{th} species.

These equations completely describe the relationship between the measured decay data as a function of excitation wavelength, emission wavelength, the kinetic scheme (quasi first-order kinetics) and the rate constants of the system on the one hand and the SAS on the other hand.

3.2. Plant cultivation

The evergreen plants (*Monstera deliciosa*, *Hedera helix* and *Prunus laurocerasus*) were cultivated at Mülheim a.d. Ruhr; whereas the non-evergreen annual plant, *Arabidopsis thaliana* was cultivated at two different locations, University of Düsseldorf and Forschungszentrum Jülich.

3.2.1. *Monstera deliciosa* - grown under fluctuating natural sunlight

Monstera deliciosa plants were grown in large pots with gardening soil and fertilized with liquid fertilizer for evergreens once per week. The plants (so called, NL-plants) were grown under natural sunlight (average maxima of 1300-1500 µmol photons m^{-2} s^{-1}) under temperature-controlled conditions (from 20°C at night to 24°C on a sunny day) behind a high glass window on the southeast side of the laboratory or in a naturally lit greenhouse.

3.2.2. *Monstera deliciosa* - grown under constant low-light

A replicate of the *Monstera* plants (herein called, LL-plants) were grown under 50-60 µmol photons m^{-2} s^{-1} provided by an array of fluorescent tubes with a 12-h light/12-h dark cycle in an indoor location of the laboratory. Room temperature was maintained at 20±2°C.

3.2.3. *Monstera deliciosa* – irradiated with high light

A second batch of aforesaid LL *Monstera* plants was irradiated to 650-700 µmol photons m^{-2} s^{-1} white light for 2 days (12 H/day) and 4 days (12 H/day). Irradiation period was later extended to 20 H/day for 2 days. For each light condition, a single mature leaf was irradiated each time under controlled room temperature of 20±2°C.

3.2.4. *Hedera helix and Prunus laurocerasus* - grown under fluctuating natural sunlight

These two evergreen plants were grown in a sunlit garden where abundant natural sunlight (average maxima of 1300-1500 µmol photons m^{-2} s^{-1}) and occasional fluctuations were available during the summer days (May-August) in 2011.

3.2.5. *Arabidopsis thaliana* - grown under constant high light

Arabidopsis wild-type (Col-0) and its mutant (*npq4*, *L17* and *npq1*) plants were put into normal light (100 µmol photons m^{-2} s^{-1}) for two to three weeks, depending on the developmental state. After initial growth the plants were singled out to 4-5 plants per pot and transferred into high light conditions (500 µmol photons m^{-2} s^{-1}) for another two to four weeks, dependent on the developmental state of the plants.

Wild-type plants were measured after five to six weeks; mutants were measured after six to eight weeks of growth.

This work was done by Tobias Schumann at the University of Düsseldorf.

3.2.6. *Arabidopsis thaliana* - grown under fluctuating light

This work was done at Forschungszentrum Jülich in the laboratory of Dr. Shizue Matsubara.

3.2.6.1. Plant cultivation

Seeds of *Arabidopsis* wildtype (wt) Columbia-0 (Col-0) as well as *npq4* and *npq1* mutants were sown on germination soil (Aussaat und Stecklingserde, Cuxin, Ottendorf) and kept for 5 days at 4°C in the dark for stratification. Germination and cultivation took place in a climate chamber. The conditions in the climate chamber were 12 h:12 h and 22°C:18°C day:night at a constant relative humidity of 60%. The photosynthetically active radiation (PAR) measured at the plant height was ca. 70 µmol photons m^{-2} s^{-1} given by fluorescent lamps (Fluora L58W/77, Osram, Munich). A small cube of soil containing a ca. 4- or 5-days-old seedling was transplanted into a pot (7cm x 7cm x 8cm) filled with cultivation soil (ED 73, Einheitserdewerk, Fröndenberg). Throughout the cultivation and experiments, plants were watered 2-3 times a week depending on the demand.

3.2.6.2. Light treatment

For each genotype, a half of the plants were kept under the cultivation conditions described above ("control-CTL"). Another half was transferred to a fluctuating light condition in the same climate chamber ("fluctuating light-SF"). These plants were exposed to a high light intensity (ca. 1000 µmol photons m^{-2} s^{-1}) for about 20 s every 5 min during the 12-h light period. The PAR between the 20-s high-light pulses was the same as for the control plants. A set of while LEDs (model 101D12, as-Schwabe, Eutingen) was used for application of high light. The treatment was started when the

plants were 4 to 5-weeks-old and continued for 8 days. On day 9 plants were transported to the MPI Mülheim, where TCSPC measurements were carried out.

3.3. Pigment characterization

Pigments were extracted from dark and actinic light adapted leaf sections pre-frozen in liquid N_2. Measurements were conducted either at the University of Düsseldorf or Forschungszentrum Jülich.

3.3.1. Pigment analysis at Düsseldorf

Pigment analysis was done on *Arabidopsis* (w.t. and mutants), *Prunus* and *Hedera* leaves, identical to what were used during fluorescence lifetime measurements. The leaf sections were either dark-adapted for 10-12 h or high light adapted for 30 min. Pigments were extracted with acetone and quantified by reversed-phase HPLC as described (Färber, Young et al. 1997).

3.3.2. Pigment analysis at Jülich

Leaf disc samples (1.6 cm^2) for pigment analysis were taken from dark-adapted plants on day 9 and immediately frozen in liquid N_2. Pigments were extracted by grinding the leaf discs in 1 ml of chilled acetone. Following centrifugation for 5 min at 13200 rpm, the extracts were syringe-filtered (0.45 µm) before injection (20 µl) in the HPLC. The HPLC analysis was performed with an instrument setup consisting of Waters 515 pumps (Waters, Eschborn), a Waters 996 PDA detector and a Merck Hitachi AS-2000A auto-sampler. The system was calibrated by using pigment standards purchased from DHI-WASY (Syke). The separation of pigments was achieved by using an Allsphere ODS-1 column (4.6 x 250 mm, Alltech) and according to a method modified from Gilmore and Yamamoto (1991). The mobile phase for separation of xanthophylls and chlorophyll b was acetonitrile:methanol:Tris (0.1M, pH 8) 80:12:8 followed by a linear gradient to hexane:methanol 1:4 for elution of chlorophyll a and β-carotene. The Tris buffer was filtered through a nylon membrane (0.45 µm, Alltech) prior to use. All solvents were of HPLC grade (Sigma-Aldrich Chemie, Taufkirchen). Peak integration was done by the Waters EmpowerPro software.

3.4. Fluorescence kinetics

Fluorescence decays were measured by the described apparatus (Miloslavina 2008) for single photon timing to high S/N ratio at several wavelengths using laser pulses of 663 nm and a repetition rate of 4 MHz. Detached plant leaves were held between two glass plates in a rotation cuvette (diameter = 10 cm, that was also oscillated sideways

(Lissajous scanner). Fluorescence was measured in a front face arrangement from the upper side of the leaves. The cuvette was filled with a sucrose solution (0.3 M).

The measurements were performed in such a way that they characterize the two conditions (F_{max} and F'_{max}/F_{NPQ}) as much as possible:

Light adaptations for *Monstera* leaves during NPQ measurement were carried out using an array of red (λ_{center} = 635 nm) high intensity light-emitting diodes providing 600 μmol photons m^{-2} s^{-1} to LL-plants and 2100 μmol photons m^{-2} s^{-1} to NL-plants. Typically lifetime measurements were started after 25-30 min of actinic illumination when the quenching had fully stabilised. For F_{max}, the DCMU [(3-(3,4-dichlorophenyl)-1,1-dimethylurea)] treatment was carried out by mild vacuum incubation (3-4 times) in a 300 µM DCMU solution for 1 hour. For achieving full PSII closure, as tested by fluorescence induction using a Hansatech HandyPea instrument and by fluorescence lifetime measurements, the lower epidermis of the leaves was mildly rubbed with extra-fine sandpaper (ISO/FEPA Grit designation: P400, average particle diameter: 35.0 µm) before the DCMU incubation. To achieve F_{max} under NPQ conditions an additional blue (λ_{center} = 460 nm) high intensity LED light, which provided high illumination for about 300 msec sufficient for closing all PSII RCs, was focused on a <1 cm diameter spot of the sample just before it entered the measuring beam.

The other two evergreen plants, such as *Hedera* and *Prunus* were similarly treated with DCMU. However, their NPQ measurements were carried out at 1,200 μmol photons m^{-2} s^{-1}.

In cases of *Arabidopsis* the leaves were cut at the stem and dipped immediately in a 45 µM DCMU solution with the main part of the leaf that was later used for measurement exposed to air. The detached leaves were incubated for 14 h in the DCMU solution in complete darkness (Tóth, Schansker et al. 2005). For F_{NPQ} actinic intensity of 1,200 μmol photons m^{-2} s^{-1} was used.

3.5. Preparation of reconstituted membrane and time-resolved fluorescence measurements

3.5.1. Native LHCII isolation

Native LHCII trimers were purified from pea leaves according to the method described in Krupa et al. (Krupa, Huner et al. 1987).

3.5.2. Expression, isolation and purification of PsbS protein and double mutant PsbS protein

PsbS cDNA of pea has been cloned in one expression vector and the PsbS protein has been expressed in *E. coli* and purified as inclusion bodies. The two Glu residues of the PsbS protein which are acting as the pH sensor sites were mutated to Gln. Expression and purification of the mutant PsbS was analogous to the WT PsbS. The functional PsbS was refolded in the preformed liposomes.

3.5.3. Proteoliposome preparation

Thylakoid lipids MGDG, DGDG, SQDG, and PG, mixed according to the lipid ratio in the thylakoid membrane, were dissolved in $CHCl_3$. The solvent was evaporated by rotary evaporation and then the lipid mixture was dissolved in Tricine-NaOH buffer (pH 7.8) (5mg lipids/ml). The liposomes were formed by sonication of this lipid suspension. LHCII and PsbS protein (wt or mutant) (molar ratio LHCII trimer: PsbS = 3.3:1), or LHCII alone, were mixed with the preformed liposomes and the mixture was then sonicated in a bath sonicator for 1 min. The sonicated mixture underwent two times freeze-thaw cycles on ice and was then sonicated again at r.t. In some experiments Z was also added to the mixture of thylakoid lipids.

3.5.4. Time-resolved fluorescence

Fluorescence kinetics as well as steady state fluorescence has been measured using a single-photon timing apparatus as described elsewhere (Müller, Griebenow et al. 1991) with temporal resolution of 2-3 ps under magic angle polarization conditions at r.t. in a 1 mm cuvette which was moved slowly in order to prevent sample deterioration by photoexcitaiton at a single spot. Before the measurements an oxygen scavenger consisting of glucose/glucose-oxidase/catalase has been added to the sample in order to prevent photooxidation. Samples were excited at 663 nm and the fluorescence decays were typically detected in the 675-750 nm wavelength region. Time-resolved fluorescence has been analyzed by global and target analysis procedures and results are presented as decay-associated emission spectra (DAES) and species-associated emission spectra (SAES) along with the kinetic models that best fitted the data (Holzwarth 1996).

3.5.5. Quantum chemical calculations

Quantum chemical calculations have in the past addressed the localized excited states of LHCII (see Ref. (Konig and Neugebauer 2011) for a review). However, various limitations in the methods used prevented the proper treatment of the important CT states: either the available computational methods were too expensive to calculate

properly the collective excited states, including the CT states, of groups of excitonically coupled chromophores together, or they lacked the required accuracy in particular in terms of the CT state energies.

For the problem at hand, we need to include at least three Chl molecules together with their protein environment. Such extensive supersystem calculations require the use of methods that are both computationally affordable and reliable at the same time. To this end, we have decided to use long-range corrected density functionals. These functionals combine the relatively low computational cost of (time-dependent) density functional theory, (TD)-DFT (Hohenberg and Kohn 1964, Kohn and Sham 1965, Casida, Jamorski et al. 1998), with a corrected long-range Coulomb interaction, *e.g.*, CAM-B3LYP (Yanai, Tew et al. 2004) or ωB97XD (Chai and Head-Gordon 2008). For the present study, these functionals offer an excellent possibility to gain insight into the collective excited states and physical processes related to CT state formation within a Chl cluster embedded in the protein environment. Our study, to the best of our knowledge, reports the first time long-range corrected TD-DFT calculations encompassing a cluster of three Chls, i.e. the minimal unit that is required to understand the mechanisms of CT state formation in LHCII. In the present stage the computational effort required has been reduced by several simplifications (*e.g.*, removal of the phytyl-chains of the Chls and the representation of the protein environment as a point charge field), but it retains all essential properties that are required to describe the involved electronic states, including in particular the CT states, and their dependence on environmental effects. Clearly further improvements in the methods are possible by e.g. employing a full state-of-the-art hybrid QM/MM approach (Senn and Thiel 2009), or testing the effects of different environment parameters, like embedding into a membrane. Such extensions would however require a very expensive computational effort at the moment. However, since we are interested at this stage in describing the electronic properties of the LHCII crystal with minimal changes to the experimental X-ray structure, the current approach suffices in our view.

Our calculations bear similarity to previous work on Chl-carotenoid coupling in LHCI (Kröner and Götze 2012). The molecular model contained the coupled Chl cluster consisting of the three Chl *a* molecules forming the supposed quenching center (residues number 601, 602 and 607 of chain A in PDB structure 2BHW (Standfuss, Terwisscha van Scheltinga et al. 2005); (cf. Figure 3.2) and the shell of amino acid (aa) residues and lipids embedding the chromophores at a distance up to 4 nm (ONIOM method) in the

crystal structure (Dapprich, Komarómi et al. 1999). A detailed list of the residues incorporated in the shell is given in Figure 3.3.

Two pairs of aa's or lipids were identified close to the proposed quenching Chl cluster of interest, which are able to easily change their protonation state and thus cause a drastic change of the charge distribution near the Chls in the quenching center: Glu175/Lys179 and Lys182/PG (note that the phosphatidylglycerole (PG) molecule is an integral constituent of the LHCII trimer structure; see discussion in Chapter 9 for details). For each of these two pairs, we calculated the point charge fields (PCFs) describing the two protonation states (i.e. four different PCF configurations in total) using AMBER99 (Wang, Cieplak et al. 2000) force field Coulomb parameters. For PG charge parameters were computed as outlined in Ref. (Kröner and Götze 2012). For each of the four PCFs, we computed the TD-CAM-B3LYP/6-31G(d) excited state energies for all vertical excitations within the Chl Q band excitation region. For comparison, we also computed the Chl cluster spectrum in vacuum.

In addition we also performed full quantum mechanical calculations for the ground state energies of the different protonation states without resorting to the PCF approximation.. The ωB97XD functional was chosen to include dispersion interactions. The conformation of the protonation states was relaxed with a 1 Å restraint for the OH bond lengths (either Glu175-OH or PG-OH), including the two aa/lipid pairs of interest in the core region of the ONIOM model.

[The quantum chemical calculations were performed by Dr. Jan Götze].

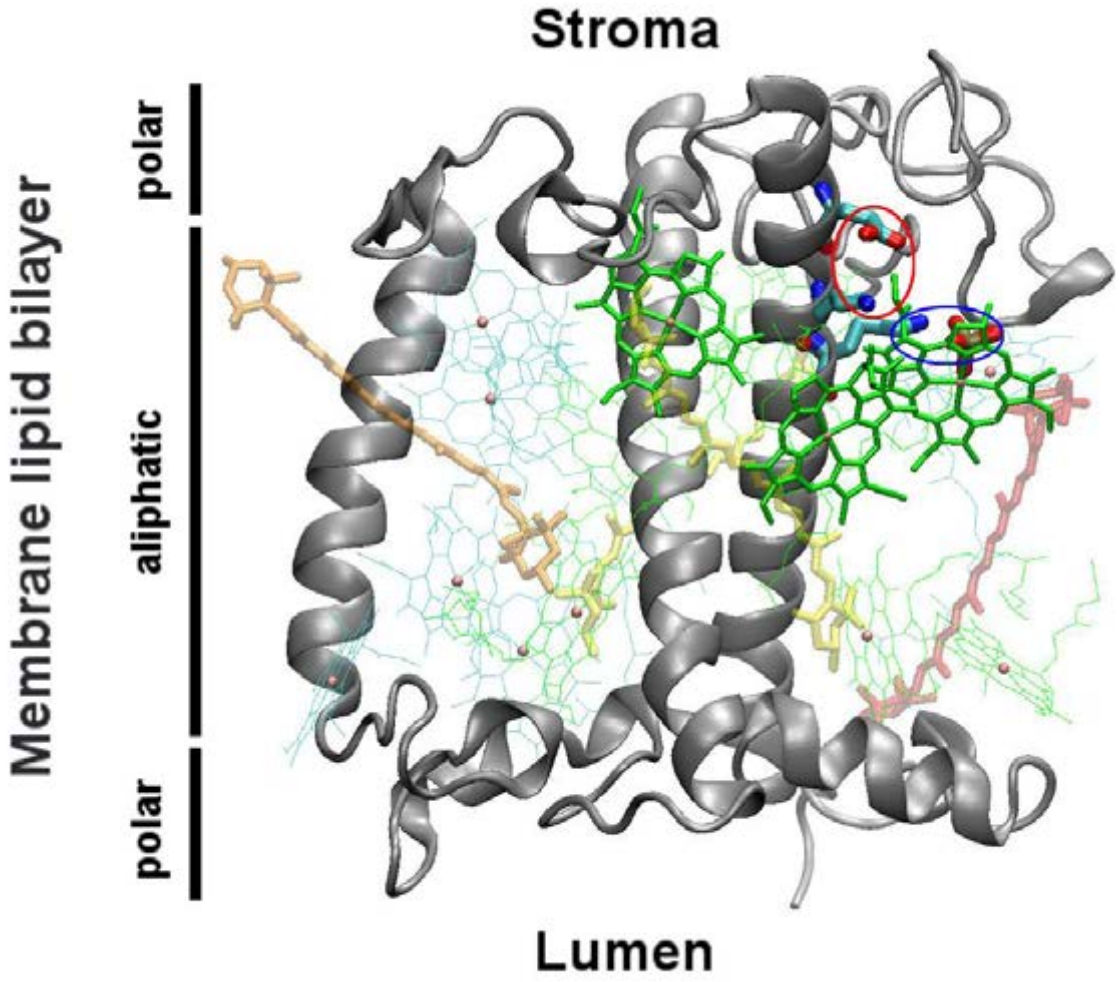

Figure 3.2: Structure of the LHCII complex indicating its position in the thylakoid membrane. The positions of the proposed quenching center and the relevant groups of the protein that are involved in quenching according to our model are highlighted. Red ellipse: Glu175/Lys179 ("gatekeeper"); blue ellipse: PG/Lys182 (passive element); green sticks: NPQ chlorophyll a cluster, f.l.t.r. chlorophyll a 601, 602, 607; yellow: lutein; orange: neaxanthin; red: violaxanthin; green lines: other chlorophyll a; cyan lines: chlorophyll b.

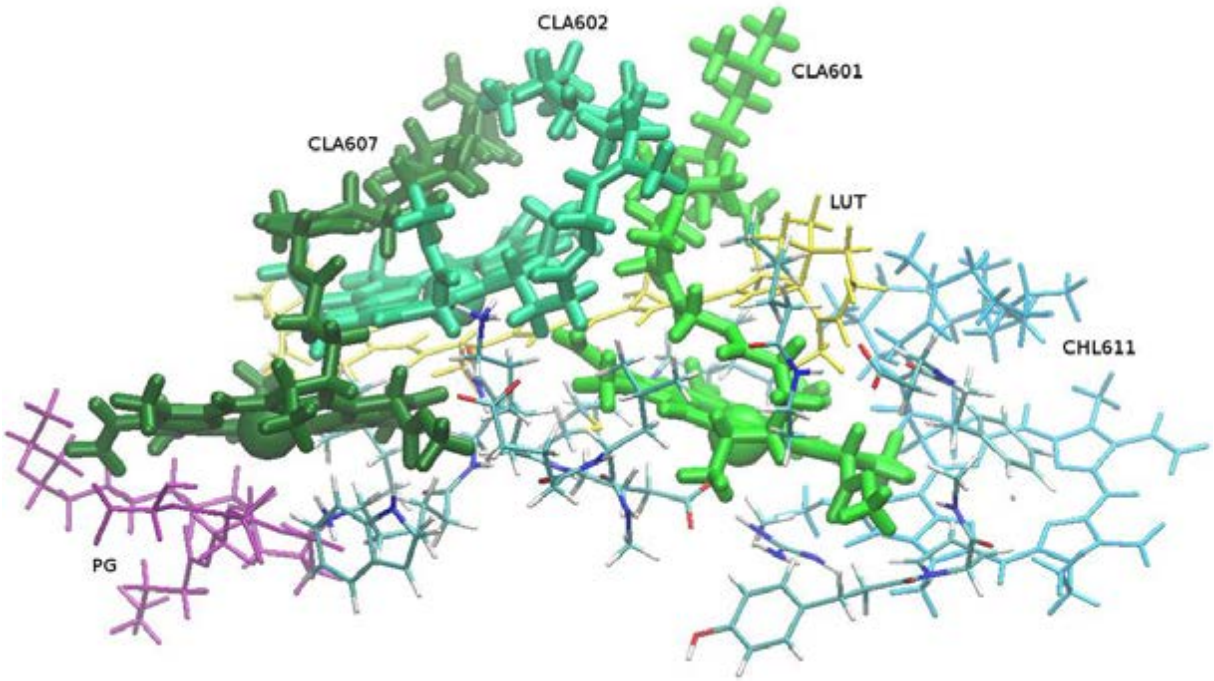

Figure 3.3: Description of aa residues and other environmental factors taken into account in the quantum mechanical calculations. View from the stromal side, with the colored residues taken as labeled. CLA: chlorophyll a; CHL: chlorophyll b; LUT: lutein; PG: phosphatidylglycerol. The unlabeled atoms correspond to the protein environment, consisting of Trp16, Arg70 (only functional part), Met73 to Leu74, Tyr156 to Pro157, Phe161 to Asp162, Leu166 to Ala167, Glu175 to Leu176, Lys179 to Glu180 and Lys182 to Asp183. N-terminal cap is methyl, C-terminal cap is hydrogen after C-α. Arg70/Glu180 pair was always charged. Core atoms were CLA porphyrin plus Mg ions for the TD calculations, together with the Glu175/Lys179 and PG/Lys182 pairs for the ground state energy calculations.

Chapter 4 : NPQ mechanisms in low-light (LL) and natural sunlight (NL) grown *Monstera deliciosa*

Harmless dissipation of potentially damaging excess absorbed light provides crucial protection to photosynthetic organisms. However, the existing photoprotection models developed so far are based on static distribution of photosynthetic pigments ignoring the actual movement of proteins induced by light, particularly caused by fluctuating natural sunlight. In the following work, the dynamic changes in thylakoid membrane that are extremely essential for photosynthetic regulation are studied.

The quenching pathways were measured, especially NPQ on the tropical evergreen plant *Monstera* grown under fluctuating natural sunlight. A comparison was made with low-light grown identical duplicates.

4.1. Results

The results from the kinetic compartment analysis of the lifetime data are shown as decay-associated fluorescence spectra (DAS) in Figure 4.1 for LL and NL-leaves. Initial analyses applied the same kinetic model previously successfully employed to describe dark-adapted and quenched kinetics in *Arabidopsis* wild-type and mutants leaves (Holzwarth, Miloslavina et al. 2009). This same model was indeed also successful for describing kinetics of dark-adapted and quenched LL *Monstera* leaves (Figure 4.1). A kinetically and spectrally homogeneous pool of PSII units not involving energy transfer to PSI (Holzwarth, Miloslavina et al. 2009, Miloslavina, de Bianchi et al. 2011) consistent with maintenance of full lateral segregation of the two photosystems (Supplementary Figure 4.1C) was observed.

For unquenched NL-leaves, however, a homogeneous PSII pool was unable to satisfactorily describe the observed kinetics (Supplementary Figure 4.4). A variety of alternative, more complex kinetic models (Supplementary Figure 4.1) were tested. A good fit of the kinetics from dark-adapted NL-leaves was finally obtained by assuming a heterogeneous PSII pool, with a fraction of about 60% of PSII units in a “non-spillover PSII” arrangement (separate from PSI) and the remaining PSII fraction requiring energy transfer to PSI (“spillover PSII”) (Supplementary Figure 4.1A and 4.4). In turn, the quenching kinetics of the high-light-irradiated NL-leaves were best described by a

homogeneous PSII pool involving fast spillover from all PSII units to PSI (Figure 4.1 and Supplementary Figure 4.1B).

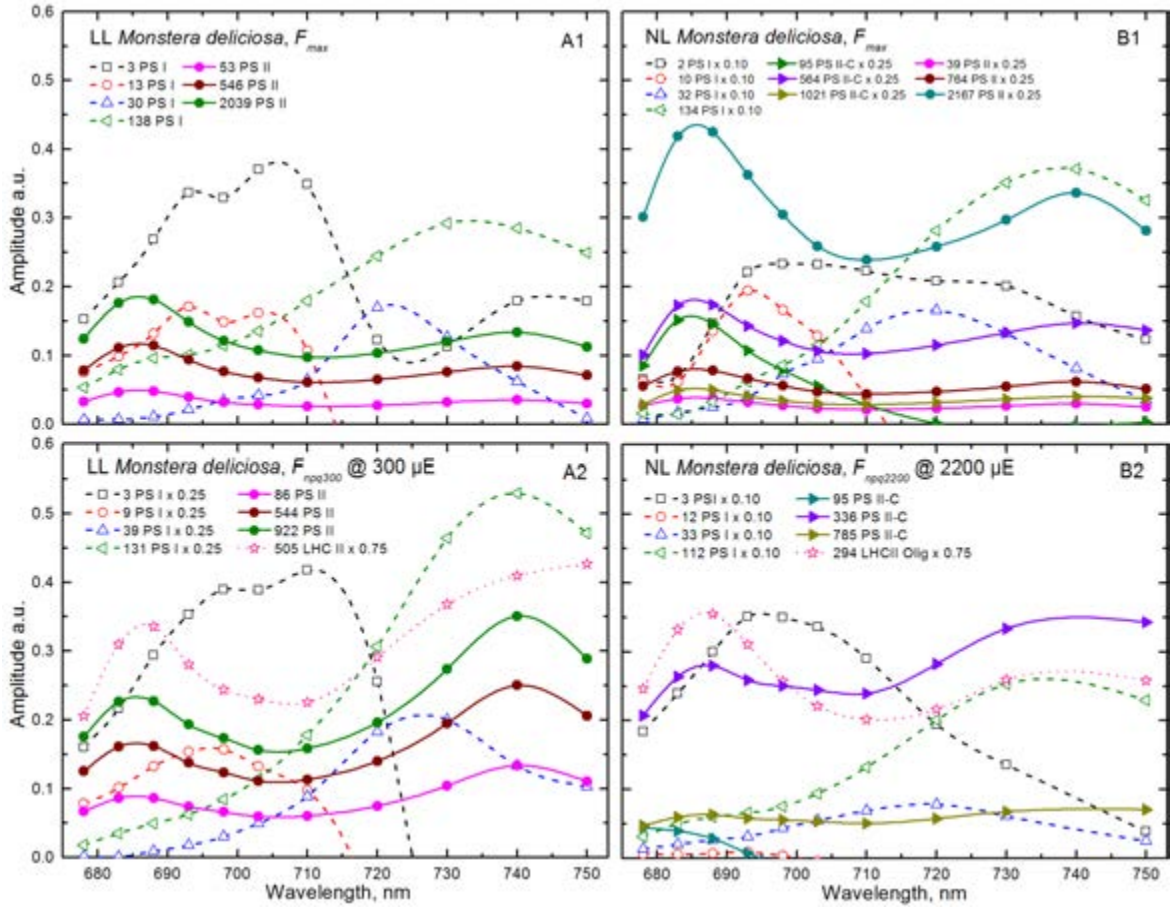

Figure 4.1: Decay-associated spectra (DAS) resulting from kinetic compartment analysis of unquenched (F_{max}) and quenched (F_{npq}/F'_{max}) states of LL and NL grown *M. deliciosa* plants. Components labeled PSII belong to unconnected (non-spillover) PSII, while those labeled PSII-C belong to connected (spillover) PSII units. PSI components are shown as dashed and detached LHCII as a dotted line. For clarity of presentation, only positive amplitude parts are shown.

Both LL- and NL-leaves in their quenched state showed a pronounced increase in thermal dissipation (assessed from an increase in the rate constant of thermal dissipation in the PSII antenna k_D from about 1.8 ns^{-1} versus 0.3 ns^{-1} in the dark-acclimated state; Table 4.1). This increase has been attributed to activation of zeaxanthin-dependent (qZ) quenching (Holzwarth, Miloslavina et al. 2009, Nilkens, Kress et al. 2010, Miloslavina, de Bianchi et al. 2011). An additional kinetic component was observed that presumably reflects PsbS-dependent detachment of LHCII from the PSII super-complex (qE) (Holzwarth, Miloslavina et al. 2009, Miloslavina, de Bianchi et al. 2011). The percentages of LHCII detachment were nearly 30% for both NL- and LL-leaves (Table 4.2), and were thus consistent with previously reported values for *Arabidopsis* leaves (Holzwarth, Miloslavina et al. 2009). These data suggest that (i) both

LL- and NL-plants exhibit the two previously described quenching mechanisms (Holzwarth, Miloslavina et al. 2009, Nilkens, Kress et al. 2010, Miloslavina, de Bianchi et al. 2011) upon high-light-exposure and (ii) that the much higher quenching capacity of NL-leaves compared to LL-leaves (Table 4.2) is related to activation of a novel NPQ quenching mechanism based on energy spillover (i.e. rapid energy transfer) (Holzwarth, Müller et al. 2006, Miloslavina, Szczepaniak et al. 2006, Szczepaniak, Sander et al. 2009) from PSII to PSI (Q_{SO}). This new mechanism is responsible for the three-times-greater maximal NPQ (8.6 versus 3.0) of NL- versus LL-leaves. In NL-plants, Q_{SO} apparently operates in addition to the previously characterized qE and qZ quenching mechanisms, while LL-plants lack Q_{SO} quenching. In NL-plants, spillover-rates from PSII to PSI reached very high levels of 1.8 ns^{-1} that are comparable to the effective rate of trapping and charge separation in the active PSII reaction centre (Table 4.1). A fast energy transfer between the large PSII-associated and PSI-associated antenna units is possible only over very short distances (in the range of <1.5 nm) of their respective peripheral antenna. The observation of efficient spillover thus demands that PSII and PSI antenna units must be in direct contact with each other in the photosynthetic membrane. Such a situation is inconsistent with a lateral segregation of the two photosystems. In turn, loss of lateral segregation is inconsistent with pronounced grana stacking. The ultrastructure of thylakoid organization by electron microscopy (EM) in LL- and NL-leaves in their dark- and high-light-adapted states were measured (Figure 4.2). EM analysis of dark-adapted LL-leaves revealed tall stacks of up to over 50 firmly appressed thylakoids (Figure 4.2A) previously described for LL-grown evergreens from the family (*Araceae*) 30 to which *Monstera* belongs, and less tall stacks (ranging between about 10 to 20 discs) for NL-plants. LL-thylakoids remained largely appressed with a few small clefts in the middle of some of the grana stacks (Figure 4.2B) upon exposure to high light. In contrast, high light exposure of NL-leaves induced a dramatic change in thylakoid organization. The previously appressed thylakoids separated widely and the whole grana structure disintegrated, turning the majority of grana thylakoids into what appeared to be extended and partially folded stroma thylakoids (Figure 4.2E). It is important to mention here that the changes occurred in the appressed region under actinic light was reversible, as can be seen from the EM images (Figure 4.2 C,F). Similar reversibility can also be judged from the recovery of Fv/Fm values (Supplementary Figure 4.5).

To conservatively quantify the extent of grana disintegration beyond the selected images shown in Figure 4.2, average width was determined for the three widest grana

stacks of 7-9 chloroplasts from the four treatments represented in Figure 4.2A-F (see Supplementary Figure 4.6). While average grana width (mean±SD) did not differ significantly for dark-(0.61±0.05 µm) versus high-light-exposed (0.57±0.05 µm) LL-plants, grana were significantly ($p<0.05$) less wide in dark-adapted NL-plants (0.48±0.09 µm) and narrowed further (0.38±0.05 µm) upon exposure to high light (Supplementary Figure 4.6).

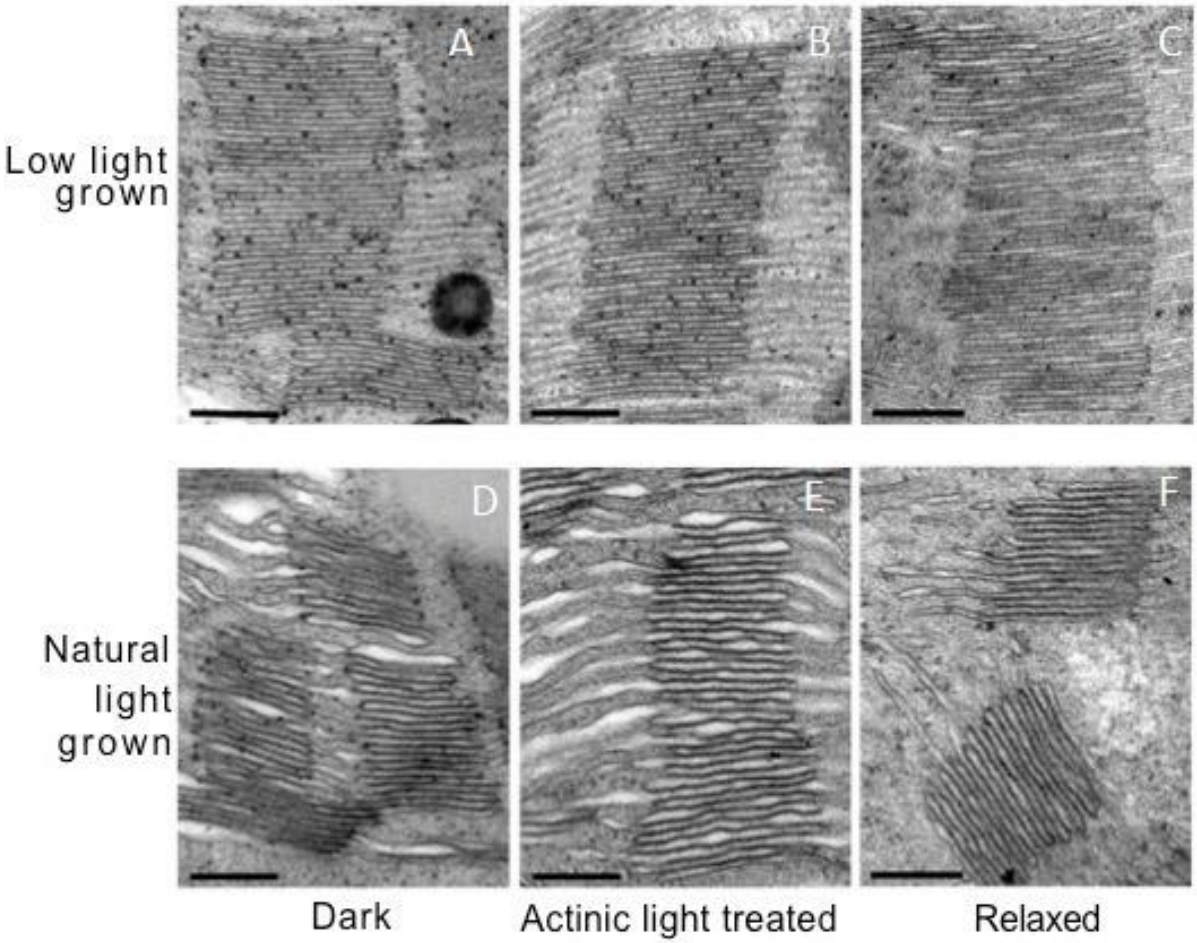

Figure 4.2: Chloroplast ultrastructure from leaves of LL (A-C) and NL (D-F) *Monstera deliciosa*. Dark-adapted leaves (A,D) were taken at the end of the 10-12 H dark period, 'actinic light treated' (B,E) represents leaf discs exposed to high light (1800 µmol photons m^{-2} s^{-1}) for 20 min in a temperature-controlled chamber at 25°C and fixated for electron microscopy as rapidly as possible (about 1 min after high light treatment) and 'relaxed' states (C,F) represent leaves fixated under room light (10 µmol photons m^{-2} s^{-1}) after 20 min exposure at aforesaid high light. The white arrow points to one of the partial destacking areas in high-light-exposed LL thylakoids. The scale (black-bar) is 250 nm. The EM experiments were performed at The University of Colorado, USA by Dr. Onno Muller and Prof. Barbara Demmig-Adams.

4.2. Discussion

4.2.1. Light-induced reorganization of thylakoid structure

As a non-invasive method, ultrafast chlorophyll fluorescence spectroscopy is very powerful in distinguishing various components of photoprotective dissipation of excess absorbed light (assessed as NPQ) (Holzwarth, Miloslavina et al. 2009, Miloslavina, Grouneva et al. 2009, Miloslavina, de Bianchi et al. 2011). This method's further advantage for the present work is its high sensitivity to structural rearrangements in the functional organization of the photosynthetic membrane. At present, the latter method is the most powerful, and likely only, non-invasive, selective technique to detect close vicinity of PSII and PSI leading to sharing of their antennae under *in vivo* conditions in either light or darkness. The results of the present fluorescence lifetime measurements (Figure 4.1) on LL- and NL-leaves are in excellent agreement with differences observed at the level of thylakoid structure (Figure 4.2). The homogenous PSII pool, not connected to PSI in both dark- and light-acclimated states of LL- plants indicated by fluorescence lifetime analysis is consistent with the pronounced stacking of the thylakoid membrane (and complete lateral segregation of the two photosystems) in both states (Figure 4.2A,B). In NL-plants, however, about 40% of PSII units were involved in spillover even in the dark-adapted state, and this fraction increased to 100% in the light-acclimated state. This result implies that unquenched NL-leaves of *Monstera* have a thylakoid organization with a large fraction of PSII complexes in direct neighbourhood to, and in energy-transfer contact with, PSI complexes. This finding is consistent with the strongly reduced width and height of grana stacks (apparently converted to stroma lamellae) in NL- versus LL-plants (Figure 4.2D). The increase of the fraction of PSII involved in spillover to 100% upon NPQ induction in NL-plants is supported by the loss of stacking in light-adapted NL-thylakoids (Figure 4.2E). A rapid, light-induced reorganization of the thylakoid membrane thus takes place in NL-plants upon transition from the dark-adapted, unquenched state to the quenched state, as illustrated by the schematic depictions of thylakoid organization in Supplementary Figure 4.2.

4.2.2. The photochemical mechanism of spillover quenching

Spillover drains away excitation energy from PSII in a similar manner as direct antenna quenching via an increase in rate k_D (qZ quenching) (Holzwarth, Miloslavina et al. 2009). Like the already described quenching mechanisms, Q_{SO} should be effective in protecting PSII from potential damage under high light. Using an analogous approach to those applied before, the rate constants in Table 4.1 can be used to calculate that Q_{SO} contributes more than 60% of the strong total quenching in NL-plants, and thus

presumably a similar amount of photoprotection of PSII (Lambrev, Miloslavina et al. 2012). In such a case, Chl triplet yield in PSII (a measure of the damage potential under high light) can be estimated to be reduced to 4% from a non-quenched value of 25% (Lambrev, Miloslavina et al. 2012). This change is what constitutes the high photoprotective capacity of Q_{SO}. Concerning the underlying photochemistry of spillover quenching, efficient Q_{SO} quenching would require tight coupling of the antenna of PSII and PSI. Such coupling should give rise to fast, energetically downhill energy transfer from PSII to PSI with a rate k_t that is nearly non-reversible due to (i) PSI's low-energy "red" antenna (Holzwarth, Miloslavina et al. 2009) and (ii) fast utilization of energy in PSI (Trissl 1997). This arrangement drains away energy from PSII and can thereby act as a PSII photoprotection mechanism. At low light intensities, PSI's reaction centre P700 is mostly in the reduced state and spillover would thus feed energy from PSII to PSI. While providing photoprotection to PSII in high light, the energy drained from PSII by the Q_{SO} mechanism can therefore serve to drive PSI when it is not oxidized. Spillover can thus serve as an efficient regulatory mechanism that redistributes excitation energy between PSII and PSI under low light conditions. Under high light intensities, when NPQ is induced by highly excessive light, the PSI-RC (reaction centre) is mostly in the oxidized form of PSI $P700^+$ (Supplementary Figure 4.3) since quenched PSII does not feed enough reducing equivalents to PSI via the electron transfer chain. In the $P700^+$ state, the PSI-RC is known to be an efficient quencher, rapidly deactivating excited-state energy into heat (Trissl 1997). The Q_{SO} quenching thus represents indirect non-photochemical quenching via oxidized PSI. In a close "spillover arrangement" of PSII and PSI units, the controlled interplay between spillover from PSII to PSI, and actual quenching in PSI, thus provide important opportunities for (i) balancing energy between PSII and PSI (without net energy loss) and (ii) regulating the efficiency of harmless, photoprotective dissipation of excess energy (NPQ).

4.2.3. LL-plants lack the ability for structural reorganization

Our results indicate that LL-leaves of Monstera lack the ability for rapid thylakoid reorganization and thus develop no Q_{SO}. LL-leaves thus achieve a maximal NPQ capacity of only about 3, which is in the range observed for laboratory-grown wild-type *Arabidopsis* and other annual higher plants that develop in high light (Li, Muller-Moulé et al. 2002, Golan, Li et al. 2004). *Monstera* grown under NL-conditions have previously been shown to accumulate higher levels of the protein PsbS and the xanthophyll zeaxanthin (both shown to be associated with NPQ) than LL-plants and a substantially higher photosynthetic capacity (Demmig-Adams, Ebbert et al. 2006). May PsbS level

promote thylakoid reorganization in NL-plants and enable the Q_{SO} quenching mechanism? The *L17* mutant of *Arabidopsis* is a PsbS overexpressor and shows enhanced NPQ (of the qE or Q1-type (Holzwarth, Miloslavina et al. 2009), with a higher total NPQ capacity than wild type (Li, Muller-Moulé et al. 2002). Despite the higher PsbS level and a corresponding higher level of LHCII detachment from PSII, this mutant did not exhibit the quenching shown here to be associated with rapid thylakoid structural reorganization in NL-leaves of *Monstera* (Holzwarth, Miloslavina et al. 2009). PsbS alone is thus unlikely to be the major factor providing thylakoid structural plasticity under NL conditions, although it cannot be excluded that PsbS may support membrane reorganization in NL-plants. Recent studies of light-induced protein phosphorylation and its regulation by light quality (Wagner, Dietzel et al. 2008, Dietzel, Bräutigam et al. 2011, Tikkanen and Aro 2012) suggest a link between acclimation to light quality and intensity, phosphorylation patterns, changes in PSI/PSII interactions (Tikkanen, Grieco et al. 2011, Alter, Dreissen et al. 2012, Tikkanen, Grieco et al. 2012) and, possibly, pronounced structural changes in thylakoid organization (Tikkanen and Aro 2012, Tikkanen, Suorsa et al. 2012). A fluctuating natural growth light environment (Alter, Dreissen et al. 2012) (as that experienced by our NL-plants) may play a key role in dynamic regulation of PSII/PSI interaction and intersystem energy transfer. Tikkanen and coauthors introduced a model of a "shared PSII/PSI antenna" (Tikkanen, Suorsa et al. 2012), which may be the closest analogue so far of the functional PSII/PSI spillover complex identified in the present study (Supplementary Figure 4.2) as evidence for rapid regulation of the degree of lateral heterogeneity of the two photosystems in response to light quality and quantity changes. Thylakoid membrane reorganization is suggested that is necessary to achieve substantially higher NPQ capacities via the Q_{SO} quenching described here may be associated with the regulation of thylakoid protein phosphorylation patterns. Changes in electrostatic surface charges associated with thylakoid protein phosphorylation may influence inter-membrane attraction/repulsion forces controlling membrane appression and inter-protein forces controlling intra-membrane interactions among thylakoid components (Chow, Kim et al. 2005). Forces controlling interaction between PSII and PSI as well as modulation of inter-membrane forces are of key interest for Q_{SO} quenching. Overall, control of interactions among membrane components by protein phosphorylation may have an impact on a wide range of regulatory mechanisms of thylakoid architecture, such as the balance between linear and cyclic electron flow (Chow, Kim et al. 2005), protein turnover (Kirchhoff, Hall et al. 2011), and balancing energy distribution between the photosystems for optimal linear electron transfer. Our data support the recently expressed view that a better

understanding of the impact of growth light intensity and short- and long-term variability on structural thylakoid dynamics (Kirchhoff, Hall et al. 2011, Anderson, Horton et al. 2012, Kouřil, Wientjes et al. 2013) is crucial for understanding the mechanisms of photosynthetic regulation and photoprotection (Tikkanen, Suorsa et al. 2012).

Table 4.1: Rate constants (ns^{-1}) for the PSII and PSI kinetics in the *Monstera deliciosa* determined from the kinetic target analysis. PSII-C: PSII fraction that is connected to the PSI-core via spillover energy transfer; k_t and k_{-t} are the forward and backward spillover rates from the PSII to the PSI core. The k_3 rate from the closed PSII units is fixed to 0.9 ns^{-1} (Holzwarth, Miloslavina et al. 2009). The error limit in the rate constants are ±10%.

		PSII-C (connected)				**PSII unconnected**			**PSI**				
		k_D	**k_{CS1}/k_{rec1}**	**k_1/k_2**	**k_t/k_{-t}**	**k_D**	**k_{CS1}/k_{rec1}**	**k_1/k_2**	**k_{r1}/k_{-r1}**	**k_{r2}/k_{-r2}**	**k_{CS}/k_{-CS}**	**k_4**	**LHCII**
LL	Fmax	-	-	-	-	0.30	3.3/12	4.1/0.71	40/16	12/37	140/90	80	-
LL	$Fnpq_{300}$	-	-	-	-	1.8	1.6/8.2	2.1/0.72	80/19	21/110	119/62	134	2.4
NL	Fmax	0.30	3.3/5.8	0.96/0.30	1.7/0.20	0.3	2.0/20	3.8/0.33	40/26	13/37	191/200	106	-
NL	$Fnpq_{2200}$	1.03	2.2/6.1	1.9/0.9	1.8/0.31				38/52	15/62	170/30	70	3.40

Table 4.2: Average lifetime τav [ps] of the fluorescence decays for the Monstera deliciosa leaves grown under NL and LL conditions were calculated from the kinetic data at 683 nm emission wavelength (excitation at 663 nm). The errors in the average lifetimes are ± 5%; errors in the other values are ±10%. NPQ values were calculated from the fluorescence decays at 683 nm according to the equation

$$PQ = \frac{\tau_{av@Fmax}}{\tau_{av@Fnpq}} - 1$$

Also shown are the lifetimes [ps] of the component appearing under NPQ conditions assigned to functionally detached and quenched LHCII, along with the percentage of LHCII detachment as measured by the decrease in total PS II cross-section in the quenched vs. the unquenched state. PSII-C denotes the PSII fraction connected by spillover to PSI.

	LL	NL
τ_{av} of PS II, ps		
F_{npq}	150	90
F_{max}	600	870
τ of quenched LHC II oligomers, ps	505	294
NPQ [a]	3.0	8.6
% of detached LHC II [b]	30	28

a) These numbers for the NPQ values derived from the lifetime measurements can be directly compared with those measured by conventional steady state NPQ induction. They fully agree within the error limits.

b) Measured as percentage of total absorption cross-section (at the excitation wavelength of 663 nm) of dark-adapted PSII that is detached as quenched LHCII

Table 4.3: Excitation vectors for the various antenna compartments resulting from kinetic compartment analysis for the time-resolved kinetic data of *Monstera deliciosa* leaves from plants grown under LL and NL conditions. The suffix 'C' denotes the PS II units connected through energy-spillover with PSI. The errors are in the range of ±10%.

	PSII-Ant/RC-C	**PSII-Ant/RC**	**PSI-Ant/RC**	**LHCII**
LL Fmax	-	0.80	1.0	-
LL Fnpq300	-	0.65	1.0	0.25
NL Fmax	0.40	0.60	1.0	-
NL Fnpq2200	0.30	-	1.0	0.20

Chapter 4: Supplementary Information

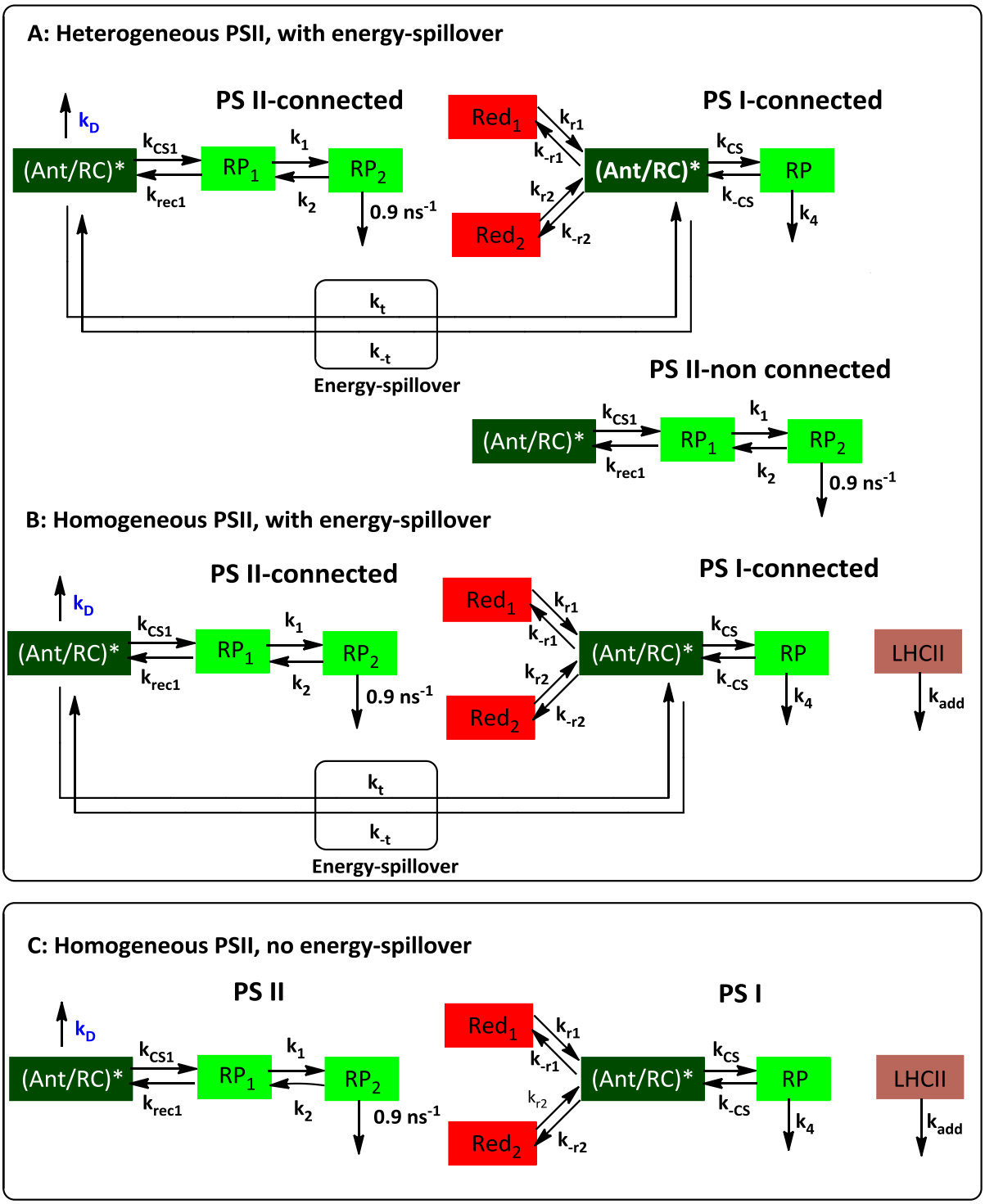

Supplementary Figure 4.1: Kinetic compartment models successful for describing the quenching kinetics of the various light adaptation conditions. The compartment models for PSI and PSII units follow those that have been demonstrated on isolated intact PSI and PSII complexes (Miloslavina, Szczepaniak et al. 2006, Slavov, Ballottari et al. 2008, Slavov, El-Mohsnawy et al. 2009) and on Arabidopsis intact leaves (Holzwarth, Miloslavina et al. 2009, Miloslavina, de Bianchi et al. 2011). The compartment labeling is as follows: Ant/ RC*: antenna/reaction center excited states of PSII or PSI; RPx: radical pairs; LHCII: functionally detached and quenched light-harvesting complex II from PSII.

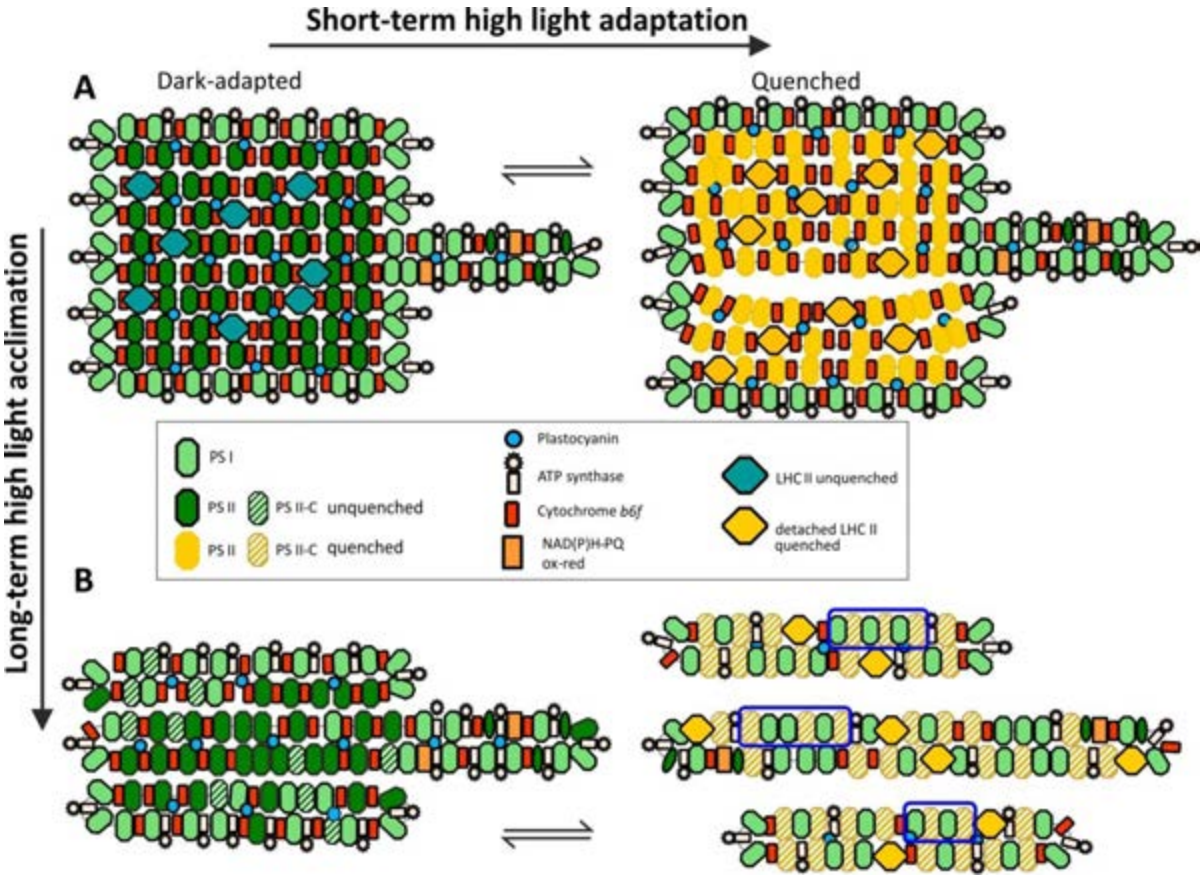

Supplementary Figure 4.2: Schematic depictions of structural and functional organization of thylakoids summarizing the present observations from time-resolved fluorescence and electron microscopy of LL- (A, top) and NL-plants (B, bottom) in their dark-adapted unquenched (left) and high-light-exposed quenched states (right). In LL-plants with pronounced grana stacking in the dark-adapted state, no or only very minor grana unstacking occurs in the quenched state and is not associated with mixing of PSII and PSI units. NL-plants possess shorter grana stacks with looser stacking and extended stroma thylakoids, and show partially mixed PSII and PSI units already in their dark-adapted state. In the quenched state, pronounced unstacking occurs in NL-plants with complete mixing of PSII and PSI units in high light. Three of the high efficiency Q_{SO} quenching units formed under these conditions in NL-plants are highlighted by blue boxes in B (right). The arrangement of membrane complexes (dark-adapted LL-plants, A) shown is based on the membrane organization of dark-adapted *Arabidopsis* thylakoids (Dekker and Boekema 2005). The yellow diamonds in the quenched structures depict detached and quenched LHCII complexes (Holzwarth, Miloslavina et al. 2009). This scheme shows only the four principal arrangement situations of thylakoid architecture suggested by our data. Intermediate architectures are likely to exist for both long-term and short-term acclimation.

Chapter 4: Supplementary Information

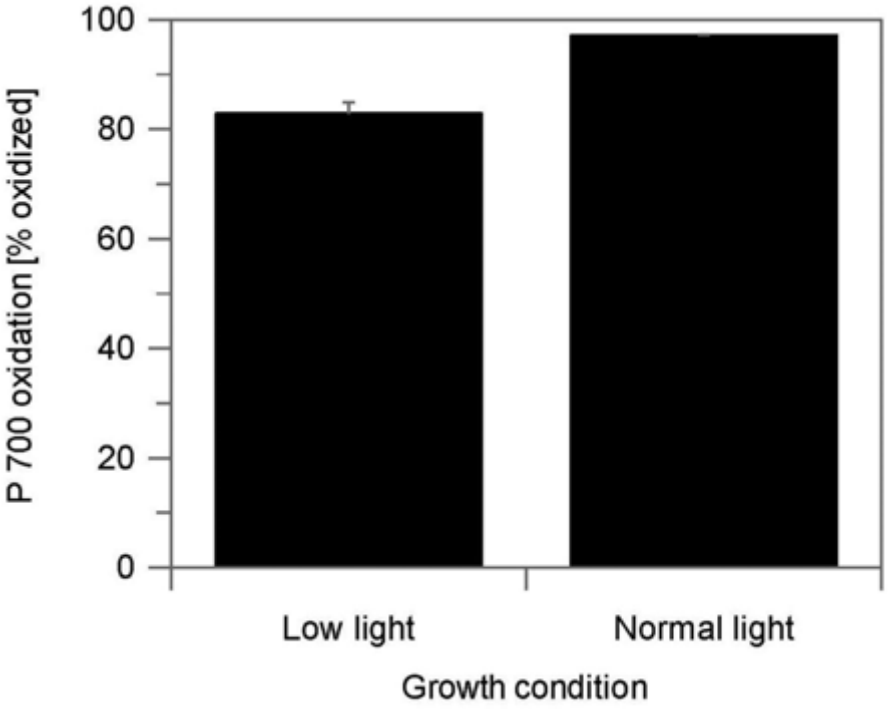

Supplementary Figure 4.3: Oxidation state of P700 in LL and NL leaves in the dark-acclimated state. Leaves were illuminated at 300 µmol photons m^{-2} s^{-1} (LL leaves) or 2000 µmol photons m^{-2} s^{-1} (NL leaves) for up to 10 min until the steady state of P700 oxidation was reached. The fraction of oxidized P700 was ascertained by determination of the fully reduced and oxidized state immediately after switching off the actinic light. Mean values and standard deviation of 3-6 independent measurements are shown.

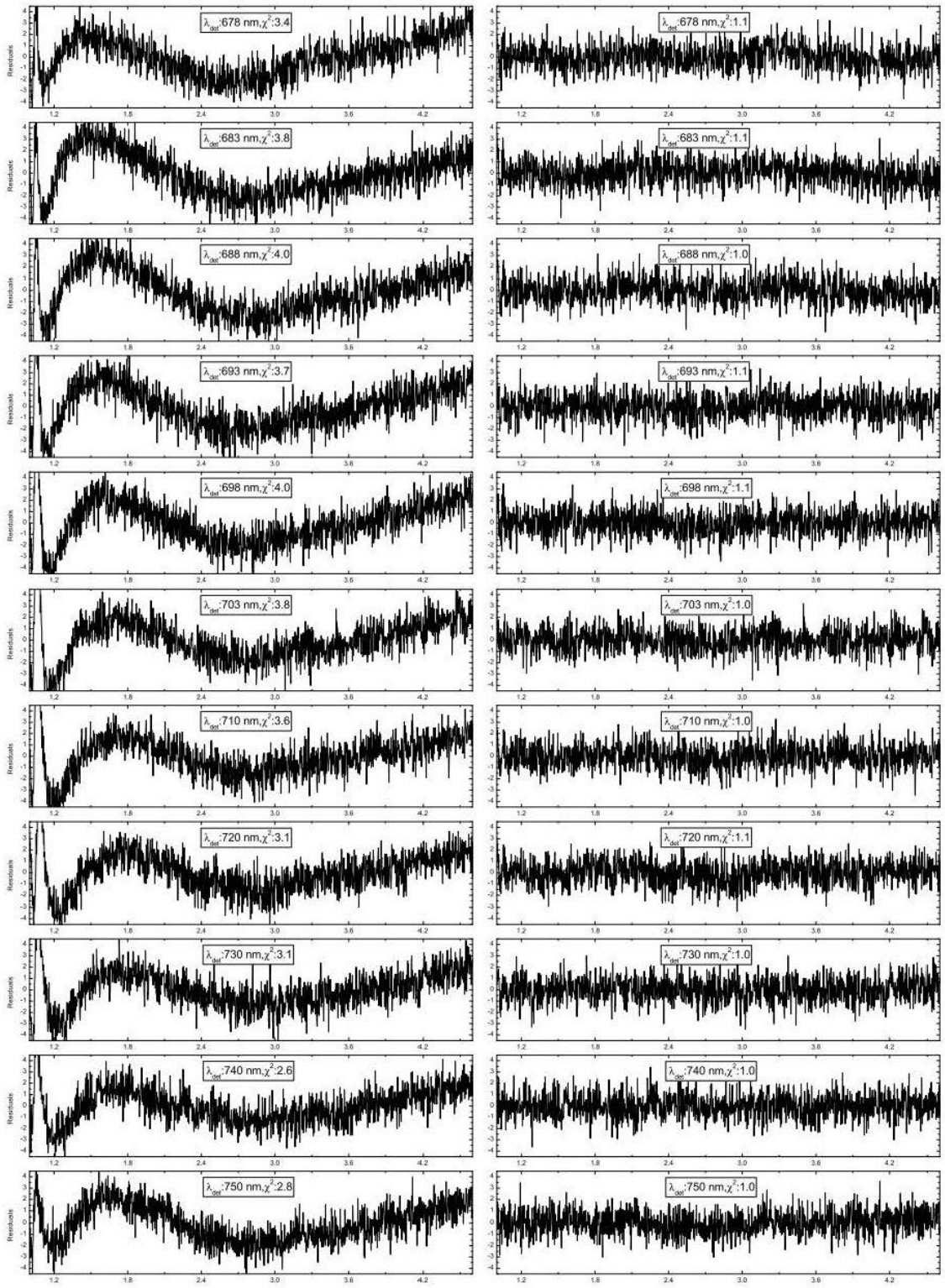

Supplementary Figure 4.4: Comparison of residual plots from global compartment analysis of the kinetics of HL grown plants. Fmax kinetics using a homogeneous spillover PSII model (left, global χ2 = 3.7) vs. a heterogeneous PSII model (spillover + non-spillover PSII, right, global χ2 = 1.08).

Chapter 4: Supplementary Information

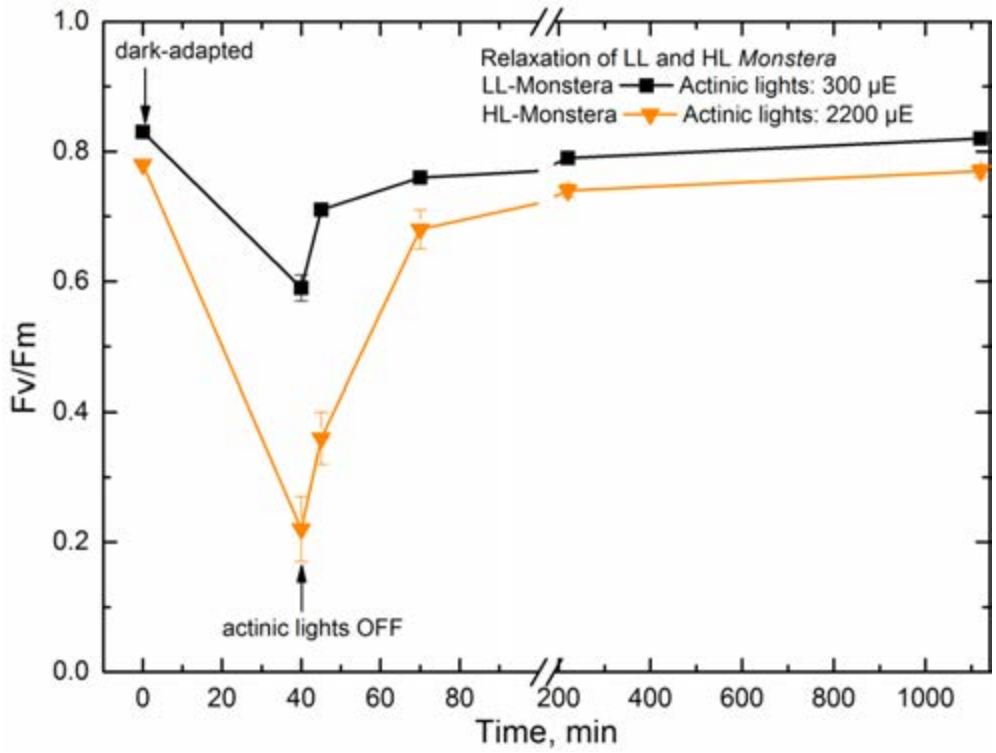

Supplementary Figure 4.5: The relaxation kinetics measured on the LL and NL *Monstera* plants after 30 min of irradiation. For LL *Monstera*, the maximum actinic light used was 300 µmol photons m^{-2} s^{-1}, whereas for NL plants it was 2200 µmol photons m^{-2} s^{-1}. The actinic lights were provided by an array of red-LEDs, identical to those used in time-resolved measurements.

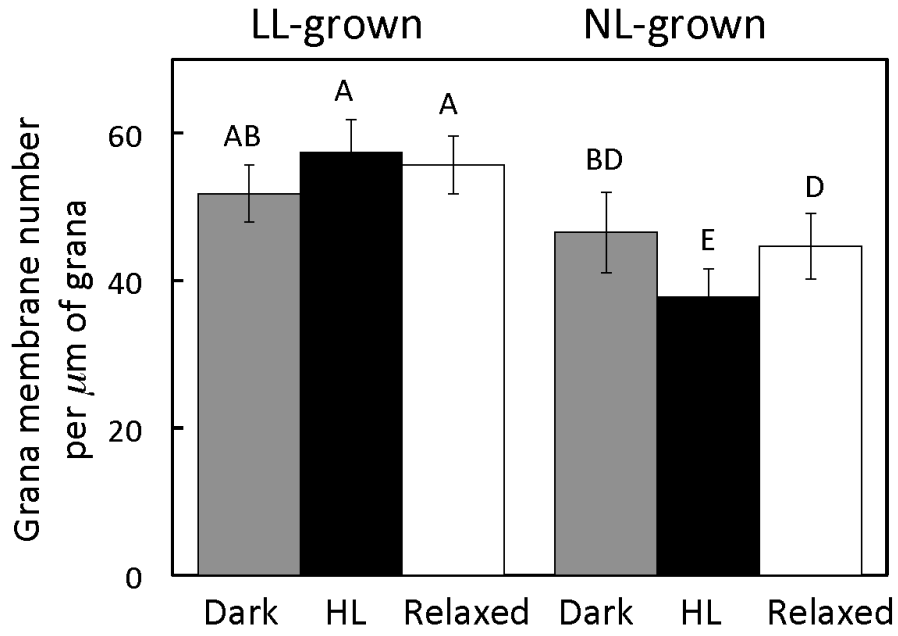

Supplementary Figure 4.6: Number of membranes (mean±SD) present in a given height of a grana stack in chloroplasts of *Monstera* grown either at low-light (LL) or natural sunlight. The measurement shows significant differences among growth environments and treatments (see Figure 4.2 and the associated text for more details).

Chapter 5 : NPQ mechanisms in low-light (LL) grown *Monstera deliciosa*, irradiated with high light (HL)

In the previous chapter, Qso i.e., spillover has been recognized as an efficient quenching mechanism in the natural sunlight grown *Monstera* leaves that transfers excess PSII energy directly to PSI. In contrast in the LL grown plants, probably due to their tighter appressed membrane regions no such PSII-PSI coupling occurred and PSII and PSI centers were functionally well separated. Consequently, the available NPQ capacity was much smaller as compared to NL plants. In the present work, the dark-adapted mature LL-grown leaves from *Monstera* were irradiated to much higher (ca. 10-15 times) light (650-700 µmol photon s^{-2} s^{-1}) intensity for 2 days (12 H/day) or 4 days (12 H/day), increased to even 20 H/day (2 days).

The aim was to study the quenching and changes in the thylakoid membrane to adapt to the increased irradiation and to elucidate the long-term acclimatization strategy employed by these typical LL grown plants to survive under HL stress.

5.1. Results

The quenched (F_{npq}) and unquenched (F_{max}) fluorescence data from the HL irradiated leaf-disks were analysed by the global target method (Holzwarth 1996). The initial kinetic model consisting of laterally segregated PSII and PSI, which was previously successful to describe the kinetics of low-light (LL) grown *Monstera deliciosa* (cf. Chapter 4), was not suitable for a good kinetic fit (see e.g., Supplementary Figure 5.1-3). For the 12-H dark-adapted leaf-samples, a good fit for the time-resolved data was obtained with heterogeneous PSII model (see Supplementary Figure 5.1-3), which was developed earlier to describe the kinetics in dark-adapted natural sunlight (NL) grown *Monstera* (cf. Chapter 4). The results are shown as decay associated spectra (DAS) in Figure 5.1A-3A and the corresponding kinetic rates are shown in Table 5.1. For a HL irradiation period of 2 days (12 H/day), it was found that nearly 40% of the PSII centers were connected to PSI via a spillover mechanism (Table 5.3), similar to our previous reports on NL grown *Monstera*. This percentage of connected PSII (labelled as PSII-C) was found to gradually increase with the HL irradiation period (Table 5.3). For unquenched, dark-adapted samples it was nearly 80%, when the HL treatment was continued for 4 days (12 H/day) and/or increased up to 20 H/day (2 days). The aforesaid changes in the PSII cross-sections of the various PSII pools (increase in PSII-C)

are consistent with the ultrastructure of the thylakoid membrane obtained on identical dark-adapted leaf-sections by electron microscopy (Figure 5.4). Like NL-*Monstera*, widening of the grana stacks and partial destacking as a result of HL-acclimatization (Figure 5.4) was found here also.

The application of strong light (by an array of red-emitting LEDs providing 1200 µmol photons^{-2} s^{-1}) induced quenching in the leaf-disks, as indicated by the NPQ parameter in Table 5.2. Increase in NPQ capacity as a result of prolonged irradiation (Table 5.2) was found. By the virtue of target analysis, we were able to dissect the changes occurred in PSII as well as in PSI, as an effect towards such HL treatment. The quenching mechanism in PSII was grossly comprised of: a) increase in the kinetic rate k_D (Table 5.1), similar to our earlier reports where the excited chlorophylls, most likely from the PSII peripheral antenna proteins are quenched by the carotenoid zeaxanthin (qZ) (Holzwarth, Miloslavina et al. 2009) and b) the PsbS-dependent formation of detached LHCII oligomers (qE) (Holzwarth, Miloslavina et al. 2009), distinguished by the characteristic far-red emission (Miloslavina, Wehner et al. 2008). The DAS are shown in Figure 5.1B-3B. A novel third quenching mechanism was required to fit the time-resolved data obtained from quenched leaf-disks. Previously this was not present in LL-*Monstera*, instead was observed in NL-leaves (cf. Chapter 4). In addition, the quenched states were accompanied by a complete dissolution of PSII heterogeneity (Table 5.3), where all the PSII were directly coupled to the PSI sites. A concomitant increase in spillover rates (k_t in Table 5.1) were also noted compared to their corresponding unquenched states.

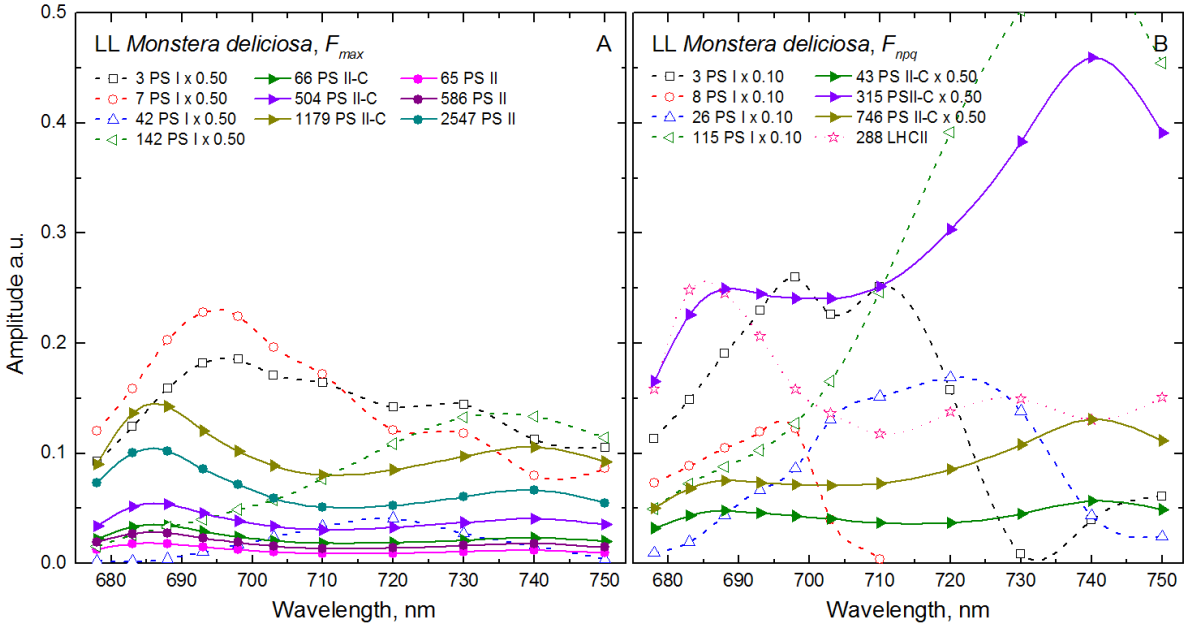

Figure 5.1: Decay-associated spectra (DAS) resulting from kinetic compartment analysis of unquenched (F_{max}) and quenched (F_{npq}) states of LL grown *M. deliciosa* plants, treated with 700 µmol photons m^{-2} s^{-1} light for 12 H/day for 2 days. Components labeled 'PSII' belong to unconnected (non-spillover) PSII, while those labeled 'PSII-C' belong to connected (spillover) PSII units. PSI components are shown as dashed and detached LHCII as a dotted line. For clarity of presentation, only positive amplitude parts are shown.

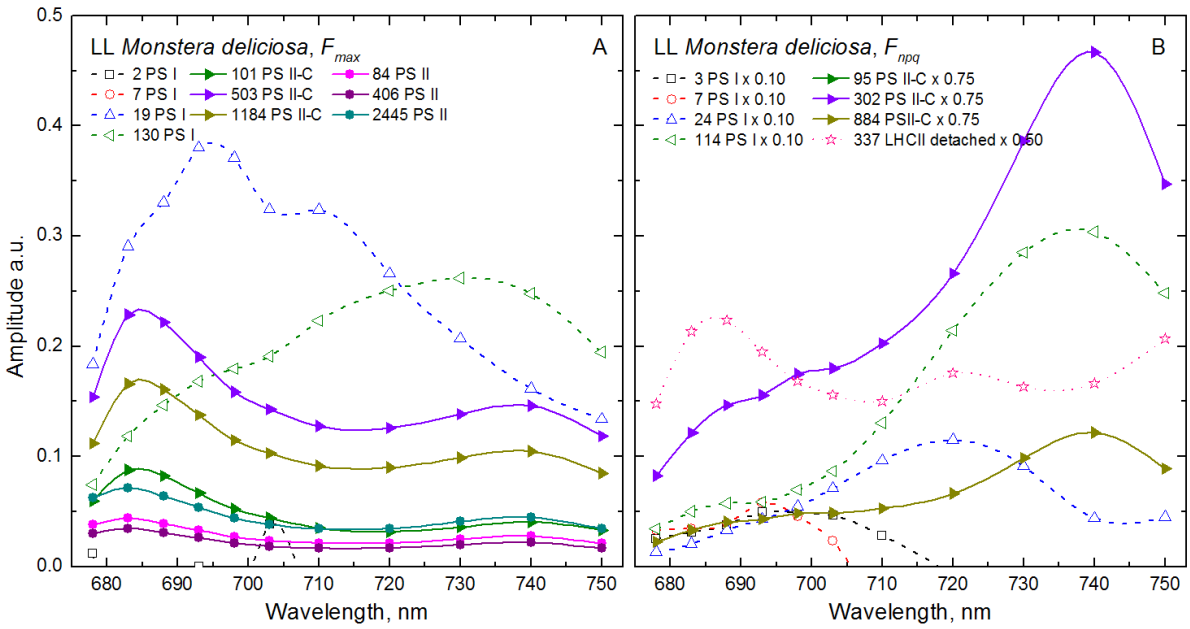

Figure 5.2: Decay-associated spectra (DAS) resulting from kinetic compartment analysis of unquenched (F_{max}) and quenched (F_{npq}) states of LL grown *M. deliciosa* plants, treated with 700 µmol photons m^{-2} s^{-1} light for 12 H/day for 4 days. Components labeled 'PSII' belong to unconnected (non-spillover) PSII, while those labeled 'PSII-C' belong to connected (spillover) PSII units. PSI components are shown as dashed and detached LHCII as a dotted line. For clarity of presentation, only positive amplitude parts are shown.

Chapter 5

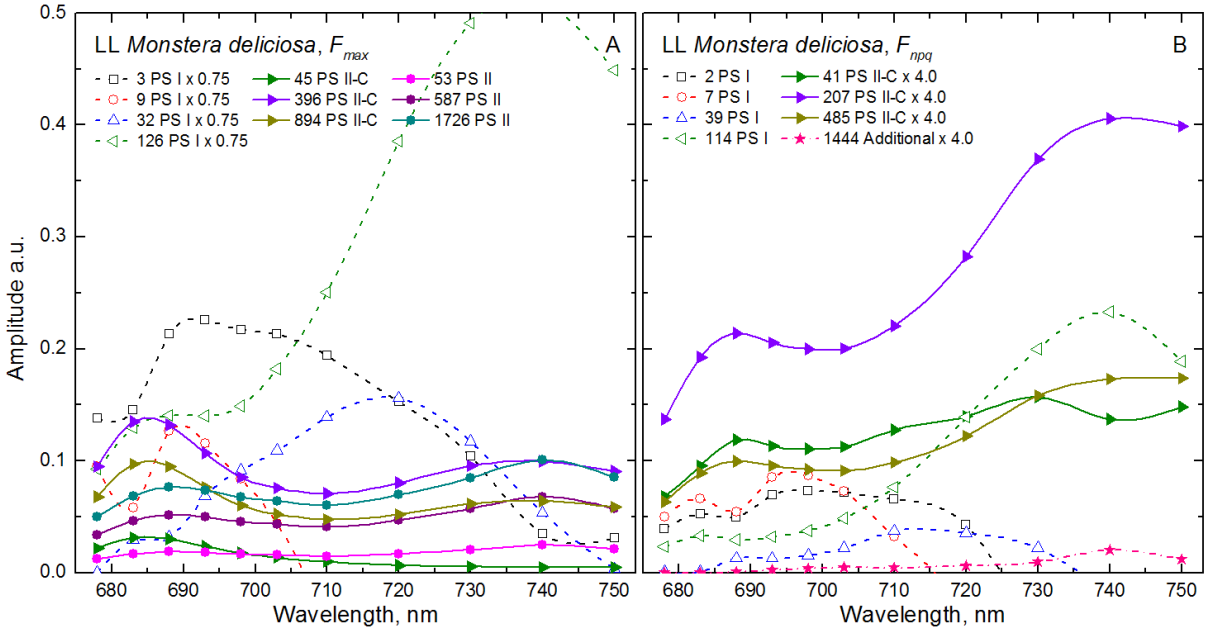

Figure 5.3: Decay-associated spectra (DAS) resulting from kinetic compartment analysis of unquenched (F_{max}) and quenched (F_{npq}) states of LL grown *M. deliciosa* plants, treated with 700 µmol photons m^{-2} s^{-1} light for 20 H/day for 2 days. Components labeled 'PSII' belong to unconnected (non-spillover) PSII, while those labeled 'PSII-C' belong to connected (spillover) PSII units. PSI components are shown as dashed and detached LHCII as a dotted line. For clarity of presentation, only positive amplitude parts are shown.

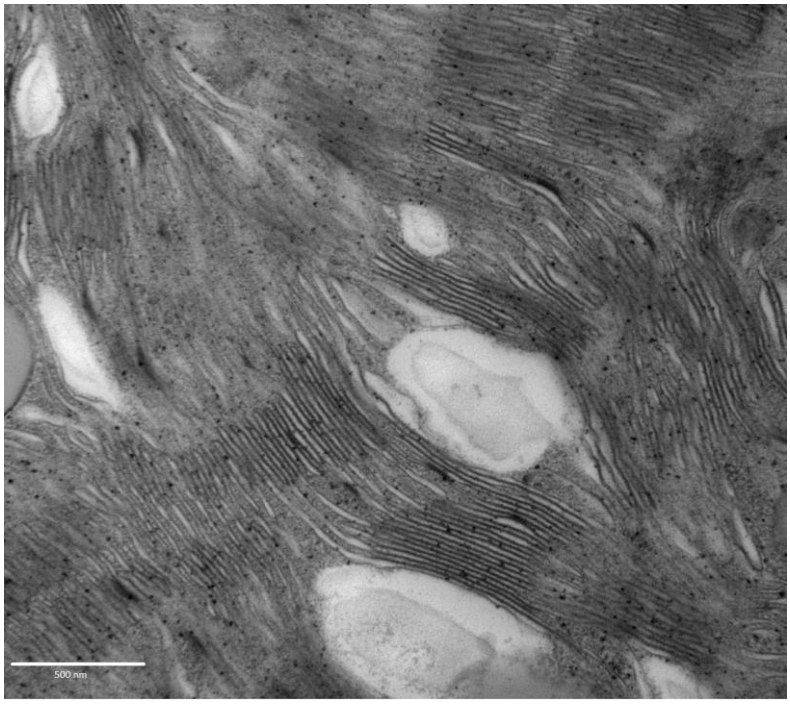

Figure 5.4: Chloroplast ultrastructure from leaves of low-light grown *Monstera deliciosa*, treated with 700 µmol photons m^{-2} s^{-1} light for 12H/day for 3 days. Dark-adapted leaves were taken at the end of the dark period and fixated for electron microscopy as rapidly as possible (in a temperature-controlled chamber at 25°C). The white arrow points to one of the partial destacking areas in high-light-exposed LL thylakoids. The scale (white-bar) is 500 nm. This EM experiment was performed by Dr. Onno Muller and Prof. Barbara Demmig-Adams at the University of Colorado, USA.

5.2. Discussion

5.2.1. HL induced reorganization in the thylakoid structure

From the time-resolved results, it is evident that LL grown *Monstera* leaves not only sustained well under HL treatment, rather they also achieved higher (ca. 2-3 times) photoprotection capacity compared to typical LL-*Monstera* (cf. Chapter 4). The increase in maximal NPQ capacity can largely be attributed to the changes occurring in the thylakoid membrane upon acclimation as seen by the EM image (Figure 5.4). Exposure of LL-leaves to high irradiation (700 µmol photons m^{-2} s^{-1} in this case) for 3 consecutive light-cycles (12 H/day) widened the grana stacks, while typical LL-plants have tightly packed and firmly appressed thylakoids (cf. Chapter 4). The widening of grana stacks correlates with the increase in the PSII fraction connected to PSI complexes (PSII-C, see Table 5.3). The fraction increased from 40% to nearly 80% when the irradiation period was continued up to 4 days (12 H/day) and/or 20 H/day (2 days). Such light induced changes in grana organization were reported in the case of *Arabidopsis* (Yin, Lundin et al. 2010), where prolonged exposure to high light irradiation was shown to modulate the phosphorylation of PSII-antenna proteins (Tikkanen and Aro 2012). The chances of grana destacking by PSII-phosphorylation are elevated under such high light treatment (Demmig-Adams, Ebbert et al. 2006, Tikkanen and Aro 2012). The immediate effects of loss in tight grana packing are revealed by randomization and mixing of PSII units with PSI complexes, leading to pronounced spillover rates (k_t in Table 5.1). The PSII to PSI energy transfers are now comparable to charge-separation kinetics in PSII (Table 5.1). Similar light induced functional changes of thylakoid organization were seen previously for NL-*Monstera* (cf. Chapter 4), where the NL-plants showed a 100% energy-spillover or a complete loss of lateral segregation under quenching state. NL grown *Hedera*, another evergreen plant also showed similar spillover mechanism and an exceptionally high NPQ capacity.

5.2.2. Spillover-type quenching and avoidance of photoinhibition

Based on other comparable experiments performed on NL and HL plants (cf. Chapter 4, 6 and 7), it seems reasonable to propose a spillover quenching (Qso), as the most efficient mechanism to avoid over-excitation and to provide high photoprotection of the PSII complex. However, it must be noted that spillover is not the only quenching mechanism; it works as a parallel third process along with the usual qE (PsbS-dependent) and qZ (Z-dependent) quenching. Interdependency among these three pathways can be expected. An elevated PsbS level (in *L17-Arabidosis*) was found to increase the spillover rate (cf. Chapter 7) as well as the percentage of LHCII detachment

(qE) (Holzwarth, Miloslavina et al. 2009). Since high irradiation is known to increase the PsbS level in *Monstera* (Demmig-Adams, Ebbert et al. 2006); we can, therefore, expect similar PsbS effect on spillover in our experiments also. However, the exact role of PsbS in the spillover mechanism is yet to be established. It is generally believed that PsbS influences the light induced fluidity of the PSII macrostructure (Goral, Johnson et al. 2012), a phenomenon of great significance to couple PSII with nearby PSI sites.

The carotenoid zeaxanthin, which is known to modulate qZ quenching (Holzwarth, Miloslavina et al. 2009) was found to have strong effects on spillover processes also (cf. Chapter 7). In HL grown *npq1-Arabidopsis*, which cannot accumulate Z upon HL treatment, spillover mechanism was totally abolished (cf. Chapter 7). It was proposed that Z is likely to be involved in the grana stacking (Rock, Bowlby et al. 1992) and during its absence, the PSII architecture tends to be more static and non-responsive towards light, possibly leading to more appressed grana stacks. This can be interpreted as strong lateral segregation among the two photosystems when Z is not accumulated and as a result, transfer of excess PSII energy as spillover is prevented. An absence of spillover mechanism was found to affect the NPQ capacity (cf. Chapter 7), as the Z-deficient HL-mutant was less photoprotected compared to the HL-wild-type (cf. Chapter 7).

The HL treatment applied in the present study was ca. 10-15 times stronger compared to the usual growth lights for these plants. Under such HL condition, an inhibition of the PSII activity or the so-called photoinhibition would be expected (Murata, Takahashi et al. 2007). In typical LL plants, the PSII remains confined to the appressed grana region and usually does not have any HL light induced mobility (cf. Chapter 4); this increases the chances of damage in PSII compared to their replenishment by D1 protein synthesis (Tikkanen, Mekala et al. 2014). However, in our study, we found that acclimation towards HL irradiation has widened the grana stacks (Figure 5.4); a major reorganization or mobility in the thylakoid structure that allowed the transfer of excess PSII energy as spillover (Table 5.1). A prolonged continuation to such HL conditions, for example, 20 H/day or 4 days, have increased the spillover rates subsequently, may be due to further loss in grana stacking (can be assumed from the increases in PSII-C fraction, as in Table 5.3). These results seem to suggest that by virtue of increasing spillover, the leaves might have prevented the damage to the PSII sites and spillover of excess energy may be the only alternative route (Quigg, Kotabová et al. 2012) to protect PSII from HL damage. Increase in spillover under photoinhibitory conditions is also supported by an earlier study (Ögren, Öquist et al. 1984), where the increase was found to occur along with partial uncoupling of electron transport chain (Samuelsson,

Lönneborg et al. 1985). In certain cases, spillover mechanism has been found to work in parallel with other regulatory measures (Santabarbara, Garlaschi et al. 1999) to avoid the loss of D1 protein (Oliver, Whittington et al. 2003). Therefore, it is evident that HL acclimation involves a significant contribution from draining the excess PSII energy as spillover and requires reorganization in the thylakoid architecture.

Table 5.1: Rate constants (ns^{-1}) for the PSII and PSI kinetics in *Monstera deliciosa*, determined from the kinetic target analysis. The LL (50-60 µmol photons m^{-2} s^{-1}) grown plants were irradiated to 700-750 µmol photons m^{-2} s^{-1} actinic lights under various light/dark regimes. PSII-C: PSII fraction that is connected to the PSI-core via spillover energy transfer; k_t and k_{-t} are the forward and backward spillover rates from the PSII to the PSI core. The k_3 rate from closed PSII units is fixed to 0.9 ns^{-1} (Holzwarth, Miloslavina et al. 2009). The errors in the kinetic rates are within ± 10%.

	PSII-C (connected)				**PSII unconnected**			**PSI**				
	k_D	k_{CS1}/k_{rec1}	k_1/k_2	k_t/k_{-t}	k_D	k_{CS1}/k_{rec1}	k_1/k_2	k_{r1}/k_{-r1}	k_{r2}/k_{-r2}	k_{CS}/k_{-CS}	k_4	**LHCII**
12H/day for 2 days												
Fmax	0.30	2.3/11	1.7/0.90	0.77/0.42	0.30	2.2/10	2.6/0.80	28/49	17/64	115/123	160	-
Fnpq	1.2	3.3/16	4.0/1.1	1.2/0.30	-	-	-	41/26	25/80	134/143	113	3.5
12H/day for 4 days												
Fmax	0.30	2.1/5.6	2.4/0.7	0.82/0.3	0.30	3.9/6.3	2.1/1.24	62/21	11/54	184/107	180	-
Fnpq	0.85	2.8/5.1	2.6/1.2	1.7/0.04	-	-	-	44/19	24/80	86/97	180	2.9
20H/day for 2 days												
Fmax	0.30	3.1/16	3.5/1.0	1.3/0.04	0.30	3.0/12	4.6/0.50	39/27	13/41	158/139	122	-
Fnpq	2.21	5.6/16	2.7/2.4	2.0/0.2	-	-	-	28/33	19/66	141/150	180	0.69

Table 5.2: Average lifetime τav [ps] of the fluorescence decays for the *Monstera deliciosa* leaves calculated from the kinetic data at 683 nm emission wavelength (excitation at 663 nm). The LL (50-60 µmol photons m^{-2} s^{-1}) grown plants were irradiated to 700-750 µmol photons m^{-2} s^{-1} actinic lights under various light/dark regimes. The errors in the average lifetimes are ±5%, errors in the other values are ±10%. NPQ values were calculated from the fluorescence decays at 683 nm according to the equation

$$\mathrm{NPQ} = \frac{\tau_{\mathrm{av@Fmax}}}{\tau_{\mathrm{av@Fnpq}}} - 1$$

Also shown are the lifetimes [ps] of the component appearing under NPQ conditions assigned to functionally detached and quenched LHCII, along with the percentage of LHCII detachment as measured by the decrease in total PS II cross-section in the quenched vs. the unquenched state. PSII-C denotes the PSII fraction connected by spillover to PSI.

	12H/day		20H/day
	2 days	4 days	2 days
τ_{av} of PS II+PSI, ps			
F_{npq}	270	150	105
F_{max}	1100	850	520
τ of quenched LHC II oligomers, ps	288	337	1444
NPQ [a]	3.0	5.6	4.0
% of detached LHC II [b]	30	30	52

a) These numbers for the NPQ values derived from the lifetime measurements can be directly compared with those measured by conventional steady state NPQ induction. They fully agree within the error limits.

b) Measured as percentage of total absorption cross-section (at the excitation wavelength of 663 nm) of dark-adapted PSII that is detached as quenched LHCII.

Table 5.3: Excitation vectors for the various antenna compartments resulting from kinetic compartment analysis for the time-resolved kinetic data of *Monstera deliciosa* leaves. The suffix 'C' denotes the PS II units connected through energy-spillover with PSI. The errors are in the range of ±10%.

	PSII-Ant/RC-C	PSII-Ant/RC	PSI-Ant/RC	LHCII
12H/day for 2 days				
Fmax	0.40	0.60	1.0	-
Fnpq	0.65	-	1.0	0.30
12H/day for 4 days				
Fmax	0.80	0.20	1.0	-
Fnpq	0.65	-	1.0	0.30
20H/day for 2 days				
Fmax	0.80	0.20	1.0	-
Fnpq	0.40	-	1.0	0.45

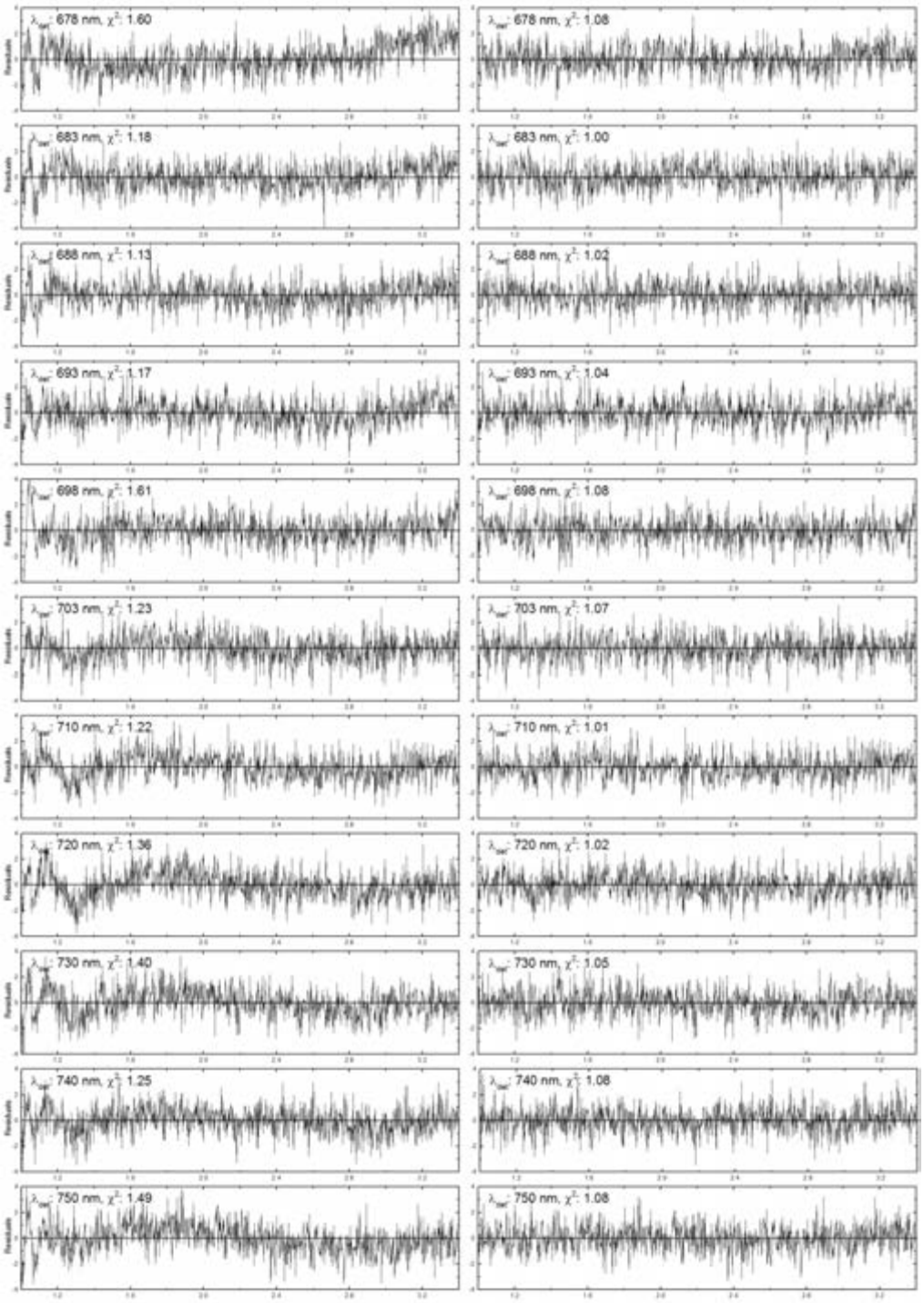

Supplementary Figure 5.1: Comparison of residual plots from global compartment analysis of the kinetics when the LL (50-60 µE) grown plants were irradiated 700 µmol photons m^{-2} s^{-1} actinic lights for 2 days (12H/day). Fmax kinetics using a homogeneous spillover PSII model (left, global χ^2 = 1.31) vs. a heterogeneous PSII model (spillover + non-spillover PSII, right, global χ^2 = 1.03).

Chapter 5: Supplementary Information

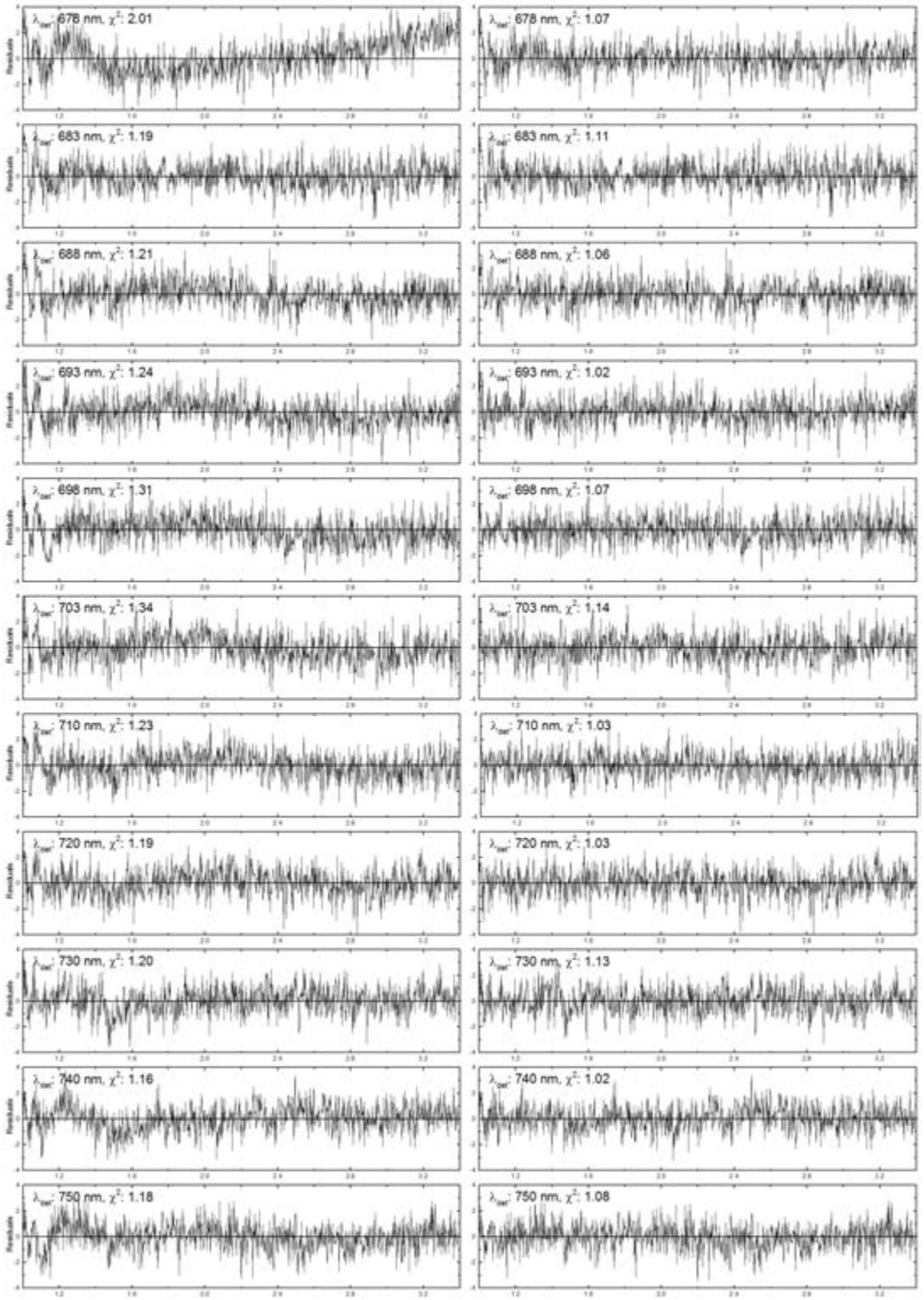

Supplementary Figure 5.2: Comparison of residual plots from global compartment analysis of the kinetics when the LL (50-60 µE) grown plants were irradiated to 700 µmol photons m^{-2} s^{-1} actinic lights for 4 days (12H/day). Fmax kinetics using a homogeneous spillover PSII model (left, global χ^2 = 1.31) vs. a heterogeneous PSII model (spillover + non-spillover PSII, right, global χ^2 = 1.03).

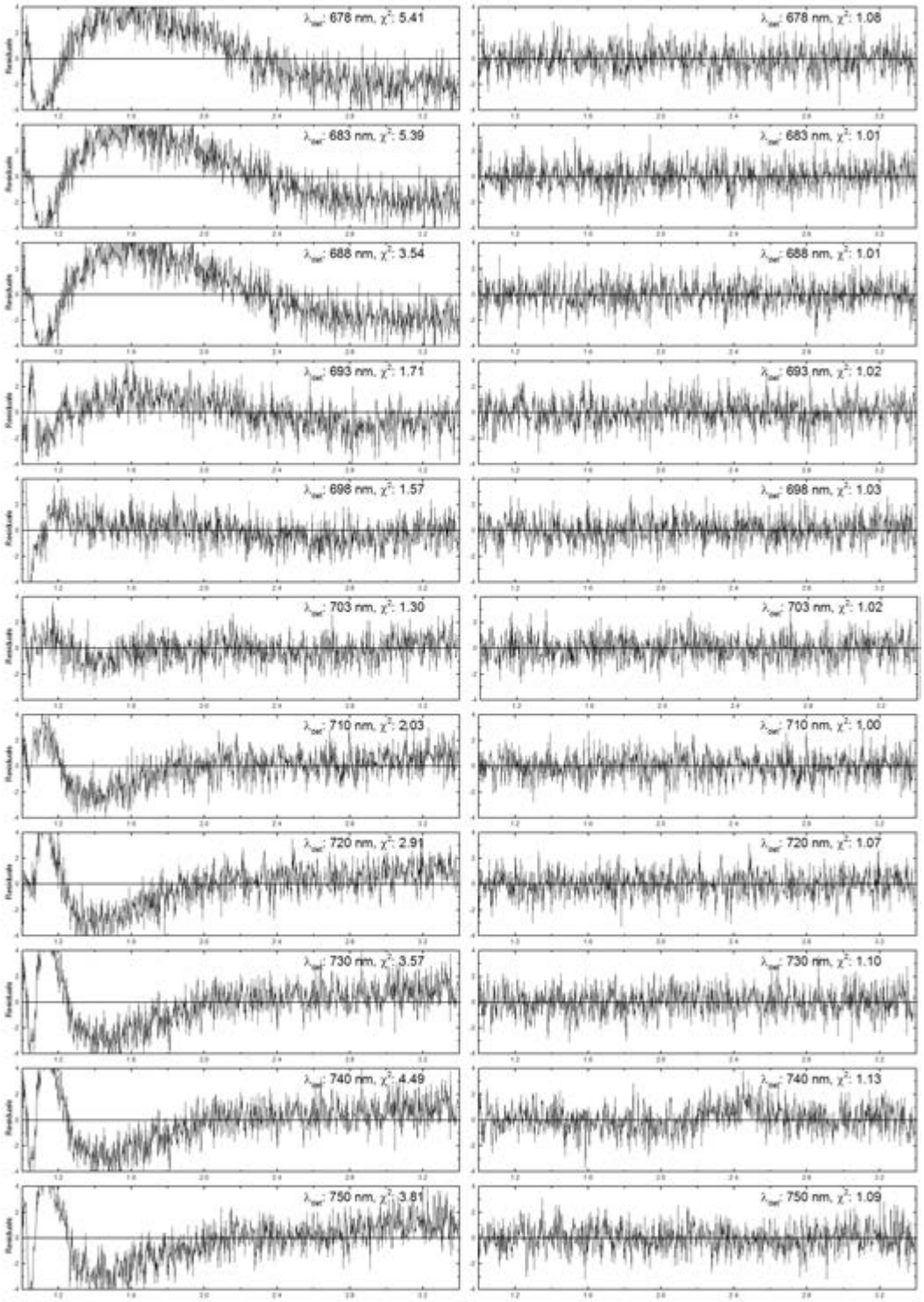

Supplementary Figure 5.3: Comparison of residual plots from global compartment analysis of the kinetics when the LL (50-60 µE) grown plants were irradiated to 700 µmol photons m^{-2} s^{-1} actinic lights for 2 days (20H/day). F_{max} kinetics using a homogeneous spillover PSII model (left, global χ^2 = 1.31) vs. a heterogeneous PSII model (spillover + non-spillover PSII, right, global χ^2 = 1.03).

Chapter 6 : NPQ mechanisms in natural sunlight grown evergreens: *Hedera helix* and *Prunus laurocerasus*

The NPQ mechanisms in two evergreen plants in addition to more extensive studies on *Monstera* are investigated to collect further information related to light induced functional reorganization in the thylakoid structure. In the following work, we have selected plants which were grown at outdoors under natural sunlight (May-August 2011) and fully sun exposed leaves were used in the measurements.

6.1. Results

6.1.1. Pigment content

The pigment content of the dark-adapted leaves and the effect of NPQ (high light treatment) on the DEPS ratio were determined by HPLC analysis. The results are presented in Table 6.1. Dark-adaptation of leaves was carried out for at least 10-12 h. For high light adaptation, leaves were illuminated for 30 min under an array of red-LED-intensity of 1,400 μmol photons m^{-2} s^{-1} (F_{npq} conditions). These two evergreen plants contained similar amounts of Chl b, Nx, Lut and β-Car relative to Chl a. However, significant differences existed in the total xanthophyll cycle pigments (VAZ). *Prunus* had a lower VAZ pool as compared to *Hedera*. High intensity light treatment increased the de-epoxidation state from virtually zero to 40-60% in these plant species.

6.1.2. Global target analysis and development of spillover model

The fluorescence measurements were performed over the whole range of Chl fluorescence from 678 to 750 nm. For target analysis we tested the kinetic models developed for analogous measurements carried on *Monstera deliciosa* (Chapters 4-5) and *Arabidopsis thaliana* (Chapter 7). The kinetic schemes that were used for the analysis of the fluorescence data are discussed in detail in Chapter 4.

The rate constants from the target analysis of the analysis are shown in Table 6.2. The simplest kinetic scheme consisting of homogenous PSII and four-PSI compartments (Holzwarth, Miloslavina et al. 2009) could not yield good fit for the unquenched (Fmax) fluorescence data (see Supplementary Figure 6.1 and 6.2 for the residuals). Rather it was found that a heterogeneous PSII kinetic scheme, containing a second pool of

'connected PSII' centres was required to deliver a good fit for the data (see the residuals plots in Supplementary Figure 6.1-2). Based on the previously developed concept of the heterogeneous scheme, the PSII-centres that are in contact with PSI are labelled as 'PSII-C'. The resulting decay-associated-spectra (DAS) for the target analysis are shown in Figure 6.1. The energy spillover rates for the connected PSII centres are labelled as k_t in Table 6.2.

In the NPQ-activated state, the PSII heterogeneity had mostly disappeared and nearly all (80% in *Prunus* and 100% in *Hedera*) of the PSII-centres were found to be in contact with PSI (Table 6.4), along with increased spillover rates vs. the dark-adapted leaves (Table 6.2). The corresponding DAS are shown in Figure 6.2 and the rate constants are compiled in Table 6.2.

Apart from these changes in the relative cross-sections of the two PSII pools (Table 6.4), connected vs. unconnected PSII, adaptation to strong actinic light changed other PSII parameters as well: a) a ca. 3-4 times increase occurred in the rate constant k_D, the PSII-attached antenna deactivation rate (Table 6.2), and b) the formation of an additional far-red emitting unconnected component was required to fit the F_{npq} quenching condition in *Hedera* (Figure 6.2 and Table 6.3). However, the leaves from *Prunus* maintained PSII heterogeneity (reduced to nearly 20%) even under strong actinic lights and no such additional far-red emitting species was observed (Figure 6.2 and Table 6.3). The other remaining PSII and PSI rate constants remained within error limits to our previous measurements on open and closed PSII particles and intact *Arabidopsis* leaves (Slavov, Ballottari et al. 2008, Holzwarth, Miloslavina et al. 2009, Miloslavina, de Bianchi et al. 2011).

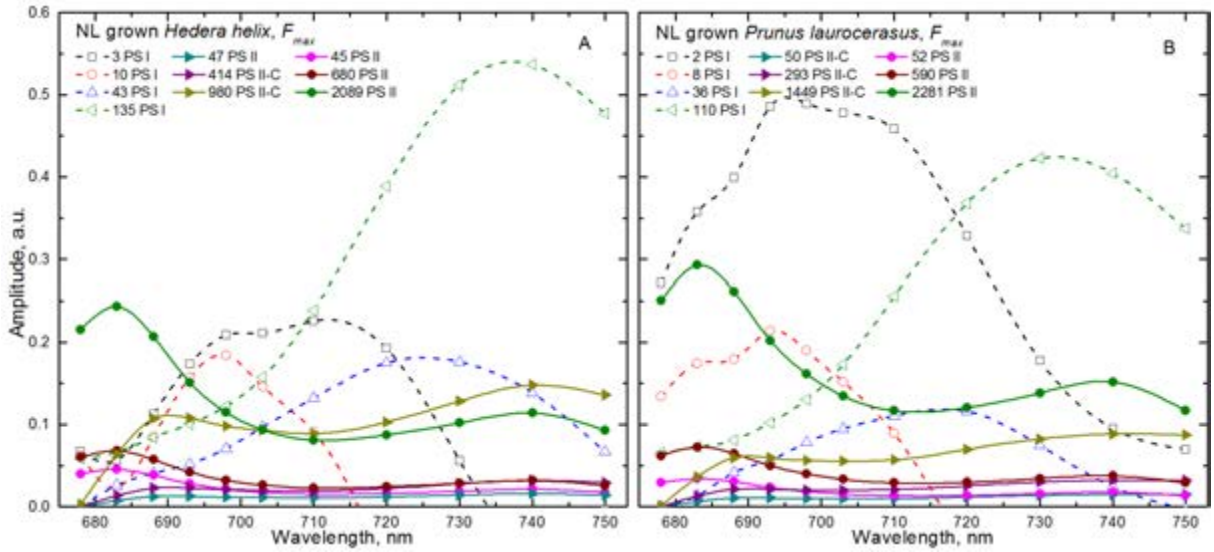

Figure 6.1: Decay-associated spectra resulting from kinetic compartment analysis of unquenched states of NL grown *Hedera* and *Prunus* plants. Components labeled PSII belong to unconnected (non-spillover) PSII, while those labeled PSII-C belong to connected (spillover) PSII units. PSI components are shown as dashed. For clarity of presentation, only positive amplitude parts are shown.

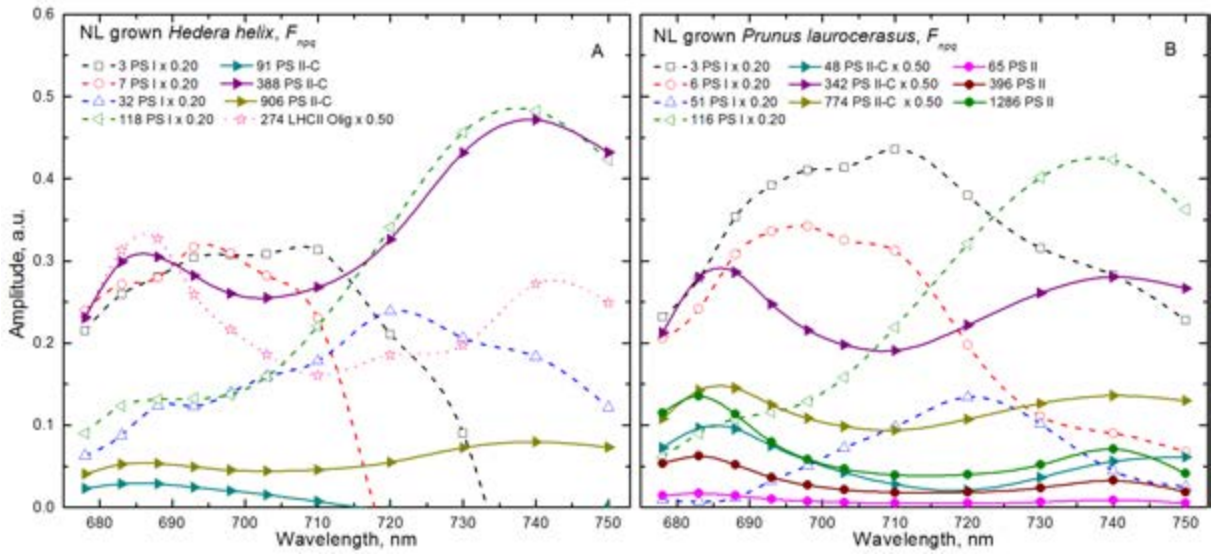

Figure 6.2: DAS resulting from kinetic compartment analysis of quenched states of NL grown *Hedera* and *Prunus* plants. Components labeled PSII belong to unconnected (non-spillover) PSII, while those labeled PSII-C belong to connected (spillover) PSII units. PSI components are shown as dashed and detached LHCII as a dotted line. For clarity of presentation, only positive amplitude parts are shown.

Chapter 6

6.2. Discussion

For NPQ conditions, the results indicate similar types of quenching mechanisms persisting among all studied evergreen species (see Chapter 4 for NL-*Monstera*). Grossly, a 2-3 fold increase in the deactivation rate of PSII-antenna from its dark-adapted value of 0.3 ns^{-1} was observed, assessed by the kinetic rate constant k_D, believed to be Z-dependent (Holzwarth, Miloslavina et al. 2009), qZ-type (Nilkens, Kress et al. 2010). This increase in k_D is, however, much lower than found previously on NL-*Monstera* leaves (cf. Chapter 4). One reason could be that the intensity of actinic lights used in the current work was not high enough as compared to the outdoor growth light intensity. Further light induced change was observed only for the PSII supercomplex of *Hedera*. Nearly 54% of the PSII antenna cross-section (mainly comprised of LHCII) (Holzwarth, Miloslavina et al. 2009) was dissociated and subsequently quenched (determined from its characteristic far-red emission) in *Hedera* (Table 6.3). This fraction reflects the quenched LHCII and was previously attributed to the centre of qE-quenching site, also observed in LL as well as NL-*Monstera* (cf. Chapter 4), although it never exceeded 30% in them (cf. Chapter 4). One reason for a higher LHCII dissociation from the PSII supercomplex in *Hedera* could be due to an elevation in PsbS level as a part of their acclimation strategy to sustain under outdoor growth condition (Demmig-Adams, Ebbert et al. 2006). PsbS protein, most likely as an allosteric factor was found to influence the formation and quenching of LHCII oligomers (Holzwarth, Miloslavina et al. 2009). Unfortunately, the actual PsbS level could not be determined for *Hedera* and *Prunus* due to a poor binding with antibody.

The maximal NPQ capacity, as shown in Table 6.3, for these two evergreen plants are analogous to plants grown under HL (cf. Chapter 7) and NL (cf. Chapter 4) and largely derive from the transfer of PSII excitation via a direct spillover pathway. In their dark-adapted unquenched states, the PSII showed a heterogeneous arrangement (as can be calculated from the PSII cross section in Table 6.4), where not many PSII centers (less than 30%) were connected with PSI. Adaptation to NPQ lights changed this fraction, increased it to a 100% connected model in *Hedera* (80% in *Prunus*). We can explain the reason for such light induced increases in PSII-C as a result of loss in grana stacking, as was recognized in NL-*Monstera* (cf. Chapter 4), perhaps, followed by a major structural reorganization leading to a tighter coupling between PSII and nearby PSI sites. The immediate effect of spillover is reflected through the higher NPQ capacity. For *Hedera*, the total NPQ was found to be 5-6 times higher compared to constant low-light grown plants (Holzwarth, Miloslavina et al. 2009). However, for *Prunus*, application of identical

actinic light did not switched on 100% spillover, nearly 20% of the PSII-fraction remained unconnected to PSI. Although the NPQ capacity in *Prunus* was higher as compared to low-light grown plants (Holzwarth, Miloslavina et al. 2009), but it was found to be 3-4 times less than *Hedera*. A higher PsbS level, as can be assumed from the higher content of detached LHCII, can also be responsible for flexible dissolution of grana stacks in *Hedera*. We found similar analogy for PsbS influence on spillover in case of HL-grown *L17-Arabidopsis* (cf. Chapter 7), which showed significantly higher spillover rates and stronger NPQ capacity among other genotypes.

As a future step, one should determine the exact levels of PsbS protein in these plants to ascertain the dependency between the mobility of photosynthetic proteins, particularly PSII and PsbS content. In this regard, it is also necessary to identify the phosphorylated percentage of PSII antenna, which may be the key to answer such architectural changes leading to most efficient energy-spillover to happen.

Table 6.1: Pigment compositions of the dark and light-adapted leaves from *Hedera helix* and *Prunus laurocerasus* grown under NL condition measured under equivalent conditions to those used in the lifetime measurements for inducing NPQ [The pigment content was determined by HPLC of leaves from five samples for each condition. Dark-adapted leaves were illuminated for 30 min under conditions equivalent to inducing NPQ (identical actinic light intensities were used during the time-resolved measurements). Mean values ± SD is shown]. The units are mmol per mol Chl (a+b).

Leaf pigments	***Hedera helix***		***Prunus laurocerasus***	
Neoxanthin	29.09± 1.77		32.27± 0.27	
VAZ	78.18± 0.94		50.00± 9.72	
Lutein	70.52± 3.45		73.48± 6.16	
β-carotene	59.25± 3.00		54.90± 5.89	
Chlorophyll a/b	4.39± 0.06		4.42± 0.21	
DEPS	0.03 ± 0.20 (dark-adapted)	0.41 ± 0.06 (high light treated)	0.05 ± 0.02 (dark-adapted)	0.60±0.08 (high light treated)

Table 6.2: Rate constants (ns-1) for the PSII and PSI kinetics in the NL grown *Hedera helix* and *Prunus laurocerasus* determined from the kinetic target analysis. PSII-C: PSII fraction that is connected to the PSI-core via spillover energy transfer; k_t and k_{-t} are the forward and backward spillover rates from the PSII to the PSI core. The k_3 rate from closed PSII units is fixed to 0.9 ns^{-1} (Holzwarth, Miloslavina et al. 2009). The errors in the rates are within ± 10%.

	PSII-C (connected)				**PSII unconnected**			**PSI**				
	k_D	k_{CS1}/k_{rec1}	k_1/k_2	k_t/k_{-t}	k_D	k_{CS1}/k_{rec1}	k_1/k_2	k_{r1}/k_{-r1}	k_{r2}/k_{-r2}	k_{CS}/k_{-CS}	k_4	**LHCII**
Hedera - Fmax	0.30	1.9/17	1.9/1.4	0.86/0.20	0.30	3.1/16	2.9/0.42	28/26	13/38	134/133	129	-
Prunus - Fmax	0.30	2.9/13	3.8/2.4	0.48/0.86	0.30	1.9/14	3.8/0.71	34/52	19/57	175/125	106	-
Hedera - Fnpq	0.81	1.4/6.0	3.5/0.74	1.2/0.17	-	-	-	14/26	59/61	108/135	150	3.6
Prunus - Fnpq	0.53	4.0/14.3	2.6/1.1	1.7/0.71	0.86	1.6/9.6	4.2/1.7	27/80	15/32	123/78	174	-

Table 6.3: Average lifetime τav [ps] of the fluorescence decays for the *Hedera helix* and *Prunus laurocerasus* leaves grown under NL condition were calculated from the kinetic data at 683 nm emission wavelength (excitation at 663 nm). The errors in the average lifetimes are ±5%, errors in the other values are ±10%. NPQ values were calculated from the fluorescence decays at 683 nm according to the equation

$$\mathrm{NPQ} = \frac{\tau_{\mathrm{av@Fmax}}}{\tau_{\mathrm{av@Fnpq}}} - 1$$

Also shown are the lifetimes [ps] of the component appearing under NPQ conditions assigned to functionally detached and quenched LHCII, along with the percentage of LHCII detachment as measured by the decrease in total PS II cross-section in the quenched vs. the unquenched state. PSII-C denotes the PSII fraction connected by spillover to PSI.

	Hedera	*Prunus*
τ_{av} of PS II, ps		
F_{npq}	68	160
F_{max}	1040	750
τ of quenched LHC II oligomers, ps	274	
NPQ [a]	14	4.0
% of detached LHC II [b]	54	-

a) These numbers for the NPQ values derived from the lifetime measurements can be directly compared with those measured by conventional steady state NPQ induction. They fully agree within the error limits.

b) Measured as percentage of total absorption cross-section (at the excitation wavelength of 663 nm) of dark-adapted PSII that is detached as quenched LHCII.

Table 6.4: Excitation vectors for the various antenna compartments resulting from kinetic compartment analysis for the time-resolved kinetic data of *Hedera helix* and *Prunus laurocerasus* leaves grown under NL condition. The suffix 'C' denotes the PS II units connected through energy-spillover with PSI. The errors are in the range of ±10%.

	PSII-Ant/RC-C	**PSII-Ant/RC**	**PSI-Ant/RC**	**LHCII**
Hedera helix - Fmax	0.30	0.60	1.0	-
Prunus laurocerasus - Fmax	0.25	0.65	1.0	-
Hedera helix - Fnpq	0.25	-	1.0	0.30
Prunus laurocerasus - Fnpq	0.40	0.10	1.0	-

Chapter 6: Supplementary Information

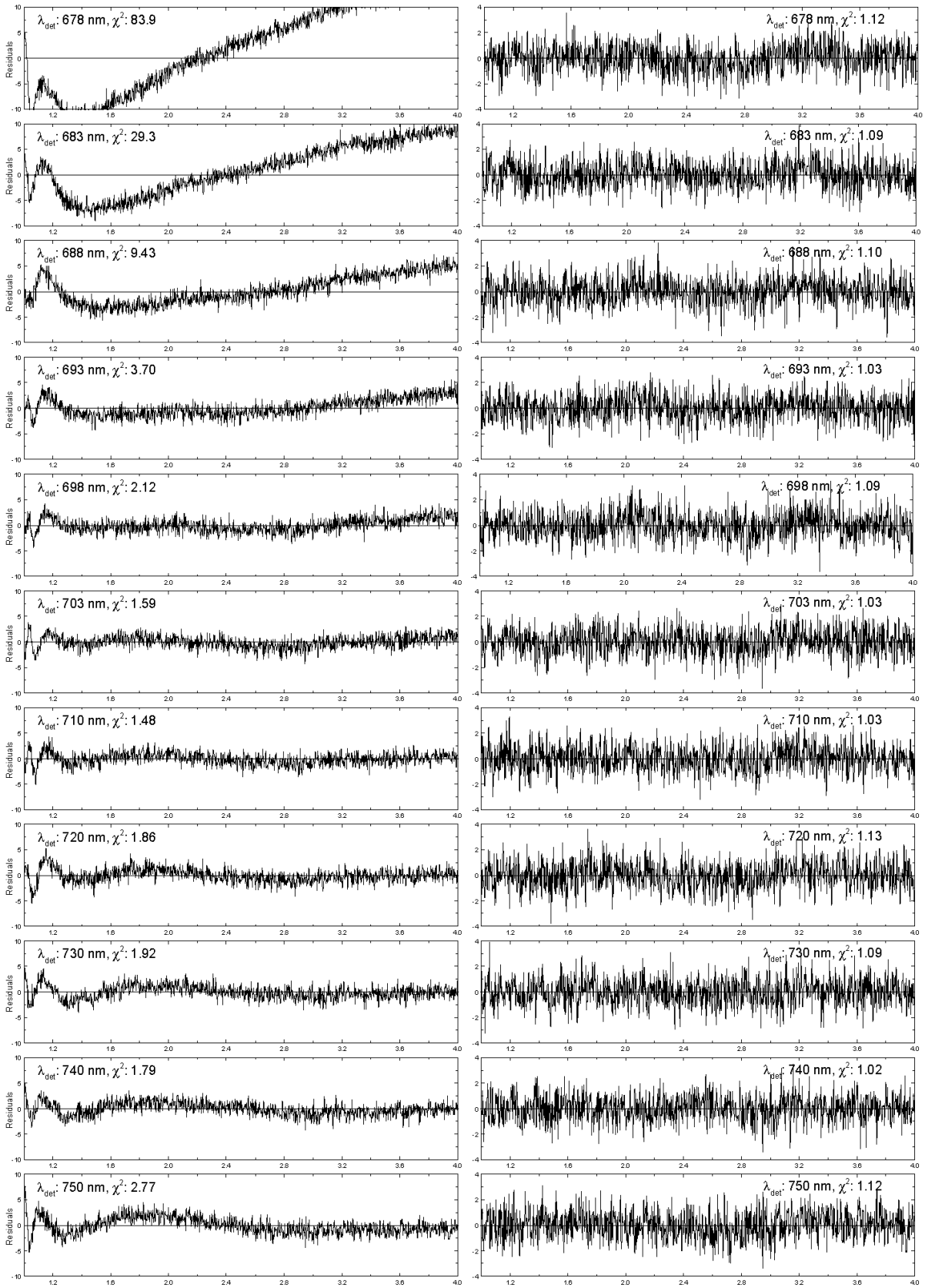

Supplementary Figure 6.1: Comparison of residual plots from global compartment analysis of the kinetics of NL grown *Hedera* plants. Fmax kinetics using a homogeneous spillover PSII model (left, global χ^2 = 12.6) vs. a heterogeneous PSII model (spillover + non-spillover PSII, right, global χ^2 = 1.06).

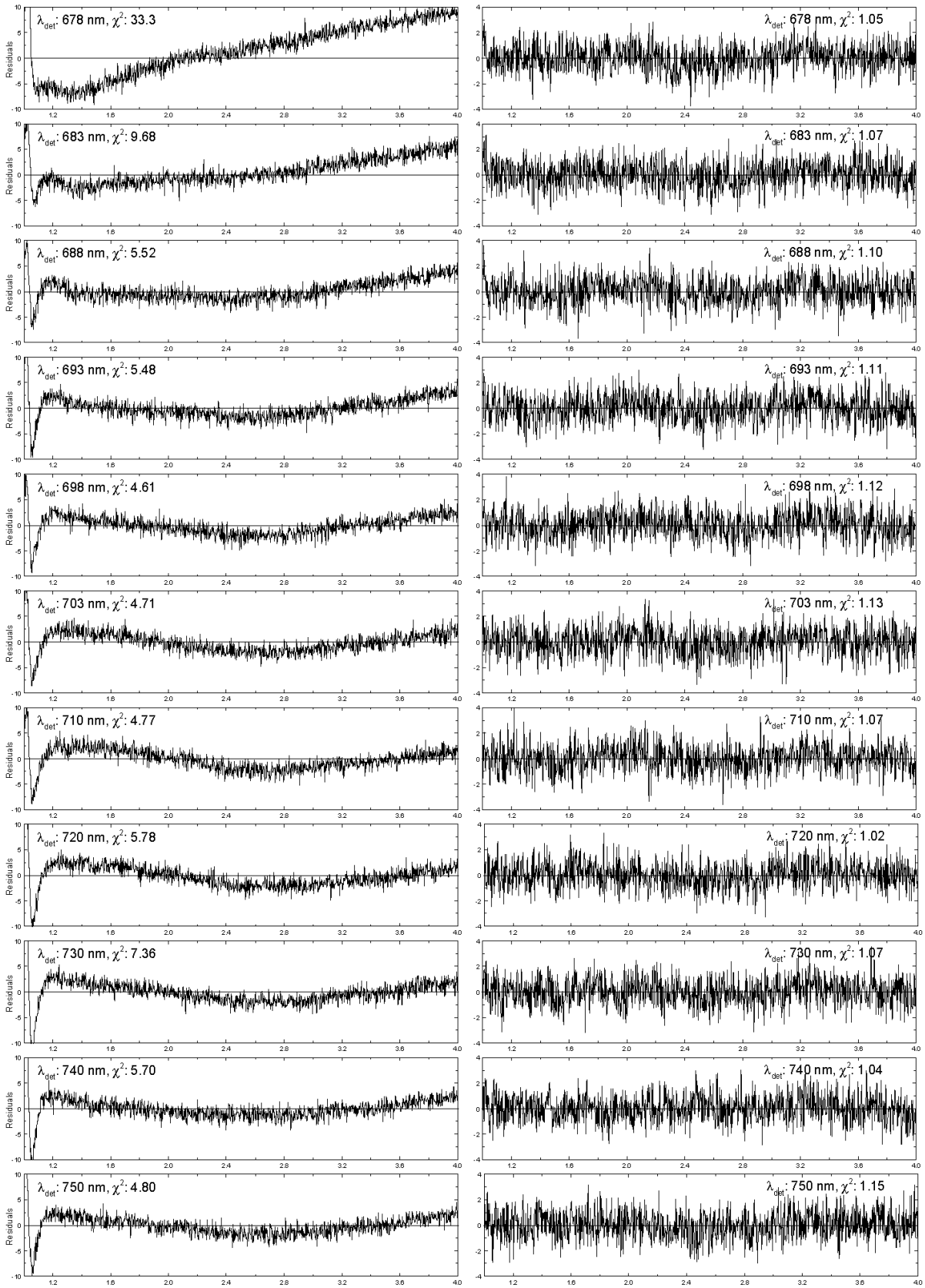

Supplementary Figure 6.2: Comparison of residual plots from global compartment analysis of the kinetics of NL grown *Prunus* plants. Fmax kinetics using a homogeneous spillover PSII model (left, global χ^2 = 8.27) vs. a heterogeneous PSII model (spillover + non-spillover PSII, right, global χ^2 = 1.07).

Chapter 7 : NPQ mechanisms in *Arabidopsis thaliana* grown under high-light (HL) condition

Arabidopsis thaliana is very well documented in the plant physiology literature, because of the availability of a large number of mutants, where desired photosynthetic pigment(s) could be abolished. In past decades, the thylakoid models developed on *Arabidopsis* served as prototype for typical low-light grown plants, with laterally segregated photosystems and reduced photoprotection. In the following work, we measured NPQ mechanisms on the plants grown under high light (500-600 µmol photons s^{-2} s^{-1}). Contrasting results were expected in terms of better photoregulation. This work has also investigated the acclimatization mechanisms for sustaining under high light, important for a plant that is long been envisaged as a typical low-light or shade plant.

7.1. Results

7.1.1. Pigment content

The effect of irradiation on the pigment composition of the leaves was estimated by making pigment extracts followed by the characterization using HPLC, as mentioned in the Materials and methods section. The results are presented in Table 7.1 for w.t., *L17*, *npq4* and *npq1* genotypes. Dark-adapted leaves were kept in the dark for at least 12 h. Light-adapted leaves were illuminated for 30 min at a light-intensity of 1,200 µmol photons m^{-2} s^{-1} (F_{npq} conditions). All genotypes contained similar amounts of Chl b, Nx, Lut, β-Car, and total XC pigments, (VAZ), relative to Chl a. These stoichiometries were not altered by the used illumination conditions. However, upon illumination the de-epoxidation state of the VAZ pool increased from virtually zero to nearly 60% in w.t. and *npq4* mutant. For *L17* mutant, this increase was only 40%. As expected, no light-induced de-epoxidation was detected in the *npq1* mutant.

7.1.2. Fluorescence decays in quenched an unquenched conditions

Figure 7.1 shows the Chl fluorescence decays for the four *Arabidopsis* genotypes at 683 nm. Measurements were performed either on dark-adapted (unquenched) or high light-adapted (quenched) leaf discs. While the unquenched kinetics were similar among these genotypes, the kinetics in the quenched states differ strongly. The PsbS overexpressor

L17 mutant had the strongest quenching capacity compared to other mutants. Wild-type plants had intermediate decay.

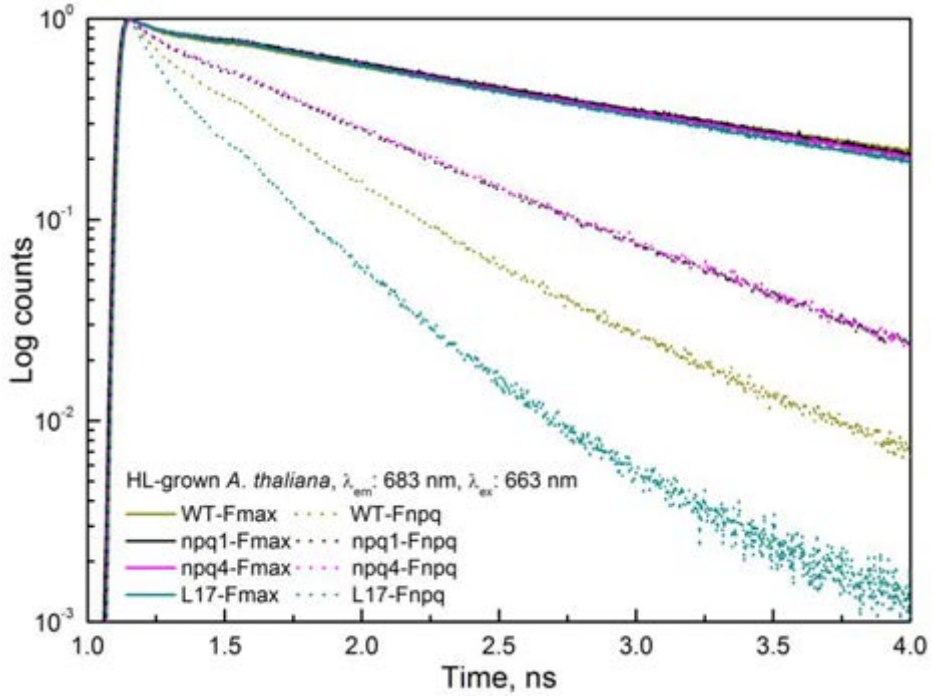

Figure 7.1: Fluorescence decays of wild-type and mutant *Arabidopsis* plants, either at unquenched or quenching conditions. Note that *L17* had the fastest decay, therefore, strongest quenching.

7.1.3. Global target analysis and component separation

The fluorescence measurements were performed over the whole range of Chl fluorescence from 675 to 750 nm. Chl fluorescence originating from PSI and PSII overlaps in this range. However their lifetimes and spectral shapes differ, depending on the origin of the fluorescence (PSI or PSII, separated antenna etc.) and the state of the PSII RC (open vs. closed RCs), etc. (Holzwarth 1988). In order to perform the target analysis we make use of the detailed knowledge that has been gained from kinetic studies of the *Arabidopsis* wild-type and mutant leaves (Holzwarth, Miloslavina et al. 2009, Lambrev, Miloslavina et al. 2012). These studies defined the principal kinetic reaction schemes underlying the fluorescence kinetics of PSI and PSII. The rate constants of the analysis are shown in Table 7.2 and the decay-associated-emission spectra (DAES) in Figures 7.2 and 7.3. The simplest kinetic scheme consistent with full lateral segregation of two photosystems in the dark-adapted unquenched state, could not yield reasonable fits for the w.t., *npq4* and *L17* plants (Supplementary Figures 7.1-3); rather a heterogeneous model was assumed, where a second pool of PSII centres (labelled as 'PSII-C') were connected to PSI via the spillover-type arrangement. The quenched states in these genotypes were, however, could be fitted well with a

homogeneous PSII model involving fast spillover, like what we observed in case of *Monstera* (Chapter 4). On the contrary, the Z deficient *npq1*-mutant maintained lateral segregation between PSII and PSI, in dark as well as light-adapted states.

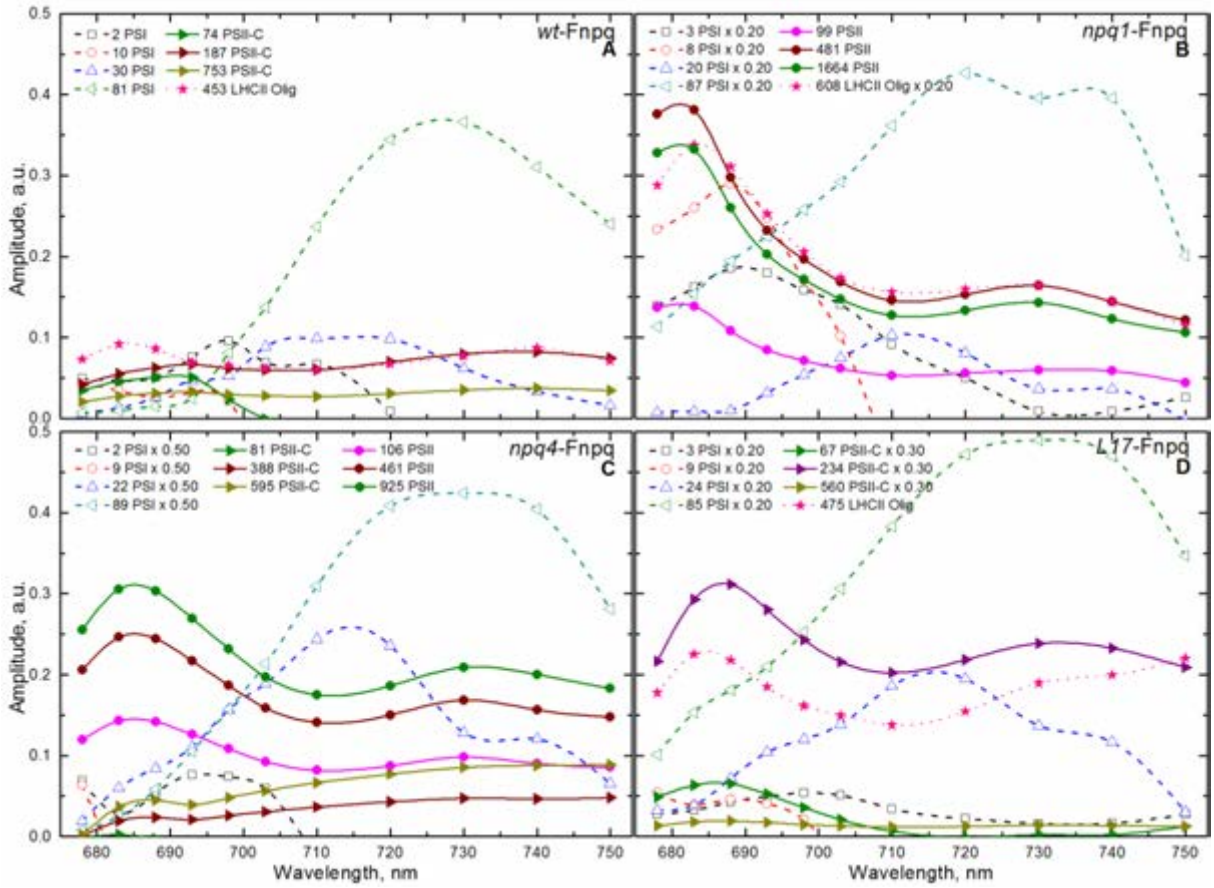

Figure 7.2: Decay-associated spectra (DAS) resulting from kinetic compartment analysis of quenched states of HL grown *A. thaliana* plants. Components labeled PSII belong to unconnected (non-spillover) PSII, while those labeled PSII-C belong to connected (spillover) PSII units. PSI components are shown as dashed and detached LHCII as a dotted line. For clarity of presentation, only positive amplitude parts are shown.

In line with our previous studies on *Arabidopsis* (Holzwarth, Miloslavina et al. 2009), the quenched states in w.t., *npq4* and *L17* plants were associated with the three-five-fold increase in the PSII-attached antenna deactivation rate constant, assessed by the rate constant k_D (ns^{-1}). This increase has been attributed to the activation of Z-dependent qZ type of quenching (Holzwarth, Miloslavina et al. 2009, Miloslavina, de Bianchi et al. 2011), as, no such increase in k_D was noted in case of *npq1*-mutant which was unable to accumulate Z under light. An additional kinetic component was required to fit the PsbS-dependent detachment of LHCII from the PSII supercomplex. This new fluorescing component could not be described within the PSI or PSII kinetic schemes and had enhanced far-red emission, strongly reminiscent of qE quenching (Lambrev, Nilkens et

al. 2010, Lambrev, Miloslavina et al. 2012). Its peak amplitude relative to total PSII were 40% for w.t., 20% for *L17* and 70% for *npq1* (Table 7.3).

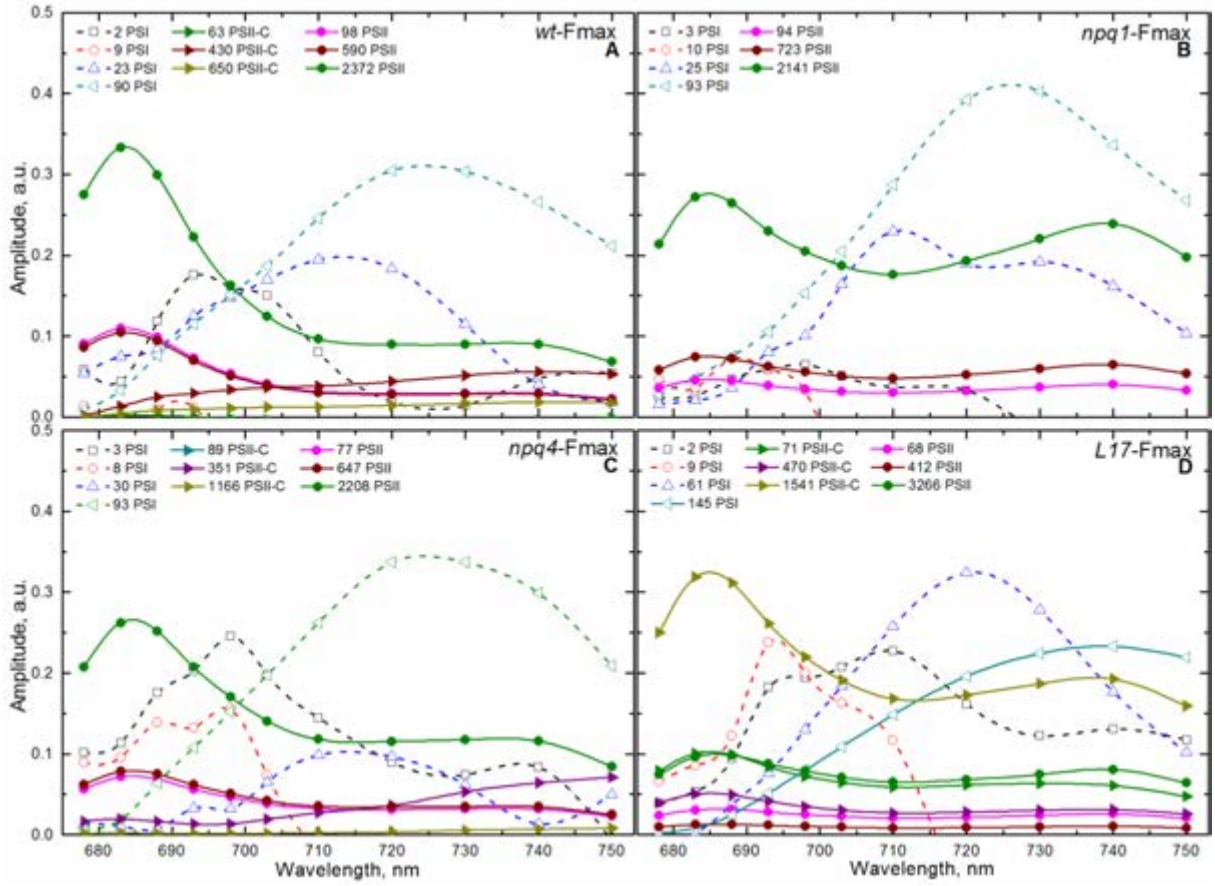

Figure 7.3: Decay-associated spectra (DAS) resulting from kinetic compartment analysis of unquenched states of HL grown *A. thaliana* plants. Components labeled PSII belong to unconnected (non-spillover) PSII, while those labeled PSII-C belong to connected (spillover) PSII units. PSI components are shown as dashed and detached LHCII as a dotted line. For clarity of presentation, only positive amplitude parts are shown.

7.2. Discussions

7.2.1. Mechanisms of non-photochemical quenching

The results indicated two major changes in the PSII kinetics, induced by high-light. The first was the 3-4 fold increase in the so-called PSII-antenna deactivation rate (k_D). Interestingly, no such increase was observed in case of *npq1*-mutant. This finding is in strong correlation with an earlier study done by Holzwarth et al. (Holzwarth, Miloslavina et al. 2009), where it was proposed that formation of Z is required for such PSII-deactivation to operate. Since, Z remains strongly attached to the minor LHC-antennas, it is therefore, reasonable to assume that the location for this quenching site is actually on the strongly coupled S-trimers. PsbS protein may not be involved in this quenching mechanism, as increase in k_D was not altered in PsbS deficient *npq4*-plants. Several mechanisms were proposed to understand this quenching. A direct deactivation

of Chl-excited states by Z (Frank, Cua et al. 1994) was later refined into the formation of carotenoid cation in $Chl^{-}Z^{+}$ charge transfer (CT) state (Holt, Zigmantas et al. 2005). These models were, however, discarded by a recent femtosecond TA measurement, where the quenching of Chl singlets were found to be independent of any carotenoid (Müller, Lambrev et al. 2010). Although, a definite mechanism remains elusive, such type of PSII deactivation is, nevertheless, very important for the plants to survive under high light stress, as can be judged from the calculated NPQ-values (Table 7.3), where the *npq1*-mutant, due to lack of Z was more susceptible to high-light stress compared to the wild-type. The conversion of Z from its precursor V is a relatively slow process (10-15 min) and reminiscent of the Q2 (or qZ) type of quenching proposed earlier (Nilkens, Kress et al. 2010). Such Z induced quenching mechanism is, however, completely reversible as can be seen from the recovery of F_v/F_m with time (Supplementary Figure 7.4) in absence of light.

The second light induced change in PSII was the formation of so-called additional far-red emitting species (Figure 7.3). Similar report was published earlier (Holzwarth, Miloslavina et al. 2009), where it was proposed that this new component was LHCII trimers, detached under quenching condition from the remaining PSII-complex. LHCII-units, after detachment gets quenched independently, believed to be via a Chl-Chl CT-mechanism (Miloslavina, Wehner et al. 2008). The percentage of detachment was found to be modulated with the level of PsbS protein and was abolished completely in PsbS deficient *npq4*-plants. The exact course of PsbS action, is however, controversial (Niyogi, Li et al. 2005), as PsbS does not bind pigments (Dominici, Caffarri et al. 2002) and can only induce a regulating effect (Holzwarth, Miloslavina et al. 2009). The function of PsbS requires protonation (Müller, Li et al. 2001) and was reported to have a very fast activation and relaxation kinetics (1-2 min), similar to Q1 (or qE) type of quenching (Lambrev, Nilkens et al. 2010).

7.2.2. Importance of energy-spillover in NPQ

Our results suggest that there remains a parallel, third type of quenching pathway, that works in addition to qE and qZ mechanisms. This novel mechanism was not seen previously in case of identical genotypes, which were grown at 150 µmol photons m^{-2} s^{-1} (Holzwarth, Miloslavina et al. 2009) that was nearly 3.5 times lower than the current growth conditions. The need of additional quenching is also apparent from the measured NPQ values (Table 7.3), which are much higher compared to reports available to date (Holzwarth, Miloslavina et al. 2009). *w.t.*, *npq4* and *L17*-plants had developed this quenching mechanism, while *npq1*-mutant did not. The rationale behind this could

be the role of Z in the function of thylakoid, grana stacking and PSII activity (Rock, Bowlby et al. 1992), which was absent in *npq1*-plants.

We call this new mechanism as energy-spillover, where PSII and PSI centres were directly connected and mutually shared the incident excitation (Chapter 4). Previously, this type of mechanism was developed as an alternative to 'mobile PSII antenna' hypothesis during state-transition (Yokono, Murakami et al. 2011). An extension to this concept for stress related studies are appearing only recently (Slavov, Reus et al. 2013), where more than 70% of the PSII quenching was attributed to spillover type direct energy transfer from PSII to PSI. There is a strong structural implication behind the feasibility of such energy transfer to operate, which in turn is directly related with the distribution of proteins, especially PSII and PSI among different regions in thylakoid membrane. A spillover type mechanism is not unreasonable in *Arabidopsis* plants, where a grana destacking is known to happen as result of prolonged exposure to high light (Yin, Lundin et al. 2010), which can promote the mobility of photosystem proteins (Kirchhoff, Sharpe et al. 2013). Time-resolved fluorescence technique is the only non-invasive method, where we were able to distinguish the relative amount of PSII and PSI based on their radiation cross section, as was determined in Table 7.4. We see a major structural rearrangement induced by actinic light, where nearly all the PSII units were connected to PSI sites; a 100% energy-spillover became operational at rates comparable to the PSII charge-separation kinetics. However, *npq4*-mutant constrained within PSII heterogeneity and only a marginal increase in spillover rates occurred. This data, when compared with PsbS overexpressor *L17*-genotype, indicates a modulation of NPQ as a function of energy-spillover. PsbS protein was recognized previously as a controller of PSII function (Kiss, Ruban et al. 2008), as well as a primary requirement for a sustained NPQ (Li, Björkman et al. 2000). We propose a similar regulatory role of the PsbS protein in spillover, where its function is, perhaps, limited to the fluidity of thylakoid, thereby, accelerating a reorganization in the PSII macrostructure (Goral, Johnson et al. 2012). PsbS protein, alone cannot be a sole contributor to spillover, as in *npq4*-mutant, where PsbS is completely abolished, a reasonable 25% of PSII centres remained in contact with PSI, even under quenching condition. The protonation of PsbS protein can also assist the excitation balance via spillover (Jajoo, Mekala et al. 2014). Light dependent protein phosphorylation can also be a major factor to enhance or suppress the energy-spillover (Zucchelli, Islam et al. 1987). Such phosphorylation may lead to unstacking and randomization of PSII and PSI centres in thylakoid that enhances spillover (Akoyunoglou and Argyroudi-Akoyunoglou 1986). The reason for unstacking was later

correlated to the slowdown of PSII D1 protein turnover (Fristedt, Willig et al. 2009) and possibly the release of oxygen-evolving proteins from damaged PSII (Baena-González and Aro 2002).

Chapter 7

Table 7.1: Pigment composition of the dark and light-adapted leaves from the HL grown *Arabidopsis thaliana* (wt and mutants) under equivalent conditions to those used in the lifetime measurements for inducing NPQ [The pigment content was determined by HPLC of leaves from five samples for each condition. Dark-adapted leaves were illuminated for 30 min under conditions equivalent to inducing NPQ (identical actinic light intensities were used during the time-resolved measurements). Mean values ± SD is shown]. The units are mmol per mol Chl (a+b).

Leaf pigments	***wild type***		***L17(psbsOE)***		***npq4 (psbs-1.3)***		***npq1***	
	dark-adapted	light-adapted	dark-adapted	light-adapted	dark-adapted	light-adapted	dark-adapted	light-adapted
Nx	33 ± 1	32 ± 0	30 ± 2	30 ± 0	33 ± 1	32 ± 1	34 ± 1	31 ± 1
VAZ	31 ± 2	33 ± 1	30 ± 5	26 ± 1	33 ± 3	34 ± 1	37 ± 7	29 ± 1
Lut	93 ± 5	96 ± 1	86 ± 8	87 ± 4	91 ± 7	93 ± 2	91 ± 5	82 ± 2
β-Car	65 ± 0	60 ± 0	47 ± 2	48 ± 1	51 ± 1	52 ± 1	51 ± 1	46 ± 2
Chl *a/b*	4.31 ± 0.06	4.51 ± 0.03	4.82 ± 0.05	4.76 ± 0.03	4.03 ± 0.15	4.05 ± 0.12	4.09 ± 0.07	4.03 ± 0.15
DEPS	0.08 ± 0.02	0.67 ± 0.01	0.10 ± 0.02	0.42 ±0.02	0.05 ± 0.01	0.62 ± 0.01	0.02 ± 0.00	0.02 ± 0.00

Table 7.2: Rate constants (ns^{-1}) for the PSII and PSI kinetics in the HL grown *Arabidopsis thaliana* (wt and mutants) determined from the kinetic target analysis. PSII-C: PSII fraction that is connected to the PSI-core via spillover-energy transfer; k_t and k_{-t} are the forward and backward spillover rates from the PSII to the PSI core. The k_3 rates from closed PSII units are fixed to 0.9 ns^{-1} (Holzwarth, Miloslavina et al. 2009). The errors in the rate constants are within ± 10%.

	PSII-C (connected)				**PSII unconnected**			**PSI**				
	k_D	**k_{CS1}/k_{rec1}**	**k_1/k_2**	**k_t/k_{-t}**	**k_D**	**k_{CS1}/k_{rec1}**	**k_1/k_2**	**k_{r1}/k_{-r1}**	**k_{r2}/k_{-r2}**	**k_{CS}/k_{-CS}**	**k_4**	**LHCII**
wt-Fmax	0.30	2.6/12	0.7/0.9	2.2/0.4	0.30	2.3/6.3	1.8/0.67	60/30	15/27	194/141	131	-
wt-Fnpq	1.6	4.2/5.6	3.0/3.1	1.8/0.2	-	-	-	41/24	17/25	196/144	123	2.21
npq1-Fmax	-	-	-	-	0.30	1.5/6.8	2.6/0.41	25/29	50/21	72/116	135	-
npq1-Fnpq	-	-	-	-	0.40	2.4/4.5	3.8/0.82	56/30	40/49	75/121	136	1.64
npq4-Fmax	0.30	2.5/3.4	6.3/0.60	0.93/0.48	0.30	2.5/8.5	2.1/0.51	43/34	13/20	166/69	161	-
npq4-Fnpq	0.50	1.1/10	1.0/1.5	1.6/0.28	1.5	1.6/6.3	1.3/1.0	60/21	17/34	188/159	137	-
L17-Fmax	0.30	2.9/10	0.9/1.1	0.5/0.9	0.30	3.4/10	1.1/1.4	21/38	10/25	162/180	161	-
L17-Fnpq	1.1	1.9/11	1.8/1.2	3.5/0.15	-	-	-	50/20	31/32	62/121	180	2.11

Table 7.3: Average lifetime τav [ps] of the fluorescence decays for the *Arabidopsis thaliana* (wt and mutants) leaves grown under HL condition were calculated from the kinetic data at 683 nm emission wavelength (excitation at 663 nm). The errors in the average lifetimes are ±5%, errors in the other values are ±10%. NPQ values were calculated from the fluorescence decays at 683 nm according to the equation

$$\mathrm{NPQ} = \frac{\tau_{\mathrm{av@Fmax}}}{\tau_{\mathrm{av@Fnpq}}} - 1$$

Also shown are the lifetimes [ps] of the component appearing under NPQ conditions assigned to functionally detached and quenched LHCII, along with the percentage of LHCII detachment as measured by the decrease in total PS II cross-section in the quenched vs. the unquenched state. PSII-C denotes the PSII fraction connected by spillover to PSI.

	wt	***npq1***	***npq4***	***L17***
τav, 683nm of PSII+PSI, ps				
F_{npq}	320	540	510	220
F_{max}	1320	1380	1400	1360
τ of quenched LHC II oligomers, ps	453	608	-	475
NPQ [a]	3.1	1.6	1.7	5.2
% of detached LHC II [b]	40	66	-	20

[a] These numbers for the NPQ values derived from the lifetime measurements can be directly compared with those measured by conventional steady state NPQ induction. They fully agree within the error limits.

[b] Measured as percentage of total absorption cross-section (at the excitation wavelength of 663 nm) of dark-adapted PSII that is detached as quenched LHCII

Table 7.4: Excitation vectors for the various antenna compartments resulting from kinetic compartment analysis for the time-resolved kinetic data from the HL grown *Arabidopsis thaliana* (wt and the other mutants). The suffix 'C' denotes the PS II units connected through energy-spillover with PSI. The errors are in the range of ±10%.

	PSII-Ant/RC-C	PSII-Ant/RC	PSI-Ant/RC	LHCII
wt - Fmax	0.4	1.0	0.7	-
wt – Fnpq	0.8	-	1.0	0.5
npq1-Fmax	-	1.0	1.0	-
npq1-Fnpq	-	0.5	1.0	0.5
npq4-Fmax	0.2	0.7	1.0	-
npq4-Fnpq	0.3	0.8	1.0	-
L17-Fmax	0.9	0.3	1.0	-
L17-Fnpq	0.6	-	1.0	0.3

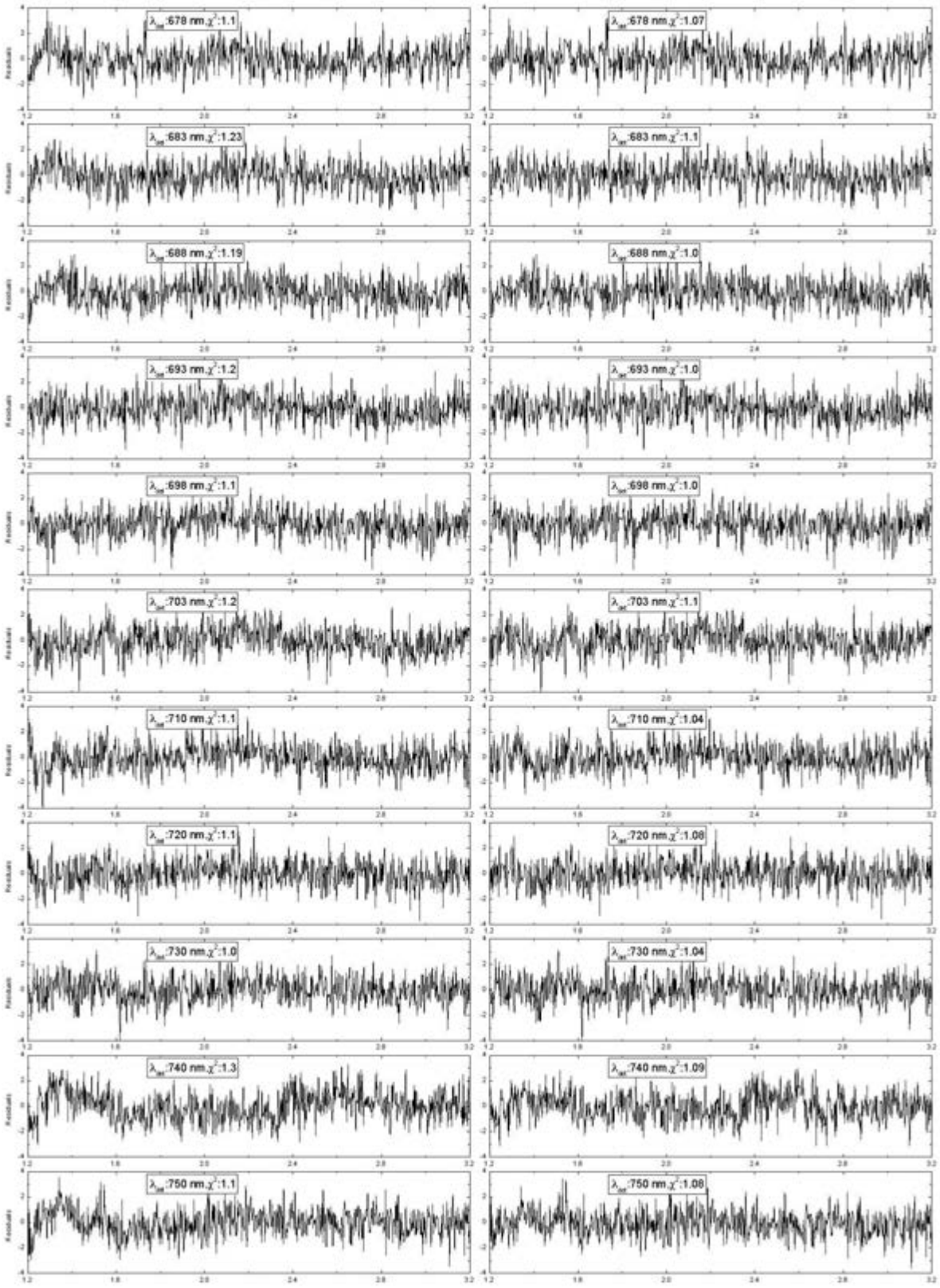

Supplementary Figure 7.1: Comparison of residual plots from global compartment analysis of the kinetics of w.t. plants. Fmax kinetics using a homogeneous spillover PSII model (left, global χ2 = 1.17) vs. a heterogeneous PSII model (spillover + non-spillover PSII, right, global χ2 = 1.08).

Chapter 7: Supplementary Information

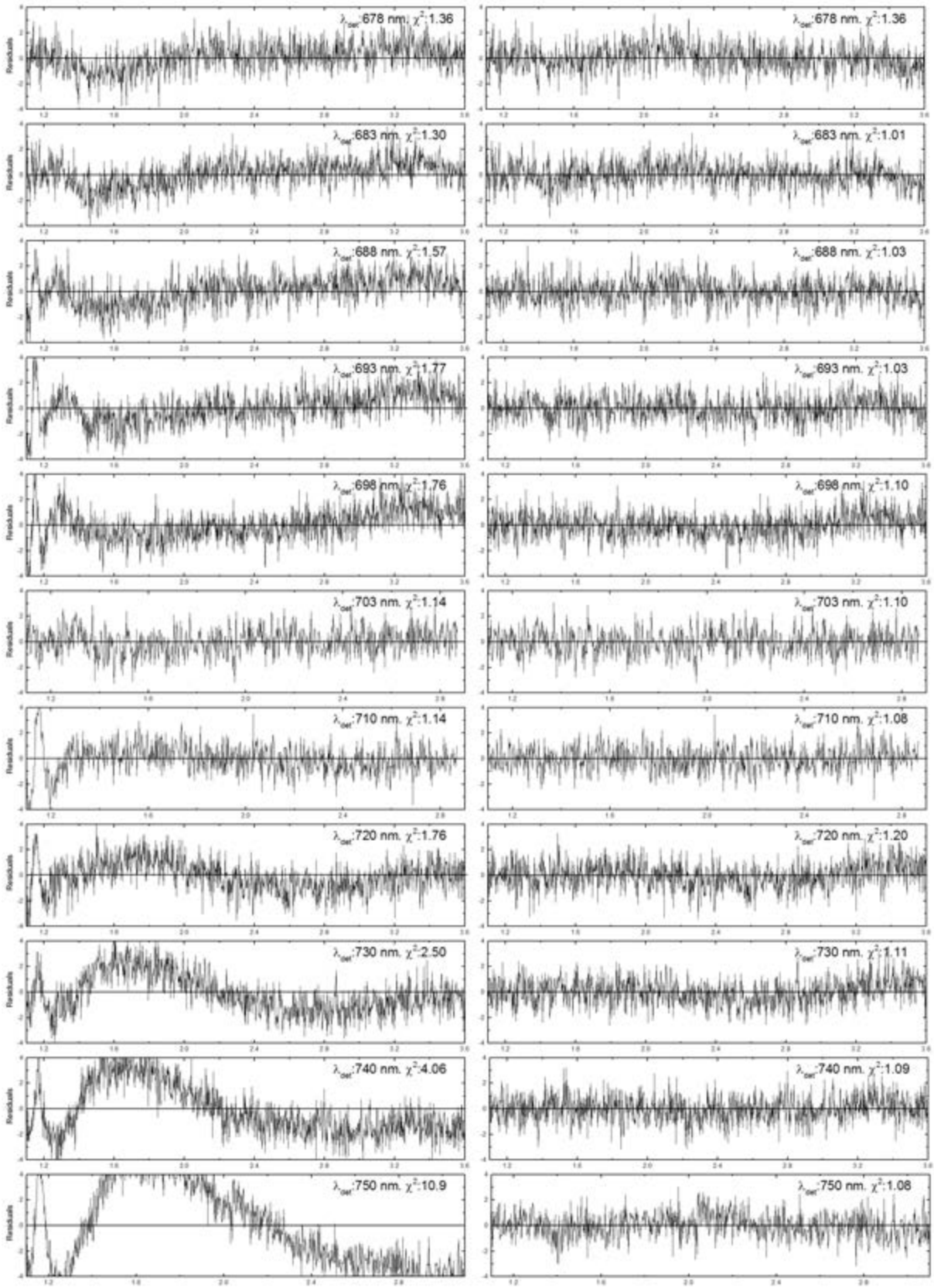

Supplementary Figure 7.2: Comparison of residual plots from global compartment analysis of the kinetics of *npq4* plants. Fmax kinetics using a homogeneous PSII model (left, global χ2 = 2.63) vs. a heterogeneous PSII model (spillover + non-spillover PSII, right, global χ2 = 1.07).

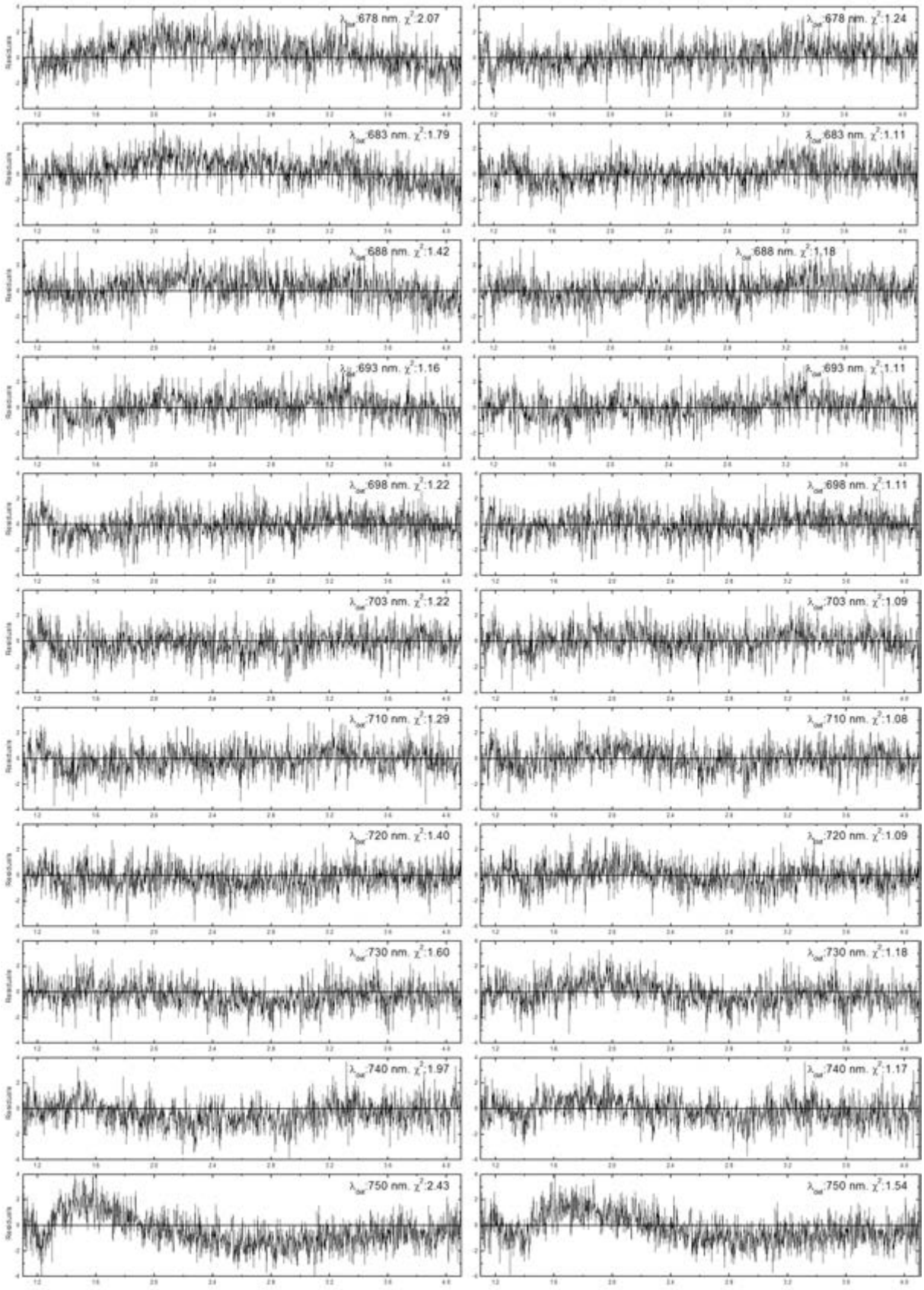

Supplementary Figure 7.3: Comparison of residual plots from global compartment analysis of the kinetics of *L17* plants. Fmax kinetics using a homogeneous PSII model (left, global χ2 = 1.58) vs. a heterogeneous PSII model (spillover + non-spillover PSII, right, global χ2 = 1.16).

Chapter 7: Supplementary Information

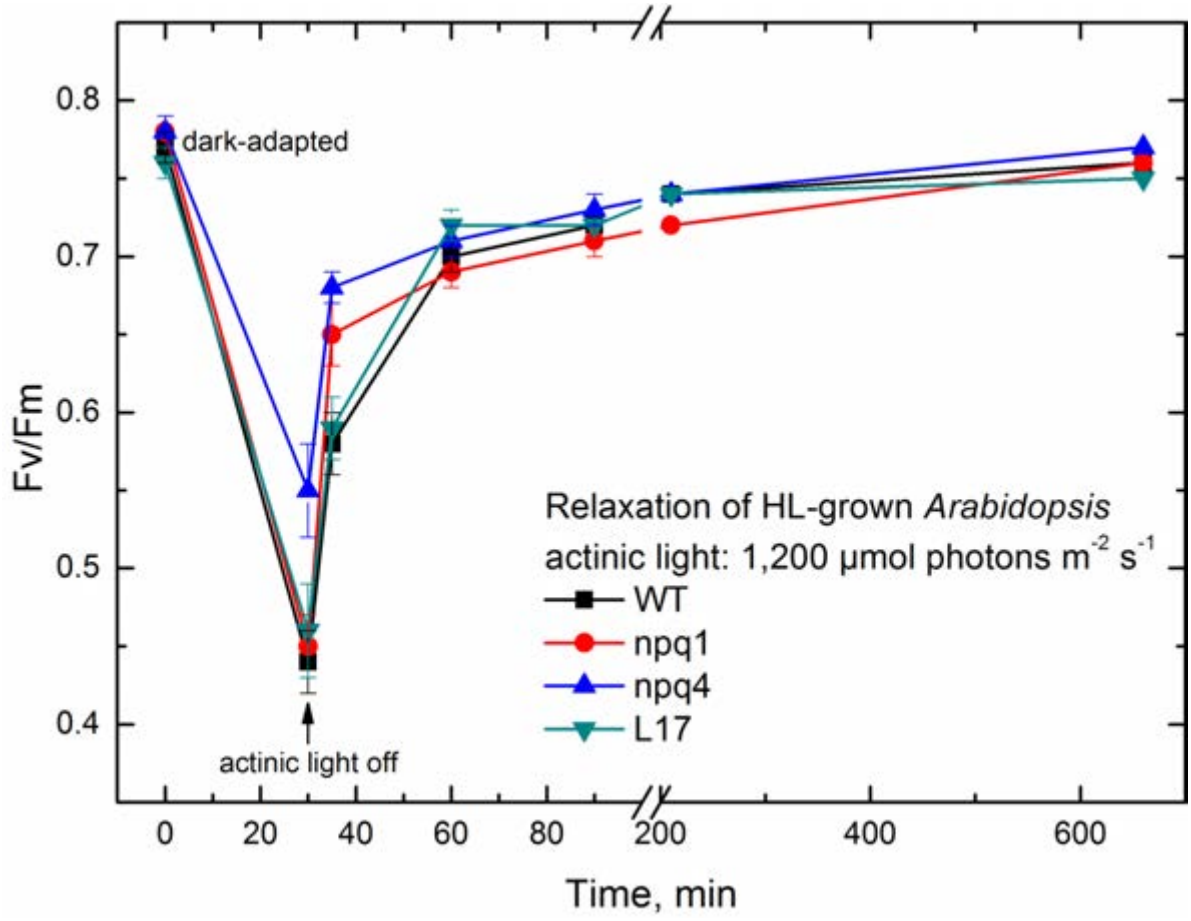

Supplementary Figure 7.4: Relaxation of HL-grown *Arabidopsis* genotypes. Fv/ Fm ratios were calculated using FluorPen FP 100, Photon System Instrument. The actinic light treatments were identical to time-resolved measurements.

Chapter 8 : NPQ mechanisms in *Arabidopsis thaliana* grown under sun-flecks (SF) condition

In the following work, time-resolved experiments on *Arabidopsis* plants grown under artificial sun-flecks condition were performed. Artificial sun-flecks during growth were caused by an array of high intensity (1000 µmol photons m^{-2} s^{-1}) white LEDs, lasting for 20 s and applied on every 5 min in addition to a constant 70 µmol photons m^{-2} s^{-1} light during the light cycle. This is an attempt to replicate the fluctuations occurring in natural sunlight (SF-plants) and possible consequences on the functional organization of the photosynthetic apparatus. This study represents a variation of the experiments in Chapter 7, where high light for growth was tested. The experiments aim to gain information on dynamic regulation of photoprotection mechanisms that actually happens in a genuine habitat. For comparison, we measured identical genotypes grown under 70 µmol photons m^{-2} s^{-1} constant light, without any sun-flecks.

8.1. Results

The Chl fluorescence decays for the SF-leaves were measured on dark (F_{max}) and high light (F_{npq}, by an array of red-emitting LEDs, providing 1,200 µmol photons m^{-2} s^{-1}) adapted leaf-disks, identical to already described procedure in former chapters. Figure 8.1 shows the decays at emission wavelength 683 nm for three *Arabidopsis* genotypes. The results are compared with replicate measurements carried out on constant low-light (CTL) grown *Arabidopsis* plants. All the plants, regardless of their growing light condition, had nearly identical F_{max}-decays; while, we found shorter fluorescence lifetimes for the NPQ-adapted SF-plants compared to their CTL-duplicates (Figure 8.1). SF-w.t. plants had the strongest quenching among all.

8.1.1. Global target analysis

The detailed analysis of decay data yielding the quenching mechanism(s) and location(s) were obtained by global target analysis (see Supplementary Figure 8.1 for the schematic of target models) (Holzwarth 1996). The results are shown as recalculated decay-associated spectra in Figure 8.2-3 and the kinetic rate constants are in Table 8.1. The initial analysis applied the simplest kinetic model, previously successful to describe the NPQ kinetics of intact *Arabidopsis* leaves (Holzwarth, Miloslavina et al. 2009). This model did not fit the data. Several models were tested. In order to fit the unquenched CTL-plants, an additional (30-40% of the total PSII, see Table 8.5) 'attached' LHCII (see

Supplementary Figure 8.2-3), transferring excitations to PSII-units (Table 8.1) and had very similar emission spectra like PSII (Figure 8.2), was required. For SF-plants, also an additional LHCII pool was required to fit the unquenched mutant data, but not for the w.t (Figure 8.3 and Table 8.1; see also Supplementary Figure 8.4 for the residual plots). The presence of such an additional LHCII pool is also expected from higher the Chl a/b ratio (Table 8.4), which indicated 10-15% more Chl b in these plants compared to *Arabidopsis* plants grown under normal light condition (ca. 150 µmol photons m^{-2} s^{-1}) (Holzwarth, Miloslavina et al. 2009).

Except for the *npq1*-mutant, high actinic light (NPQ state) in these plants had the usual well-known effects: a) increase in thermal dissipation of the PSII antenna (qZ), assessed by the rate constant k_D (Table 8.1) (Holzwarth, Miloslavina et al. 2009) and b) detachment of LHCII from the PSII-supercomplex (Table 8.2-3) (qE) (Holzwarth, Miloslavina et al. 2009). In contrast to the previous reports (Holzwarth, Miloslavina et al. 2009), detached LHCII oligomer was also found in *npq4*-mutant (see Supplementary Figure 8.5-6); This will be discussed separately.

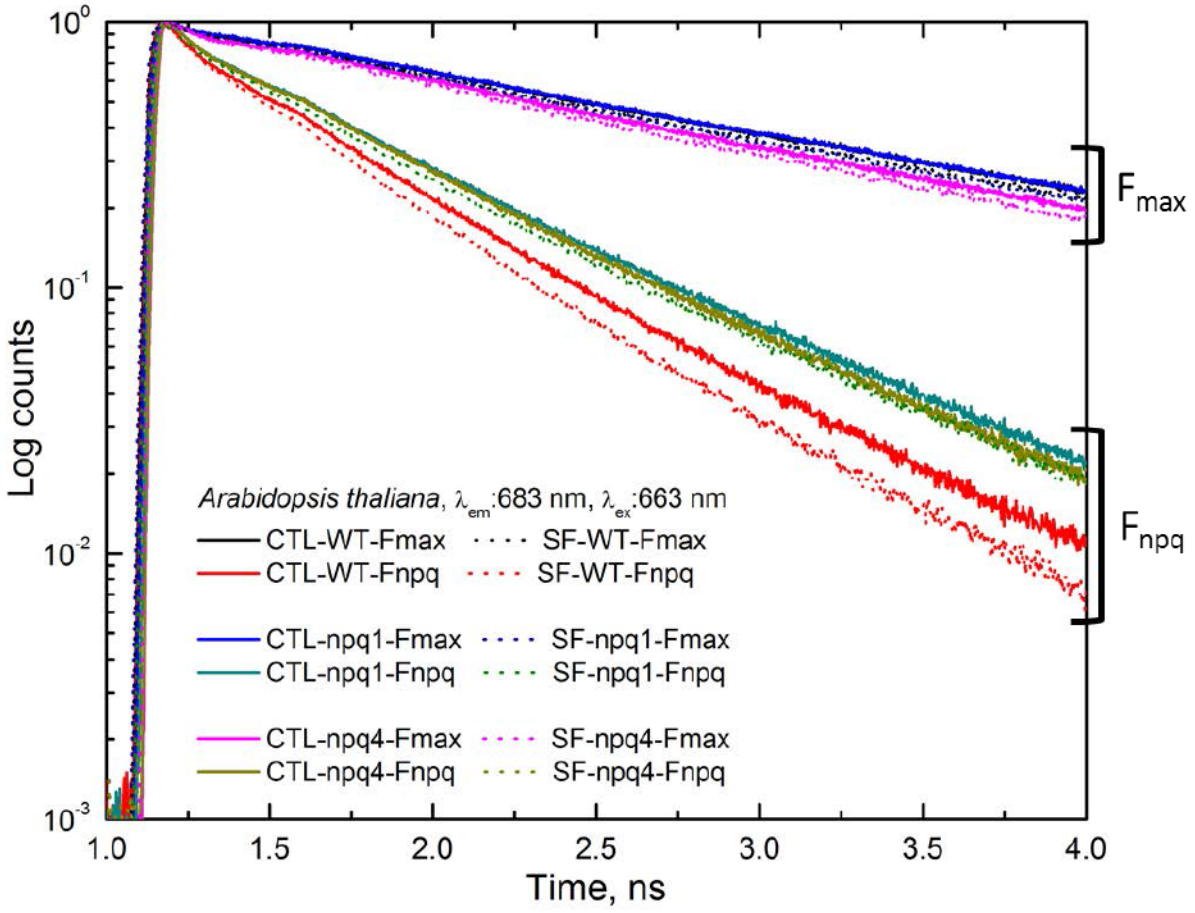

Figure 8.1: Fluorescence decays of wild-type and mutant *Arabidopsis* plants, either at unquenched (Fmax) or quenching (Fnpq) conditions. The sun-flecks (SF) plants had shorter fluorescence lifetimes, therefore, stronger quenching compared to the controlled light (CTL) plants. SF-w.t. had the fastest decay.

8.2. Discussion

8.2.1. NPQ mechanisms in SF-plants

NPQ-quenching in SF-plants is known to be faster and stronger as compared to plants grown under constant low-light (Alter, Dreissen et al. 2012). The time-resolved data agree with that general finding (Figure 8.1). The direct calculation of the NPQ parameter from their corresponding quenched and unquenched states lifetimes (Table 8.2-3) yielded matching values (Alter, Dreissen et al. 2012). In line with other studies on *Arabidopsis* (Holzwarth, Miloslavina et al. 2009), the w.t. plants sustained higher NPQ capacities compared to Z- and/or PsbS-deficient mutants. The quenching in fully functional w.t. PSII can be well described by the 4-state-2-site model (Holzwarth and Jahns 2014), where the PSII antennae are quenched by qE and qZ mechanisms. The present study also supports this model, where, in Z-deficient *npq1*-mutant, there was no light induced increase in rate constant k_D (Table 8.1). However, the quenched state in PsbS deficient *npq4*-mutant required an additional detached LHCII to improve the fits (see Supplementary Figure 8.6 for the residual plots). This result deviates from the

normal light grown *Arabidopsis* (Holzwarth, Miloslavina et al. 2009, Miloslavina, de Bianchi et al. 2011), where the PsbS protein is required for LHCII detachment. The most plausible origin for a detached LHCII in absence of PsbS could be the unusually large LHCII pool size (present as poorly attached antenna in the unquenched states, see Table 8.1 for the energy-transfer rates). From this very large LHCII pool a significant 30-40% (Table 8.5) portion was 'loosely' attached, as was revealed in the low kinetic rate k_{LH1}, the forward energy transfer to PSII (Table 8.1). No such large, loosely bound LHCII antenna was present in normal light grown *Arabidopsis* (Holzwarth, Miloslavina et al. 2009, Miloslavina, de Bianchi et al. 2011), where the kinetic model was based on a PSII-$C_2S_2M_2$ architecture. The presence of large LHCII antenna in unquenched state is also consistent with the lower Chl a/b ratio (Table 8.4). As the presence of loosely coupled LHCII is now confirmed, it is reasonable to assume that under NPQ lights, a section from this 'extra' LHCII was detached, apparently without any involvement of the PsbS protein, which explains the detached LHCII also in *npq4*-plants.

8.2.2. Effects of Sun-flecks over CTL-lights – responses in terms of plants photoprotection

The study of photosynthetic machinery towards sun-flecks (SF)-light provides a more realistic description of the natural habitat, where the sunlight also fluctuates on regular (short-term and long-term) as well as irregular intervals. Application of SF-light to mature leaves grown under controlled low-light (CTL) is known result in the up-regulation of electron transport and in certain cases also affected carbon gains, in form of starch-accumulation (Alter, Dreissen et al. 2012). The time-resolved studies revealed the effect of SF on PSII and PSI organization. Apart from the superior photoprotection in SF plants (Table 8.3), the tighter coupling among the PSII antennas, resulted in the absence of loosely bound LHCII complexes in the analysis, which were rather present in the low-light CTL-plants. The role of carotenoid zeaxanthin and PsbS protein were also studied by experiments performed on *npq1* and *npq4* mutants. These two important cofactors are present in the w.t. membrane, where the former is a de-epoxide homologue of violaxanthin, accumulates under light and believed to be responsible for the regular functioning of thylakoid, particularly in the grana stacking and PSII activity (Rock, Bowlby et al. 1992). It is reasonable to assume for the plants to develop unusual PSII architecture (with loosely bound LHCII antenna) when such a vital cofactor, is missing, as in *npq1*-mutant. There was barely any difference in the photoprotection capacities between the SF and low-light CTL-plants (Table 8.2 and 8.3). Similar

conclusion can also be made on behalf of the other cofactor PsbS, which was absent in *npq4*-mutant, resulted in the synthesis of loosely attached feigned LHCII pool.

8.2.3. The limitation of SF-condition

Although, artificial SF lights could replicate the sunlight scenario to a large extent, however, the photoprotection capacity, as judged by their maximal NPQ (Table 8.3), achieved by this method is less compared to plants grown at high-light (HL) (cf. Chapter 7). The primary reason is revealed in the distribution of PSII and PSI in the thylakoid membrane and their mobility induced by light (Kirchhoff 2013, Kirchhoff 2013). In a normal light grown thylakoid (see (Holzwarth, Miloslavina et al. 2009)), PSII and PSI are believed to be laterally segregated into grana and stroma lamella respectively (Andersson, Åkerlund et al. 1982, Pribil, Labs et al. 2014), where NPQ photoprotection is performed by PSII antenna (Lambrev, Miloslavina et al. 2012, Ruban, Johnson et al. 2012) and are located on two-sites, qE and qZ (Holzwarth and Jahns 2014). Results from the present study are in line with these findings. However, recent reports suggested that the NPQ capacities achieved by the qE and qZ sites are less, compared to the superior photoprotection obtained by mixing the PSII and PSI sites (Slavov, Reus et al. 2013). Recent studies on HL plants confirmed a tight coupling between PSII and PSI via the so-called 'energy-spillover' pathway, where excess PSII excitations are directly transmitted to PSI (cf. Chapter 7 and 4). The mixing two photosystems enables a third highly efficient quenching mechanism, Qso, which makes PSII centers more protective to higher light intensity. This mechanism has been shown to operate in natural sunlight (NL) grown evergreen plants (cf. Chapter 4). The electron micrographs as shown in for NL-grown plants (cf. Chapter 4 and 5) showed destacking in grana membrane resulted a pronounced mixing between the two photosystems. It must be mentioned here that the quenching mechanisms qE and qZ remain operative despite the presence of Qso.

Therefore, it can be concluded that thylakoid membrane is actually very responsive to the growth lights. For very low-light (CTL) grown plants, the thylakoid produces loosely attached LHCII pool, which apparently does not have any well-defined role, neither in light harvesting nor in photoprotection. Under normal growth lights (similar to SF used in the present study), on contrary, the LHCII antennae are firmly attached to the PSII-complex and efficiently funnel the energy to the reaction-centers. LHCII antennae from such normal light grown thylakoids also help to dissipate the excess PSII energy via the qE-quenching mechanism. Whereas, a major reorganization in the thylakoid membrane occurs under natural sunlight (cf. Chapter 4) or when the plants are grown under high irradiation (cf. Chapter 7). Disintegration in the grana stacks expands the lamella region

which brings PSII and PSI at proximate locations, thereby enabling spillover of excess PSII energy towards PSI. This spillover quenching mechanism has been found to provide the most efficient photoprotection in these HL or NL plants.

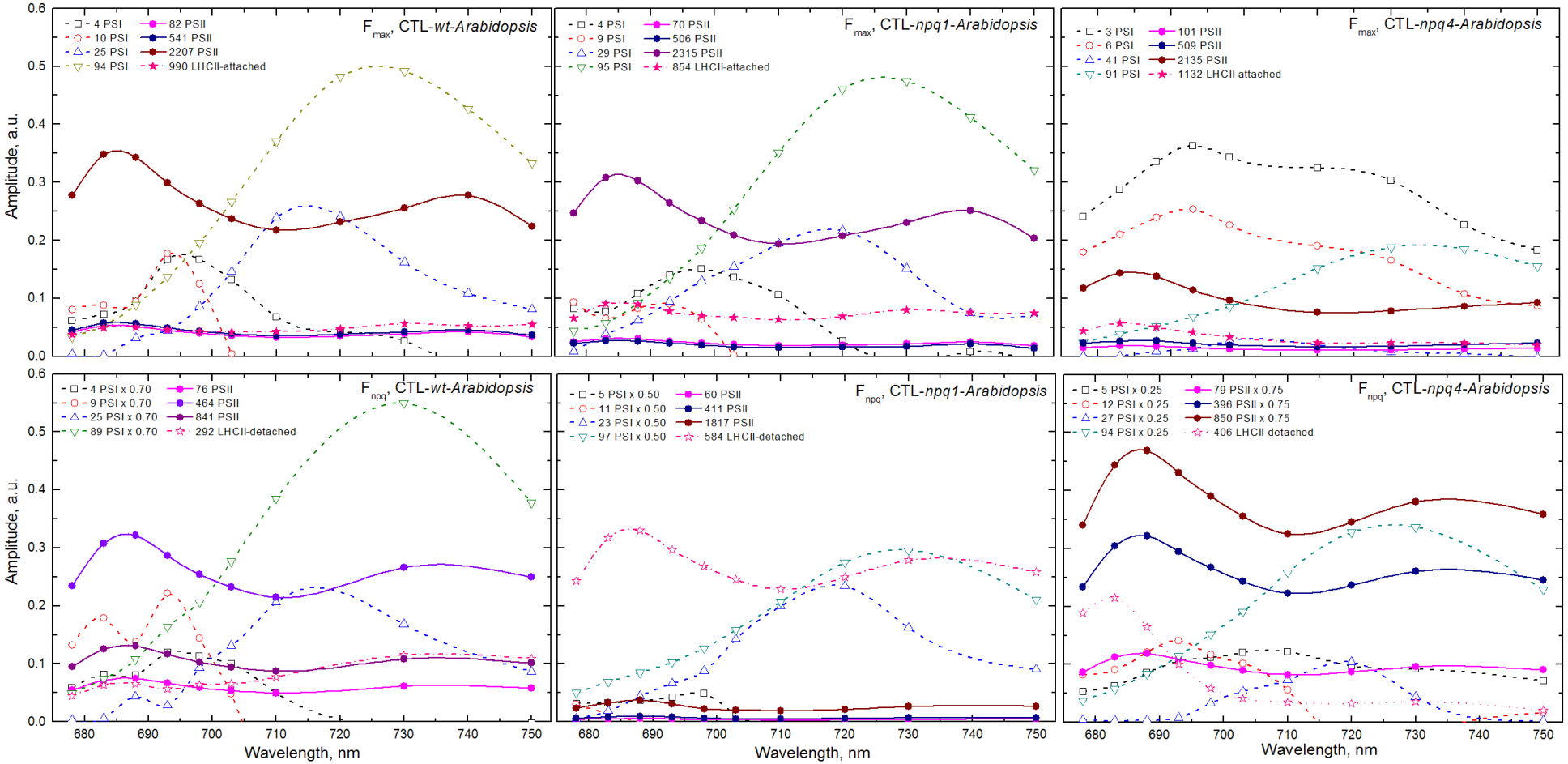

Figure 8.2: Decay-associated spectra (DAS) resulting from kinetic compartment analysis of unquenched (Fmax) and quenched (Fnpq) states of controlled low-light grown (CTL) *A. thaliana* plants. PSI components are shown as dashed and LHCII as dotted lines. For clarity of presentation, only positive amplitude parts are shown. Note that the unquenched states are characterized by the presence of 'loosely attached' extra LHCII.

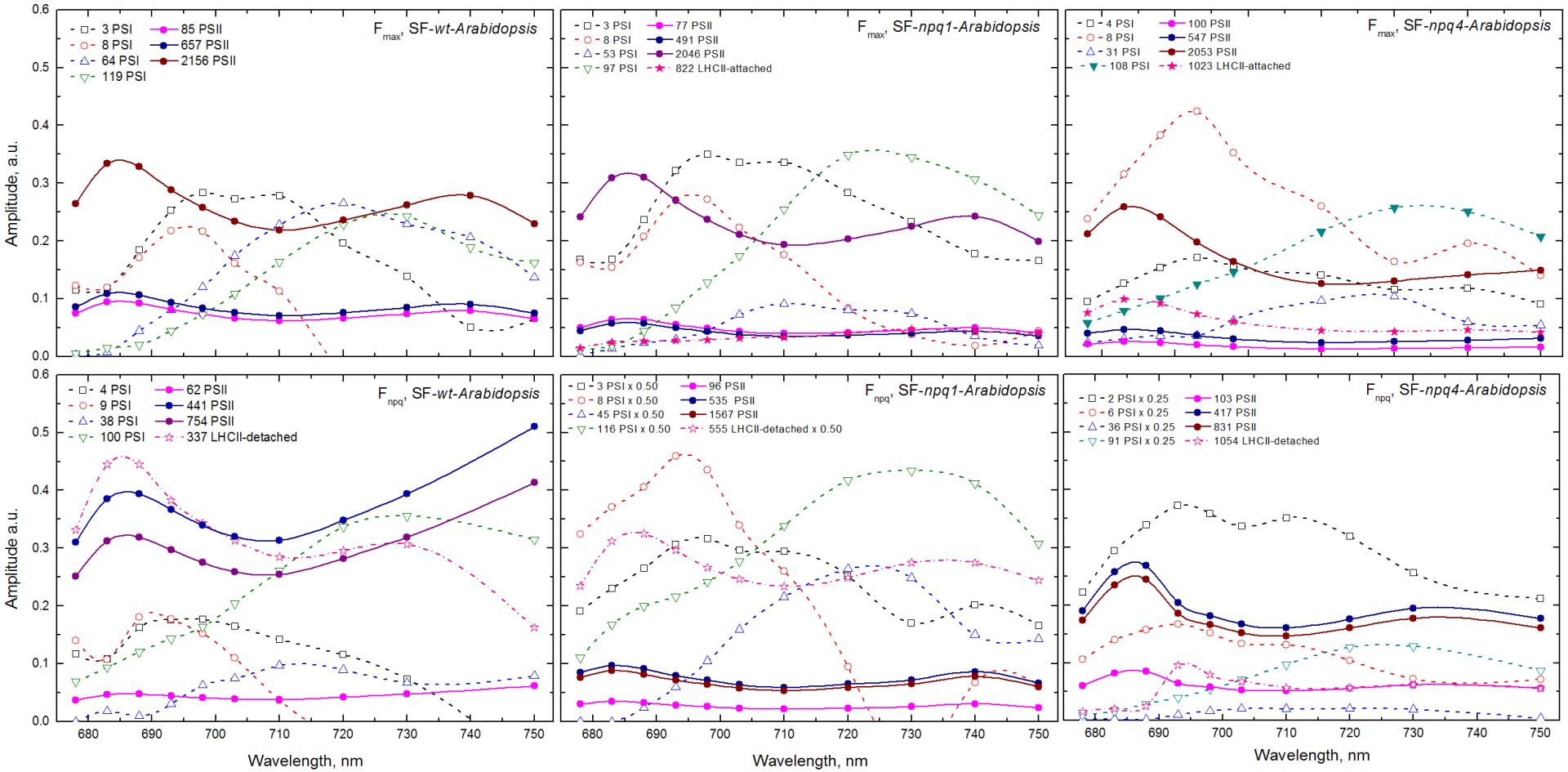

Figure 8.3: : Decay-associated spectra (DAS) resulting from kinetic compartment analysis of unquenched (Fmax) and quenched (Fnpq) states of sunflecks light grown (SF*) A. thaliana* plants. PSI components are shown as dashed and LHCII as dotted lines. For clarity of presentation, only positive amplitude parts are shown. Note that in wild-type (w.t.) plants, the aforesaid 'loosely attached' LHCII segment is no longer present, whereas for the Z and PsbS deficient mutants, such 'attached LHCII' exists.

Table 8.1: Rate constants (ns^{-1}) for the PSII and PSI kinetics in the controlled (CTL) and sunflecks (SF) grown *Arabidopsis thaliana* determined from the kinetic target analysis. k_{LH1} and k_{-LH1} are the forward and backward energy-transfer rates from LHCII antenna to PSII-core. The k_3 rates from closed PSII units are fixed to 0.9 ns^{-1} (Holzwarth, Miloslavina et al. 2009). The errors in the rate constants are within ± 10%.

		PSII				**PSI**				
		k_D	**k_{CS1}/k_{rec1}**	**k_1/k_2**	**k_{LH1}/k_{-LH1}**	**k_{r1}/k_{-r1}**	**k_{r2}/k_{-r2}**	**k_{CS}/k_{-CS}**	**k_4**	**LHCII**
CTL-WT	Fmax	0.30	2.2/7.4	2.8/0.81	0.70/0.0	45/16	29/44	66/67	111	0.31, fixed
CTL-npq1	Fmax	0.30	2.2/9.1	3.3/0.86	0.78/0.17	41/26	21/40	87/62	134	0.31, fixed
CTL-npq4	Fmax	0.30	2.1/5.1	3.1/0.85	0.51/0.10	24/14	20/82	164/60	186	0.31, fixed
CTL-WT	Fnpq	1.8	1.7/9.4	2.0/0.71	LHCII-detached	43/17	28/47	69/71	152	3.4
CTL-npq1	Fnpq	0.55	2.1/11.7	2.9/1.5	LHCII-detached	57/18	23/29	60/63	105	1.7
CTL-npq4	Fnpq	1.6	1.6/8.8	2.1/1.4	LHCII-detached	41/11	25/32	61/60	102	2.5
SF-WT	Fmax	0.30	2.4/7.8	2.2/0.48	-	18/25	10/20	164/62	162	-
SF-npq1	Fmax	0.30	2.8/7.4	3.2/0.85	0.89/0.0	21/20	14/31	161/60	158	0.31, fixed
SF-npq4	Fmax	0.30	1.7/5.1	3.6/0.77	0.62/0.10	44/36	21/32	61/60	155	0.31, fixed
SF-WT	Fnpq	1.7	1.0/12	3.1/1.1	LHCII-detached	30/22	18/40	103/61	146	2.9
SF-npq1	Fnpq	0.45	2.3/5.0	3.7/0.62	LHCII-detached	22/7.0	16/60	131/115	180	1.8
SF-npq4	Fnpq	1.7	1.2/6.3	1.9/1.2	LHCII-detached	30/31	16/70	230/70	180	0.95

Table 8.2: Average lifetime τ_{av} [ps] of the fluorescence decays for the controlled (CTL) light grown *Arabidopsis thaliana* were calculated from the kinetic data at 683 nm emission wavelength (excitation at 663 nm). The errors in the average lifetimes are ±5%, errors in the other values are ±10%. NPQ values were calculated from the fluorescence decays at 683 nm according to the equation

$$\mathrm{NPQ} = \frac{\tau_{\mathrm{av@Fmax}}}{\tau_{\mathrm{av@Fnpq}}} - 1$$

Also shown are the lifetimes [ps] of the component appearing under NPQ conditions assigned to functionally detached and quenched LHCII; along with the percentage of LHCII detachment as measured by the decrease in total PSII cross-section in the quenched vs the unquenched state.

Controlled-light grown	wt	*npq1*	*npq4*
$\tau_{av,\ 683nm}$ of PSII+PSI, ps			
F_{npq}	380	480	390
F_{max}	1380	1390	1250
τ of quenched LHC II oligomers, ps	292	584	406
NPQ [a]	2.6	1.9	2.2
% of detached LHC II [b]	30	60	30

a) These numbers for the NPQ values derived from the lifetime measurements can be directly compared with those measured by conventional steady state NPQ induction. They fully agree within the error limits.

b) Measured as percentage of total absorption cross-section (at the excitation wavelength of 663 nm) of dark-adapted PSII that is detached as quenched LHCII

Table 8.3: Average lifetime τ_{av} [ps] of the fluorescence decays for the sun-flecks (SF) light grown *Arabidopsis thaliana* were calculated from the kinetic data at 683 nm emission wavelength (excitation at 663 nm). The errors in the average lifetimes are ±5%, errors in the other values are ±10%. NPQ values were calculated from the fluorescence decays at 683 nm according to the equation

$$\mathrm{NPQ} = \frac{\tau_{\mathrm{av@Fmax}}}{\tau_{\mathrm{av@Fnpq}}} - 1$$

Also shown are the lifetimes [ps] of the component appearing under NPQ conditions assigned to functionally detached and quenched LHCII; along with the percentage of LHCII detachment as measured by the decrease in total PSII cross-section in the quenched vs the unquenched state.

Sunflecks-light grown	wt	*npq1*	*npq4*
$\tau_{av,\ 683nm}$ of PSII+PSI, ps			
F_{npq}	290	450	360
F_{max}	1010	1240	1140
τ of quenched LHC II oligomers, ps	337	555	1054
NPQ [a]	2.5	1.8	2.2
% of detached LHC II [b]	30	62	30

a) These numbers for the NPQ values derived from the lifetime measurements can be directly compared with those measured by conventional steady state NPQ induction. They fully agree within the error limits.

b) Measured as percentage of total absorption cross-section (at the excitation wavelength of 663 nm) of dark-adapted PSII that is detached as quenched LHCII

Table 8.4: Chl a/b ratios of the dark-adapted *Arabidopsis* leaves grown under controlled (CTL) and sunflecks (SF) light conditions. The pigment was determined by HPLC from three replicates for each case. Mean value ± SD is shown.

	wt	***npq1***	***npq4***
CTL	3.5 ± 0.1	3.4 ± 0.1	3.5 ± 0.1
SF	3.4 ± 0.1	3.5 ± 0.1	3.7 ± 0.1

Table 8.5: Excitation vectors for the various antenna compartments resulting from kinetic compartment analysis for the time-resolved kinetic data from the controlled (CTL) and sunflecks (SF) grown *Arabidopsis thaliana*. The errors are in the range of ±10%.

	Excitation vectors used in SAES		
	PSII	**PSI**	**LHCII**
CTL-WT-Fmax	0.65	1.0	0.25
CTL-npq1-Fmax	0.62	1.0	0.40
CTL-npq4-Fmax	0.60	1.0	0.25
CTL-WT-Fnpq	0.65	1.0	0.25
CTL-npq1-Fnpq	0.35	1.0	0.50
CTL-npq4-Fnpq	0.65	1.0	0.25
SF-WT-Fmax	1.0	1.0	-
SF-npq1-Fmax	0.65	1.0	0.25
SF-npq4-Fmax	0.65	1.0	0.25
SF-WT-Fnpq	0.65	1.0	0.25
SF-npq1-Fnpq	0.25	1.0	0.45
SF-npq4-Fnpq	0.65	1.0	0.25

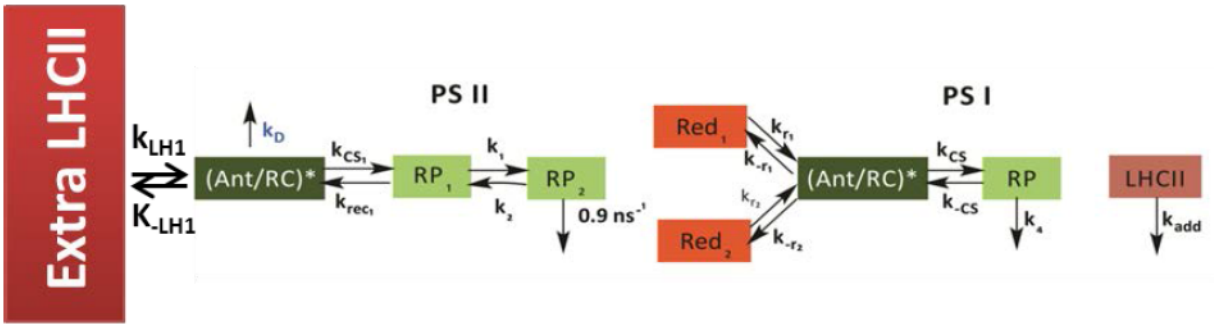

Supplementary Figure 8.1: Kinetic compartment models successful for describing the quenching kinetics of the various light adaptation conditions. The compartment models for PSI and PSII units follow those that have been demonstrated on isolated intact PSI and PSII complexes (Miloslavina, Szczepaniak et al. 2006, Slavov, Ballottari et al. 2008, Slavov, El-Mohsnawy et al. 2009) and on *Arabidopsis* intact leaves (Holzwarth, Miloslavina et al. 2009, Miloslavina, de Bianchi et al. 2011). The compartment labeling is as follows: Ant/RC*: antenna/reaction center excited states of PSII or PSI; RPx: radical pairs; LHCII: functionally detached and quenched light-harvesting complex II from PSII. A second pool of extra LHCII remains connected to the PSII during unquenched condition.

Chapter 8: Supplementary Information

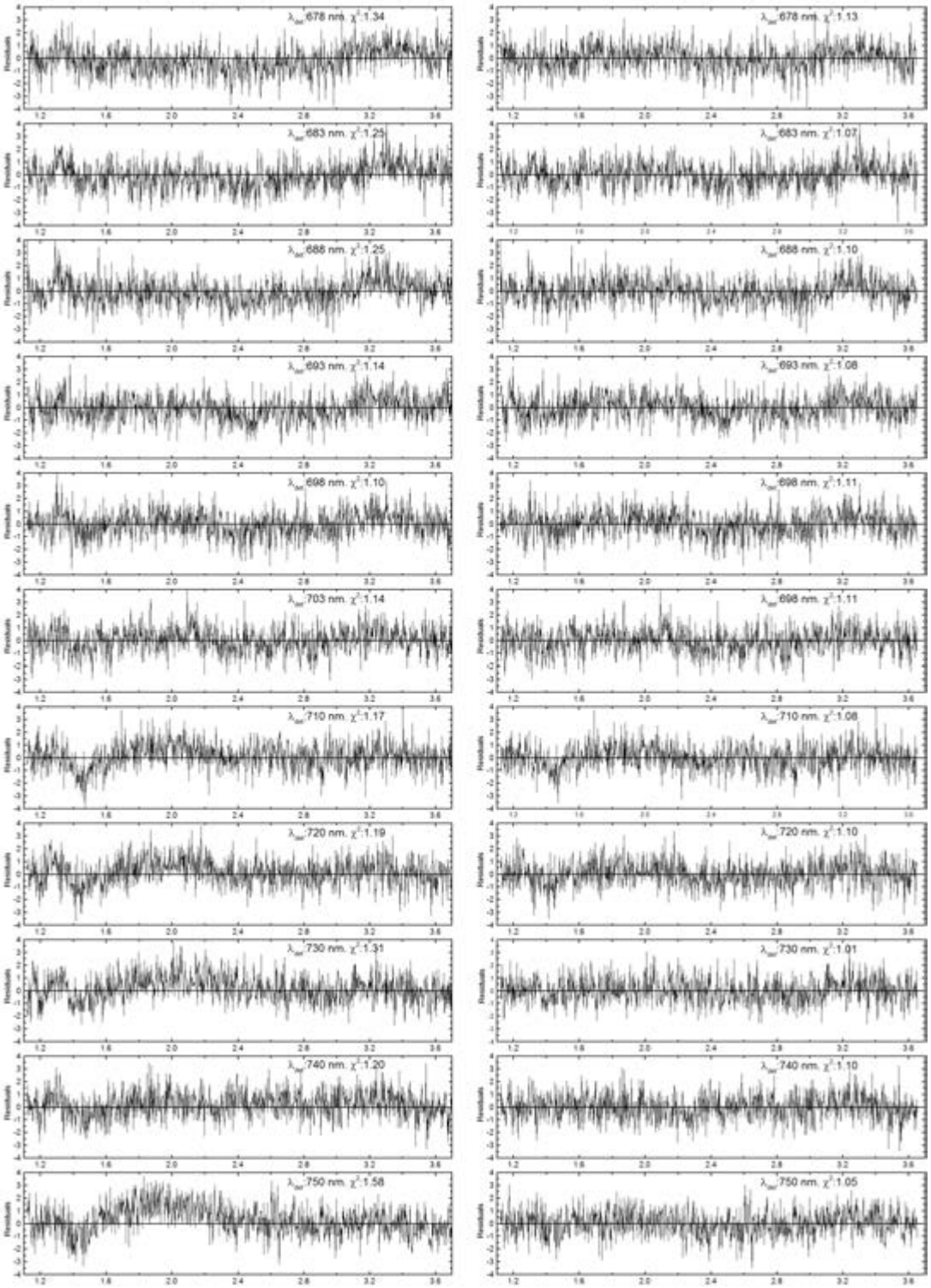

Supplementary Figure 8.2: Comparison of residual plots from global compartment analysis of the kinetics of CTL-w.t. plants. Fmax kinetics 'without' an additional LHCII antenna in the PSII model (left, global χ2 = 1.23) vs. 'with' an additional LHCII in the PSII model (right, global χ2 = 1.09).

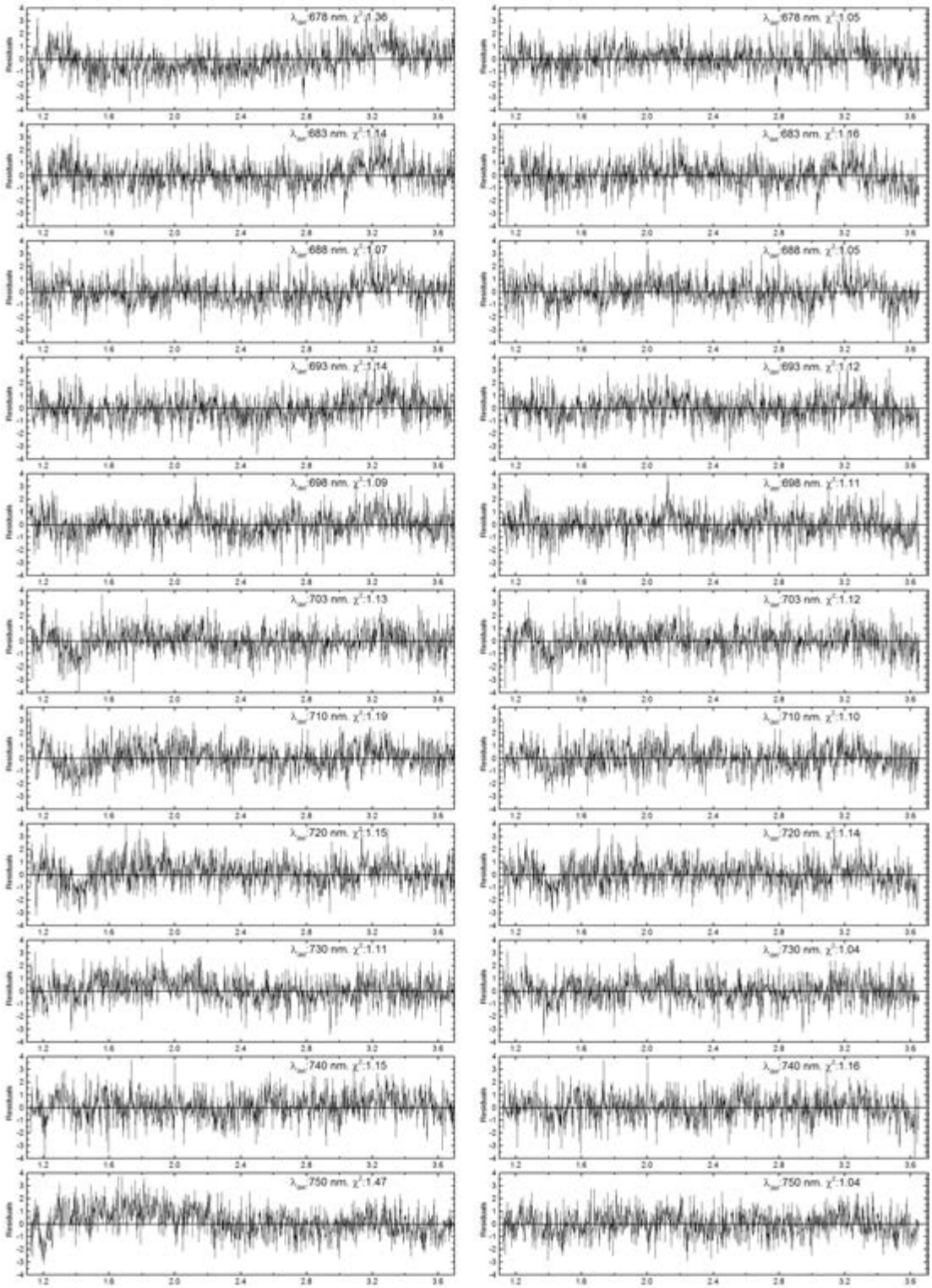

Supplementary Figure 8.3: Comparison of residual plots from global compartment analysis of the kinetics of CTL-*npq1* plants. Fmax kinetics 'without' an additional LHCII antenna in the PSII model (left, global χ2 = 1.18) vs. 'with' an additional LHCII in the PSII model (right, global χ2 = 1.10).

Chapter 8: Supplementary Information

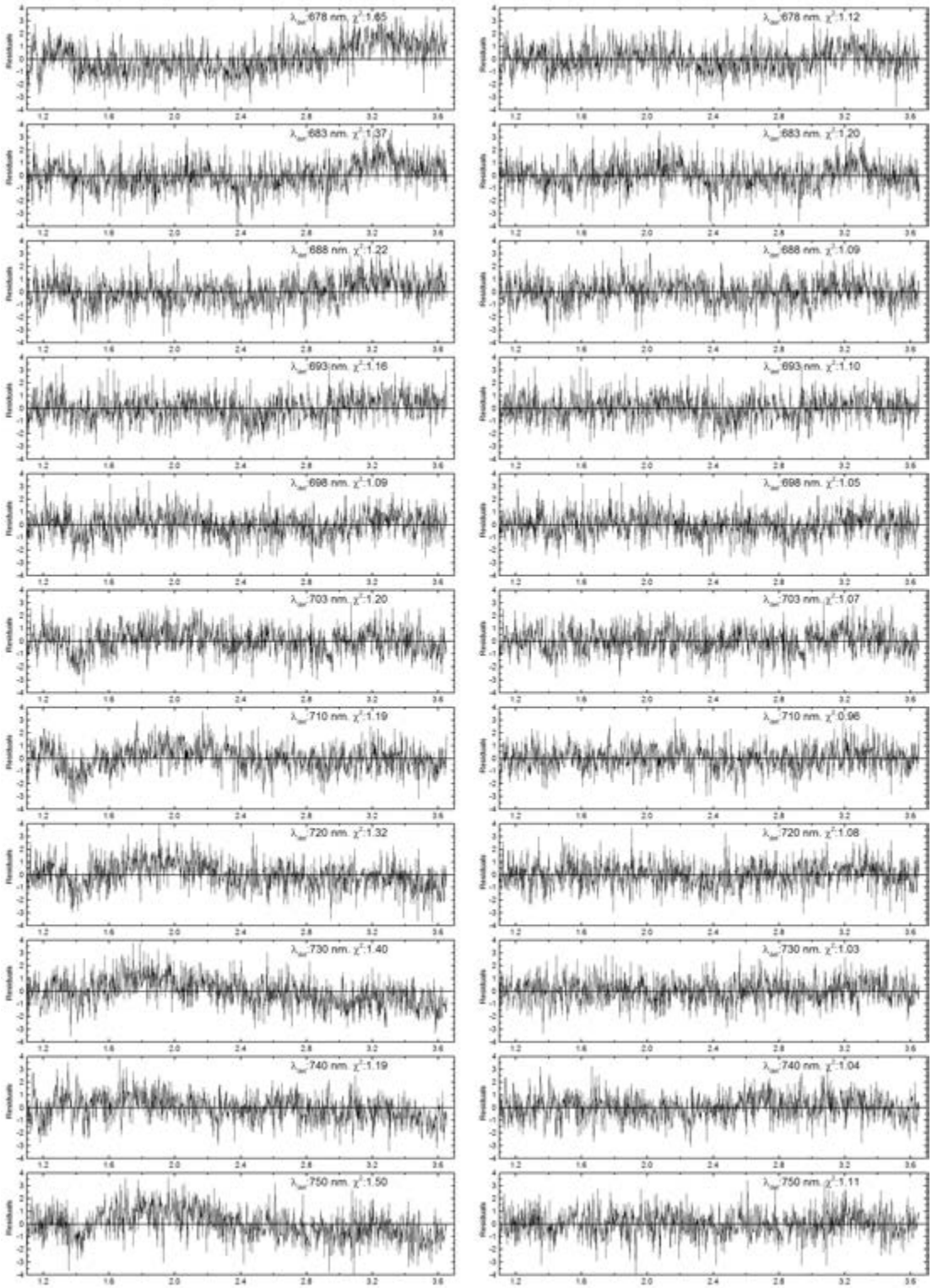

Supplementary Figure 8.4: Comparison of residual plots from global compartment analysis of the kinetics of SF-*npq1* plants. Fmax kinetics 'without' an additional LHCII antenna in the PSII model (left, global χ2 = 1.29) vs. 'with' an additional LHCII in the PSII model (right, global χ2 = 1.07).

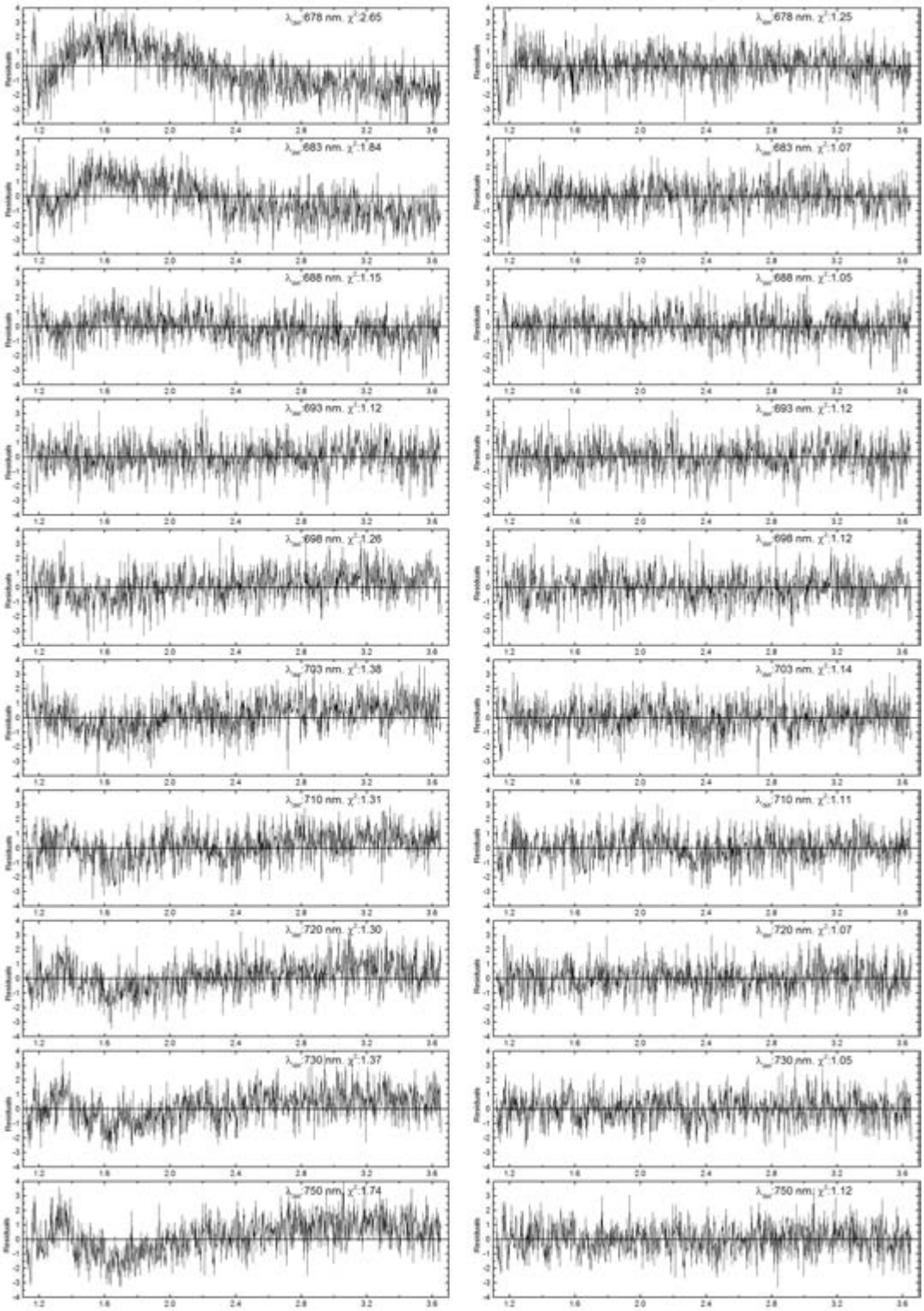

Supplementary Figure 8.5: Comparison of residual plots from global compartment analysis of the kinetics of CTL-*npq4* plants. Fnpq kinetics 'without' an additional LHCII antenna in the PSII model (left, global χ2 = 1.51) vs. 'with' an additional LHCII in the PSII model (right, global χ2 = 1.10).

Chapter 8: Supplementary Information

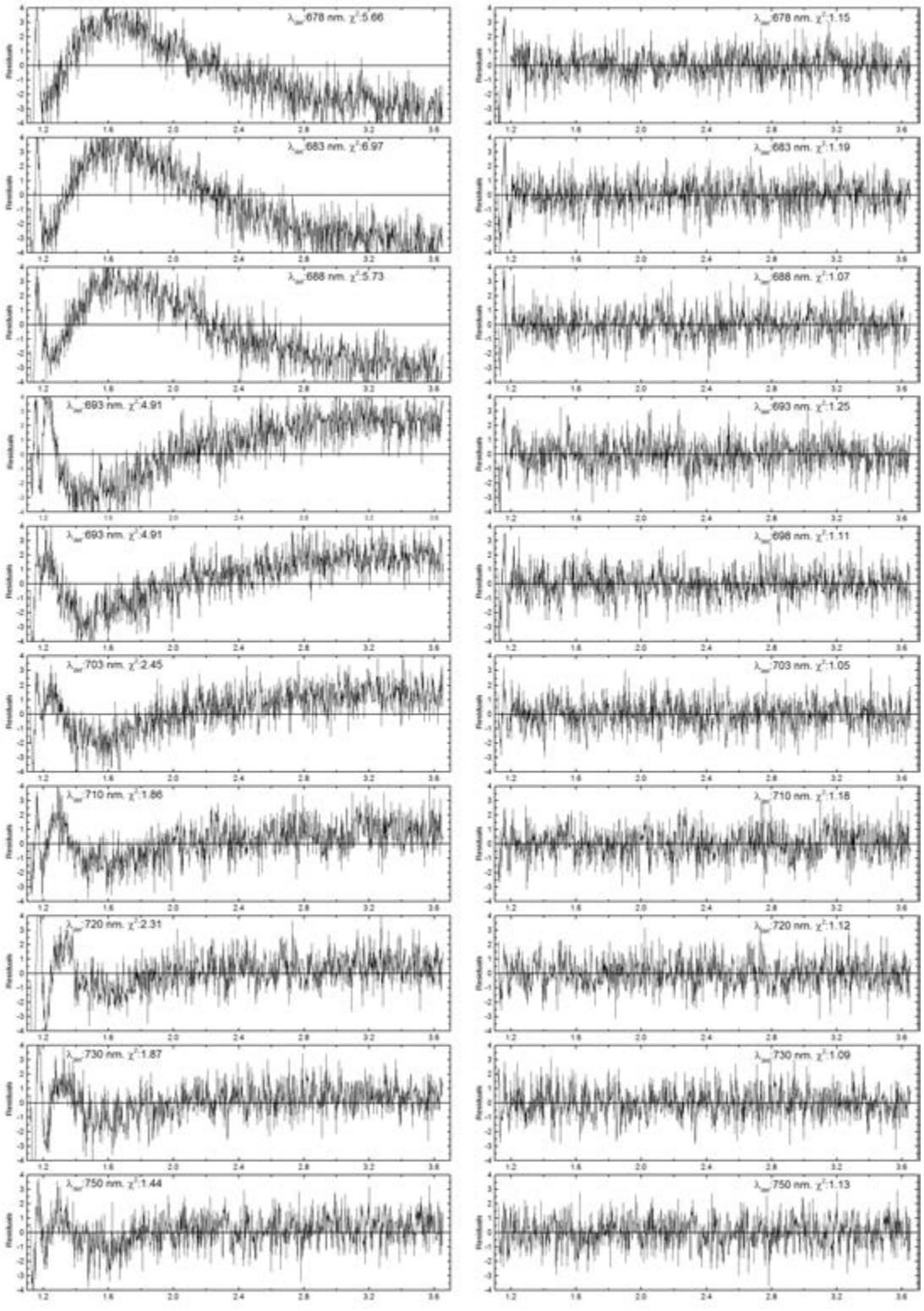

Supplementary Figure 8.6: Comparison of residual plots from global compartment analysis of the kinetics of SF-*npq4* plants. Fnpq kinetics 'without' an additional LHCII antenna in the PSII model (left, global χ2 = 3.63) vs. 'with' an additional LHCII in the PSII model (right, global χ2 = 1.12).

Chapter 9 : On the molecular mechanism of quenching and photoprotection in the major light-harvesting complex LHCII of photosystem II

LHCII is the major antenna complex in photosystem II that is attached to the periphery of the PSII supercomplex and collects more than 50% of the light absorbed by PSII. The qE quenching mechanism proposed in former chapters is based on the hypothesis of LHCII oligomerization, thought to be triggered by ΔpH and had a strong PsbS-dependency. In the following work, we reconstituted the LHCII and PsbS duo inside proteoliposomes and studied the quenching mechanism in time-resolved fluorescence technique. Various other factors like ΔpH or addition of protons into the medium and/or carotenoid Z were also investigated.

9.1. Results

9.1.1. Fluorescence lifetime measurements on LHCII in proteoliposomes and kinetic modelling

The fluorescence decays of quenched (with PsbS) and unquenched (without PsbS) LHCII in reconstituted proteoliposomes are compared in Figure 9.1 for two typical emission wavelengths. In addition to the PsbS effect on quenching, we also tested the effects of different pH and of DCCD or Z addition. Furthermore the kinetics of samples reconstituted with a mutated PsbS, having deleted the external pH sensing groups, have been measured. Supplementary Figure 9.1 shows the results of the global lifetime analysis for various conditions of LHCII reconstituted without PsbS. Typically 3-4 lifetime components were necessary for a good fit, but the associated DAES have essentially the same spectral shape for all the components, indicating that these different lifetime components decay independently from very similar excited states. This is different for all the samples reconstituted with PsbS. The lifetimes are generally much shorter in these samples reconstituted with PsbS (Supplementary Figure 9.2) than without PsbS, and new red-shifted low amplitude components show up which are specifically correlated with quenching. Together with the shorter lifetimes the increased intensity of the spectra in the FR region is reminiscent of the corresponding situation for the spectra of quenched LHCII both *in vivo* and in quenched oligomers. We further analysed these data by global target analysis using a kinetic model that had been established previously in detailed quenching studies on LHCII oligomers (without

detergent) (Miloslavina, Wehner et al. 2008). The kinetic target models with resulting rate constants and the corresponding SAES are shown in Figure 9.2 (proteoliposomes with LHCII but no PsbS) and 9.3 (proteoliposomes with LHCII and PsbS). The SAES of all the samples reconstituted with PsbS show two red-emitting states that are formed sequentially from the initially excited state. The samples reconstituted without PsbS show also multi-exponential decays. But these decays have essentially the same spectra within the error limits and the best-fit kinetic analysis suggests that they decay independently from each other (non-connected compartments, cf. Figure 9.2). The spectral dependence of the average fluorescence lifetimes for all the samples are shown for proteoliposomes without PsbS (Figure 4a) and with PsbS (Figure 4b). Note that the lifetimes are essentially wavelength independent for the (unquenched) samples without PsbS, except for the shortest wavelengths, while the average lifetime shows a pronounced peak around 710 nm for the quenched samples with PsbS.

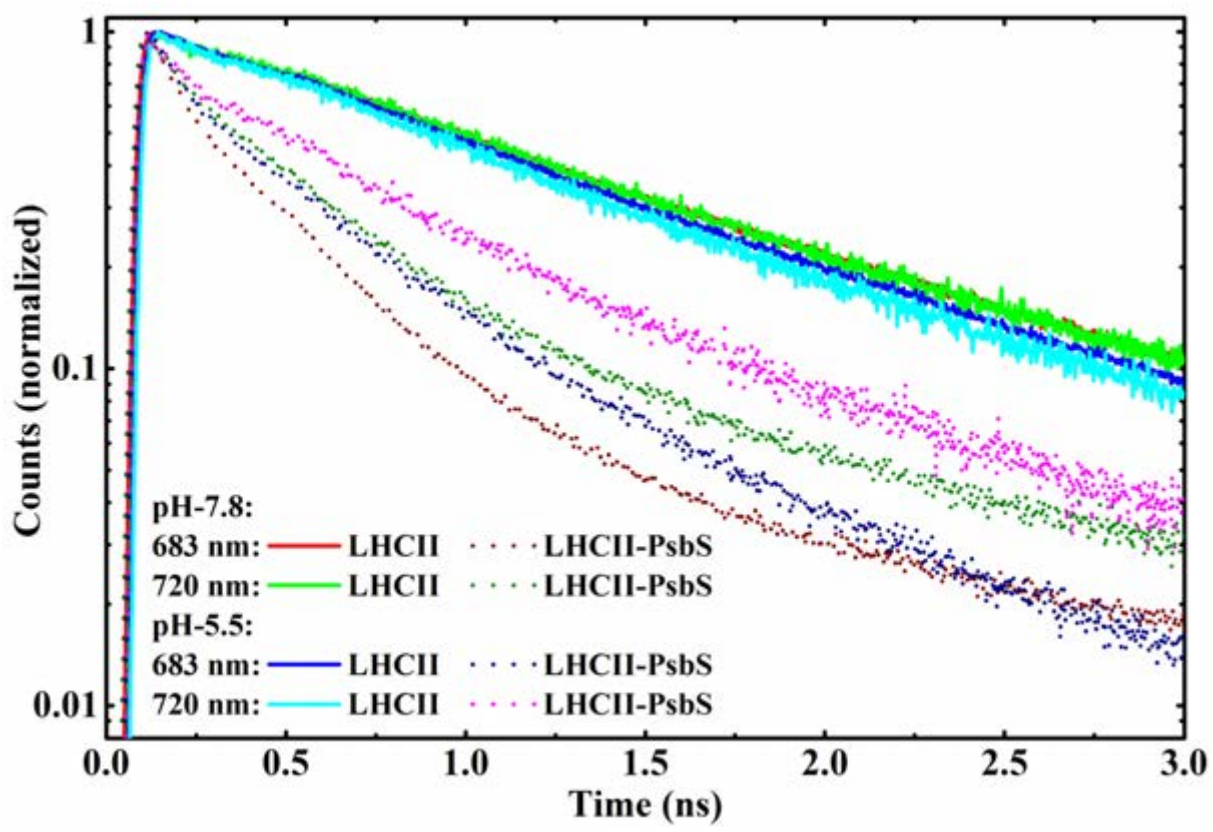

Figure 9.1: Fluorescence decays (semilogarithmic scale) at two selected emission wavelengths for various conditions of LHCII reconstituted in proteoliposomes without (full lines) and with (dotted lines) PsbS.

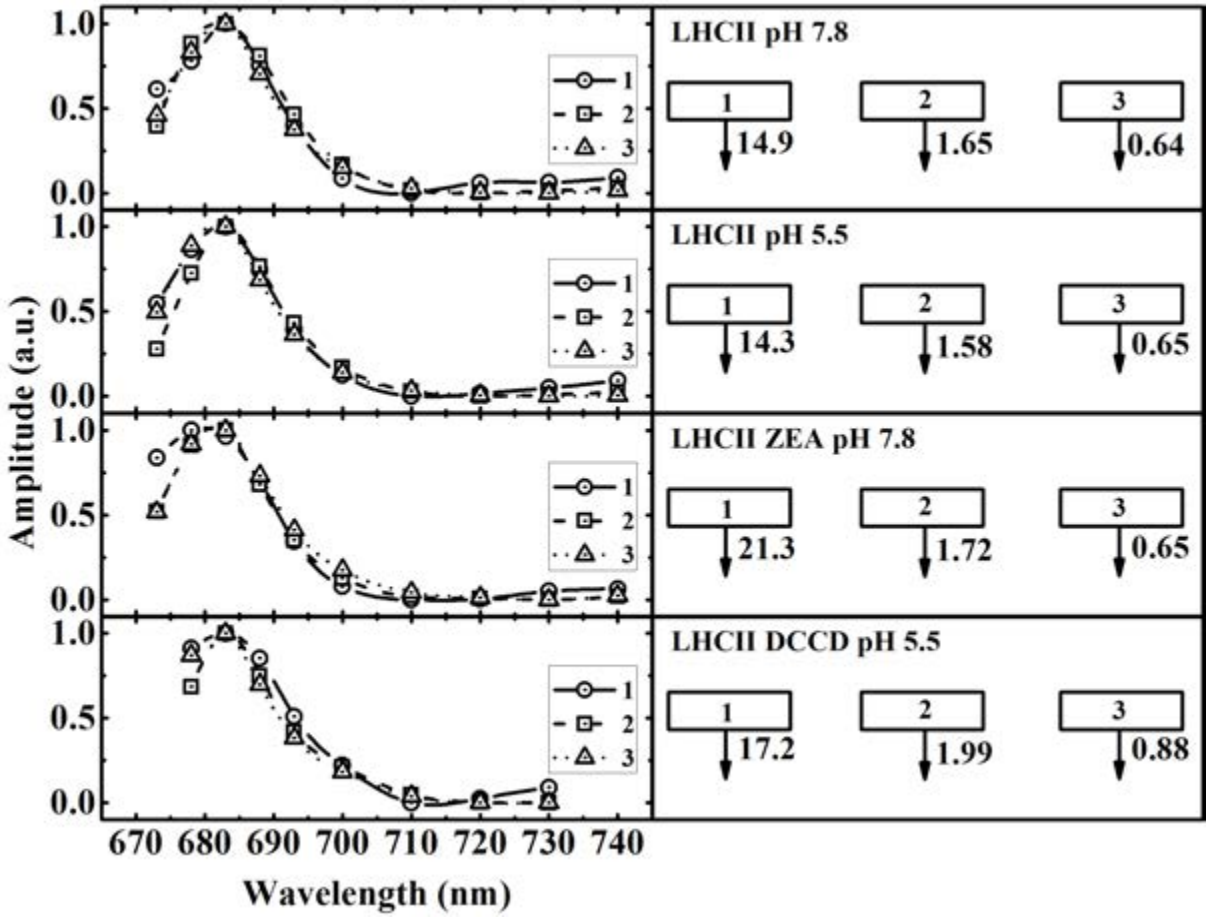

Figure 9.2: SAES and kinetic target models for proteoliposomes containing LHCII only and various conditions of pH and additives. Left side: SAES of the compartments shown on the right side. Note: The SAES amplitudes are normalized for better visibility. Right side: The numbers in the boxes denominate the compartments, and the numbers at the arrows give the rate constants in units of ns^{-1}.

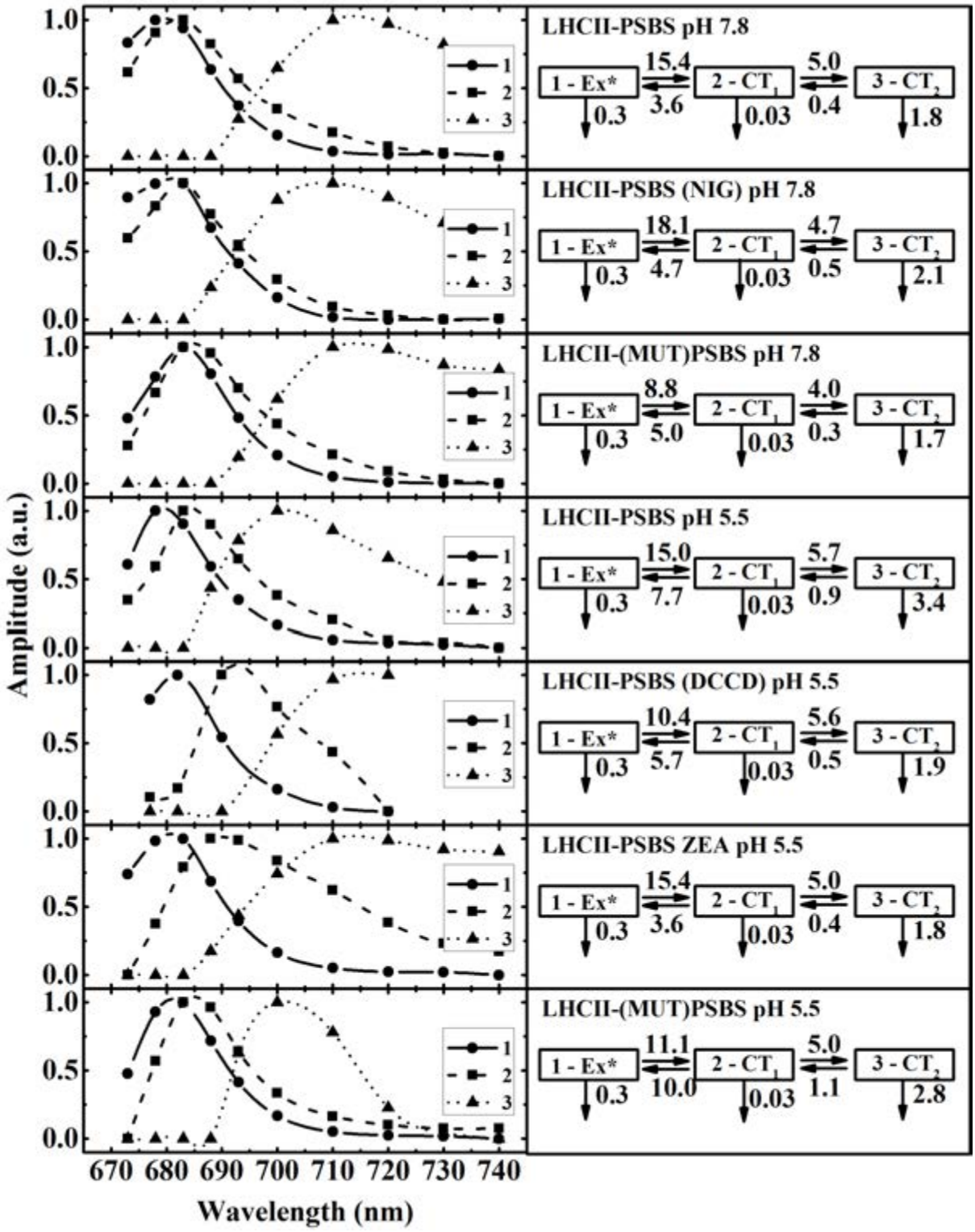

Figure 9.3: SAES and kinetic target models for proteoliposomes containing both LHCII and PsbS and various other conditions. Left side: SAES corresponding to the model compartments shown on the right side (numbered boxes). Note: The SAES amplitudes are normalized for better visibility. Right side: The numbers in the boxes denominate the compartments, and the numbers at the arrows give the rate constants in units of ns^{-1}. Note: The SAES amplitudes are normalized for better visibility. The real amplitudes of the SAES of the CT states are typically 7-15 times smaller than those of the originally excited exciton state reflecting the much lower oscillator strength of the CT states vs. Chl excited states.

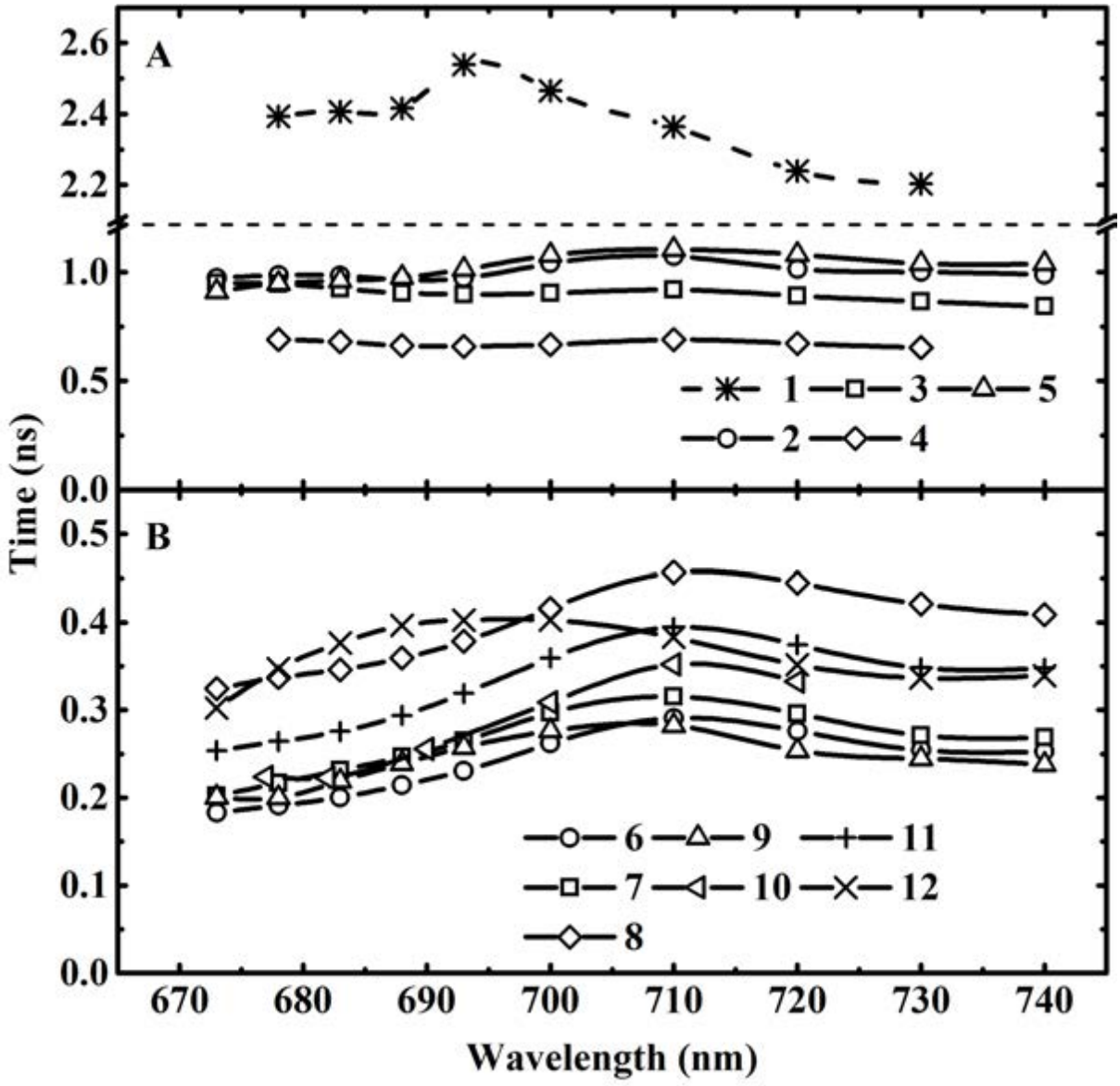

Figure 9.4: Wavelength dependence of the average lifetimes of the fluorescence decays for proteoliposomes reconstituted with LHCII only (A) or with LHCII and PsbS (B) for various conditions of pH and other additions: **1** – LHCII pH 7.8 LHCII/LIP-200; **2** - LHCII pH 7.8 LHCII/LIP-160; **3** - LHCII pH 5.5; **4** - LHCII DCCD pH 5.5; **5** - LHCII ZEA pH 7.8; **6** – LHCII-PsbS pH 7.8; **7** - LHCII-PsbS NIG pH 7.8; **8** - LHCII-(MUT)PsbS pH 7.8; **9** - LHCII-PsbS pH 5.5; **10** - LHCII-PsbS DCCD pH 5.5; **11** - LHCII-PsbS ZEA pH 5.5; **12 -** LHCII-(MUT)PsbS pH 5.5.

9.1.2. Results from quantum chemical calculations

The results of the quantum-chemical calculations of the localized excited states and the CT states for the cluster of three excitonically coupled Chls forming the supposed quenching center in LHCII (Chls 601, 602 and 607 of chain A in PDB structure 2BHW (Standfuss, Terwisscha van Scheltinga et al. 2005) embedded in the protein environment are shown in Figure 9.5. The molecular model contained the coupled Chl cluster consisting of the three Chl *a* molecules forming the supposed quenching center

(residues number 601, 602 and 607 of chain A in PDB structure 2BHW (Standfuss, Terwisscha van Scheltinga et al. 2005); (cf. Supplementary Figure 9.3 and 9.4) and the shell of aa residues and lipids embedding the chromophores at a distance up to 4 nm (Supplementary Figure 9.4, for details of the calculations see Materials and Methods). Without any protein environment (gas phase), we find only local Q band excitations, e.g., Q_y excitations at 579, 567 and 563 nm with oscillator strengths of 0.62, 0.17 and 0.05, respectively. Excitonic coupling is indicated for the lowest and the highest Q_y bands as they display similar orbital character, being delocalized mainly over Chls 601 and 607. Yet, analysis of the wavefunctions and charge distribution of the excited states yields no indication of any charge transfer state (CT) in the energy region of the Q_y spectrum in the absence of the protein surrounding. However in the presence of the protein surrounding, represented by the respective PCFs, the calculations yield several CT states within and below the Q_y band region (Figure 9.5). The energies of these CT states are strongly dependent on the specific protonation state configuration at the two main protonation/deprotonation centers considered here. Whereas some CT states are also found in the vicinity of the Qy energies for the neutral Glu175/Lys179 protonation state, the lowest CT states drop in energy by ca. 2000 cm^{-1} in the charged protonation state $Glu175^{-}$/H-$Lys179^{+}$ state, thus producing CT states that are located well below the localized excited states. These low-lying CT states could then be formed rapidly by electron transfer after initial Qy excitation. Also a significant dependence of the CT state energies is suggested by the calculations on the protonation state of the PG/Lys182 pair (cf. Figure 9.5). Another important question refers to the ground-state energy of the three-Chl cluster in dependence on the protonation state. We calculated those energies for the neutral Glu175/Lys179 protonation state without the PCF approximation, taking into account fully the protein environment based on the crystal structure. This site is of particular interest since the Glu175 is surface-exposed and its protonation state could be thus be easily controlled by any closely located external molecules or charges. The environment corresponding to the X-ray structure interestingly yields the charged $Glu175^{-}$/H-$Lys179^{+}$ state as the lowest energy ground state, and thus the state that would be present before excitation. This state has the very low-lying CT states, and would thus be ideal to effect CT state formation after excitation. With a negative charge placed near the Glu175 (located on the stromal side), simulating the effect of an external negatively charged environment, the energy of the Chl ground state increases drastically however, and in this situation the neutral Glu175/Lys179 protonation state represents the lowest energy ground state. This would open the possibility that a negative charge located near the Glu175 could switch off the possibility for CT state formation.

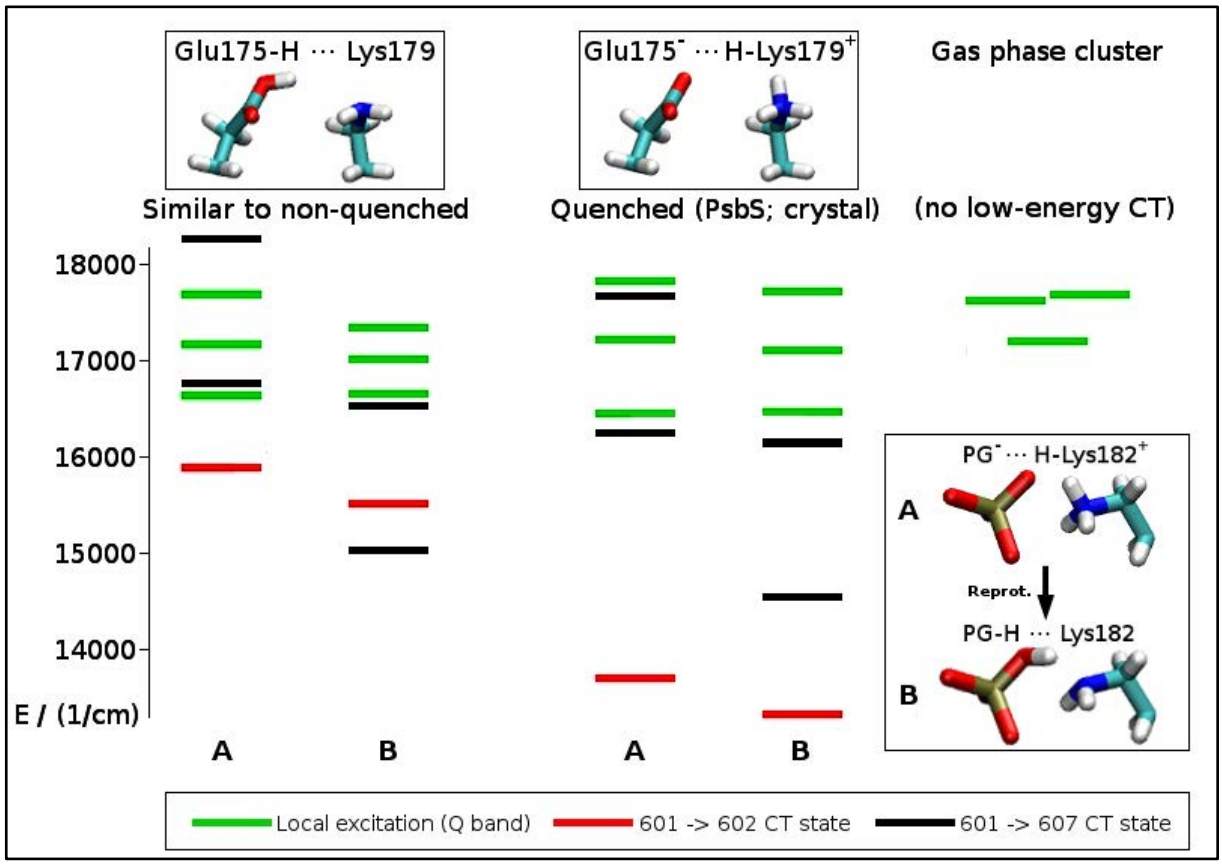

Figure 9.5: Energy level diagram for localized excited states (green lines) and CT states (black and red lines) of the quenching center formed by the excitonically coupled cluster containing three Chls. The energies are calculated for the four different protein protonation states of the surrounding protein as indicated in the boxes. On the right-hand side the energies are shown for comparison for the same Chls in the gas phase.

9.2. Discussion

9.2.1. PsbS induces quenching via CT states

Comparison of the lifetime data for proteoliposomes containing PsbS/LHCII vs. those containing LHCII alone reveals that PsbS induces efficient quenching. As judged from the average lifetime in the 680 nm emission region the initially excited state is quenched by a factor of approx. 5 by PsbS as compared to the same LHCII/lipid ratio without PsbS. However the LHCII/lipid ratio has some effect in the average lifetime even without PsbS present. For a low protein/lipid ratio the average LHCII lifetime reaches a value of 2.5 ns, while for the high protein/lipid ratio (characteristic of thylakoids) used in this work the average lifetime without PsbS is only ca. 1 ns (Figure 4). This finding is in line with an earlier observation on reconstituted LHCII in proteoliposomes (Moya, Silvestri et al. 2001). We note however that the quenching effect of a high LHCII/lipid ratio is not reflecting *the in vivo* PsbS or qE quenching mechanism since it is PsbS independent, and

it is in particular also not correlated with the formation of FR-emitting states (see below). This quenching apparently occurs due to LHCII/LHCII interaction alone and its molecular origin is not well understood at present.

In all cases where LHCII and PsbS have been co-reconstituted into liposomes two new red-shifted kinetic fluorescence components were found, and the overall kinetics was best fitted by a reversible sequential reaction model (Figure 3) and a very short-lived initially excited state (200-300 ps). In all these cases these FR-emitting states have longer lifetimes but smaller SAES amplitudes than the initially excited states of LHCII. In order to explain the quenching effect we have to assume that PsbS interacts with LHCII in a specific manner in order to cause this effect. Our general results in that respect are in line with a previous report on PsbS-induced quenching in liposomes studied by steady state spectroscopy (Wilk, Grunwald et al. 2013). The time-resolved data presented here allow however a detailed evaluation of the kinetics and mechanism of quenching. Red-shifted fluorescence (FR) states have been observed previously under various quenched conditions and were identified as Chl-Chl CT states (Miloslavina, Wehner et al. 2008, Müller, Lambrev et al. 2010). The properties of these states involved in LHCII quenching have been characterized more recently by Stark fluorescence (47) (Wahadoszamen, Berera et al. 2012) and by hole burning spectroscopy (Kell, Feng et al. 2014) and both methods further strengthened their interpretation in terms of Chl-Chl CT states. Most interestingly however these red-shifted states were found previously *in vivo* in intact leaves to reflect the characteristics of the PsbS-dependent qE quenching (Holzwarth, Miloslavina et al. 2009, Lambrev, Nilkens et al. 2010, Miloslavina, de Bianchi et al. 2011). We thus conclude that PsbS-induced quenching of LHCII in proteoliposomes very well reproduces the processes and mechanisms of *in vivo* qE quenching and thus represent an excellent model system to study the molecular mechanism of qE-quenching in an environment that is much simpler to study than the intact leaf. Several observations are very important with respect of the mechanism of this quenching: First, no lowering of the pH is required in order to induce the major part of the PsbS-induced quenching (Figure 9.3). Rather only a small but distinct increase in quenching occurs if the pH is lowered from 7.8 to 5.5, and this effect can be eliminated again by adding DCCD, which is a molecule that blocks pH sensing groups in proteins. Interestingly only a very minor quenching effect (average lifetime reduction by about 10-20%; cf. Figure 3A) was observed (and only in the long-wavelength range) upon lowering the pH for proteoliposomes that contained only LHCII without PsbS, although it has been proposed in the literature that LHCII itself contains pH sensing groups. Our observations are thus

partially at variance with pH sensitivity of LHCII quenching studied in detergents of varying concentration. For LHCII in a membrane this effect seems to be minor. More interesting in this connection is our observation of a lack of pH sensitivity of the quenching for LHCII reconstituted together with PsbS (Figure 9.3 and 9.4). The quenching is essentially identical at pH 7.8 and at pH 5.5. This finding is in contrast with present models explaining the activation of PsbS quenching *in vivo*. It has been shown that in order for inducing the *in vivo* qE quenching a low lumen pH (or ΔpH across the membrane) is required. We note that Wilk et al. did not study the effect of lowering of the pH in the reconstituted proteoliposomes, but also found the strong PsbS quenching effect already at neutral pH and our results are thus in agreement with their findings. One additional note is that we did not find any effect of nigericin on the PsbS-induced low pH quenching. If we reasonably assume that the liposomes do not transmit protons, and thus acidification on the outside of the liposomes would only be able to activate those PsbS molecules which have an orientation such that the pH-sensing groups are located also on the outside (assuming that PsbS is oriented randomly in the membrane). Thus addition of nigericin might be able to pH-activate also PsbS with proton sensing groups on the inside. However no such effect was observed. In this connection it is also very interesting to compare the quenching effect of the PsbS mutant which lacks the pH sensing groups. *In vivo* deletion of these groups knocks out the qE quenching. However, in the reconstituted liposomes this mutant also effects substantial quenching already at pH 7.8, with little difference to pH 5.5 (Figure 9.3 and 9.4). The overall quenching effect of the PsbS mutant is however somewhat smaller than for the w.t. PsbS (at 680 nm the initially excited state has a lifetimes of 300 ps with the mutant PsbS vs. 200 ps with the w.t.; Note that some dependence upon pH exists for the intensity of the FR state emission above 710 nm). From this discrepancy between *in vivo* and *in vitro* quenching results follow interesting questions regarding the exact role of these pH sensing groups for inducing qE quenching. Are these groups indeed required to affect the quenching when PsbS is bound to LHCII, or does the pH sensing via PsbS serve some other purpose? Literature reports provided evidence that PsbS *in vivo* may have several different roles and bind to different components of the thylakoid membrane and not only to LHCII (Teardo, de Laureto et al. 2007). Possible other roles of the pH sensing groups could thus be the activation of the PsbS transition from a dimer to a monomer, the detachment of LHCII from the PSII supercomplex. We speculate here that the first possibility might provide at least one of the relevant answers. We can infer this from the fact that in our reconstituted liposomes the PsbS is present already in the monomeric

form, and not in the dimeric form. However, a final understanding of the role of the pH sensing groups in particular *in vivo* in PsbS will need further clarification.

We also studied the effect on the lifetimes by the combined action of PsbS and added Z (Note: this Z is not directly bound by LHCII, but present external to the protein in the liposome membrane). Interestingly we did not find any quenching effect of Z in this case (Figure 3), at variance to the report of Wilk et al. (Wilk, Grunwald et al. 2013) who found a pronounced quenching effect of added Z in steady state fluorescence measurements. We note however that lifetime measurements are a more direct measurement of quenching than comparison of steady state measurements between different samples and thus do allow a more reliable evaluation of the effects as compared to steady state data. Finally we also studied the effect of DCCD on a possible pH-induced quenching. Interestingly without PsbS present the non-specific LHCII quenching at low pH was increased, rather than decreased by DCCD. This indicates that DCCD may somehow affect the LHCII-LHCII trimer interaction. For liposomes reconstituted with both LHCII and PsbS, DCCD had no pronounced effect on the quenching of the initially excited state around 680 nm at low pH 5.5. However the FR fluorescence that is related to quenching increased somewhat with the addition of DCCD. This is definitely the opposite effect that what would be expected from DCCD effects on quenching reported in the literature.

9.2.2. Molecular mechanism of LHCII quenching and of qE

We have previously shown that LHCII quenching in detergent-free oligomers occurs by an excited state deactivation via FR fluorescing Chl-Chl CT states (Miloslavina, Wehner et al. 2008, Müller, Lambrev et al. 2010). Essentially the same findings were also obtained by us recently on LHCII crystals which are highly quenched) (Pascal, Liu et al. 2005, Ostroumov, Lambrev et al. 2014). This mechanistic interpretation is also supported by recent hole-burning studies (Kell, Feng et al. 2014) as well as by the observation of a Stark effect on the FR fluorescence that is associated with LHCII quenching (Wahadoszamen, Berera et al. 2012). The observations on the PsbS-induced LHCII quenching in the proteoliposomes are fully in line with this interpretation, i.e. the data strongly suggest that the same or very similar quenching mechanism is operative for *in vitro* LHCII oligomers, in crystals, in PsbS-containing proteoliposomes, and *in vivo* in the qE quenching mechanism (Miloslavina, Wehner et al. 2008, Holzwarth, Miloslavina et al. 2009, Lambrev, Nilkens et al. 2010). We had proposed that the quenching via Chl-Chl CT states can be explained in principle by a polarity-switching

model, where the energetic position of the Chl-Chl CT states, either above (no quenching) or below (quenching switched on) the energy of the local (excitonic) Chl excited states is controlled by a polarity change in the immediate environment of the Chls constituting the quenching centre. The rationale is that this polarity switching is induced by PsbS when it binds to LHCII. The present data should thus in principle provide a detailed insight into the molecular mechanism of this polarity-switch and thus the molecular mechanism of quenching. PsbS contains several charged amino acid (AA) sites that might interact with LHCII and thus provide that function. However for proposing a detailed molecular mechanism we would need to know the interaction region and the precise interaction geometry of PsbS with LHCII. Mainly due to a lack of a high resolution structure of PsbS we unfortunately do not have that information available and would thus have to refer to some molecular interaction modelling for the PsbS/LHCII complex resulting in speculative assumptions. However, in view of the finding that PsbS-induced quenching *in vitro* (in reconstituted liposomes) as well as *in vivo* and that strong quenching in LHCII crystals and aggregated LHCII all occur via very similar intermediate states, as inferred from the FR fluorescence induced in all cases, and thus likely via the same mechanism. This gives us a handle on proposing a detailed molecular mechanism on the basis of the well-resolved LHCII X-ray structure (Liu, Yan et al. 2004, Standfuss, Terwisscha van Scheltinga et al. 2005). We thus describe in the following the basis for a detailed molecular quenching model based on LHCII crystals, and then discuss the relationship and similarity of this model to PsbS-induced quenching.

9.2.3. The molecular model

We focus our search for a quenching mechanism to the molecular region that has been identified by several independent observations as the most likely quenching center in LHCII, i.e. the three Chls of the strongly excitonically coupled Chl cluster Chl 601, 602, and 607 (Ruban, Berera et al. 2007, Mozzo, Passarini et al. 2008, Bode, Quentmeier et al. 2009 (note that we use here the Chl nomenclature of Standfuss et al {Standfuss, 2005 #4251, Ostroumov, Lambrev et al. 2014)). Inspection of that region in the crystal structure around the relevant Chls reveals three groups that could potentially play a key role in a polarity switch model. The easiest way to switch between a polar and a non-polar environment in a protein is a proton transfer between neighboring groups (protonation/deprotonation reaction). Three different aa/aa or aa/lipid pairs were found which could in principle be reversibly protonated/unprotonated (i.e.

charged/uncharged) in the immediate vicinity to the three Chl cluster (see also Methods section). These sites are (i) Asp162, close to Chl 601, (ii) a pair formed by Glu175/Lys179, located between Chls 602 and 607, and (iii) a pair formed by Lys182 and a PG molecule (labelled LHG in PDB structure 2BHW (Standfuss, Terwisscha van Scheltinga et al. 2005)), which coordinates the Mg ion of Chl 607. Preliminary simplified quantum chemical calculations indicated that only the latter two sites would have any significant influence on the energies of the CT states of the Chl cluster. Consequently all four protonation/deprotonation states resulting from these two pairs were calculated by precise QM/QM calculations as described above (Figure 9.5 and 9.6). The results of the calculations support the idea of a polarity switch controlling the energies of the CT states of the system and thus a quenching mechanism that would be controlled by an externally affected internal proton-transfer reaction. The protonation state with the lowest Chl cluster electronic ground state energy in the crystal corresponds to $Glu175^{-}$/$Lys179^{-}H^{+}$ (Figure 9.6). This state has several low energy CT states located well below the local excited states of the excitonically coupled Chl triple cluster (Figure 9.4). Thus the formation of one or more Chl-Chl CT states after excitation of the lowest excitonic state is energetically possible. After the first electron transfer step corresponding to the formation of the first CT state (Figure 9.5 and 9.7) a proton transfer at the Lys182/PG, pair, driven by the charges created by the first electron transfer step, would allow another electron transfer step to reach a second group of still lower-lying CT states. These two (groups) of CT states can be identified with the CT_1 and CT_2 states observed in the results of the target analysis of the PsbS-induced quenching in the reconstituted liposomes (Figure 9.3) and also with the similar FR-fluorescence CT states observed in LHCII crystals (paper to be submitted (Ostroumov, Lambrev et al. 2014)). In the absence of other relaxation possibilities the lowest energy CT state(s) would recombine to the ground state and quenching of the excited state would be completed. The whole reaction scheme as supported strongly by our QM/QM calculations is depicted in Figure 9.7 together with its intermediates on an energy level scale. We note that this model is also in line with the electronic properties of the intermediates deduced from both ultrafast fluorescence as well as transient absorption spectroscopy (Miloslavina, Wehner et al. 2008, Holzwarth, Miloslavina et al. 2009, Müller, Lambrev et al. 2010, Miloslavina, de Bianchi et al. 2011).

In this model the Chl-Chl CT states act as intermediates in excited state quenching. The formation of the first CT state out of the Qy excitonic state occurs very rapidly (with time constants in the range of 50 ps, Figure 9.3). The quantum chemical calculations result in

the local Qy band excitation energies being fairly unaffected by the different protonation states. This agrees with the experimental finding that the absorption spectrum of quenched aggregates and crystals, as compared to unquenched trimeric LHCII, does not differ substantially in the main absorption bands, but only shows a weak far-red tailing in the quenched LHCII reflecting absorption of low-lying mixed CT states (Magdaong, Enriquez et al. 2013, Kell, Feng et al. 2014).

The Glu175/Lys179 protonation state controls specifically the energetic position of the 601 -> 602 states (red lines in Figure 9.5). The 601 -> 602 CT states (Figure 9.5 and 9.7) can thus act as acceptors of energy from, e.g., the 601 -> 607 CT states, thus forming a downhill ladder of CT states. According to the calculations, the sequential downhill relaxation of the CT states promotes a transfer of the (buried) Lys182 proton to the close by PG residue. In the charged Glu175/Lys179 configuration, the 601 -> 602 states are about 2000 cm^{-1} lower in energy than in the uncharged configuration. A note of caution is required here: due to the approximations that were necessary to perform this calculation on such a large system comprising three Chls and its surrounding, we are clearly faced with some substantial error in the calculation of the absolute energies of the CT states relative to the excited states. However, we note that it is less important here to get the absolute energies of the CT states right, but rather the relative changes in these energies upon the changes in protonation states. The very large effect of the Glu175/Lys179 reprotonation upon the energy of the 601/602 CT state (CT energy down-shift of ca. 2000 cm^{-1}) and also the smaller but still relatively large effect of the reprotonation of the PG/Lys182 pair thus provides us quite a safe margin for our conclusions.

The calculations show that (i) the 601 -> 602 CT state energies depend critically on the Glu175/Lys179 protonation state, being energetically lower for a charged Glu175/Lys179 pair, and (ii) the PG/Lys182 proton transfer appears to be energetically favorable for any CT state formed, but more so for 601 -> 607 CT states which are strongly stabilized. Thus, we can conclude that formation of the first CT state depends critically on the proton configuration of the system at the Glu175/Lys179 site. This site is thus likely to play the role of the initial switch or “gate-keeper” which decides whether quenching by CT state formation can occur or not. With the electrically neutral protonation state Glu175/Lys179 the gate for CT state formation would be closed, as the CT states are strongly shifted up in energy. Consequently, initial transfer of the proton in that pair to Lys179 will open the gate to start a sequence reaction of CT states. This is the ground-state preferred in the LHCII crystal according to our calculations and thus

explains very well why the LHCII crystal is quenched. In contrast the PG/Lys182 protonation site is buried in the protein and inaccessible from the surface. We thus cannot expect that it plays an externally switchable gate-keeper role but rather it should be expected to control the rate of an intermediate CT reaction in the reaction sequence.

It is now of interest to speculate how the quenching can be switched off. According to our model this would have to occur via a switching of the Glu175/Lys179 site to the neutral state. This could be affected by interaction with an external (charged) agent since the Glu175 is located at the surface of the protein, directly accessible to interaction with external cofactors, like e.g. ions, external proteins like e.g. PsbS, or polar water molecules, as in the case of detergent-free LHCII aggregates. We have tried to simulate in our calculations what would be needed to switch this site to a neutral state by proton transfer toward Glu175. Our calculations show that it is possible to switch the Glu175/Lys179 protonation state preference to neutral by simply approaching a chloride ion from the stromal side towards the aa pair. The energetically optimal (ωB97XD/6-31G(d)) position for the ion is at 3.85 Å for the uncharged, and at 4.10 Å for the charged configuration. This places the Cl- just halfway towards the stromal surface, right in the middle of the polar part of the (missing) thylakoid membrane (see Supplementary Figure 9.3). The simulation thus shows that in the presence of an intact membrane, the charge preference of the Glu175/Lys179 pair will be inverted, favoring the neutral configuration (note that the Cl anion just stands as a proxy in the calculation for a suitable negative charge near the Glu175 site, we definitely do not propose here that actually a Cl anion would be present *in vivo*). Thus such a negative charge would have the desired effect for switching off the quenching. At present we do not have a detailed structural proposal how this could happen *in vivo*. To some extent these results indicate however that the preferred "natural" state of LHCII may in fact be the quenched state, and that switching off the quenching may in fact require a special interaction in the membrane. Interaction of negatively charged phosphate head groups of the lipids with Glu175 may provide the answer, but more work needs to be done on that.

From the full set of CT states (not shown), including test calculations using different PCF configurations, as well as TD-ωB97XD calculations, we conclude that the 601 -> 607 CT states always represent the lowest CT states at the ground state geometry, with the 601 -> 602 states serving as intermediates. Thus, it is likely that the system ends up first in a Chl 601^{+}/Chl 607^{-} CT configuration. This CT state would then promote/induce the PG/Lys182 proton transfer.

9.2.4. Hypothesis on the PsbS-induced polarity-switching

The Glu moiety of the Glu175/Lys179 pair is surface-exposed in LHCII (Figure 9.8). It is thus accessible to interaction with the surrounding. We suggest that in the crystal (and also in LHCII oligomers) Glu175 interacts with a polar surrounding, unprotected by the non-polar tail groups of the membrane lipids or detergent in the case of detergent-isolated LHCII. This environment is favorable to stabilize the charged $Glu175^{-}/Lys179^{-}H^{+}$ pair. Thus the gate for the formation of CT states is open and quenching occurs as depicted in Figure 9.7. We suggest that *in vivo* binding of PsbS to LHCII has the analogous but more specifically controlled effect on Glu175 as has the relatively unspecific polar environment in the crystal (where the LHCII complex is not fully surrounded by a detergent micelle) and in detergent-free oligomers of LHCII. If our hypothesis of a lipid phosphate-group interaction with Glu175 in the unquenched state in the membrane would be correct, one could infer that PsbS upon binding to LHCII would remove this Glu175/phosphate group interaction which prevents quenching and the protonation gate at $Glu175^{-}/Lys179^{-}H^{+}$ would be opened. Further work will be necessary to verify this hypothesis.

Chapter 9

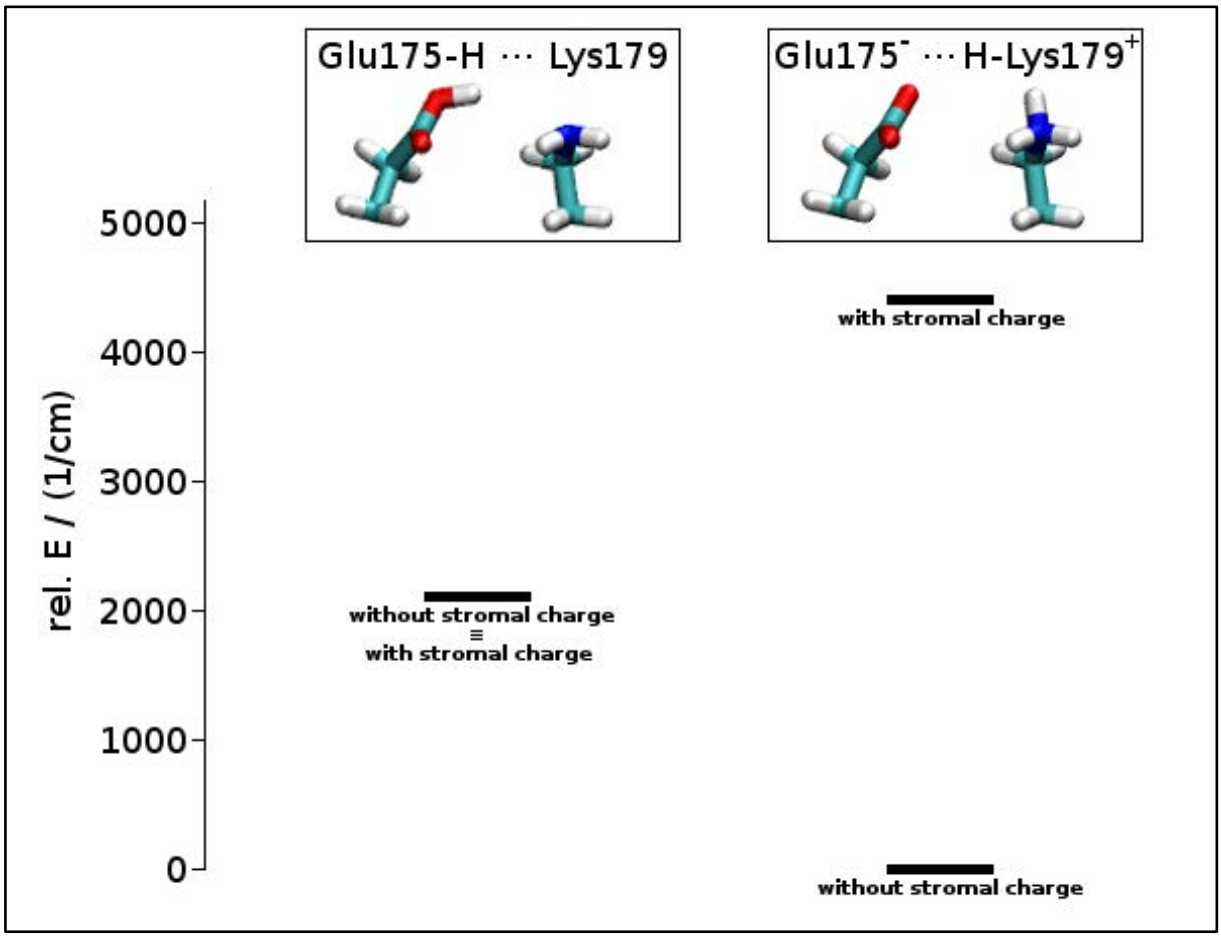

Figure 9.6: Molecular structure of the proposed quenching center showing the arrangement of the molecular groups relevant for quenching. The figure shows the chlorophyll a cluster as labeled. PG (violet) is phosphatidylglycerol, next to buried Lys182 (not shown). Red ellipse: surface-exposed Glu175/Lys179 gatekeeper pair (red/blue). Other elements are protein (grey), lutein (yellow), neaxanthin (orange), violaxanthin (light orange), other chlorophyll a (bright green) and chlorophyll b (cyan). Structure is based on the X-ray structure data of {Standfuss, 2005 #4251}.

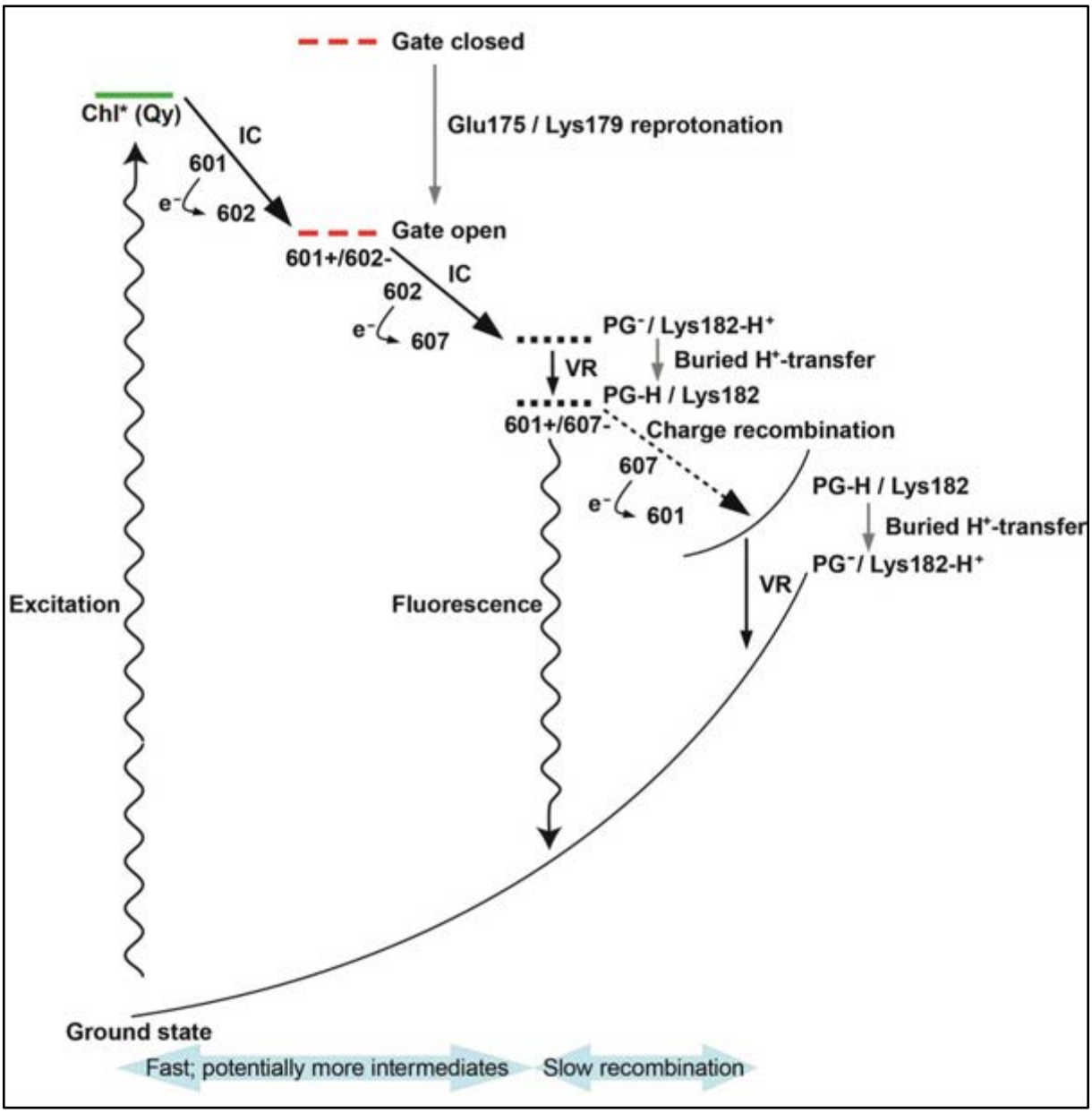

Figure 9.7: Mechanistic model for the sequence of reaction steps in quenching in the crystal. The same model is proposed to occur in PsbS-induced qE quenching. The CT state energy is likely controlled by the protonation state of the Glu175/Lys179 pair, and passively lowered upon CT state formation by reprotonation of the PG/Lys182 pair. IC is internal conversion, VR is vibrational relaxation.

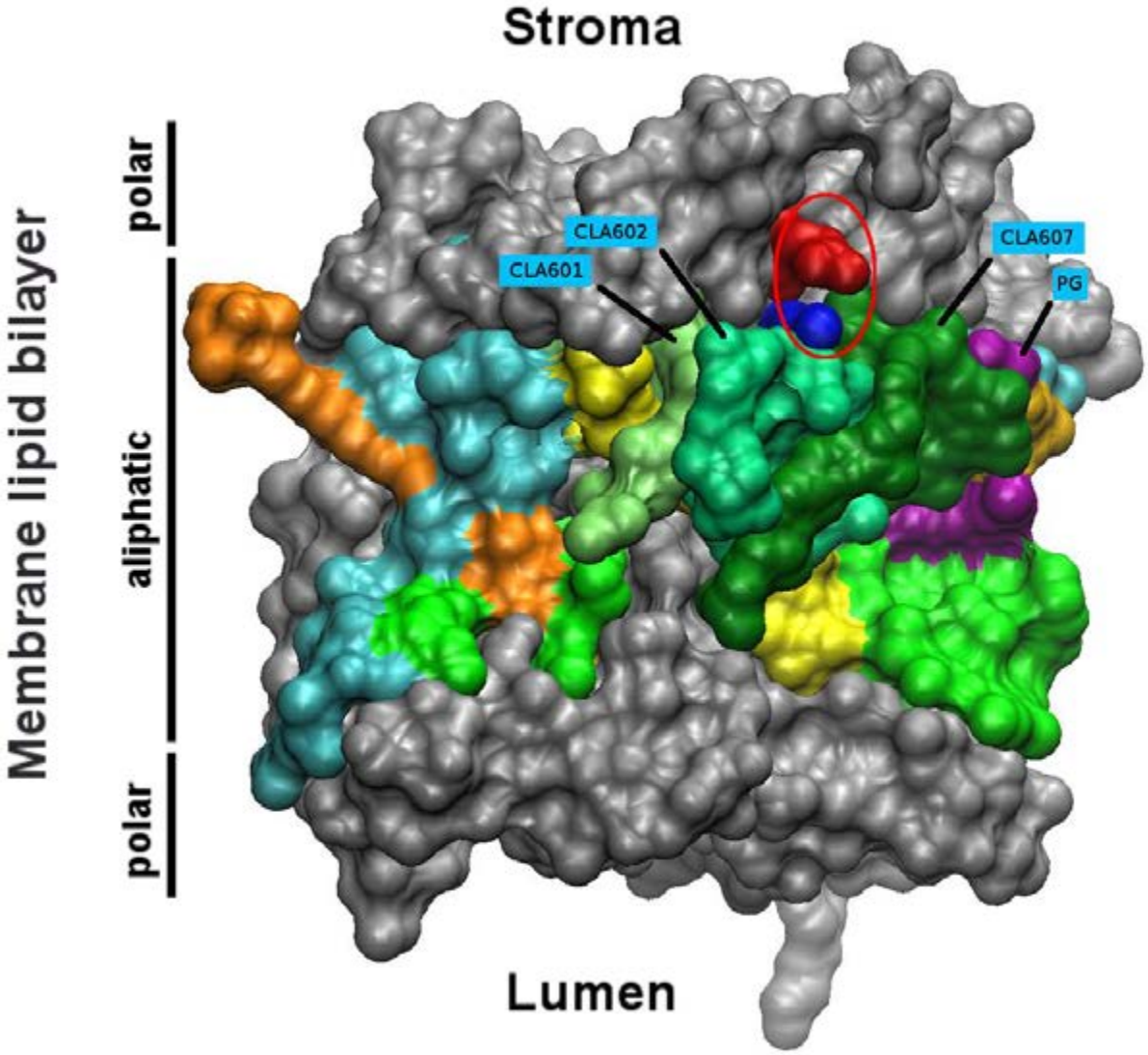

Figure 9.8: Molecular structure of the proposed quenching center showing the arrangement of the molecular groups relevant for quenching. The figure shows the chlorophyll a cluster as labeled. PG (violet) is phosphatidylglycerol, next to buried Lys182 (not shown). Red ellipse: surface-exposed Glu175/Lys179 gatekeeper pair (red/blue). Other elements are protein (grey), lutein (yellow), neaxanthin (orange), violaxanthin (light orange), other chlorophyll a (bright green) and chlorophyll b (cyan). Structure is based on the X-ray structure data of (Standfuss, Terwisscha van Scheltinga et al. 2005).

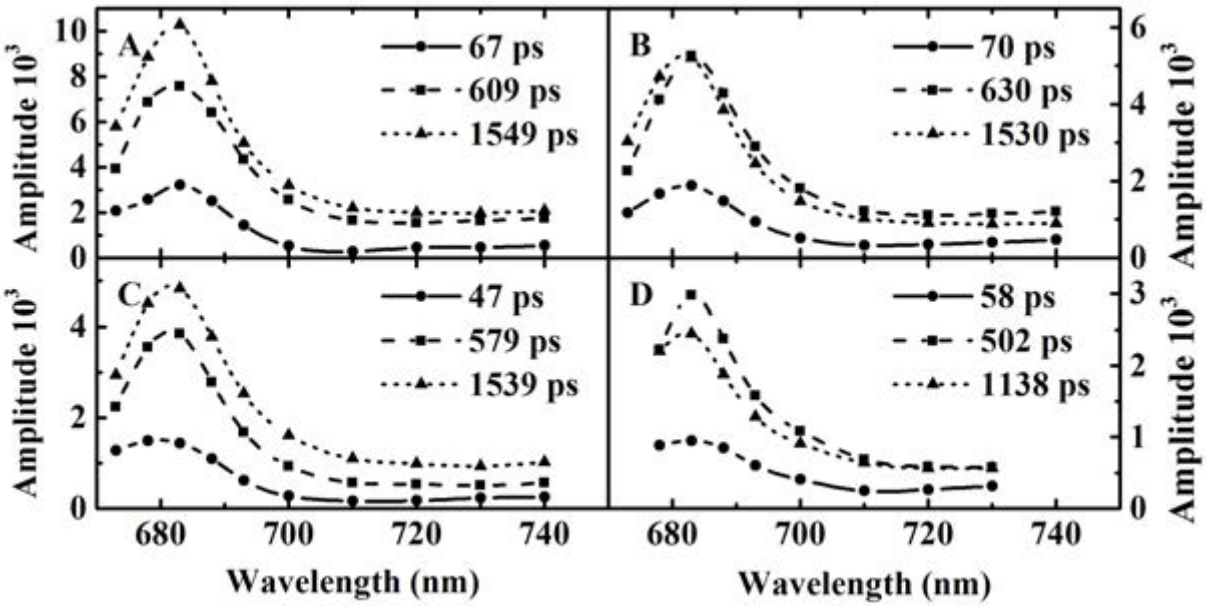

Supplementary Figure 9.1: DAES resulting from global lifetime analysis of fluorescence decays of proteoliposomes containing LHCII only for different pH and additives.

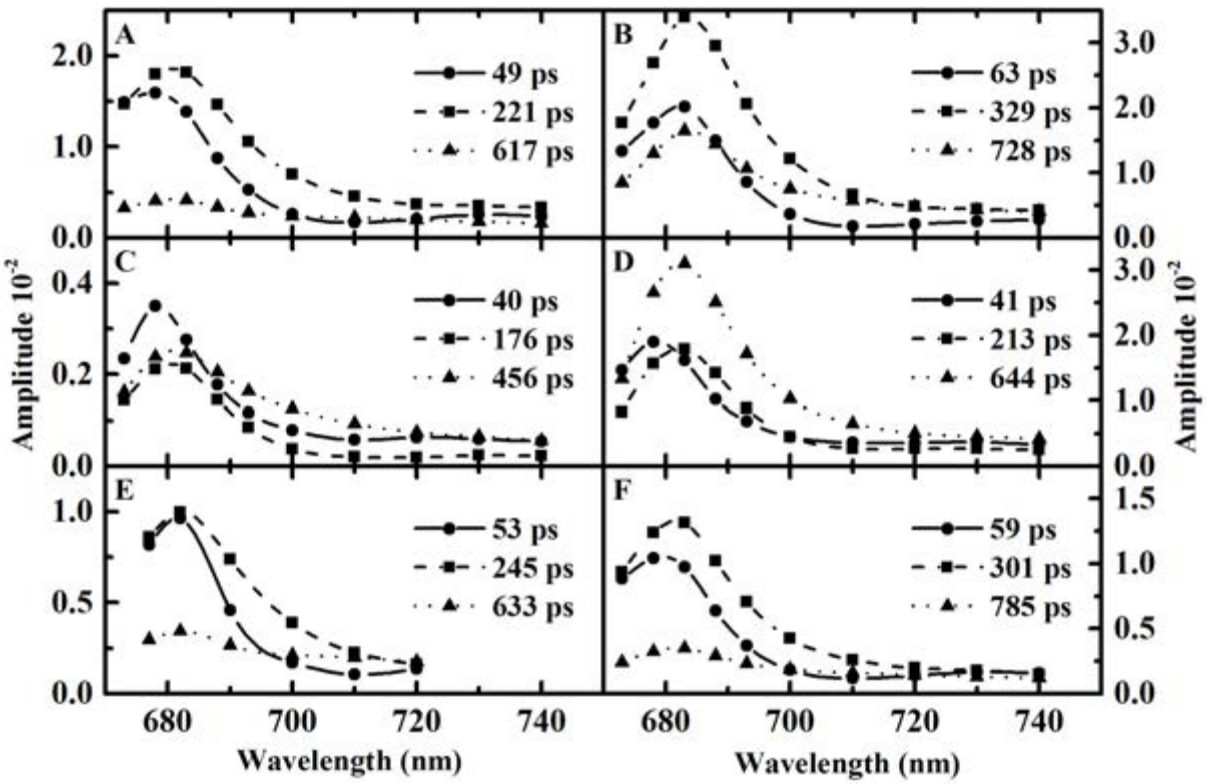

Supplementary Figure 9.2: DAES resulting from global lifetime analysis of fluorescence decays of proteoliposomes containing LHCII and PsbS for different pH conditions and various additives.

Chapter 9: Supplementary Information

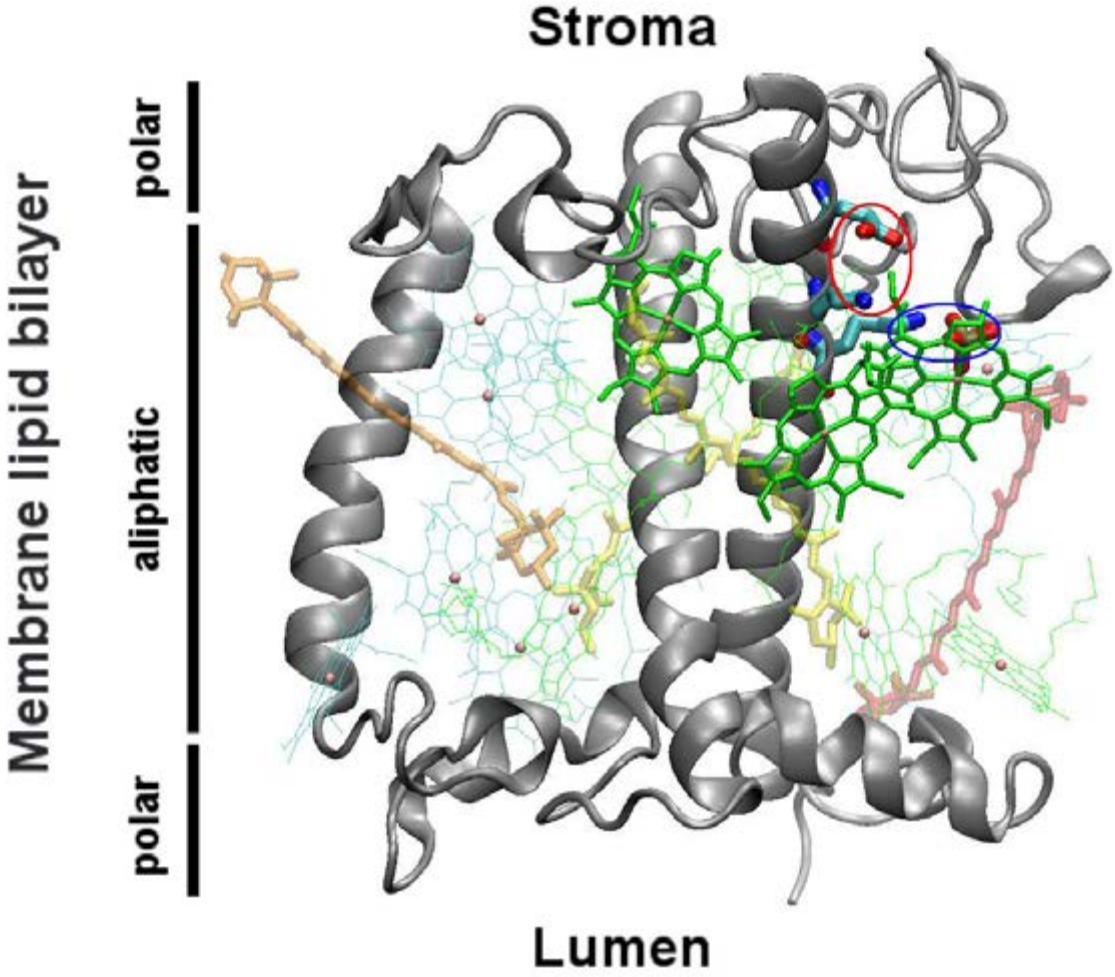

Supplementary Figure 9.3: Energy level diagram for localized excited states (green lines) and CT states (black and red lines) of the quenching center formed by the excitonically coupled cluster containing three Chls. The energies are calculated for the four different protein protonation states of the surrounding protein as indicated in the boxes. On the right-hand side the energies are shown for comparison for the same Chls in the gas phase.

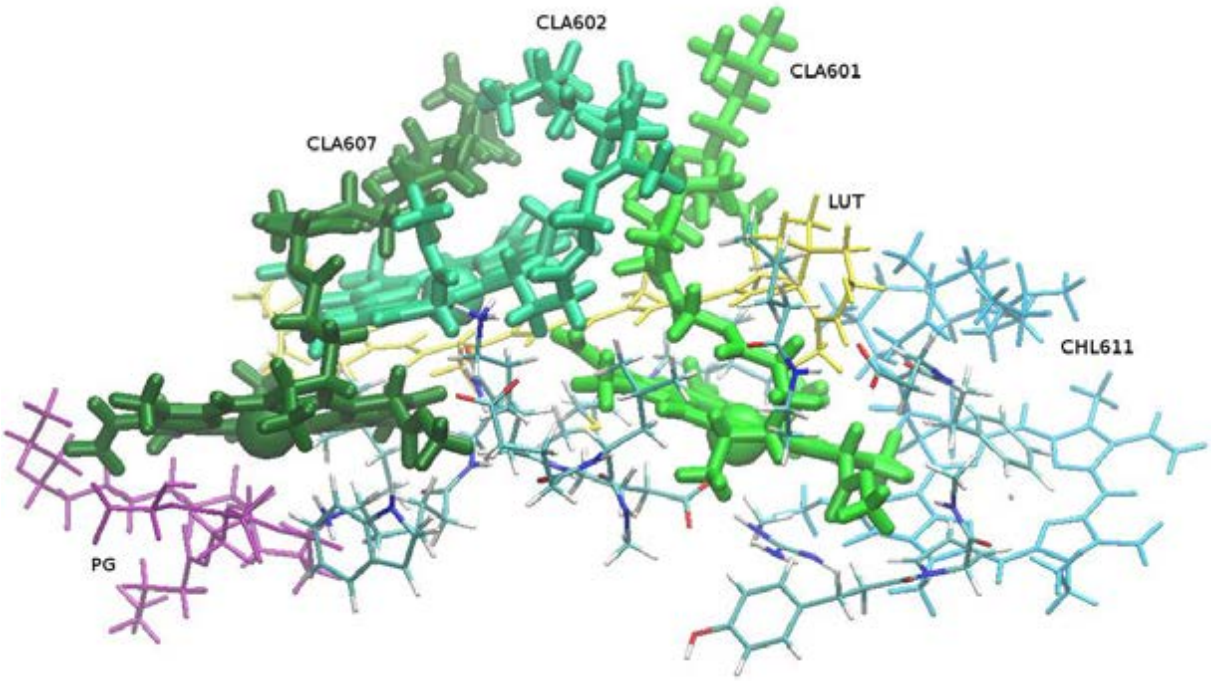

Supplementary Figure 9.4: Description of aa residues and other environmental factors taken into account in the quantum mechanical calculations. View from the stromal side, with the colored residues taken as labeled. CLA: chlorophyll a; CHL: chlorophyll b; LUT: lutein; PG: phosphatidylglycerol. The unlabeled atoms correspond to the protein environment, consisting of Trp16, Arg70 (only functional part), Met73 to Leu74, Tyr156 to Pro157, Phe161 to Asp162, Leu166 to Ala167, Glu175 to Leu176, Lys179 to Glu180 and Lys182 to Asp183. N-terminal cap is methyl, C-terminal cap is hydrogen after C-α. Arg70/Glu180 pair was always charged. Core atoms were CLA porphyrin plus Mg ions for the TD calculations, together with the Glu175/Lys179 and PG/Lys182 pairs for the ground state energy calculations.

Chapter 10 : Conclusion

The superiority of time-correlated single photon counting (TCSPC) technique in plant biophysics dwells with its high sensitivity, allowing measurements with low-light signals and detailed kinetic information can be extracted with the help of very powerful 'target-analysis' methods. This technique is probably the only non-invasive approach proven till date, capable of obtaining primary energy and electron transfer kinetics including the functional changes in the thylakoid membrane organization affecting the interaction of the primary components. So far, antenna-localized non-photochemical quenching (NPQ) mechanisms like, the qE and qZ have been considered as the main photoprotection mechanisms. However, our new data show that this picture is incomplete and not sufficient to explain the strong NPQ situations where the maximal NPQ reaches up to 10-12.

The current available structure of thylakoid membrane distributes two photosystems, PSII and PSI, into laterally segregated appressed and non-appressed regions. Such separation of photosynthetic complexes is too static and not adequate for plants grown under natural fluctuating sunlight (NL). Recently, considerable efforts are being made to follow the real dynamics of thylakoid membranes during the course of an actual photoregulation scenario. One approach would be to replicate the natural sun-flecks (SF; which is a major cause of NPQ) under controlled condition. In this context, it would also be interesting to study the functional and structural response of thylakoid membranes towards extreme light conditions, which can be either very low (LL) or very high (HL). The picture would be incomplete without measuring the actual NL grown plants.

In the present study, we addressed these questions at organizational level of the thylakoid membrane with the help of non-invasive ultrafast fluorescence technique (TCSPC) as a primary measuring tool, along with electron microscopy (EM) and biochemical analyses, wherever possible. We used plants grown under various light regimes, such as, LL, HL, NL and SF.

The most important conclusions resulting from our work are as follows:

- Evergreen plants, such as *Monstera* (Chapter 4), *Hedera* and *Prunus* (Chapter 6) grown under NL-condition, dissipate the excess PSII excitation very strongly by means of three principal pathways, viz., the zeaxanthin-dependent qZ

mechanism, the PsbS-dependent qE mechanism and the spillover of excess energy to PSI (Qso), which requires reorganization in the thylakoid membrane. The spillover mechanism has been demonstrated as a novel highly efficient quenching process. It is facilitated by the phosphorylation of PSII proteins that may lead to softening the grana stacking, a phenomenon that allows coupling of PSII with nearby PSI-proteins.

- These three quenching mechanisms are also operational in the HL grown plant *Arabidopsis* (Chapter 7), although the extent of spillover is less compared to the natural fluctuating light grown evergreens. It is apparent that growth lights have major impact on the photoregulation processes, at least on the spillover mechanism. A better mixing of PSII and PSI was evident in NL-plants, resulted in stronger Qso quenching and reorganization in the thylakoid structure.
- Low growth lights (LL condition) cause larger grana stacks because of higher LHCII content (Chapter 8). A tighter appressed region may be one of the reasons that prevent reorganization in the thylakoid and does not enable the Qso quenching. As a result, photoregulation is less (quenching is caused by qE and qZ) compared to HL and NL grown plants. In certain cases, like CTL-*Arabidopsis*, low-light promoted the synthesis of additional loosely attached of LHCII antennae. We did not find any particular role for such extra LHCII antennas, neither in photosynthesis nor in photoprotection.
- Our SF condition was found to provide only moderate light intensity, similar to what have been studied previously as normal light (ca. 150 µmol photons m^{-2} s^{-1}) in literature, where qE and qZ were the only two quenching mechanisms, located on the PSII-antennae (Chapter 8). No Qso, spillover, was detected and the overall photoregulation was not much different to normal light grown *Arabidopsis*.
- Acclimatization of a typical LL plant into HL ambience can be fast, as we gradually increased the HL irradiation (Chapter 5). Our LL grown *Monstera* plants were acclimatized to high lights within 2 days of exposure (12 H/day) and it sustained a fully functional PSII even after 20 H/day of irradiation. At the thylakoid level, HL irradiation was found to widen the grana stacks, thereby promoted the coupling between PSII and nearby PSI-sites. As an effect, its NPQ capacity was found to be elevated (ca. 2-3 times) compared to typical LL-plants, where the dominant contribution came from Qso, which was previously absent in LL growth lights.
- The quenching in detached LHCII was found to be directly dependent on the monomeric PsbS (Chapter 9). A chlorophyll-chlorophyll (Chl-Chl) charge-transfer

(CT) state in oligomerized LHCII was confirmed, which shows its characteristic far-red fluorescence as is observed also for detached LHCII during qE-mechanism *in vivo*. We did not find any quenching in LHCII caused by low pH and/or Z.

Based on these findings and related reports published in literature, we are now able to distinguish at least three different quenched mechanisms and locations, *in vivo*, in higher plants. The exact ratios of these states contributing to NPQ are dependent on their growth lights and actinic light intensity. The following discussion summarizes these quenching mechanisms and outlines their structural basis and location.

1. Quenching scenario-1

   Quenching in this scenario is executed by 2-distinguished dissipating sites (Q1 or qE quenching) and (Q2 or qZ quenching) (Holzwarth and Jahns 2014), as depicted in Figure 10.1. The former dissipating site is a Chl-Chl CT state, which is located in the dissociated LHCII when it is quenched by activated PsbS protein ((Miloslavina, Wehner et al. 2008), see also Chapter 9). qZ quenching is most likely located on the peripheral minor antenna proteins of PSII and the heat dissipation is caused by de-epoxidised carotenoid zeaxanthin (Jahns and Holzwarth 2012, Holzwarth and Jahns 2014). In time-resolved measurements, qZ is assessed by the increase in the PSII rate constant k_D. Quenched scenario-1 is realized in low to moderate light grown plants, including some of our experiments too (LL-*Monstera* in Chapter 4 and CTL-*Arabidopsis* in Chapter 8). SF-plants, also exhibited alike quenched states (Chapter 8). Overall the situation is reflected in the 4-state-2-site quenching model (Holzwarth and Jahns 2014).

2. Quenching scenario-2

   This scenario is an intermediate between scenarios 1 and 3 and can occur in natural (NL) and high light (HL) grown plants. The quenched state has PSII-heterogeneity, and a 100% spillover is not obtained as shown in Figure 10.2. This scenario is expected when the NPQ lights are not strong enough in comparison to actual growth light. In Chapter 6, NL-*Prunus* had this type of quenched state. The maximal NPQ capacity is primarily obtained from partial spillover of PSII energy and is less compared to scenario 3, where all the PSII are coupled with PSI-proteins. The two aforesaid qE and qZ mechanisms (scenario-1), however, remain functional (not shown in here) in the quenched state.

Chapter 10

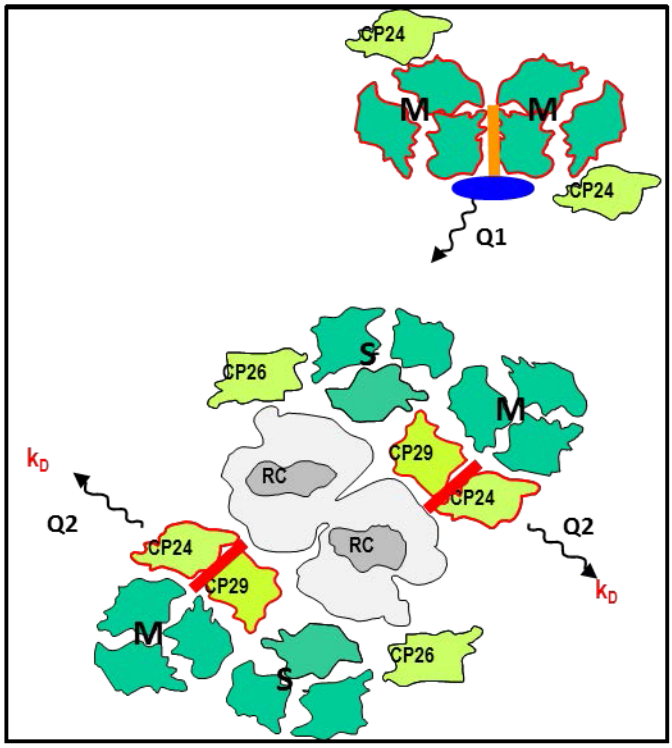

Figure 10.1: Schematic representation of plausible quenching sites in 'quenching scenario-1'. Q1 or qE quenching site is the detached LHCII antenna, believed to be associated with minor antenna protein, CP24 (Miloslavina, de Bianchi et al. 2011). The quenching in this site has strong PsbS dependency (see Chapter 9). The second heat-dissipation site (Q2 or qZ) is located on the PSII-attached antenna proteins and the quenching is dependent on Z (Jahns and Holzwarth 2012).

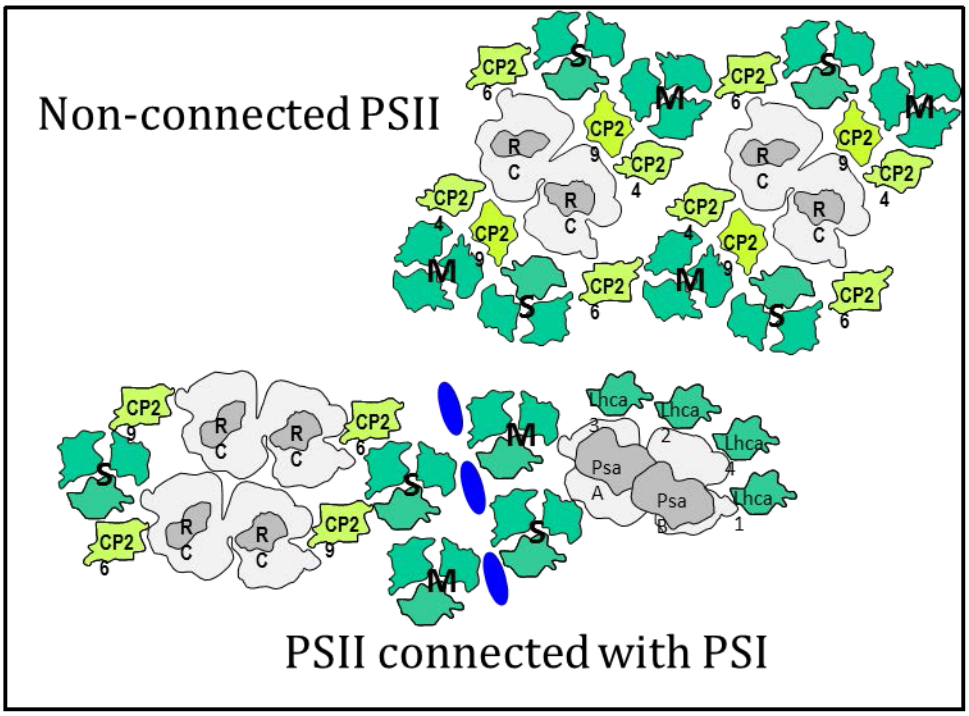

Figure 10.2: Schematic drawing of the 'quenching scenario-2' with connected and non-connected PSII. The connected PSII are responsible for spillover of excess energy to PSI.

3. Quenching scenario-3

   The studies on NL and HL grown plants have revealed detailed information for 'quenching scenario 3'. It is the most efficient form of photoprotection, where light regulation is controlled by the reorganization in thylakoid membrane, leading to 100% spillover of excess PSII energy (Figure 10.3). As a result, the NPQ capacity is ca. 4-6 times higher compared to 'quenching scenario-1'. For the evergreen plants, studied in this thesis, an NPQ value 10-14 was obtained. Structurally, this quenching scenario is revealed in electron microscopy by the softening of grana stacks that may have a direct consequence on the migration of PSI proteins towards grana which may be up to 100%.

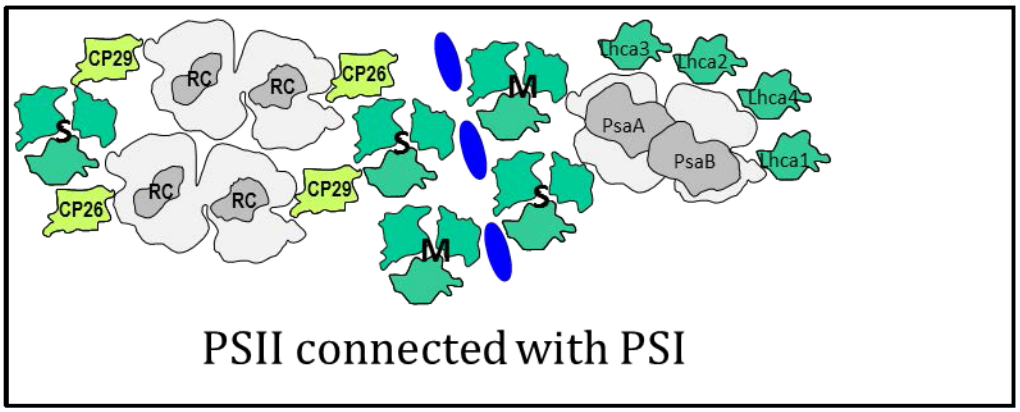

Figure 10.3: Schematic drawing of the 'quenching scenario -3' with connected PSII responsible for spillover of excess energy to PSI. In this state, PSII heterogeneity is completely abolished.

The formation of these quenching states and their dependence on the structural organization of the thylakoid is shown schematically in Figure 10.4.

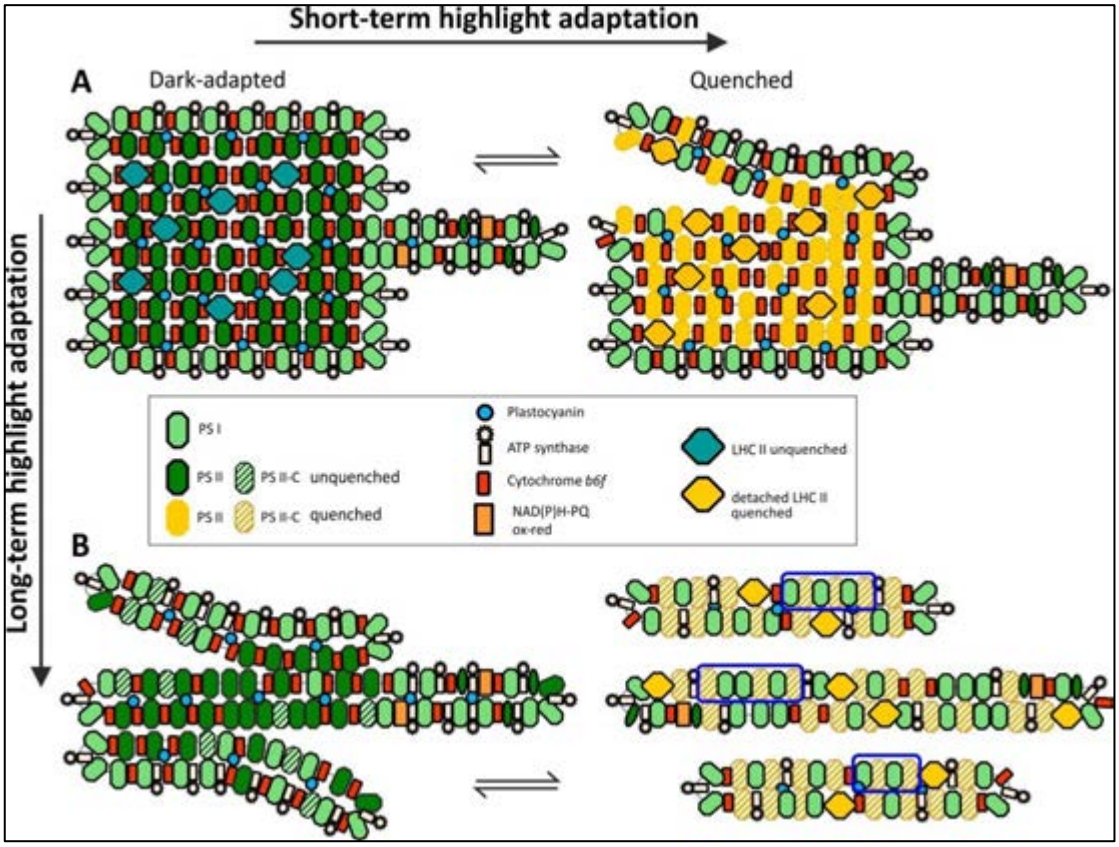

Figure 10.4: Schematic depictions of structural and functional organization of thylakoids based on time-resolved fluorescence and electron microscopy of LL- (A, top) and HL and/or NL-plants (B, bottom) in their dark-adapted unquenched (left) and high-light-exposed quenched states (right).

- Figure 10.4A shows the formation of 'quenching scenario-1' from the corresponding relaxed state. In LL-plants with pronounced grana, no or only very minor grana unstacking occurs in the quenched state and does not give rise to significant mixing of PSII and PSI units. The NPQ capacity in this scenario is limited to the qE and qZ mechanisms and much smaller compared to NL-plants (Figure 10.4B). Acclimatization from 'quenching scenario-1' (Figure 10.4A) to 'quenching scenario-3' (Figure 10.4B) is possible with HL irradiation (see also Chapter 5). Figure 10.4B represents the formation of 'quenching scenario-3' typical in NL and HL plants. These plants possess widened grana stacks and extended stroma thylakoids. A partial coupling between the PSII and PSI proteins occur even in the dark-adapted state also. The quenched state in these plants show a 100% spillover of excess PSII energy to PSI antenna proteins and sustain an exceptionally high NPQ capacity.
- For the plants grown under very low-light (such as CTL-*Arabidopsis* in Chapter 8), the photosynthetic machinery produces an 'extra LHCII' pool which is loosely attached to the PSII-supercomplex in the relaxed state. In the corresponding quenched state, not all LHCII is detached (as is seen in case of 100-150 µmol

photons m^{-2} s^{-1} light grown *Arabidopsis* during qE-quenching (Holzwarth, Miloslavina et al. 2009)).

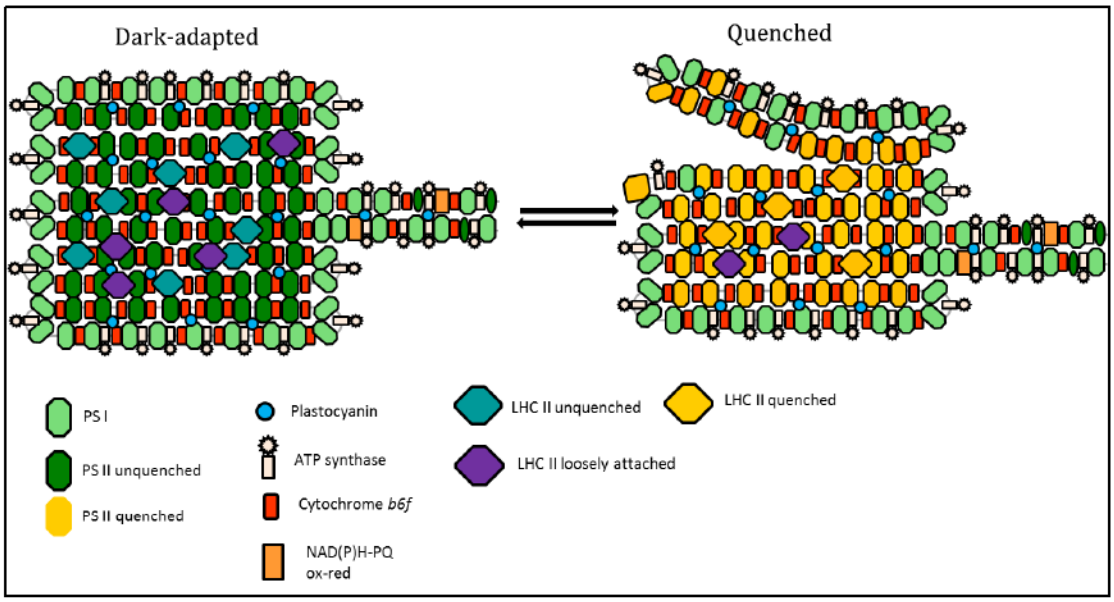

Figure 10.5: Schematic presentation of structural and functional organization of very low-light grown thylakoids. The dark-state is characterized by the presence of large extra LHCII pool loosely attached to the PSII-supercomplex and does not participate in the photoregulation.

List of Publications

- Paul, S., Götze, J. P., Liu, C., Pawlak, K., Reus, M., Yang, C. and Holzwarth, A. R. (2014). "On the molecular mechanism of quenching and photoprotection in the major light- harvesting complex LHCII of photosystem II." submitted.
- Paul, S., Matsubara, S. and Holzwarth, A. R. (2014). "Picosecond fluorescence studies on the fluctuating light acclimation strategies in *Arabidopsis thaliana*." in preparation.
- Paul, S., Muller, O., Schumann, T., Demmig-Adams, B., Adams III, W. W., Jahns, P. and Holzwarth, A. R. (2014). "A new photoprotection mechanism in plants grown under natural light regime involves major thylakoid reorganization." submitted.
- Paul, S., Schumann, T., Jahns, P. and Holzwarth, A. R. (2014). "A novel energy-transfer mechanism reveals the light induced dynamics in the thylakoid organization for *Arabidopsis thaliana*." in preparation.

Acknowledgement

I would like to offer my special thanks to my advisor Prof. Dr. Alfred R. Holzwarth for his continuous support, patience, motivation and enthusiasm in course of my PhD study. His guidance and immense knowledge helped me in research and writing of my thesis.

Besides my advisor, I am deeply grateful to Prof. Dr. Claus A. M. Seidel for his evaluation of my work, encouragement and insightful comments.

I want to thank Prof. Dr. Peter Jahns for his overwhelming support and continuous encouragement in this work and developing my interest in plant biophysics.

I am also grateful to Max-Planck-Institut für Chemische Energiekonversion for providing me all the facilities and funding. I acknowledge generous financial support from Marie-Curie HARVEST program for sponsoring my research and travels.

I gratefully acknowledge my collaborators, Prof. Barbara Demmig-Adams, Dr. Shizue Matsubara, Dr. Marc Müller, Dr. Krzysztof Pawlak, Michael Reus and Tobias Schumann.

I owe a very important debt to my parents for their understanding and loving support. I would like express my deepest appreciation to my beloved wife Dr. Shivani Tanwar, who spent sleepless nights in proof-checking and providing constructive advices and comments at every step when there was no one to answer my queries. A big thank to her.

References

Adams III, W. W., Muller, O., Cohu, C. M. and Demmig Adams, B. (2013). "May photoinhibition be a consequence, rather than a cause, of limited plant productivity?" Photosynth Res 17(1 3): 31 44.

Ahmad, M. and Cashmore, A. R. 1996). Seeing lue: he iscovery f yptochrome." Plant Mol Biol 0(5): 851 861.

Ahn, T. K., Avenson, T. J., Ballottari, M., Cheng, Y. C., Niyogi, K. K., Bassi, R. and Fleming, G. R. (2008). "Architecture of a charge transfer state regulating light harvesting in a plant antenna protein." Science 320(5877): 794 797.

Akoyunoglou, G. and Argyroudi Akoyunoglou, J. H. (1986). "Organization of the photosynthetic units, and onset of electron transport and excitation energy distribution in greening leaves." Photosynth Res 0(3): 171 180.

Allen, J. F., Bennett, J., Steinback, K. E. and Arntzen, C. J. (1981). "Chloroplast protein phosphorylation couples plastoquinone redox state to distribution of excitation energy between photosystems." Nature 291(5810): 25 29.

Allen, J. F. and Forsberg, J. (2001). "Molecular recognition in thylakoid structure and function." Trends Plant Sci (7): 17 326.

Alter, P., Dreissen, A., Luo, F. L. and Matsubara, S. (2012). "Acclimatory responses of *Arabidopsis* o fluctuating light environment: comparison of different sunfleck regimes and accessions." Photosynth Res 113(1 3): 221 237.

Amunts, A., Drory, O. and Nelson, N. (2007). "The structure of a plant photosystem I supercomplex at 3.4 Å resolution." Nature 47(7140): 8 63.

Anderson, J. M., Horton, P., Kim, E. H. and Chow, W. S. (2012). "Towards elucidation of dynamic structural changes of plant thylakoid architecture." Philos Trans R Soc Lond B Biol Sci 67(1608): 515 3524.

Andersson, B., Åkerlund, H. E., Jergil, B. and Larsson, C. (1982). "Differential phosphorylation of the light harvesting chlorophyll protein complex in appressed and non appressed regions of the thylakoid membrane." FEBS Lett 49(2): 81 185.

Andersson, B. and Anderson, J. M. (1980). "Lateral heterogeneity in the distribution of chlorophyll protein complexes of the thylakoid membranes of spinach chloroplasts." Biochim Biophys Acta 93(2): 27 440.

Andersson, J., Walters, R. G., Horton, P. and Jansson, S. (2001). "Antisense inhibition of the photosynthetic antenna proteins CP29 and CP26: Implications for the mechanism of protective energy dissipation." Plant Cell 3(5): 193 1204.

Armstrong, G. A., Runge, S., Frick, G., Sperling, U. and Apel, K. (1995). "Identification of NADPH:protochlorophyllide oxidoreductases A and B: a branched pathway for light dependent chlorophyll biosynthesis in *Arabidopsis thaliana*." Plant Physiol 08(4): 505 1517.

Aro, E. M. and Ohad, I. (2003). "Redox regulation of thylakoid protein phosphorylation." Antioxid Redox Signal (1): 5 67.

Aro, . ., irgin, . nd ndersson, . 1993). Photoinhibition f hotosystem I. nactivation, rotein damage and turnover." Biochim Biophys Acta 143(2): 13 134.

Aspinall O'Dea, M., Wentworth, M., Pascal, A., Robert, B., Ruban, A. and Horton, P. (2002). "In vitro reconstitution of the activated zeaxanthin state associated with energy dissipation in plants." Proc Natl Acad Sci U S A 9(25): 6331 16335.

Avenson, T. J., Ahn, T. K., Zigmantas, D., Niyogi, K. K., Li, Z., Ballottari, M., Bassi, R. and Fleming, . . 2008). "Zeaxanthin radical cation formation in minor light harvesting complexes of higher plant antenna." J Biol Chem 83(6): 550 3558.

Baena González, E. and Aro, E. M. (2002). "Biogenesis, assembly and turnover of photosystem II units." Philos Trans R Soc Lond B Biol Sci 57(1426): 451 1459; discussion 1459 1460.

Bailey, S., Walters, R. G., Jansson, S. and Horton, P. (2001). "Acclimation of *Arabidopsis thaliana* o he ight environment: The existence of separate low light and high light responses." Planta 13(5): 94 801.

Baker, N. R. (2008). "Chlorophyll fluorescence: a probe of photosynthesis in vivo." Annu Rev Plant Biol 9: 89 113.

Ballaré, C. L., Scopel, A. L., Roush, M. L. and Radosevich, S. R. (1995). "How plants find light in patchy canopies. A comparison between wild type and phytochrome B deficient mutant plants of cucumber." Funct Ecol (6): 59 868.

Ballottari, M., Girardon, J., Betterle, N., Morosinotto, T. and Bassi, R. (2010). "Identification of the chromophores involved in aggregation dependent energy quenching of the monomeric photosystem II antenna protein Lhcb5." J Biol Chem 85(36): 8309 28321.

Barbato, R., Friso, G., de Laureto, P. P., Frizzo, A., Rigoni, F. and Giacometti, G. M. (1992). "Light induced degradation of D2 protein in isolated photosystem II reaction center complex." FEBS Lett 11(1): 3 36.

Barber, J. (1982). "Influence of surface charges on thylakoid structure and function." Annu Rev Plant Physiol 33(1): 261 295.

Barber, J., Chow, W. S., Scoufflaire, C. and Lannoye, R. (1980). "The relationship between thylakoid stacking and salt induced chlorophyll fluorescence changes." Biochim Biophys Acta 91(1): 2 103.

Barber, J., Ferreira, K., Maghlaoui, K. and Iwata, S. (2004). "Structural model of the oxygen evolving centre of photosystem II with mechanistic implications." Phys Chem Chem Phys (20): 737 4742.

Barera, S., Pagliano, C., Pape, T., Saracco, G. and Barber, J. (2012). "Characterization of PSII LHCII supercomplexes isolated from pea thylakoid membrane by one step treatment with α nd dodecyl D maltoside." Philos Trans R Soc Lond B Biol Sci 67(1608): 389 3399.

Beauregard, M., Martin, I. and Holzwarth, A. R. (1991). "Kinetic modelling of exciton migration in photosynthetic systems. (1) Effects of pigment heterogeneity and antenna topography on exciton kinetics and charge separation yields." Biochim Biophys Acta 060: 71 283.

Becker, W. (2005). The bh TCSPC handbook, ecker ickl mbH.

Bellafiore, S., Barneche, F., Peltier, G. and Rochaix, J. D. (2005). "State transitions and light adaptation require chloroplast thylakoid protein kinase STN7." Nature 33(7028): 92 895.

Bergantino, E., Segalla, A., Brunetta, A., Teardo, E., Rigoni, F., Giacometti, G. M. and Szabo, I. (2003). "Light and pH dependent structural hanges n he sbS ubunit f hotosystem I." Proc Natl Acad Sci U S A 100(25): 15265 15270.

Betterle, N., Ballottari, M., Zorzan, S., de Bianchi, S., Cazzaniga, S., Dall'Osto, L., Morosinotto, T. and Bassi, R. (2009). "Light induced dissociation of an antenna hetero oligomer is needed for non photochemical quenching induction." J Biol Chem 84(22): 5255 15266.

Biswal, A. K., Pattanayak, G. K., Pandey, S. S., Leelavathi, S., Reddy, V. S., Govindjee and Tripathy, B. C. (2012). "Light intensity dependent modulation of chlorophyll b biosynthesis and photosynthesis by overexpression of chlorophyllide a oxygenase in tobacco." Plant Physiol 59(1): 33 449.

Boardman, N. K. (1977). "Comparative photosynthesis of sun and shade plants." Annu Rev Plant Physiol Plant Mol Biol 8: 55 377.

Bode, S., Quentmeier, C. C., Liao, P. N., Hafi, N., Barros, T., Wilk, L., Bittner, F. and Walla, P. J. (2009). "On the regulation of photosynthesis by excitonic interactions between carotenoids and chlorophylls." Proc Natl Acad Sci 06(30): 2311 12316.

Boekema, E. J., van Roon, H., Calkoen, F., Bassi, R. and Dekker, J. P. (1999). "Multiple types of association of photosystem II and its light harvesting antenna in partially solubilized photosystem II membranes." Biochemistry 8(8): 2233 2239.

Boichenko, V. A., Hou, J. M. and Mauzerall, D. (2001). "Thermodynamics of electron transfer in oxygenic photosynthetic reaction centers: Volume change, enthalpy, and entropy of electron transfer reactions in the intact cells of the cyanobacterium *Synechocystis* PCC 6803." Biochemistry 0(24): 126 7132.

Bonardi, V., Pesaresi, P., Becker, T., Schleiff, E., Wagner, R., Pfannschmidt, T., Jahns, P. and Leister, D. (2005). "Photosystem II core phosphorylation and photosynthetic acclimation require two different protein kinases." Nature 37(7062): 179 1182.

Bonente, G., Ballottari, M., Truong, T. B., Morosinotto, T., Ahn, T. K., Fleming, G. R., Niyogi, K. K. and Bassi, R. (2011). "Analysis of LhcSR3, a protein essential for feedback de excitation in the green alga *Chlamydomonas reinhardtii*." PLoS Biol (1): 1000577.

Bonente, G., Howes, B. D., Caffarri, S., Smulevich, G. and Bassi, R. (2008). "Interactions between the photosystem II subunit PsbS and xanthophylls studied in vivo and in vitro." J Biol Chem 83(13): 434 8445.

Bradshaw, A. D. (1965). "Evolutionary significance of phenotypic plasticity in plants." Advan Genet 3: 115 155.

Briggs, W. R. and Olney, M. A. (2001). "Photoreceptors in plant photomorphogenesis to date. Five phytochromes, two cryptochromes, one phototropin, and one superchrome." Plant Physiol 25(1): 5 88.

Brooks, M. D., Sylak Glassman, E. J., Fleming, G. R. and Niyogi, K. K. (2013). "A thioredoxin like/β propeller protein maintains the efficiency of light harvesting in *Arabidopsis*." Proc Natl Acad Sci U S A 10(29): E2733 2740.

Broser, M., Gabdulkhakov, A., Kern, J., Guskov, A., Muh, F., Saenger, W. and Zouni, A. (2010). "Crystal structure of monomeric photosystem II from Thermosynechococcus elongatus at 3.6 Å resolution." J Biol Chem 85(34): 6255 26262.

Brown, G. and Mies, A. B. (2012). Chapter 5 cology nd daptive trategies. Vegetation Ecology of Socotra, pringer. : 388.

Brugnoli, E. and Björkman, O. (1992). "Chloroplast movements in leaves: Influence on chlorophyll fluorescence and measurements of light induced absorbance changes related to ΔpH and zeaxanthin formation." Photosynth Res 2(1): 3 35.

Casida, M. E., Jamorski, C., Casida, K. C. and Salahub, D. R. (1998). "Molecular excitation energies to high lying bound tates rom ime dependent density functional response theory: Characterization and correction of the time dependent local density approximation ionization threshold." J Chem Phys 08(11): 4439 4449.

Chai, J. D. and Head Gordon, M. (2008). "Long range corrected hybrid density functionals with damped atom atom dispersion corrections." Phys Chem Chem Phys 0(44): 615 6620.

Chow, W. S., Goodchild, D. J., Miller, C. and Anderson, J. M. (1990). "The influence of high levels of brief or prolonged supplementary far red illumination during growth on the photosynthetic characteristics, composition and morphology of *Pisum sativum* hloroplasts." Plant Cell Environ 3(2): 35 145.

Chow, W. S., Kim, E. H., Horton, P. and Anderson, J. M. (2005). "Granal stacking of thylakoid membranes in higher plant chloroplasts: the physicochemical forces at work and the functional consequences that ensue." Photochem Photobiol Sci (12): 081 1090.

Chow, W. S., Melis, A. and Anderson, J. M. (1990). "Adjustments of photosystem stoichiometry in chloroplasts improve the quantum efficiency of photosynthesis." Proc Natl Acad Sci U S A 7(19): 502 7506.

Connelly, J. P., Müller, M. G., Bassi, R., Croce, R. and Holzwarth, A. R. (1997). "Femtosecond transient absorption study of carotenoid to chlorophyll energy transfer in the light harvesting complex II of photosystem II." Biochemistry 6(2): 81 287.

Cramer, W. A., Martinez, S. E., Huang, D., Tae, G. S., Everly, R. M., Heymann, J. B., Cheng, R. H., Baker, T. S. and Smith, J. L. (1994). "Structural aspects of the cytochrome *b6f* omplex; tructure f he umen side domain of cytochrome *f*." J Bioenerg Biomembr 6(1): 1 47.

Croce, R., Chojnicka, A., Morosinotto, T., Ihalainen, J. A., van Mourik, F., Dekker, J. P., Bassi, R. and van Grondelle, R. (2007). "The low energy forms of photosystem I light harvesting complexes: spectroscopic properties and pigment pigment interaction characteristics." Biophys J 3(7): 418 2428.

Crouchman, S., Ruban, A. and Horton, P. (2006). "PsbS enhances nonphotochemical luorescence quenching in the absence of zeaxanthin." FEBS Lett 80(8): 053 2058.

Dapprich, S., Komarómi, I., Byun, K. S., Morokuma, K. and Frisch, M. J. (1999). "A new ONIOM implementation in Gaussian98. Part I. The calculation of energies, gradients, vibrational frequencies and electric field derivatives." J Mol Struct 61 462: 1 21.

Daum, B., Nicastro, D., Austin, J. I., McIntosh, J. R. and Kühlbrandt, W. (2010). "Arrangement of photosystem II and ATP synthase in chloroplast membranes of spinach and pea." Plant Cell 2(4): 299 1312.

de Bianchi, S., Dall'Osto, L., Tognon, G., Morosinotto, T. and Bassi, R. (2008). "Minor antenna proteins CP24 and CP26 affect the interactions between photosystem II Subunits and the electron transport rate in grana membranes of *Arabidopsis*." Plant Cell 0(4): 012 1028.

Dekker, J. P. and Boekema, E. J. (2005). "Supramolecular organization of thylakoid membrane proteins in green plants." Biochim Biophys Acta 706(1 2): 12 39.

Demmig Adams, B. and Adams II, W. W. 1990). The carotenoid zeaxanthin and 'high energy state quenching' of chlorophyll fluorescence." Photosynth Res 5(3): 87 197.

Demmig Adams, B., Cohu, C. M., Muller, O. and Adams II, W. W. 2012). Modulation f hotosynthetic energy conversion efficiency in nature: from seconds to seasons." Photosynth Res 13(1 3): 75 88.

Demmig Adams, B., Ebbert, V., Mellman, D. L., Mueh, K. E., Schaffer, L., Funk, C., Zarter, C. R., Adamska, I., Jansson, S. and Adams II, W. W. (2006). "Modulation of PsbS and flexible vs sustained energy dissipation by light environment in different species." Physiol Plant 27(4): 70 680.

Demmig-Adams, B., Ebbert, V., Zarter, C. R. and Adams, W. W., III (2006). Chapter 4: Characteristics and species dependent employment of flexible versus sustained thermal dissipation and photoinhibition. Advances in Photosynthesis and Respiration. B. Demmig Adams, Adams III, W. W. and Matto, Autark. Springer Netherlands: 39 48.

Depège, N., Bellafiore, S. and Rochaix, J. D. (2003). "Role of chloroplast protein kinase Stt7 in LHCII phosphorylation and state transition in *Chlamydomonas*." Science 99(5612): 572 1575.

Dietzel, L., Bräutigam, K., Steiner, S., Schuffler, K., Lepetit, B., Grimm, B., Schottler, M. A. and Pfannschmidt, T. (2011). "Photosystem II supercomplex remodeling serves as an entry mechanism for state transitions in *Arabidopsis*." Plant Cell 3(8): 964 2977.

Dominici, P., Caffarri, S., Armenante, F., Ceoldo, S., Crimi, M. and Bassi, R. (2002). "Biochemical properties of the PsbS subunit of photosystem I ither urified rom hloroplast r ecombinant." J Biol Chem 277(25): 22750 22758.

Engelbrecht, S. and Junge, W. (1997). "ATP synthase: a tentative structural model." FEBS Lett 14(3): 85 491.

Fan, D. Y., Hope, A. B., Smith, P. J., Jia, H., Pace, R. J., Anderson, J. M. and Chow, W. S. (2007). "The stoichiometry of the two photosystems in higher plants revisited." Biochim Biophys Acta 767(8): 064 1072.

Färber, A., Young, A. J., Ruban, A. V., Horton, P. and Jahns, P. (1997). "Dynamics of xanthophyll cycle activity in different antenna subcomplexes in the photosynthetic membranes of higher plants: The relationship between zeaxanthin conversion and nonphotochemical fluorescence quenching." Plant Physiol 15(4): 609 1618.

Ferroni, L., Angeleri, M., Pantaleoni, L., Pagliano, C., Longoni, P., Marsano, F., Aro, E. M., Suorsa, M., Baldisserotto, C., Giovanardi, M., Cella, R. and Pancaldi, S. (2014). "Light dependent reversible phosphorylation of the minor photosystem II antenna Lhcb6 (CP24) occurs in lycophytes." Plant J.

Finazzi, G., Johnson, G. N., Dall'Osto, L., Joliot, P., Wollman, F. A. and Bassi, R. (2004). "A zeaxanthin independent nonphotochemical quenching mechanism localized in the photosystem II core complex." Proc Natl Acad Sci U S A 01(33): 2375 12380.

Finazzi, G., Zito, F., Barbagallo, R. P. and Wollman, F. A. (2001). "Contrasted effects of inhibitors of cytochrome b6*f* omplex n tate ransitions n *Chlamydomonas reinhardtii*: the role of Qo site occupancy in LHCII kinase activation." J Biol Chem 76(13): 770 9774.

Foyer, C. H., Neukermans, J., Queval, G., Noctor, G. and Harbinson, J. (2012). "Photosynthetic control of electron transport and the regulation of gene expression." J Exp Bot 3(4): 637 1661.

Frank, H. A., Cua, A., Chynwat, V., Young, A., Gosztola, D. and Wasielewski, M. R. (1994). "Photophysics of the carotenoids associated with the xanthophyll cycle in photosynthesis." Photosynth Res 1(3): 89 395.

Fristedt, R., Willig, A., Granath, P., Crèvecoeur, M., Rochaix, J. D. and Vener, A. V. (2009). "Phosphorylation of photosystem II controls functional macroscopic folding of photosynthetic membranes in *Arabidopsis*." Plant Cell 1(12): 950 3964.

Fufezan, C., Simionato, D. and Morosinotto, T. (2012). "Identification of key residues for pH dependent activation of violaxanthin de epoxidase from *Arabidopsis thaliana*." Plos One (4).

Fujita, Y., Ohki, K. and Murakami, A. (1987). "Chromatic regulation of photosystem composition in the Cyanobacterial photosynthetic system inetic elationship etween change of photosystem composition and cell proliferation." Plant Cell Physiol 8(2): 27 234.

Gilmore, A. M., Shinkarev, V. P., Hazlett, T. L. and Govindjee (1998). "Quantitative analysis of the effects of intrathylakoid pH and xanathophyll cycle pigments on chlorophyll a fluorescence lifetime distributions and intensity in thylakoids." Biochemistry 7(39): 3582 13593.

Golan, T., Li, X. P., Muller Moulé, P. and Niyogi, K. K. (2004). Chapter 20: Using mutants to understand light stress acclimation in plants. Chlorophyll a Fluorescence. G. C. Papageorgiou and Govindjee, Springer Netherlands. 19**:** 525 554.

Goral, T. K., Johnson, M. P., Duffy, C. D., Brain, A. P., Ruban, A. V. and Mullineaux, C. W. (2012). "Light harvesting antenna composition controls the acrostructure nd ynamics f hylakoid embranes n *Arabidopsis*." Plant J 9(2): 89 301.

Grinvald, A. and Steinberg, I. Z. (1974). "On the analysis of fluorescence decay kinetics by the method of least squares." Anal.Biochem. 9: 83 598.

Gruissem, W. and Tonkyn, J. C. (1993). "Control mechanisms of plastid gene expression." CRC Crit Rev Plant Sci 2(1 2): 19 55.

Gruszecki, W. I., Grudzinski, W., Gospodarek, M., Patyra, M. and Maksymiec, W. (2006). "Xanthophyll induced aggregation of LHCII as a switch between light harvesting and energy dissipation systems." Biochim Biophys Acta 757(11): 504 1511.

Hager, A. (1966). "Die Zusammenhänge zwischen lichtinduzierten Xanthophyll Umwandlungen und Hill Reaktion." Ber Dtsch Bot Ges 9: 4 107.

Hager, A. (1969). "Light dependent decrease of the pH value in a chloroplast compartment causing the enzymatic interconversion of violaxanthin to zeaxanthin; relations to photophosphorylation." Planta 89(3): 224 243.

Hakala Yatkin, M., Mantysaari, M., Mattila, H. and Tyystjärvi, E. (2010). "Contributions of visible and ultraviolet parts of sunlight to photoinhibition." Plant Cell Physiol 1(10): 745 1753.

Heijde, M. and Ulm, R. (2012). "UV B photoreceptor mediated signalling in plants." Trends Plant Sci 7(4): 230 237.

Heldmaier, G. and Werner, D. (2003). Chapter 1: Environmental signal processing and adaptation. Environmental Signal Processing and Adaptation. G. Heldmaier and Werner, D., Springer Berlin Heidelberg**:** 1 8.

Herbstová, M., Tietz, S., Kinzel, C., Turkina, M. V. and Kirchhoff, H. (2012). "Architectural switch in plant photosynthetic membranes induced by light stress." Proc Natl Acad Sci U S A 09(49): 0130 20135.

Hohenberg, P. and Kohn, W. (1964). "Inhomogenous electron gas." Physical Review B 36(3B): 864 B871.

Holt, N. E., Zigmantas, D., Valkunas, L., Li, X. P., Niyogi, K. K. and Fleming, G. R. (2005). "Carotenoid cation formation and the regulation of photosynthetic light harvesting." Science 07(5708): 33 436.

Holzwarth, A. R. (1988). Time resolved chlorophyll luorescence. hat ind f nformation n photosynthetic systems does it provide? Applications of Chlorophyll Fluorescence. H. K. Lichtenthaler. Dordrecht, Kluwer Academic**:** 21 31.

Holzwarth, A. R. (1991). Excited state kinetics in chlorophyll systems and its relationship to the functional organization of the photosystems. Chlorophylls. . cheer. oca aton, RC ress**:** 1125 1151.

Holzwarth, A. R. (1995). Time resolved fluorescence spectroscopy. Methods in Enzymology. Vol.246 Biochemical Spectroscopy. . auer. San Diego, Academic Press**:** 334 362.

Holzwarth, A. R. (1996). Data analysis of time resolved measurements. Biophysical Techniques in Photosynthesis. Advances in Photosynthesis Research. J. Amesz and Hoff, A. J. Dordrecht, Kluwer Academic Publishers**:** 75 92.

Holzwarth, A. R. (2004). Light absorption and harvesting. Molecular to Global Photosynthesis. M. D. Archer and Barber, J. London, Imperial College Press**:** 43 115.

Holzwarth, A. R. (2008). Ultrafast primary reactions in the photosystems of oxygen evolving organisms. Ultrashort Laser Pulses in Biology and Medicine. M. Braun, Gilch, P. and Zinth, W., Springer Berlin Heidelberg**:** 141 164.

Holzwarth, A. R. and Jahns, P. (2014). NPQ mechanisms in intact organisms as derived from ultrafast fluorescence kinetics tudies. Non Photochemical Quenching and Thermal Energy Dissipation In Plants, Algae and Cyanobacteria, pringer cience, ordrecht.

Holzwarth, A. R., Miloslavina, Y., Nilkens, M. and Jahns, P. (2009). "Identification of two quenching sites active in the regulation of photosynthetic light harvesting studied by time resolved fluorescence." Chem Phys Lett 483(4 6): 262 267.

Holzwarth, A. R., Müller, M. G., Niklas, J. and Lubitz, W. (2005). "Charge recombination fluorescence in photosystem I reaction centers from Chlamydomonas reinhardtii." J Phys Chem B 09(12): 903 5911.

Holzwarth, A. R., Müller, M. G., Reus, M., Nowaczyk, M., Sander, J. and Rogner, M. (2006). "Kinetics and mechanism of electron transfer in intact photosystem II and in the isolated reaction enter: heophytin s the primary electron acceptor." Proc Natl Acad Sci U S A 03(18): 895 6900.

Holzwarth, A. R., Wendler, J. and Haehnel, W. (1985). "Time resolved picosecond fluorescence spectra of the antenna chlorophylls in *Chlorella vulgaris*. Resolution of Photosystem I fluorescence." Biochim Biophys Acta 07(2): 55 167.

Horton, P. (2012). "Optimization of light harvesting and photoprotection: molecular mechanisms and physiological consequences." Philos Trans R Soc Lond B Biol Sci 67(1608): 455 3465.

Horton, P. and Black, M. T. (1981). "Light dependent quenching of chlorophyll fluorescence in *Pea* chloroplasts induced by adenosine 5' triphosphate." Biochim Biophys Acta 35(1): 3 62.

Horton, P., Johnson, M. P., Perez Bueno, M. L., Kiss, A. Z. and Ruban, A. V. (2008). "Photosynthetic acclimation: does the dynamic structure and macro organisation of photosystem II in higher plant grana membranes regulate light harvesting states?" FEBS J 75(6): 069 1079.

Horton, P., Ruban, A. V., Rees, D., Pascal, A. A., Noctor, G. and Young, A. J. (1991). "Control of the light harvesting function of chloroplast membranes by aggregation of the LHCII chlorophyll protein complex." FEBS Lett 92(1 2): 1 4.

Horton, P., Ruban, A. V. and Walters, R. G. (1996). "Regulation of light harvesting in green plants." Annu Rev Plant Physiol Plant Mol Biol 7(1): 55 684.

Horton, P., Ruban, A. V. and Young, A. J. (1999). Regulation of the structure and function of the light harvesting complexes of photosystem II by the xanthophyll cycle. Carotenoids in plants. Advances in photosynthesis. H. Frank, Cogdell, R. and Young, A. J. Dordrecht, The Netherlands, Kluwer Academic Publishers. 6**:** 271 291.

Horton, P., Wentworth, M. and Ruban, A. (2005). "Control of the light harvesting function of chloroplast membranes: the LHCII aggregation model for non photochemical quenching." FEBS Lett 79(20): 201 4206.

Hubbart, S., Ajigboye, O. O., Horton, P. and Murchie, E. H. (2012). "The photoprotective protein PsbS exerts control over CO2 assimilation rate in fluctuating light in rice." Plant J 1(3): 02 412.

Ihalainen, J. A., Croce, R., Morosinotto, T., van Stokkum, I. H., Bassi, R., Dekker, J. P. and van Grondelle, R. (2005). "Excitation decay pathways of Lhca proteins: a time resolved fluorescence study." J Phys Chem B 109(44): 21150 21158.

Ivanov, A. G., Hurry, V., Sane, P. V., Oquist, G. and Huner, N. P. A. (2008). "Reaction centre quenching of excess light energy and photoprotection of photosystem II." Journal of Plant Biology 1(2): 5 96.

Jahns, P. and Holzwarth, A. R. (2012). "The role of the xanthophyll cycle and of lutein in photoprotection of photosystem II." Biochim Biophys Acta 817(1): 82 193.

Jajoo, A., Mekala, N. R., Tongra, T., Tiwari, A., Grieco, M., Tikkanen, M. and Aro, E. M. (2014). "Low pH induced regulation of excitation energy between the two photosystems." FEBS Lett.

Jansen, M. A., Mattoo, A. K. and Edelman, M. (1999). "D1 D2 protein degradation in the chloroplast. Complex light saturation kinetics." Eur J Biochem 60(2): 27 532.

Jegerschöld, C., Virgin, I. and Styring, S. (1990). "Light dependent degradation of the D1 protein in photosystem II is accelerated after inhibition of the water splitting reaction." Biochemistry 9(26): 179 6186.

Johnson, G. N., Young, A. J. and Horton, . 1994). Activation f on photochemical quenching in thylakoids and leaves." Planta 94(4): 50 556.

Johnson, M. P., Havaux, M., Triantaphylides, C., Ksas, B., Pascal, A. A., Robert, B., Davison, P. A., Ruban, A. V. and Horton, P. (2007). "Elevated zeaxanthin bound to oligomeric LHCII enhances the resistance of *Arabidopsis* o hotooxidative tress y ipid protective, antioxidant mechanism." J Biol Chem 82(31): 22605 22618.

Johnson, M. P., Pérez Bueno, M. L., Zia, A., Horton, P. and Ruban, A. V. (2009). "The zeaxanthin independent and zeaxanthin dependent qE components of nonphotochemical quenching involve common conformational changes within the photosystem II antenna in *Arabidopsis*." Plant Physiol 49(2): 061 1075.

Johnson, M. P. and Ruban, A. V. (2010). "*Arabidopsis* lants acking sbS rotein ossess hotoprotective energy dissipation." Plant Journal 1(2): 83 289.

Johnson, M. P. and Ruban, A. V. (2011). "Restoration of rapidly reversible photoprotective energy dissipation in the absence of PsbS rotein y nhanced pH." J Biol Chem 86(22): 9973 19981.

Joliot, P. and Johnson, G. N. (2011). "Regulation of cyclic and linear electron flow in higher plants." Proc Natl Acad Sci U S A 08(32): 3317 13322.

Jung, J. and Kim, H. S. (1990). "The chromophores as endogenous sensitizers involved in the photogeneration of singlet oxygen in spinach thylakoids." Photochem Photobiol 2(5): 003 1009.

Kaftan, D., Brumfeld, V., Nevo, R., Scherz, A. and Reich, Z. (2002). "From chloroplasts to photosystems: in situ canning orce icroscopy n ntact hylakoid embranes." Embo Journal 1(22): 146 6153.

Kamiya, N. and Shen, J. R. (2003). "Crystal structure of oxygen evolving photosystem II from *Thermosynechococcus vulcanus* t .7 Å resolution." Proc Natl Acad Sci U S A 00(1): 8 103.

Kell, A., Feng, X., Lin, C., Reus, M., Holzwarth, A. R. and Jankowiak, R. (2014). "On the charge transfer character of the low energy Chl a Qy absorption band in aggregated LHCII pigmentprotein complexes." J Phys Chem B ubmitted.

Kereïche, S., Kiss, A. Z., Kouřil, R., Boekema, E. J. and Horton, P. (2010). "The PsbS protein controls the macro organisation of photosystem II complexes in the grana membranes of higher plant chloroplasts." FEBS Lett 84(4): 59 764.

Keren, N., Berg, A., VanKan, P. J. M., Levanon, H. and Ohad, I. (1997). "Mechanism of photosystem II photoinactivation and D1 protein degradation at low light: The role of back electron flow." Proc Natl Acad Sci U S A 4(4): 579 1584.

Kern, J., Biesiadka, J., Loll, B., Saenger, W. and Zouni, A. (2007). "Structure of the Mn4 Ca cluster as derived from X ray diffraction." Photosynth Res 2(3): 89 405.

Kim, J. H., Glick, R. E. and Melis, A. (1993). "Dynamics of photosystem stoichiometry adjustment by light quality in chloroplasts." Plant Physiol 02(1): 81 190.

Kim, S., Sandusky, P., Bowlby, N. R., Aebersold, R., Green, B. R., Vlahakis, S., Yocum, C. F. and Pichersky, E. (1992). "Characterization of a spinach *psbS* cDNA encoding the 22 kDa protein of photosystem II." FEBS Lett 14(1): 67 71.

Kirchhoff, H. (2013). "Architectural switches in plant thylakoid membranes." Photosynth Res.

Kirchhoff, H. (2013). "Diffusion of molecules and macromolecules in thylakoid membranes." Biochim Biophys Acta.

Kirchhoff, H., Hall, C., Wood, M., Herbstova, M., Tsabari, O., Nevo, R., Charuvi, D., Shimoni, E. and Reich, Z. (2011). "Dynamic control of protein diffusion within the granal thylakoid lumen." Proc Natl Acad Sci U S A 108(50): 20248 20253.

Kirchhoff, H., Sharpe, R. M., Herbstova, M., Yarbrough, R. and Edwards, G. E. (2013). "Differential mobility of pigment protein complexes in granal and agranal thylakoid membranes of c3 and c4 plants." Plant Physiol 61(1): 97 507.

Kiss, A. Z., Ruban, A. V. and Horton, P. (2008). "The PsbS protein controls the organization of the photosystem II antenna in higher plant thylakoid membranes." J Biol Chem 83(7): 972 3978.

Kohn, W. and Sham, L. J. (1965). "Self consistent equations including exchange and correlation effects." Physical Review A 40(4A): 1133 A1138.

Kok, B. (1956). "On the inhibition of photosynthesis by intense light." Biochim Biophys Acta 1(2): 34 244.

Koller, D., Björkman, O. and Ritter, S. (1995). "Role of pulvinar chloroplasts in light driven leaf movements of the trifoliate leaf of bean (*Phaseolus vulgaris* .)." J Exp Bot 6(290): 215 1222.

Kong, S. G. and Wada, M. (2014). "Recent advances in understanding the molecular mechanism of chloroplast photorelocation movement." Biochim Biophys Acta 837(4): 22 530.

Konig, C. and Neugebauer, J. (2011). "First principles calculation of electronic spectra of light harvesting complex II." Phys Chem Chem Phys 3(22): 0475 10490.

Kouřil, R., Wientjes, E., Bultema, J. B., Croce, R. and Boekema, E. J. (2013). "High light vs. low light: effect of light acclimation on photosystem II composition and organization in *Arabidopsis thaliana*." Biochim Biophys Acta 827(3): 11 419.

Kovács, L., Damkjær, J., Kereïche, S., Ilioaia, C., Ruban, A. V., Boekema, E. J., Jansson, S. and Horton, P. (2006). "Lack of the light harvesting complex CP24 affects the structure and function of the grana membranes of higher plant chloroplasts." Plant Cell 8(11): 106 3120.

Krause, G. H. (1988). "Photoinhibition of photosynthesis n valuation f amaging nd rotective mechanisms." Physiol Plant 4(3): 66 574.

Krause, G. H., Vernotte, C. and Briantais, J. M. (1982). "Photoinduced quenching of chlorophyll fluorescence in intact chloroplasts and algae esolution nto omponents." Biochim Biophys Acta 679(1): 116 124.

Krause, G. H. and Weis, E. (1991). "Chlorophyll fluorescence and photosynthesis he asics." Annu Rev Plant Physiol Plant Mol Biol 2: 13 349.

Krinsky, N. I. (1964). "Carotenoid de epoxidations in algae. I. photochemical transformation of antheraxanthin to zeaxanthin." Biochim Biophys Acta 8: 87 491.

Kröner, D. and Götze, J. P. (2012). "Modeling of a violaxanthin chlorophyll b chromophore pair in its LHCII environment using CAM B3LYP." J Photochem Photobiol B 09: 2 19.

Krupa, Z., Huner, N. P., Williams, J. P., Maissan, E. and James, D. R. (1987). "Development at cold hardening temperatures : The structure and composition of purified Rye light harvesting complex II." Plant Physiol 84(1): 19 24.

Krupnik, T., Kotabov, E., van Bezouwen, L. S., Mazur, R., Garstka, M., Nixon, P. J., Barber, J., Kana, R., Boekema, E. J. and Kargul, J. (2013). "A reaction centre dependent photoprotection mechanism in a highly robust photosystem II from an extremophilic red alga Cyanidioschyzon merolae." J Biol Chem.

Kudoh, H. and Sonoike, K. (2002). "Irreversible damage to photosystem I by chilling in the light: cause of the degradation of chlorophyll after returning o ormal rowth emperature." Planta 15(4): 41 548.

Kurisu, G., Zhang, H., Smith, J. L. and Cramer, W. A. (2003). "Structure of the cytochrome b6*f* omplex f oxygenic photosynthesis: tuning the cavity." Science 02(5647): 009 1014.

Lambrev, P. H., Miloslavina, Y., Jahns, P. and Holzwarth, A. R. (2012). "On the relationship between non photochemical quenching and photoprotection of Photosystem II." Biochim Biophys Acta 817(5): 60 769.

Lambrev, P. H., Nilkens, M., Miloslavina, Y., Jahns, P. and Holzwarth, A. R. (2010). "Kinetic and spectral resolution of multiple nonphotochemical quenching components in *Arabidopsis* eaves." Plant Physiol 152(3): 1611 1624.

Li, X. P., Björkman, O., Shih, C., Grossman, A. R., Rosenquist, M., Jansson, S. and Niyogi, K. K. (2000). "A pigment binding protein essential for regulation of photosynthetic light harvesting." Nature 03(6768): 391 395.

Li, X. P., Gilmore, A. M., Caffarri, S., Bassi, R., Golan, T., Kramer, D. and Niyogi, K. K. (2004). "Regulation of photosynthetic light harvesting involves intrathylakoid lumen pH sensing by the PsbS protein." J Biol Chem 79(22): 2866 22874.

Li, X. P., Muller Moulé, P., Gilmore, A. M. and Niyogi, K. K. (2002). "PsbS dependent enhancement of feedback de excitation protects photosystem I rom hotoinhibition." Proc Natl Acad Sci U S A 9(23): 15222 15227.

Lisitsky, I., Liveanu, V. and Schuster, G. (1995). "RNA binding characteristics of a ribonucleoprotein from spinach chloroplast." Plant Physiol 07(3): 33 941.

Liu, Z., Yan, H., Wang, K., Kuang, T., Zhang, J., Gui, L., An, X. and Chang, W. (2004). "Crystal structure of spinach major light harvesting complex at 2.72 Å resolution." Nature 28(6980): 87 292.

Ljungberg, U., Akerlund, H. E. and Andersson, B. (1986). "Isolation and characterization of the 10 kDa and 22 kDa polypeptides of higher plant photosystem 2." Eur J Biochem 58(3): 77 482.

Magdaong, N. M., Enriquez, M. M., Lafountain, A. M., Rafka, L. and Frank, H. A. (2013). "Effect of protein aggregation on the spectroscopic properties and excited state kinetics of the LHCII pigment protein complex from green plants." Photosynth Res.

Marquardt, D. W. (1963). "An algorithm for least squares estimation of nonlinear parameters." J Soc Ind Appl Math 1(2): 31 441.

Martinez Junza, V., Szczepaniak, M., Braslavsky, S. E., Sander, J., Nowaczyk, M., Rogner, M. and Holzwarth, A. R. (2008). "A photoprotection mechanism involving the D2 branch in photosystem II cores with closed reaction centers." Photochem Photobiol Sci (11): 337 1343.

Maxwell, K., Marrison, J. L., Leech, R. M., Griffiths, H. and Horton, P. (1999). "Chloroplast acclimation in leaves of *Guzmania monostachia* n esponse o igh ight." Plant Physiol 21(1): 9 96.

McCarty, R. E. (1992). "A plant biochemist's view of H+ ATPases and ATP synthases." J Exp Biol 72(Pt): 431 441.

Melis, A. (1984). "Light regulation of photosynthetic membrane structure, organization, and function." J Cell Biochem 4(3): 71 285.

Mellis, A. (1999). "Photosystem II damage and repair cycle in chloroplasts: What modulates the rate of photodamage in vivo?" Trends Plant Sci (4): 30 135.

Menke, W. (1962). "Uber die Chloroplasten von Anthoceros punctatus." Zeitschrift fur Naturforschung 6: 334 336.

Miloslavina, Y. (2008). On the mechanisms of non photochemical quenching in plants and diatoms. Ph. D. Thesis Heinrich Heine Universität Düsseldorf.

Miloslavina, Y., de Bianchi, S., Dall'Osto, L., Bassi, R. and Holzwarth, A. R. (2011). "Quenching in *Arabidopsis thaliana* utants acking onomeric ntenna roteins of photosystem II." J Biol Chem 86(42): 6830 36840.

Miloslavina, Y., Grouneva, I., Lambrev, P. H., Lepetit, B., Goss, R., Wilhelm, C. and Holzwarth, A. R. (2009). "Ultrafast fluorescence study on the location and mechanism of non photochemical quenching in diatoms." Biochim Biophys Acta 787(10): 189 1197.

Miloslavina, Y., Szczepaniak, M., Müller, M. G., Sander, J., Nowaczyk, M., Rögner, M. and Holzwarth, A. R. (2006). "Charge separation kinetics in intact photosystem II core particles is trap limited. A picosecond fluorescence study." Biochemistry 5(7): 436 2442.

Miloslavina, Y., Wehner, A., Lambrev, P. H., Wientjes, E., Reus, M., Garab, G., Croce, R. and Holzwarth, A. R. (2008). "Far red fluorescence: a direct spectroscopic marker for LHCII oligomer formation in non photochemical quenching." FEBS Lett 82(25 26): 3625 3631.

Minagawa, J. and Takahashi, Y. (2004). "Structure, function and assembly of Photosystem II and its light harvesting proteins." Photosynth Res 2(3): 41 263.

Mishra, R. K. and Ghanotakis, D. F. (1993). "Selective extraction of 22 kDa and 10 kDa polypeptides from Photosystem II without removal of 23 kDa and 17 kDa extrinsic proteins." Photosynth Res 6(1): 1 16.

Morosinotto, T., Baronio, R. and Bassi, R. (2002). "Dynamics of chromophore binding to Lhc proteins in vivo and in vitro during operation of the xanthophyll cycle." J Biol Chem 77(40): 6913 36920.

Moya, I., Silvestri, M., Vallon, O., Cinque, G. and Bassi, R. (2001). "Time resolved fluorescence analysis of the photosystem I ntenna roteins n etergent icelles nd iposomes." Biochemistry 0(42): 2552 12561.

Mozzo, M., Passarini, F., Bassi, R., van Amerongen, H. and Croce, R. (2008). "Photoprotection in higher plants: the putative quenching site is conserved in all outer light harvesting complexes of Photosystem II." Biochim Biophys Acta 777(10): 263 1267.

Müller, M. G. (1992). Picosekundenuntersuchungen an Photosyntheseantennen. Schriftenreihe des MPI für Strahlenchemie Nr. 65, SSN 932 5131.

Müller, M. G., Griebenow, K. and Holzwarth, A. R. (1991). "Primary processes in isolated photosynthetic bacterial reaction centres from *Chloroflexus aurantiacus* studied by picosecond fluorescence spectroscopy." Biochim Biophys Acta 098(1): 12.

Müller, M. G., Lambrev, P., Reus, M., Wientjes, E., Croce, R. and Holzwarth, A. R. (2010). "Singlet energy dissipation in the photosystem II light harvesting complex does not involve energy transfer to carotenoids." Chemphyschem 1(6): 289 1296.

Müller, P., Li, X. P. and Niyogi, K. K. (2001). "Non photochemical quenching. A response to excess light energy." Plant Physiol 25(4): 558 1566.

Mullineaux, C. W. and Emlyn Jones, D. (2005). "State transitions: an example of acclimation to low light stress." J Exp Bot 6(411): 89 393.

Mullineaux, C. W., Pascal, A. A., Horton, P. and Holzwarth, A. R. (1993). "Excitation energy quenching in aggregates of the LHC II chlorophyll protein complex: A time resolved fluorescence study." Biochim Biophys Acta 141(1): 3 28.

Murata, N., Takahashi, S., Nishiyama, Y. and Allakhverdiev, S. I. (2007). "Photoinhibition of photosystem II under environmental stress." Biochim Biophys Acta 767(6): 14 421.

Murty, N. R. and Rabinowitch, E. (1965). "Fluorescence decay studies of chlorophyll A in vivo." Biophys J 5(5): 655 661.

Mustárdy, L., Buttle, K., Steinbach, G. and Garab, G. (2008). "The three dimensional network of the thylakoid membranes in plants: quasihelical model of the granum stroma assembly." Plant Cell 0(10): 2552 2557.

Nilkens, M., Kress, E., Lambrev, ., iloslavina, ., üller, ., olzwarth, . . nd ahns, . 2010). "Identification of a slowly inducible zeaxanthin dependent component of non photochemical quenching f chlorophyll fluorescence generated under steady state conditions in *Arabidopsis*." Biochim Biophys Acta 1797(4): 466 475.

Niyogi, K. K., Li, X. P., Rosenberg, V. and Jung, H. S. (2005). "Is PsbS the site of non photochemical quenching in photosynthesis?" J Exp Bot 6(411): 75 382.

Niyogi, K. K. and Truong, T. B. (2013). "Evolution of flexible non photochemical quenching mechanisms that regulate light harvesting in oxygenic photosynthesis." Curr Opin Plant Biol 6(3): 07 314.

O'Connor, D. V. and Phillips, D. (1984). Time correlated single photon counting. ondon, cademic ress.

Ögren, ., quist, . nd ällgren, . . 1984). Photoinhibition f hotosynthesis n emna ibba s induced by the interaction between light and temperature. I. Photosynthesis in vivo." Physiol Plant 2: 181 186.

Ohnishi, N., Allakhverdiev, S. I., Takahashi, S., Higashi, S., Watanabe, M., Nishiyama, Y. and Murata, N. (2005). "Two step mechanism of photodamage to photosystem II: Step 1 occurs at the oxygen evolving complex and step 2 occurs at the photochemical reaction center." Biochemistry 4(23): 494 8499.

Oliver, R. L., Whittington, J., Lorenz, Z. and Webster, I. T. (2003). "The influence of vertical mixing on the photoinhibition of variable chlorophyll a fluorescence and its inclusion in a model of phytoplankton photosynthesis." J Plankton Res 5(9): 107 1129.

Ostroumov, E. E., Lambrev, P., Barros, T., Reus, M. and Holzwarth, A. R. (2014). "Fluorescent chlorophyll charge transfer states as intermediates in the excited state quenching of light harvesting complex II." J Biol Chem ubmitted.

Papageorgiou, G. C. and Govindjee (2011). "Photosystem II fluorescence: slow changes scaling from the past." J Photochem Photobiol B 04(1 2): 258 270.

Pascal, A. A., Liu, Z., Broess, K., Van Oort, B., Van Amerongen, H., Wang, C., Horton, P., Robert, B., Chang, W. and Ruban, A. (2005). "Molecular basis of photoprotection and control of photosynthetic light harvesting." Nature 36(7047): 34 137.

Pearcy, R. W. (1990). "Sunflecks and photosynthesis in plant canopies." Annu Rev Plant Physiol Plant Mol Biol 1(1): 21 453.

Peterson, R. B. and Havir, E. A. (2000). "A nonphotochemical quenching deficient mutant of *Arabidopsis thaliana* ossessing ormal igment omposition nd anthophyll cycle activity." Planta 10(2): 05 214.

Petrou, K., Belgio, E. and Ruban, A. V. (2013). "pH sensitivity of chlorophyll fluorescence quenching is determined by the detergent/protein ratio and the state of LHCII aggregation." Biochim Biophys Acta.

Pfannschmidt, T., Nilsson, A. and Allen, J. F. (1999). "Photosynthetic control of chloroplast gene expression." Nature 97(6720): 25 628.

Pfannschmidt, T., Nilsson, A., Tullberg, A., Link, G. and Allen, J. F. (1999). "Direct transcriptional control of the chloroplast genes *psbA* nd *psaAB* djusts hotosynthesis o ight nergy istribution n lants." IUBMB ife 8(3): 71 276.

Pogson, B. J. and Albrecht, V. (2011). "Genetic dissection of chloroplast biogenesis and development: an overview." Plant Physiol 55(4): 545 1551.

Pribil, M., Labs, M. and Leister, D. (2014). "Structure and dynamics of thylakoids in and lants." J Exp Bot.

Pribil, M., Pesaresi, P., Hertle, A., Barbato, R. and Leister, D. (2010). "Role of plastid protein phosphatase TAP38 in LHCII dephosphorylation and thylakoid electron flow." PLoS Biol (1): 1000288.

Quick, W. P. and Stitt, M. (1989). "An examination of factors contributing to non photochemical quenching of chlorophyll fluorescence in barley leaves." Biochim Biophys Acta 77(3): 87 296.

Quigg, A., Kotabová, E., Jarešová, J., Kaňa, R., Setlik, J., Šedivá, B., Komárek, O. and Prášil, O. (2012). "Photosynthesis in Chromera velia represents a simple system with high efficiency." PLoS One (10): e47036.

Rees, D., Young, A., Noctor, G., Britton, G. and Horton, P. (1989). "Enhancement of the ΔpH dependent dissipation of excitation energy in spinach chloroplasts by light activation: correlation with the synthesis of zeaxanthin." FEBS Lett 56(1 2): 85 90.

Remelli, R., Varotto, C., Sandonà, D., Croce, R. and Bassi, R. (1999). "Chlorophyll binding to monomeric light harvesting complex. A mutation analysis of chromophore binding residues." J Biol Chem 74(47): 33510 33521.

Rochaix, J. D. (2001). "Posttranscriptional control of chloroplast gene expression. From RNA to photosynthetic complex." Plant Physiol 25(1): 42 144.

Rock, C. D., Bowlby, N. R., Hoffmann Benning, S. and Zeevaart, J. A. (1992). "The *aba* utant f *Arabidopsis thaliana* L.) eynh. as educed hlorophyll luorescence ields nd educed thylakoid stacking." Plant Physiol 00(4): 796 1801.

Rozak, P. R., Seiser, R. M., Wacholtz, W. F. and Wise, R. R. (2002). "Rapid, reversible alterations in spinach thylakoid appression upon changes in light intensity." Plant Cell and Environ 5(3): 21 429.

Ruban, A. V., Berera, R., Ilioaia, C., van Stokkum, I. H., Kennis, J. T., Pascal, A. A., van Amerongen, H., Robert, B., Horton, P. and van Grondelle, R. (2007). "Identification of a mechanism of photoprotective energy dissipation in higher plants." Nature 50(7169): 75 578.

Ruban, A. V., Johnson, M. P. and Duffy, C. D. (2012). "The photoprotective molecular switch in the photosystem II antenna." Biochim Biophys Acta 817(1): 67 181.

Ryrie, I. J., Anderson, J. M. and Goodchild, D. J. (1980). "The role f he ight harvesting chlorophyll a/b protein complex in chloroplast membrane stacking. Cation induced aggregation of reconstituted proteoliposomes." Eur J Biochem 07(2): 45 354.

Samuelsson, G., Lönneborg, A., Rosenqvist, E., Gustafsson, P. and Öquist, G. (1985). "Photoinhibition and reactivation of photosynthesis in the cyanobacterium Anacystis nidulans." Plant Physiol 9(4): 92 995.

Santabarbara, S., Garlaschi, F. M., Zucchelli, G. and Jennings, R. C. (1999). "The effect of excited state population in photosystem II on the photoinhibition induced changes in chlorophyll fluorescence parameters." Biochim Biophys Acta 409(3): 65 170.

Sapozhnikov, D. I., Krasovskaya, T. A. and Maevskaya, A. N. (1957). "Change in the interrelationship of the basic carotenoids of the plastids of green leaves under the action of light." Dokl Akad Nauk USSR 13: 65 467.

Sarvikas, P., Hakala, M., Pätsikkä, E., Tyystjärvi, T. and Tyystjärvi, E. (2006). "Action spectrum of photoinhibition in leaves of wild type and *npq1-2* nd *npq4-1* mutants of *Arabidopsis thaliana*." Plant Cell Physiol 7(3): 91 400.

Schrubar, H., Wanner, G. and Westhoff, P. (1991). "Transcriptional control of plastid gene expression in greening Sorghum seedlings." Planta 83(1): 01 111.

Schuster, G., Timberg, R. and Ohad, I. (1988). "Turnover of thylakoid photosystem II proteins during photoinhibition of *Chlamydomonas reinhardtii*." Eur J Biochem 77(2): 03 410.

Senn, H. M. and Thiel, W. (2009). "QM/MM methods for biomolecular systems." Angew Chem Int Ed Engl 48(7): 1198 1229.

Shapiguzov, A., Ingelsson, B., Samol, I., Andres, C., Kessler, F., Rochaix, J. D., Vener, A. V. and Goldschmidt Clermont, M. (2010). "The PPH1 phosphatase is specifically involved in LHCII dephosphorylation and state transitions in *Arabidopsis*." Proc Natl Acad Sci U S A 07(10): 782 4787.

Sharrock, R. A. (2008). "The phytochrome red/far red photoreceptor superfamily." Genome Biol (8): 230.

Shiau, Y. G. and Franck, J. (1947). "Chlorophyll fluorescence and photosynthesis in algae, leaves and chloroplasts." Arch Biochem 4(3): 53 295.

Slavov, C., Ballottari, M., Morosinotto, T., Bassi, R. and Holzwarth, A. R. (2008). "Trap limited charge separation kinetics in higher plant photosystem I complexes." Biophys J 4(9): 601 3612.

Slavov, C., El Mohsnawy, E., Rogner, M. and Holzwarth, A. R. (2009). "Trapping kinetics in isolated cyanobacterial PS I complexes." Chemical Physics 57(1 3): 163 170.

Slavov, C., Reus, M. and Holzwarth, A. R. (2013). "Two different mechanisms cooperate in the desiccation induced excited state quenching in *Parmelia* ichen." J Phys Chem B 17(38): 1326 11336.

Smith, H. (2000). "Phytochromes and light signal perception by plants an emerging synthesis." Nature 407(6804): 585 591.

Sonoike, K., Hihara, Y. and Ikeuchi, M. (2001). "Physiological significance of the regulation of photosystem stoichiometry upon high light acclimation of *Synechocystis* p CC 803." Plant Cell Physiol 2(4): 79 384.

Standfuss, J., Terwisscha van Scheltinga, A. C., Lamborghini, M. and Kühlbrandt, . 005). Mechanisms f photoprotection and nonphotochemical quenching in pea light harvesting complex at 2.5 Å resolution." EMBO J 4(5): 19 928.

Stirbet, A. and Govindjee (2011). "On the relation between the Kautsky effect (chlorophyll a fluorescence induction) and Photosystem II: basics and applications of the OJIP fluorescence transient." J Photochem Photobiol B 04(1 2): 236 257.

Stransky, H. and Hager, A. (1970). "The carotenoid pattern and the occurrence of the light induced xanthophyll cycle in various classes of algae. VI. Chemosystematic study." Arch Mikrobiol 3(4): 15 323.

Styring, S., Virgin, I., Ehrenberg, A. and Andersson, B. (1990). "Strong light photoinhibition of electrontransport in Photosystem II. Impairment of the function of the first quinone acceptor, QA." Biochim Biophys Acta 015(2): 69 278.

Suetsugu, N. and Wada, M. (2007). "Chloroplast photorelocation movement mediated by phototropin family proteins in green plants." Biol Chem 88(9): 27 935.

Suorsa, M., Grieco, M., Järvi, S., Gollan, P. J., Kangasjärvi, S., Tikkanen, M. and Aro, E. M. (2013). "PGR5 ensures photosynthetic control to safeguard photosystem I under fluctuating light conditions." Plant Signal Behav (1): 67 172.

Suorsa, M., Järvi, S., Grieco, M., Nurmi, M., Pietrzykowska, M., Rantala, M., Kangasjärvi, S., Paakkarinen, V., Tikkanen, M., Jansson, S. and Aro, E. M. (2012). "PROTON GRADIENT REGULATION5 is essential for proper acclimation of *Arabidopsis* hotosystem o aturally nd rtificially luctuating ight onditions." Plant Cell 4(7): 934 2948.

Szczepaniak, M., Sander, J., Nowaczyk, M., Müller, M. G., Rögner, M. and Holzwarth, A. R. (2009). "Charge separation, stabilization, and protein relaxation in photosystem II core particles with closed reaction center." Biophys J 6(2): 21 631.

Takahashi, H., Clowez, S., Wollman, F. A., Vallon, O. and Rappaport, F. (2013). "Cyclic electron flow is redox controlled but independent of state transition." Nat Commun .

Teardo, E., de Laureto, P. P., Bergantino, E., Dalla Vecchia, F., Rigoni, F., Szabò, I. and Giacometti, G. M. (2007). "Evidences for interaction of PsbS with photosynthetic complexes in maize thylakoids." Biochimica et Biophysica Acta ioenergetics 767(6): 03 711.

Tikkanen, M. and Aro, E. M. (2012). "Thylakoid protein phosphorylation in dynamic regulation of photosystem II in higher plants." Biochim Biophys Acta 817(1): 32 238.

Tikkanen, M., Grieco, M. and Aro, E. M. (2011). "Novel insights into plant light harvesting complex II phosphorylation and 'state ransitions'." Trends Plant Sci 6(3): 26 131.

Tikkanen, M., Grieco, M., Kangasjarvi, S. and Aro, E. M. (2010). "Thylakoid protein phosphorylation in higher plant chloroplasts optimizes electron transfer under fluctuating light." Plant Physiol 52(2): 23 735.

Tikkanen, M., Grieco, M., Nurmi, M., Rantala, M., Suorsa, M. and Aro, E. M. (2012). "Regulation of the photosynthetic apparatus under fluctuating growth light." Philos Trans R Soc Lond B Biol Sci 67(1608): 3486 3493.

Tikkanen, M., Mekala, N. R. and ro, . . 2014). Photosystem I hotoinhibition repair cycle protects Photosystem I from irreversible damage." Biochim Biophys Acta 837(1): 10 215.

Tikkanen, M., Suorsa, M., Gollan, P. J. and Aro, E. M. (2012). "Post genomic insight into thylakoid membrane lateral heterogeneity and redox balance." FEBS Lett 86(18): 911 2916.

Tóth, S. Z., Schansker, G. and Strasser, R. J. (2005). "In intact leaves, the maximum fluorescence level (F(M)) is independent of the redox state of the plastoquinone pool: a DCMU inhibition study." Biochim Biophys Acta 708(2): 75 282.

Trissl, H. W. (1997). "Determination of the quenching efficiency of the oxidized primary donor of Photosystem I, P700(+): Implications for the trapping mechanism." Photosynth Res 4(3): 37 240.

Umena, Y., Kawakami, K., Shen, J. R. and Kamiya, N. (2011). "Crystal structure of oxygen evolving photosystem II at a resolution of 1.9 Å." Nature 73(7345): 5 60.

Van Breusegem, F. and Dat, J. F. (2006). "Reactive oxygen species in plant cell death." Plant Physiol 41(2): 384 390.

van Wijk, K. J. (2004). Plastid proteomics. Plant Physiology and Biochemistry. 2**:** 963 977.

Vass, I., Styring, S., Hundal, T., Koivuniemi, A., Aro, E. and Andersson, B. (1992). "Reversible and irreversible intermediates during photoinhibition of photosystem II: stable reduced QA species promote chlorophyll triplet formation." Proc Natl Acad Sci U S A 9(4): 408 1412.

Wagner, R., Dietzel, L., Bräutigam, K., Fischer, W. and Pfannschmidt, T. (2008). "The long term response to fluctuating light quality is an important and distinct light acclimation mechanism that supports survival of *Arabidopsis thaliana* under low light conditions." Planta 28(4): 73 587.

Wahadoszamen, M., Berera, R., Ara, A. M., Romero, E. and van Grondelle, R. (2012). "Identification of two emitting sites in the dissipative state of the major light harvesting antenna." Phys Chem Chem Phys 4(2): 759 766.

Walters, R. G. (2005). "Towards an understanding of photosynthetic acclimation." J Exp Bot 6(411): 35 447.

Wang, J., Cieplak, P. and Kollman, P. A. (2000). "How well does a restrained electrostatic potential (RESP) model perform in calculating conformational energies of organic and biological molecules?" J Comput Chem 1(12): 049 1074.

Wilk, L., Grunwald, M., Liao, P. N., Walla, P. J. and Kühlbrandt, W. (2013). "Direct interaction of the major light harvesting complex II and PsbS in nonphotochemical quenching." Proc Natl Acad Sci U S A 10(14): 5452 5456.

Yakushevska, A. E., Keegstra, W., Boekema, E. J., Dekker, J. P., Andersson, J., Jansson, S., Ruban, A. V. and Horton, P. (2003). "The structure of photosystem II in *Arabidopsis*: Localization of the CP26 and CP29 antenna complexes." Biochemistry 2(3): 08 613.

Yamamoto, H. Y., Nakayama, T. O. and Chichester, C. O. 1962). Studies n he ight nd ark interconversions of leaf xanthophylls." Arch Biochem Biophys 7(1): 68 173.

Yamamoto, Y. and Akasaka, T. (1995). "Degradation of antenna chlorophyll binding protein CP43 during photoinhibition of photosystem II." Biochemistry 4(28): 038 9045.

Yanai, T., Tew, D. P. and Handy, N. C. (2004). "A new hybrid exchange correlation functional using the Coulomb attenuating method (CAM B3LYP)." Chem Phys Lett 93(1 3): 51 57.

Yin, ., undin, ., ertrand, ., urmi, ., olymosi, K., Kangasjärvi, S., Aro, E. M., Schoefs, B. and Spetea, C. (2010). "Role of thylakoid ATP/ADP carrier in photoinhibition and photoprotection of photosystem II in *Arabidopsis*." Plant Physiol 53(2): 66 677.

Yokono, M., Murakami, A. and Akimoto, S. (2011). "Excitation energy transfer between photosystem II and photosystem I in red algae: larger amounts of phycobilisome enhance spillover." Biochim Biophys Acta 1807(7): 847 853.

Zer, H. and Ohad, I. (1995). "Photoinactivation of photosystem II induces changes in the photochemical reaction center II abolishing the regulatory role of the QB site in the D1 protein degradation." Eur J Biochem 31(2): 48 453.

Zito, F., Finazzi, G., Delosme, R., Nitschke, W., Picot, D. and Wollman, F. A. (1999). "The Qo site of cytochrome b6f complexes controls the activation of the LHCII kinase." EMBO J 8(11): 961 2969.

Zucchelli, G., Islam, K. and Jennings, R. C. (1987). The kinetics of phosphorylation of the light harvesting chlorophyll a/b protein and associated changes in photosystem cross section and energy spillover. Progress in Photosynthesis Research. . iggins, pringer etherlands**:** 725 728.